Estimation non-paramétrique dans les problèmes inverses à opérateur bruité

Thomas Vareschi

Université Paris Diderot - Paris VII
UFR de Mathématiques

Thèse de doctorat

présentée pour obtenir le titre de
Docteur en sciences de l'université Paris VII
Spécialité : **Mathématiques appliquées**

soutenue par
Thomas Vareschi

Estimation Non-paramétrique Dans Les Problèmes Inverses À Opérateur Bruité

Directrice de thèse : **Dominique Picard**

Soutenue publiquement le 6 décembre 2013 devant le jury composé de:

Mme Cristina Butucea	*Université Paris-Est Marne-la-Vallée*	Rapporteur
M. Markus Reiss	*Humboldt-Universität zu Berlin*	Rapporteur
M. Stéphane Boucheron	*Université Paris Diderot*	Examinateur
Mme Fabienne Comte	*Université Paris Descartes*	Examinatrice
M. Sylvain Delattre	*Université Paris Diderot*	Examinateur
M. Marc Hoffmann	*Université Paris Dauphine*	Examinateur
Mme Dominique Picard	*Université Paris Diderot*	Directrice

Remerciements

Mes premiers remerciements vont à ma directrice Dominique Picard. Dominique, merci de m'avoir fait découvrir le monde de la recherche dans ce domaine passionnant qu'est celui de la statistique (non paramétrique, mais pas que). Merci pour ton soutien constant, pour la patience dont tu as fait preuve et pour ta gentillesse à mon égard au cours de ces trois années.

Je remercie chaleureusement Cristina Butucea et Markus Reiß d'avoir accepté de rapporter ma thèse. Je leur en suis très reconnaissant.

Je remercie Fabienne Comte, Stéphane Boucheron, Sylvain Delattre et Marc Hoffmann d'avoir accepté de participer à mon jury de thèse. Leur présence dans mon jury est un honneur, et leurs travaux ont été une source d'inspiration pendant ces trois ans.

Un des travaux de cette thèse est le résultat d'une collaboration avec plusieurs auteurs. J'en profite donc pour remercier (au risque d'être redondant) Dominique Picard, Sylvain Delattre, et Marc Hoffmann pour cette agréable expérience. Je remercie particulièrement Marc pour son énergie et son initiation pédagogique (et patiente) aux lowers bounds. Certaines parties de cette thèse lui doivent beaucoup.

Ce fut un plaisir d'assurer les travaux dirigés du cours de Karine Tribouley au cours de ces trois ans. Je la remercie de m'avoir donné cette opportunité.

Ces trois années furent également l'occasion de rencontres agréables et enrichissantes au sein du laboratoire du LPMA. Je remercie donc Stéphane Boucheron, Sylvain Delattre, Gérard Kerkyacharian, Erwan Le Pennec, Mathilde Mougeot, et Karine Tribouley pour m'avoir accordé ne serait-ce qu'un peu de leur temps en explications ou conseils. Un grand merci également au personnel administratif du laboratoire et de l' U.F.R : Nathalie Bergame, Pascal Chiettini et Valérie Juvé pour leur efficacité et leur sympathie.

Enfin, ce préambule est l'occasion pour moi d'exprimer ma sincère gratitude à mes compagnons de route thésards qui ont entre autres rendu les moments difficiles plus supportables et moins solitaires. Pour ne vexer personne, merci donc par ordre alphabétique à Anna Benhamou, Guillaume Barraquand, Oriane Blondel, Jiatu Cai, Sébastien Choukroun, Sophie Coquan, Aser Cortines, Pierre Gruet, Lorick Huang, Nicolas Langrené, Victor Perez, Christophe Poquet et Maud Thomas pour la bonne ambiance que vous avez maintenue lors des pauses café ou bien des soirées passées ensemble. Qu'ils m'excusent pour l'absence de remerciements personnalisés, mais le temps me manque actuellement! Je porte une attention particulière à mes 'frères de thèse' Jean-Baptiste

Monnier et Marc-Antoine Giuliani pour leur solidarité, leur gentillesse et leur sens de l'humour régénérateurs. Je remercie enfin mon camarade rennais Laurent Pater de m'avoir remercié dans son manuscrit de thèse.

Cette thèse n'aurait pas été la même sans le soutien de ma famille qui tient une place de premier plan pour moi et que je tiens à remercier ici. J'ai bien entendu une pensée pour mes amis, qui me pardonneront ma non-exhaustivité.

Pour finir, merci à celle qui a patiemment supporté, sans (trop) se plaindre, ces trois années parfois difficiles. Amélie, ces travaux te doivent aussi beaucoup et les mots seuls ne peuvent exprimer toute ma reconnaissance, et plus encore...

Contents

1 Introduction aux problèmes inverses **11**

1.1 Qu'est-ce qu'un problème inverse? 11
1.2 Cadre statistique des problèmes inverses 13
1.2.1 Différents modèles statistiques 13
1.2.2 Critère de performance et cadre minimax 14
1.3 Méthodes de résolution 15
1.3.1 La méthode SVD 16
1.3.2 La méthode SVD par blocs 16
1.4 Généralisation: méthode de Galerkin 19
1.4.1 Choix des bases 20
1.4.2 Décomposition biais-variance 22
1.5 Degree of ill-posedness, espaces de régularité, adaptativité 23
1.6 Nécessité de considérer des opérateurs bruités 24

2 Problèmes inverses à opérateurs bruités **27**

2.1 Modèle 27
2.1.1 Conséquence sur le compromis biais-variance 29
2.2 Schémas génériques de résolution 30
2.2.1 Régularisation de l'opérateur bruité 31
2.2.2 Procedures IR et RI 33
2.2.3 Détermination de bornes inférieures pour le risque minimax . . 35
2.3 Retour sur la déconvolution aveugle par ondelettes 35
2.4 Traitement des opérateurs diagonaux par blocs 37
2.4.1 Modèle 37
2.4.2 Algorithme 38
2.5 Traitement des opérateurs intégraux de Volterra 41
2.5.1 Hypothèses du modèle 43
2.5.2 Algorithme et vitesse de convergence 44
2.5.3 Aspects pratiques 45
2.6 Opérateurs diagonaux par blocs : cas $\mathbb{L}^p$ 47
2.6.1 Needlets 50
2.6.2 Algorithme et résultats 51

3 Blockwise SVD with error in the operator **55**
3.1 Introduction . . . 56
3.1.1 Motivation . . . 56
3.1.2 Main results and organisation of the paper . . . 57
3.2 Estimation by blockwise SVD . . . 58
3.2.1 The blockwise SVD property . . . 58
3.2.2 Blockwise SVD reconstruction with noisy data . . . 60
3.3 Main results . . . 60
3.3.1 Minimax rates of convergence . . . 60
3.3.2 Discussion . . . 61
3.4 Application to blind deconvolution . . . 64
3.4.1 Spherical deconvolution . . . 64
3.4.2 Circular deconvolution . . . 68
3.5 Proofs . . . 71
3.5.1 Preliminary estimates . . . 71
3.5.2 Proof of Theorem 3.3.1 . . . 73
3.5.3 Proof of Theorem 3.3.2 . . . 80

4 Noisy Laplace deconvolution with error in the operator **87**
4.1 Introduction . . . 88
4.2 Discretization of Laplace deconvolution . . . 90
4.2.1 Laguerre functions . . . 90
4.2.2 Galerkin method . . . 90
4.2.3 Application to the regression model with irregular design . . . 91
4.2.4 Error in the operator . . . 93
4.3 Features of the target function and the kernel . . . 93
4.3.1 Sobolev spaces associated to Laguerre functions . . . 93
4.3.2 Banded Toeplitz matrices . . . 94
4.3.3 Degree of ill posedness . . . 95
4.3.4 A first algorithm of estimation . . . 96
4.4 Adaptation to the standard framework . . . 97
4.5 Practical performances . . . 99
4.6 Proofs . . . 104
4.6.1 Proof of Proposition 4.4.2 . . . 104
4.6.2 Proofs of theorems 4.3.3 and 4.4.5 . . . 105
4.6.3 Proof of theorem 4.4.6 . . . 114

5 Needlets on $\mathbb{S}^2$ and the NEED-VD procedure **119**
5.1 A brief introduction to frame theory . . . 119
5.2 Needlets . . . 121
5.2.1 The needlet framework . . . 122
5.2.2 Properties of needlets . . . 124
5.2.3 Besov spaces . . . 125

5.3 The NEED-VD procedure 126

6 Needlets and blind spherical deconvolution 129
6.1 Introduction 130
6.1.1 Statistical framework 130
6.1.2 Harmonic analysis on SO(3) and $\mathbb{S}^2$ 132
6.2 Estimation procedure 135
6.2.1 Main procedure 136
6.2.2 Practical study 140
6.3 Proofs 142
6.3.1 Proof of Theorem 6.2.2 148
6.3.2 Proof of Theorem 6.2.3 151

A Wavelets and statistical estimation 155
A.1 Multi Resolution Analysis 155
A.2 Wavelets and approximation theory 157
A.2.1 Besov spaces 157
A.2.2 Besov spaces and Littlewood-Paley decomposition 157
A.2.3 Characterization of Besov spaces via wavelet expansion 158
A.3 Statistical estimation using wavelets 159
A.3.1 Direct estimation using wavelets 159
A.3.2 Application of wavelets to inverse problems 160

B Proof of the lower bound in section 2.1.1 163

Sommaire et notations

Cette thèse est consacrée à l'étude des problèmes inverses avec opérateur bruité. Nous exposerons donc dans un premier temps au Chapitre 1, de manière introductive, le cadre mathématique des problèmes inverses ainsi que différentes méthodes de résolution. Nous expliquerons au Chapitre 2 comment la question de la résolution avec opérateur bruité se pose naturellement pour certains opérateurs, avant de passer en revue plusieurs solutions dans le cadre non paramétrique. Nous aborderons ensuite aux Chapitres 3, 4 et 6 les principales contributions de cette thèse au domaine des problèmes inverses avec opérateur bruité, à savoir :

- Au Chapitre 3, le traitement d'opérateurs diagonaux par blocs dans un cas L^2.
- Au Chapitre 6, l'adaptation de cette procédure à une perte de type L^p, dans le cas précis de la déconvolution sphérique.
- Au Chapitre 4, le traitement d'opérateurs de convolution de Laplace/Volterra.

Une version résumée de ces trois chapitres, ayant chacun fait l'objet d'une publication ou d'une soumission dans une revue scientifique, se trouve dans le Chapitre 2. Le Chapitre 5 sert d'interlude entre les Chapitres 3 et 6. On y présente les needlets, sorte d'équivalent des ondelettes sur la sphère, mises en oeuvre dans le Chapitre 6.

Au cours de ce manuscrit, nous définirons le plus souvent les notations en jeu. Nous apportons ici quelques précisions sur certaines d'entre elles:

- Les notations $a \lesssim b$, $a \gtrsim b$ ou $a \leqslant Cb$, $a \geqslant Cb$ signifient inégalité à une constante multiplicative près. La constante C peut dépendre de données annexes, que nous ne préciserons pas lorsque le contexte sera clair.
- La norme spectrale d'un opérateur ou bien d'une matrice sera désignée par $\|.\|_{\mathrm{op}}$, la norme de Hilbert-Schmidt d'une matrice par $\|A\|_{\mathrm{HS}} = \mathrm{Tr}({}^tAA)$.
- Enfin, lorsque ce ne sera pas précisé, la norme $\|.\|$ sera la norme associée à l'espace de Hilbert $\mathbb{H}$ ou $\mathbb{K}$ sous-jacent.

Chapter 1

Introduction aux problèmes inverses

Ce chapitre est dédié à la présentation et au traitement des problèmes inverses (section 1.1). On s'intéressera en particulier au cadre statistique sous-jacent à l'ensemble de cette thèse en section 1.2 avant de passer en revue diverses méthodes de résolution (section 1.3). Nous verrons que l'étude du compromis biais variance induit par une méthode de Galerkin (section 1.4) introduit naturellement les notions d'espace de régularité et de 'degree of ill-posedness' (section 1.5). Enfin, un bref exemple pratique (section 1.6) motivera l'introduction du cadre des problèmes inverses avec erreur dans l'opérateur au chapitre suivant.

Contents

1.1 Qu'est-ce qu'un problème inverse? 11
1.2 Cadre statistique des problèmes inverses 13
1.3 Méthodes de résolution 15
1.4 Généralisation: méthode de Galerkin 19
1.5 Degree of ill-posedness, espaces de régularité, adaptativité 23
1.6 Nécessité de considérer des opérateurs bruités 24

1.1 Qu'est-ce qu'un problème inverse?

Un problème inverse consiste en la détermination de l'antécédent d'un état par un procédé évolutif. Ou bien, formulé de manière plus simpliste, à déterminer des causes connaissant leurs effets. Bien évidemment, cette formulation est trop générale dans un contexte mathématique, aussi nous précisons maintenant notre cadre de travail.
La modélisation d'un tel procédé se fait par le biais d'un opérateur $\boldsymbol{K}$, agissant sur un ensemble $\mathbb{H}$ (de causes), à valeurs dans un ensemble $\mathbb{K}$ (d'effets). Un problème inverse consiste donc, étant donné un élément $\boldsymbol{g} \in \mathbb{K}$ image d'un élément $\boldsymbol{f} \in \mathbb{H}$ selon l'équation

$$\boldsymbol{g} = \boldsymbol{K}\boldsymbol{f}\,, \tag{1.1}$$

à déterminer l'inconnue $\boldsymbol{f}$. Dans notre cas, l'ensemble $\mathbb{H}$ est un ensemble de fonctions, que nous supposerons définies sur un espace mesurable $(\mathcal{Y}, d\mu)$. Nous omettrons parfois la mesure μ lorsque le contexte sera clair. Avant de poursuivre, donnons-en quelques exemples afin de motiver leur étude:

- *Opérateur de convolution*: L'exemple le plus emblématique est sans doute celui de la déconvolution. Ici, la fonction $\boldsymbol{f} \in \mathbb{L}^2([0,1])$ est observée au travers d'un dispositif bruitant qui moyenne localement la fonction, selon l'équation

$$\boldsymbol{g}(x) = \boldsymbol{K}\boldsymbol{f}(x) = \boldsymbol{k} * \boldsymbol{f}(x) = \int_0^1 \boldsymbol{f}(x-t)\boldsymbol{k}(t)dt\,, \tag{1.2}$$

  où $\boldsymbol{k}$ est une fonction de $\mathbb{L}^2([0,1])$. Plus généralement, on observe

$$\boldsymbol{g}(x) = \boldsymbol{K}\boldsymbol{f}(x) = \boldsymbol{k} * \boldsymbol{f}(x) = \int_H \boldsymbol{f}(h^{-1}x)\boldsymbol{k}(h)dh\,,$$

  où H est un groupe agissant sur $\mathcal{Y}$, et dh est la mesure de Haar sur H. Cette modélisation très générique recouvre des domaines très variés, incluant par exemple le traitement d'images, la spectroscopie, ou bien l'astrophysique.

- *Opérateur de Wicksell*: Supposons que des sphères, dont le rayon suit une loi de probabilité de densité $\boldsymbol{f}$, baignent dans un milieu. On désire retrouver $\boldsymbol{f}$ à partir de coupes planaires. Ce modèle possède des applications en biologie et en stéréologie entre autres. Johnstone and Silverman [45] ont montré qu'il conduisait à l'inversion de l'opérateur

$$\begin{aligned}\boldsymbol{K} : \mathbb{L}^2\big([0,1],(4x)^{-1}dx\big) &\to \mathbb{L}^2\big([0,1],4\pi^{-1}(1-y^2)^{1/2}dy\big)\\ \boldsymbol{f} &\mapsto \boldsymbol{K}\boldsymbol{f}(y) = \frac{\pi}{4}y(1-y^2)^{-1/2}\int_y^1 (x^2-y^2)^{-1/2}\boldsymbol{f}(x)(4x)^{-1}dx\,.\end{aligned}$$

- *Opérateur intégral de Volterra*: Soit $\boldsymbol{f} \in \mathbb{L}^2(\mathbb{R}_+)$. On observe, pour $t \geqslant 0$,

$$\boldsymbol{g}(t) = \int_0^t \boldsymbol{k}(\tau)\boldsymbol{f}(t-\tau)d\tau\,. \tag{1.3}$$

  Cet opérateur est l'analogue de l'opérateur de convolution pour des systèmes non anticipants, c'est-à-dire que $\boldsymbol{g}(t)$ ne dépend que des valeurs de $\boldsymbol{k}$ et de $\boldsymbol{f}$ prises aux temps $\tau < t$. Encore une fois, les applications sont nombreuses et incluent par exemple la dynamique des populations et la spectroscopie par fluorescence. On pourra par exemple se référer à [59, Chap. 2].

Cette liste est bien sûr hautement non exhaustive, et on pourra consulter [53, Chap. 1] pour y apporter de nouveaux exemples. De plus, remarquons que nous n'avons mentionné que des opérateurs linéaires. La théorie des problèmes inverses à opérateur non linéaires étant autrement plus complexe, nous ne l'aborderons pas ici, et nous nous restreindrons donc à l'étude d'**opérateurs linéaires**. Revenons donc à la formulation du problème. En toute généralité, ce dernier est mal posé au sens de Hadamard. De manière plus précise, plusieurs facteurs peuvent entraver sa résolution:

- **Existence**: en pratique, on n'observe jamais $\boldsymbol{Kf}$, mais plutôt une version bruitée $\boldsymbol{Kf}+\boldsymbol{\xi}$. Si la fonction observée n'appartient pas à $\mathrm{Im}(\boldsymbol{K})$, alors l'inversion directe comme dans (1.1) est impossible.

- **Unicité**: si plusieurs antécédents conduisent à la même observation, le choix de l'un d'entre eux seulement prête à confusion. Il est donc nécessaire de disposer d'informations additionnelles permettant de discriminer entre les différentes solutions. On supposera dans notre cas l'opérateur injectif.

- **Stabilité**: malgré l'injectivité supposée, un dernier problème subsiste. Sachant qu'en pratique, d'une part, la fonction $\boldsymbol{g}$ n'est jamais observée qu'à travers une approximation, et que d'autre part l'inversion de l'opérateur $\boldsymbol{K}$ est elle-même sujette à approximation, on voit qu'une notion de continuité vis-à-vis des données ainsi qu'une notion de stabilité de l'opérateur sont indispensables. C'est en particulier ce dernier problème que nous tenterons de résoudre dans certains cas précis. Le caractère mal posé se traduira par le fait que l'opérateur $\boldsymbol{K}$ est compact. Dans ce cas, $\boldsymbol{K}^{-1}$ n'est pas continu et même une erreur très faible commise sur l'observation de $\boldsymbol{g}$ peut conduire à un résultat radicalement différent de $\boldsymbol{f}$. Il est donc nécessaire de régulariser $\boldsymbol{K}$, c'est à dire de trouver $\widetilde{\boldsymbol{K}}$ 'proche' de $\boldsymbol{K}$ en un certain sens, compatible avec l'inversion de (1.1), mais aux propriétés plus attrayantes (stabilité, simplicité et rapidité computationnelle de l'inversion).

Pour plus de précisions concernant ces questions, on pourra se référer à Kirsch [53].

1.2 Cadre statistique des problèmes inverses

1.2.1 Différents modèles statistiques

Nous venons d'exposer le cadre générique d'un problème inverse. Dans l'optique de sa résolution, la problématique déterministe consiste à majorer l'erreur (déterministe!) commise sur $\boldsymbol{f}$ en fonction de l'erreur commise sur $\boldsymbol{g}$. En statistique, l'approche adoptée est différente, et on suppose que le terme d'erreur est le résultat d'un procédé aléatoire dont on contrôle l'amplitude. Ce type d'approche recouvre en réalité plusieurs cadres statistiques distincts (mais connexes, voir [82, Chap. 1]), dont nous présentons trois cas particuliers :

(1) **Estimation de densité**: On observe $(Y_1, ..., Y_n)$ un n-échantillon de loi commune Z à densité $\boldsymbol{f}_Z$, tel que $\boldsymbol{f}_Z$ est l'image par $\boldsymbol{K}$ de la densité cible $\boldsymbol{f}$. En particulier, il faut que $\boldsymbol{K}$ conserve l'ensemble

$$\left\{ f \in \mathbb{H},\ \int f = 1 \right\}.$$

Un exemple très simple d'application est celui de la convolution de deux densités définies sur $\mathbb{R}$: si X et Y sont deux variables aléatoires à valeurs réelles, de densités

respectives $\boldsymbol{f}$ et $\boldsymbol{g}$, alors la variable $Z = X + Y$ a pour densité $\boldsymbol{f}_Z = \boldsymbol{g} * \boldsymbol{f}$ où $*$ est le produit de convolution sur $\mathbb{R}$. L'opérateur $\boldsymbol{K} : f \mapsto \boldsymbol{g} * f$ conserve bien l'ensemble des fonctions mesurables d'intégrale 1. La version 'sphérique' de cette exemple est présentée au Chapitre 3.

(2) **Modèle de régression**: Soit $t_1, ..., t_n \in \mathcal{Y}$. On observe les valeurs

$$Y_i = \boldsymbol{K}\boldsymbol{f}(t_i) + \xi_i,\ i = 1, ..., n\,,$$

où les variables ξ_i sont i.i.d et $\mathbb{E}[\xi_1] = 0$. La qualité de l'estimation de $\boldsymbol{f}$ est bien sûr intrinsèquement liée à celle de la grille $t_1, .., t_n$.

(3) **Modèle de bruit blanc**: Ce modèle est un modèle idéalisé, mais très utile en théorie: on observe des réalisations du processus

$$d\boldsymbol{Y}_\varepsilon(s) = \boldsymbol{K}\boldsymbol{f}(s)ds + \varepsilon d\boldsymbol{W}(s)\,, \tag{1.4}$$

où $\boldsymbol{W}$ est un processus de Wiener standard. On écrira de manière plus succincte $\boldsymbol{Y}_\varepsilon = \boldsymbol{K}\boldsymbol{f} + \varepsilon\dot{\boldsymbol{W}}$, et on réfèrera indifféremment à $\boldsymbol{Y}_\varepsilon$ ou $\boldsymbol{Y}$. L'acquisition d'informations sur $\boldsymbol{Y}_\varepsilon$ se fait par le biais de fonctions tests. Plus précisément, pour deux fonctions test $\xi, \xi' \in \mathbb{H}$, les quantités observables prennent la forme

$$\langle \boldsymbol{Y}_\varepsilon, \xi\rangle_{\mathbb{K}} = \langle \boldsymbol{K}\boldsymbol{f}, \xi\rangle_{\mathbb{K}} + \varepsilon\langle\dot{\boldsymbol{W}}, \xi\rangle_{\mathbb{K}}\,,$$

où $\langle\dot{\boldsymbol{W}}, \xi\rangle_{\mathbb{K}} \sim \mathcal{N}(0, \|\xi\|^2)$ et $\mathbb{E}[\langle\dot{\boldsymbol{W}}, \xi\rangle_{\mathbb{K}}\langle\dot{\boldsymbol{W}}, \xi'\rangle_{\mathbb{K}}] = \langle\xi, \xi'\rangle_{\mathbb{K}}$.
Le parallèle avec le modèle de densité et le modèle de régression lorsque $t_i = i/n$ s'opère en posant $\varepsilon = n^{-1/2}$.

1.2.2 Critère de performance et cadre minimax

La bonne performance d'un estimateur est quantifiée par un critère de performance à minimiser. Nous nous plaçons dans le modèle de bruit blanc (3), mais les résultats sont aisément transcriptibles aux cadres (1) et (2) en remplaçant ε par $n^{-1/2}$. Etant donné $\boldsymbol{f}$ et un estimateur $\widetilde{\boldsymbol{f}}$, on peut par exemple considérer la perte $\mathbb{L}^p$

$$d(\widetilde{\boldsymbol{f}}, \boldsymbol{f}) = \int_{\mathcal{Y}} |\widetilde{\boldsymbol{f}} - \boldsymbol{f}|^p d\mu,\ 1 \leqslant p \leqslant +\infty\,.$$

De manière générale, on peut considérer n'importe quelle distance d définie sur $\mathbb{H} \times \mathbb{H}$. Bien sûr, cette perte est aléatoire et dépend des observations générées par les modèles (1), (2),ou (3). Il est donc naturel de considérer plus précisément le risque moyenné

$$\mathcal{R}_\varepsilon = \mathbb{E}_{\boldsymbol{f}}\left[d(\widetilde{\boldsymbol{f}}, \boldsymbol{f})\right],$$

que l'on cherche à minimiser en $\widetilde{\boldsymbol{f}}$ lorsque $\boldsymbol{f}$ vit dans un espace X. On voit que deux entités antagonistes interviennent lors de cette minimisation: d'une part, la nature

prodigue une fonction inconnue a priori $\boldsymbol{f}$, d'autre part le statisticien propose un estimateur $\widetilde{\boldsymbol{f}}$ destiné à l'approcher. Nous adoptons la stratégie dite du minimax, qui consiste à se parer contre le pire cas possible du choix de $\boldsymbol{f}$. En d'autres termes, nous cherchons un estimateur $\widetilde{\boldsymbol{f}}$ tel que

$$\sup_{\boldsymbol{f}\in X} \mathbb{E}_{\boldsymbol{f}}[d(\widetilde{\boldsymbol{f}}, \boldsymbol{f})] = \inf_{\widetilde{f}} \sup_{\boldsymbol{f}\in X} \mathbb{E}_{\boldsymbol{f}}[d(\widetilde{f}, \boldsymbol{f})]\,. \tag{1.5}$$

On note

$$\mathcal{R}^*_\varepsilon = \inf_{\widetilde{f}} \sup_{\boldsymbol{f}\in X} \mathbb{E}_{\boldsymbol{f}}[d(\widetilde{f}, \boldsymbol{f})]$$

le risque minimax associé au problème. De manière générale, cette notion est trop restrictive si l'espace X est suffisament vaste. On introduit donc la notion relaxée de vitesse de convergence optimale pour le cadre minimax:

Definition 1.2.1. *Une fonction positive ψ_ε est appelée vitesse de convergence optimale pour le problème (3) s'il existe deux constantes $0 < c, C < +\infty$ tel que*

$$\limsup_{\varepsilon\to 0} \psi_\varepsilon^{-1}\mathcal{R}^*_\varepsilon \leqslant C \;\; et \;\; \liminf_{\varepsilon\to 0} \psi_\varepsilon^{-1}\mathcal{R}^*_\varepsilon \geqslant c\,.$$

Dans la suite, on dira qu'un algorithme est optimal s'il atteint une vitesse de convergence optimale (au sens minimax) sur l'espace considéré.
Le choix de l'espace X est crucial car il dicte la forme d'une procédure d'estimation (ou réciproquement le choix de l'espace X découle de la méthode utilisée). Par exemple, la décomposition (1.21) incite à choisir des espaces dans lesquels $\boldsymbol{f}$ est bien approchée par la base $(u_k)_{k\geqslant 0}$ utilisée. De manière générale, l'espace X choisi sera un compact d'un espace métrique.

1.3 Méthodes de résolution

La résolution de (1.1) fait l'objet d'une très vaste littérature que nous ne pouvons nous permettre d'aborder de manière exhaustive. Les méthodes les plus populaires sont sans doute la régularisation de Tikhonov (voir e.g. [73, Chap. 2]), la décomposition en valeurs singulières (SVD) ainsi que les méthodes de projection. Nous n'aborderons que les deux dernières dans la suite.
De manière générale, le principe de ces méthodes est d'approcher ce problème par une suite de problèmes bien posés $\mathcal{P}_h$ dont la solution $\boldsymbol{f}_h$ converge vers $\boldsymbol{f}$ lorsque $h \to 0$. Dans un cadre statistique, la réduction du paramètres h diminue le biais mais augmente la variance du modèle, l'enjeu étant de calibrer de manière optimale le compromis entre les deux. Nous verrons que ceci est possible sous certaines hypothèses concernant les données du problème.
Nous prodiguons maintenant la liste des méthodes de régularisation qui nous intéresseront par la suite, à savoir la méthode SVD (et son corollaire la troncature spectrale), la généralisation de cette méthode à un cadre de SVD par blocs, et enfin la méthode de projection dite de Galerkin qui englobe en réalité les deux précédentes.

1.3.1 La méthode SVD

La méthode SVD repose sur le choix de bases des espaces $\mathbb{H}$ et $\mathbb{K}$, adaptées au comportement de $\boldsymbol{K}$. Plus précisément, on a le

Theorem 1.3.1. *Soit $\mathbb{H}$ et $\mathbb{K}$ deux espaces de Hilbert, et $\boldsymbol{K} : \mathbb{H} \to \mathbb{K}$ un opérateur compact. Alors il existe $(u_\ell)_{\ell\geqslant 0}$ une base hilbertienne de $\mathbb{H}$, $(v_\ell)_{\ell\geqslant 0}$ une base hilbertienne de $\mathbb{K}$ et une suite $\lambda_\ell \to 0$ tel que*

$$\boldsymbol{K}u_\ell = \lambda_\ell v_\ell \text{ et } \boldsymbol{K}^* v_\ell = \lambda_\ell u_\ell \,. \tag{1.6}$$

Ainsi, par choix de la base $(v_\ell)_{\ell\geqslant 0}$ comme fonctions tests dans le modèle (3), on obtient, pour tout $\ell \geqslant 0$:

$$\begin{aligned}\langle \boldsymbol{Y}_\varepsilon, v_\ell\rangle &= \langle \boldsymbol{K}\boldsymbol{f}, v_\ell\rangle + \varepsilon\langle \dot{\boldsymbol{W}}, v_\ell\rangle \\ &= \lambda_\ell \langle \boldsymbol{f}, u_\ell\rangle + \varepsilon\xi_\ell\end{aligned}$$

où, grâce à la propriété d'orthonormalité de la base v_ℓ, la suite de variables $(\xi_\ell)_{\ell\geqslant 0}$ est i.i.d $\mathcal{N}(0,1)$. On s'est donc ramené à un modèle **séquentiel** à composantes de bruit normales i.i.d. Déterminer $\boldsymbol{f}$ est équivalent à déterminer la séquence des $(\langle \boldsymbol{f}, u_\ell\rangle)_{\ell\geqslant 0}$, dont on peut désormais aisément proposer un estimateur sans biais:

$$\widehat{\boldsymbol{f}}_\ell = \lambda_\ell^{-1}\langle \boldsymbol{Y}_\varepsilon, v_\ell\rangle \,. \tag{1.7}$$

On applique ensuite un filtre à chacun des coefficients $\widehat{\boldsymbol{f}}_\ell$, le filtre pouvant être:

1. linéaire, avec un estimateur final de la forme $\widetilde{\boldsymbol{f}}^{\,\ell} = \gamma_\ell \widehat{\boldsymbol{f}}_\ell$ où $(\gamma_\ell) \in [0,1]^{\mathbb{N}}$, cadre recouvrant par exemple: les filtres de Tikhonov ($\gamma_\ell = \big(1 + (\ell/\alpha)^\beta\big)^{-1}$), les filtres de Pinsker $(\gamma_\ell = (1 - (\ell/\alpha)^\beta)_+)$.
2. non linéaire, comme le seuillage doux $\widetilde{\boldsymbol{f}}_\ell = \mathrm{sgn}(\widehat{\boldsymbol{f}}_\ell)\big(|\widehat{\boldsymbol{f}}_\ell| - S\big)_+$ ou le seuillage dur $\widetilde{\boldsymbol{f}}_\ell = \widehat{\boldsymbol{f}}_\ell \mathbf{1}_{\{|\widehat{\boldsymbol{f}}_\ell|\geqslant S\}}$.

En pratique, on ne calcule bien sûr qu'un nombre fini de coefficients $\widetilde{\boldsymbol{f}}_\ell$ en stoppant l'expansion avant un niveau maximal de résolution L.

1.3.2 La méthode SVD par blocs

On peut généraliser l'approche précédente. La SVD permet de réduire $\boldsymbol{K}$ à une séquence dénombrable d'homothéties. La méthode SVD par blocs (ou 'Blockwise SVD') réduit $\boldsymbol{K}$ à une séquence dénombrable d'applications linéaires sur des espaces de dimensions finies.

Definition 1.3.2. *On dit que $\boldsymbol{K}$ admet une SVD par blocs s'il existe $(\mathbb{H}_\ell)_{\ell\geqslant 0}$ et $(\mathbb{K}_\ell)_{\ell\geqslant 0}$ une suite d'espaces orthogonaux de $\mathbb{H}$ (resp. $\mathbb{K}$) tel que $\mathbb{H} = \bigoplus_{\ell\geqslant 0}\mathbb{H}_\ell$ (resp. $\mathbb{K} = \bigoplus_{\ell\geqslant 0}\mathbb{K}_\ell$) et, pour tout $\ell \geqslant 0$, $\boldsymbol{K}(\mathbb{H}_\ell) \subset \mathbb{K}_\ell$.*

Notant $\boldsymbol{P}_V$ la projection orthogonale sur le sous-espace vectoriel V, on se ramène donc à l'inversion séquentielle des problèmes

$$\boldsymbol{P}_{\mathbb{K}_\ell}\boldsymbol{K}\boldsymbol{P}_{\mathbb{H}_\ell}\boldsymbol{f} = \boldsymbol{P}_{\mathbb{K}_\ell}\boldsymbol{g}\,. \tag{1.8}$$

Par commodité, on supposera $\dim(\mathbb{H}_\ell) = \dim(\mathbb{K}_\ell)$ (on peut toujours se ramener à ce cas autrement) et on notera $|\Lambda_\ell|$ cette dimension commune. Notons $u_{\ell,1}, ..., u_{\ell,|\Lambda_\ell|}$ (resp. $v_{\ell,1}, ..., v_{\ell,|\Lambda_\ell|}$) une base de $\mathbb{H}_\ell$ (res. $\mathbb{K}_\ell$). En utilisant $v_{\ell,m}$ comme fonction test dans (3), on obtient

$$\langle \boldsymbol{g}, v_{\ell,m}\rangle = \langle \boldsymbol{K}\boldsymbol{f}, v_{\ell,m}\rangle = \langle \boldsymbol{K}\boldsymbol{P}_{\mathbb{H}_\ell}\boldsymbol{f}, v_{\ell,m}\rangle = \sum_{n=1}^{|\Lambda_\ell|}\langle \boldsymbol{K}u_{\ell,n}, v_{\ell,m}\rangle\langle \boldsymbol{f}, u_{\ell,n}\rangle\,,$$

ce qui, en notant

$$\begin{aligned}
\boldsymbol{K}_\ell &= \big(\langle \boldsymbol{K}u_{\ell,n}, v_{\ell,m}\rangle\big)_{n,m=1,...,|\Lambda_\ell|}\,,\\
\boldsymbol{f}_\ell &= \big(\langle \boldsymbol{f}, u_{\ell,n}\rangle\big)_{n=1,...,|\Lambda_\ell|}\,,\\
\boldsymbol{g}_\ell &= \big(\langle \boldsymbol{Y}_\varepsilon, v_{\ell,m}\rangle\big)_{m=1,...,|\Lambda_\ell|}\,,
\end{aligned}$$

se traduit par l'égalité matricielle $\boldsymbol{K}_\ell\boldsymbol{f}_\ell = \boldsymbol{g}_\ell$. Si $\boldsymbol{g}$ est observée selon le modèle de bruit blanc (3), alors les coefficients accessibles deviennent

$$\langle \boldsymbol{Y}_\varepsilon, v_{\ell,m}\rangle = \langle \boldsymbol{g}, v_{\ell,m}\rangle + \varepsilon\langle \dot{\boldsymbol{W}}, v_{\ell,m}\rangle$$

ou bien de manière synthétique $\boldsymbol{Y}_{\varepsilon,\ell} = \boldsymbol{g}_\ell + \varepsilon\dot{\boldsymbol{W}}_\ell$, où $\dot{\boldsymbol{W}}_\ell \in \mathbb{R}^{|\Lambda_\ell|}$ est une séquence de vecteurs gaussiens indépendants dont chacune des composantes est normale $\mathcal{N}(0,1)$. On peut alors adapter les stratégies de la section 1.3.1 en adoptant par exemple un seuillage par bloc du type

$$\widetilde{\boldsymbol{f}}_\ell = \boldsymbol{K}_\ell^{-1}\boldsymbol{Y}_{\varepsilon,\ell}\mathbf{1}_{\left\{\|\boldsymbol{K}_\ell^{-1}\boldsymbol{Y}_{\varepsilon,\ell}\|_{\mathbb{R}^{|\Lambda_\ell|}} > S\right\}},\ \ell \leqslant L(\varepsilon)\,.$$

Déconvolution sphérique

Un exemple notable de déconvolution par blocs est celui de la déconvolution sphérique. Etant donné qu'il intervient en tant qu'exemple ou que sujet d'étude dans les Chapitres 3, 5 et 6, attardons nous quelque peu sur son cas.
Cette modélisation a été initialement introduite par Van Rooij and Ruymgaart [83] et traitée par Healy et al. [39]. L'optimalité (au sens minimax) de la procédure développée a été établie par Kim and Koo [52] pour la perte MSE. Plus récemment, l'extension des performances $\mathbb{L}^2$ des algorithmes ainsi développés à des performances $\mathbb{L}^p$, $p \geqslant 1$ a été réalisée par des stratégies de seuillage sur des systèmes de needlets par Kerkyacharian et al. [51]. Nous reviendrons en détail sur ce dernier point au Chapitre 5. Les domaines d'applications couvrent par exemple l'imagerie médicale, l'astrophysique ainsi que les géosciences. Passons maintenant à la présentation du cadre mathématique.

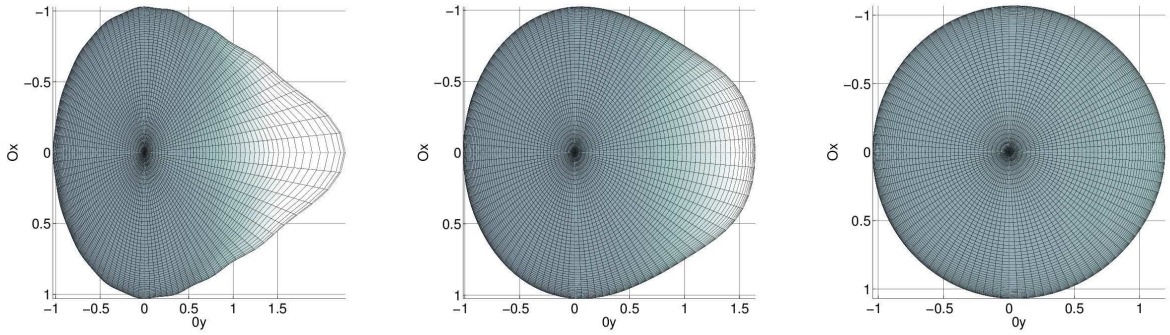

Figure 1.1: 'Vue de dessus' de la fonction $\boldsymbol{f}$ (à gauche) et de $\boldsymbol{K}\boldsymbol{f}$ lorsque $\boldsymbol{K}$ est un opérateur de Rosenthal de degré $p = 1$ (au centre) et un opérateur de Laplace (à droite). Pour tout $\omega \in \mathbb{S}^2$ de coordonnées sphériques $(\theta, \varphi, 1)$, on a tracé le point $(\theta, \varphi, 1 + \boldsymbol{f}(\theta, \varphi))$. L'opérateur de Laplace a un effet régularisant plus prononcé.

Soit $\mathbb{H} = \mathbb{K} = \mathbb{L}^2(\mathbb{S}^2)$ où $\mathbb{S}^2$ est muni de la mesure de Lebesgue. On considère l'opérateur de convolution sur la sphère défini par

$$\boldsymbol{K} : \boldsymbol{f} \mapsto \int_{\mathrm{SO}(3)} \boldsymbol{h}(r)\boldsymbol{f}(r^{-1}.)dr\,, \tag{1.9}$$

où $\boldsymbol{h} \in \mathbb{L}^2(\mathrm{SO}(3))$ et dr est la mesure de Haar sur $\mathrm{SO}(3)$. $\boldsymbol{K}$ a un effet moyennant autour de chaque point $\omega \in \mathbb{S}^2$, quantifié par l'étalement de $\boldsymbol{h}$ autour de l'élément neutre du groupe $\mathrm{SO}(3)$. Afin d'illustrer cet effet, nous avons représenté en Figure 1.1 la fonction $\boldsymbol{K}\boldsymbol{f}$ pour $\boldsymbol{K}_{\ell,m,n} = \big(1 + \ell(\ell+1)\big)^{-1}\delta_{m,n}$ (opérateur de Laplace), $\boldsymbol{K}_{\ell,m,n} = \sin\big((\ell + 1/2)\pi\big)\big((2\ell+1)\sin(\pi/2)\big)^{-1}\delta_{m,n}$ (opérateur de Rosenthal) et lorsque $\boldsymbol{f}$ est la version tronquée à la résolution $\ell = 16$ de la fonction $\boldsymbol{f}_0(\omega) = 1/\exp(-2\|\omega - (0,1,0)\|_{\ell^1(\mathbb{R}^3)})$. Pour une illustration de cet effet dans le modèle de l'estimation de densité, on pourra consulter les Figures 3.1 et 3.2.
On a la décomposition

$$\mathbb{H} = \bigoplus_{\ell \geqslant 0}^{\perp} \mathbb{H}_\ell$$

où $\mathbb{H}_\ell$ est l'espace des harmoniques sphériques de degré ℓ, définies par

$$Y_{\ell,m}(\omega) = Y_{\ell,m}(\theta,\varphi) = (-1)^m \sqrt{\tfrac{2\ell+1}{4\pi}\tfrac{(\ell-m)!}{(\ell+m)!}} P_{\ell,m}\big(\cos(\theta)\big)e^{im\varphi}\,, \tag{1.10}$$

pour $\ell \in \mathbb{N}$, $-\ell \leqslant m \leqslant \ell$ et où $P_{\ell,m}$ sont les fonctions de Legendre définies par exemple dans Vilenkin [84]. De plus, on peut montrer (voir [39]) que pour tout $\ell \geqslant 0$, $\boldsymbol{K}(\mathbb{H}_\ell) \subset \mathbb{H}_\ell$. L'inversion de (1.9) est donc équivalente à l'inversion des équations

$$\boldsymbol{P}_{\mathbb{H}_\ell}\boldsymbol{K}\boldsymbol{P}_{\mathbb{H}_\ell}\boldsymbol{f} = \boldsymbol{P}_{\mathbb{H}_\ell}\boldsymbol{K}\boldsymbol{f} \tag{1.11}$$

sur $\mathbb{H}_\ell$. Chacune de ces inversions correspond à la résolution d'un système linéaire de taille $|\Lambda_\ell| = 2\ell + 1$. Par la suite, on notera, pour toute fonction $\boldsymbol{f} \in \mathbb{L}^2(\mathbb{S}^2)$ et tout opérateur $\boldsymbol{K}$

$$\boldsymbol{f}_\ell = \boldsymbol{P}_{\mathbb{H}_\ell}\boldsymbol{f} \text{ et } \boldsymbol{K}_\ell = \boldsymbol{P}_{\mathbb{H}_\ell}\boldsymbol{K}\boldsymbol{P}_{\mathbb{H}_\ell}\,.$$

1.4 Généralisation: méthode de Galerkin

Les méthodes de SVD et de SVD par blocs requièrent donc la connaissance et la manipulation des bases u et v. De manière générale, ces bases sont potentiellement 1) soit inconnues ou 2) soit difficiles à manipuler numériquement, d'où un besoin de généraliser ces méthodes à des choix de bases quelconques.
La méthode Galerkin repose sur la projection de (1.1) sur une suite croissante de sous espaces vectoriels $V_\ell \subset \mathbb{H}, W_\ell \subset \mathbb{K}$. Notons $u_1, ..., u_\ell$ une base de V_ℓ et $v_1, ..., v_\ell$ une base de W_ℓ (on suppose que $\dim V_\ell = \dim W_\ell = \ell$). Alors l'approximation de Galerkin $\boldsymbol{f}_G$ de $\boldsymbol{f}$ est définie comme la solution du problème

$$\begin{cases} \boldsymbol{f}_G \in V_\ell\,, \\ \langle \boldsymbol{K}\boldsymbol{f}_G, y\rangle = \langle \boldsymbol{g}, y\rangle \text{ pour tout } y \in W_\ell\,. \end{cases} \tag{1.12}$$

Ainsi, on a

$$\boldsymbol{P}_{W_\ell}\boldsymbol{K}\boldsymbol{P}_{V_\ell}\boldsymbol{f}_G = \boldsymbol{P}_{V_\ell}\boldsymbol{g}\,. \tag{1.13}$$

Comme précédemment, en notant

$$\boldsymbol{K}^\ell = (\langle \boldsymbol{K}u_m, v_n\rangle)_{m,n\leqslant\ell},\ \boldsymbol{f}_G^\ell = (\langle \boldsymbol{f}_G, u_m\rangle)_{m\leqslant\ell},\ \boldsymbol{g}^\ell = (\langle \boldsymbol{g}, v_n\rangle)_{n\leqslant\ell}, \tag{1.14}$$

l'inversion de (1.12) est en réalité l'inversion du système linéaire

$$\boldsymbol{K}^\ell \boldsymbol{f}_G^\ell = \boldsymbol{g}^\ell\,. \tag{1.15}$$

On voit bien désormais que les deux méthodes évoquées auparavant sont deux cas particuliers où 1) la matrice $\boldsymbol{K}^\ell$ est diagonale et 2) la matrice $\boldsymbol{K}^\ell$ est diagonale par blocs (avec blocs $\boldsymbol{K}_i$).
Ainsi, une méthode de Galerkin repose sur une double approximation: approximation de $\boldsymbol{K}$ par $\boldsymbol{K}^\ell$, et approximation de $\boldsymbol{g}$ par $\boldsymbol{g}^\ell$. La décomposition orthogonale

$$\boldsymbol{f} - \boldsymbol{f}_G = \left(\boldsymbol{f} - \boldsymbol{P}_{V_\ell}\boldsymbol{f}\right) + \boldsymbol{G}^\ell\boldsymbol{f}\,, \tag{1.16}$$

avec $\boldsymbol{G}^\ell = (\boldsymbol{K}^\ell)^{-1}\boldsymbol{P}_{W_\ell}\boldsymbol{K}\boldsymbol{P}_{V_\ell^\perp}$, implique

$$\|\boldsymbol{f} - \boldsymbol{f}_G\|^2 = \|\boldsymbol{f} - \boldsymbol{P}_{V_\ell}\boldsymbol{f}\|^2 + \|\boldsymbol{G}^\ell\boldsymbol{f}\|^2\,.$$

La décomposition de l'erreur fait apparaître deux termes: le premier terme est le biais d'approximation de $\boldsymbol{f}$ par sa projection sur l'espace V_ℓ, tandis que le second contrôle les résidus associés au choix des espaces V_ℓ, W_ℓ. Par conséquent, la bonne marche d'une méthode de Galerkin requiert que ces deux termes tendent vers 0.

1.4.1 Choix des bases

Les bases (u_ℓ) et (v_ℓ) doivent répondre à une double exigence: premièrement, la simplicité et la rapidité computationnelle de l'inversion du système linéaire (1.15), et deuxièmement, la représentation efficace de la fonction cible $\boldsymbol{f}$ dans la base (u_ℓ). Le choix d'une base de SVD ou bien de SVD par blocs de l'opérateur privilégie la première qualité au détriment potentiel de la seconde. En effet les bases réalisant la SVD ne représentent usuellement $\boldsymbol{f}$ de manière efficace que dans un cadre hilbertien pour une perte de type $\mathbb{L}^2$. Le choix d'une base d'ondelette lorsque l'espace sous-jacent est un espace de Besov (voir Appendix A) inverse le compromis, et nécessite bien souvent des hypothèses plus restrictives sur l'opérateur $\boldsymbol{K}$. Nous en présentons trois exemples ci-dessous.

Ondelettes et méthode de Galerkin

Cohen et al. [17] ont eu recours à une méthode de Galerkin utilisant des bases d'ondelettes $(u_\ell) = (v_\ell) = (\boldsymbol{\psi}_\lambda)$ sur $[0,1]$ (où λ représente le double indice (j,k)). Dans cette section, on supposera de plus l'opérateur symétrique (mais le raisonnement s'adapte au cas d'un opérateur non symétrique). Pour un indice maximal J, on notera $\Lambda = \{(j,k), j \leqslant J, k \leqslant 2^j\}$. Pour un bref rappel théorique sur les ondelettes, on pourra consulter l'Appendix A. Les méthodes d'estimation développées dans ces travaux mettent en évidence une distinction entre deux types de méthodes, qui réapparaîtra dans le Chapitre 2. Ici, $\boldsymbol{K}$ est un opérateur auto-adjoint, vérifiant la relation

$$\forall f \in \mathbb{L}^2([0,1]),\ \langle \boldsymbol{K} f, f\rangle \sim \|f\|^2_{H^{-\nu/2}}\,. \tag{1.17}$$

Sous cette hypothèse on peut montrer ([40]) que la constante

$$Q_j = \sup_{j\geqslant 0} 2^{-j\nu} \|(\boldsymbol{K}^j)^{-1}\|_{op}$$

est finie, et donc que cette notion rejoint la condition (1.22) définie plus bas. L'estimation par méthode de Galerkin requiert la résolution de

$$\langle \boldsymbol{K}\boldsymbol{f}_G, \boldsymbol{\psi}_{j,k}\rangle = \langle \boldsymbol{Y}_\varepsilon, \boldsymbol{\psi}_{j,k}\rangle \text{ pour tout } (j,k) \in \Lambda\,. \tag{1.18}$$

La présence de bruit sur la fonction image $\boldsymbol{g} = \boldsymbol{K}\boldsymbol{f}$ est traitée à l'aide d'une méthode de seuillage. Deux choix distincts se présentent:

1. Opérer un seuillage sur le signal image $\boldsymbol{Y}_\varepsilon$ **puis** résoudre l'équation ci-dessus en remplaçant $\boldsymbol{Y}_\varepsilon$ par sa version seuillée dans (1.18).

2. Résoudre (1.18) et appliquer le seuillage sur le résultat.

Ces deux cas mettent naturellement en jeu des procédures et des hypothèses différentes. Par exemple, le premier cas impose l'efficacité d'un seuillage appliqué sur $\boldsymbol{Y}_\varepsilon$, donc l'appartenance de $\boldsymbol{g}$ à un certain espace de Besov (typiquement $B^{s+\nu}_{p,p}$ si $\boldsymbol{K}$ vérifie (1.17))

et par là la continuité de $\boldsymbol{K} : B^s_{p,p} \to B^{s+\nu}_{p,p}$. Le seuillage pratiqué sur $\boldsymbol{Y}_\varepsilon$ prend la forme naturelle (voir Appendix A)

$$\mathcal{T}(.) = \sum_{\lambda \leqslant \Lambda} \langle ., \boldsymbol{\psi}_\lambda \rangle \mathbf{1}_{\left\{|\langle ., \boldsymbol{\psi}_\lambda \rangle| > \tau\varepsilon\sqrt{|\log\varepsilon|}\right\}} \boldsymbol{\psi}_\lambda \, .$$

Le deuxième cas n'impose aucune hypothèse supplémentaire sur $\boldsymbol{K}$. Cependant, la procédure de seuillage appliquée à $\left(\boldsymbol{K}^\Lambda\right)^{-1}\boldsymbol{Y}_\varepsilon$ requiert le contrôle des variables aléatoires $\langle \left(\boldsymbol{K}^\Lambda\right)^{-1}\dot{\boldsymbol{W}}^J, \boldsymbol{\psi}_{j,k}\rangle$. Du fait de (1.17), ces estimateurs possèdent une variance croissante en j, qui est incorporée au seuillage. Ce dernier, pratiqué sur $\left(\boldsymbol{K}^\Lambda\right)^{-1}\boldsymbol{Y}_\varepsilon$, devient alors

$$\mathcal{T}(.) = \sum_{\lambda \leqslant \Lambda} \langle ., \boldsymbol{\psi}_\lambda \rangle \mathbf{1}_{\left\{|\langle ., \boldsymbol{\psi}_\lambda \rangle| > \tau 2^{j\nu}\varepsilon\sqrt{|\log\varepsilon|}\right\}} \boldsymbol{\psi}_\lambda \, .$$

Décomposition WVD

Il est parfois possible d'améliorer substantiellement la procédure ci-dessus pour certains opérateurs spécifiques. L'existence d'une WVD (pour Wavelet-Vaguelette Decomposition, initialement introduite par Donoho [26]) ou bien d'une VWD (voir Abramovich and Silverman [2]) offre un cadre intermédiaire entre SVD et ondelettes par méthode de Galerkin. Par exemple, la WVD repose sur l'hypothèse qu'il existe une base d'ondelettes $(\boldsymbol{\psi}_\lambda)$, un système de vaguelettes $(\boldsymbol{\nu}_\lambda)$ et une suite $\beta_j > 0$ tel que, pour tout $\lambda = (j,k)$,

$$\boldsymbol{K}^*(\boldsymbol{\nu}_\lambda) = \beta_j \boldsymbol{\psi}_\lambda \, . \tag{1.19}$$

En conséquence, en décomposant $\boldsymbol{f}$ sur la base $(\boldsymbol{\psi}_\lambda)$, on obtient

$$\begin{aligned}\langle \boldsymbol{Y}_\varepsilon, \boldsymbol{\nu}_\lambda \rangle &= \sum_{\lambda'} \langle \boldsymbol{K}\boldsymbol{\psi}_{\lambda'}, \boldsymbol{\nu}_\lambda \rangle \langle \boldsymbol{f}, \boldsymbol{\psi}_{\lambda'} \rangle + \varepsilon \langle \dot{\boldsymbol{W}}, \boldsymbol{\nu}_\lambda \rangle \\ &= \beta_j \langle \boldsymbol{f}, \boldsymbol{\psi}_\lambda \rangle + \varepsilon \langle \dot{\boldsymbol{W}}, \boldsymbol{\nu}_\lambda \rangle\end{aligned}$$

où l'on a successivement appliqué (1.19) ainsi que l'orthogonalité des ondelettes. Par conséquent, on obtient un estimateur sans biais de $\langle \boldsymbol{f}, \boldsymbol{\psi}_\lambda \rangle$ en posant

$$\langle \widetilde{\boldsymbol{f}}, \boldsymbol{\psi}_\lambda \rangle = \beta_j^{-1} \langle \boldsymbol{Y}_\varepsilon, \boldsymbol{\nu}_\lambda \rangle$$

On couple ensuite cet estimateur à un seuillage doux ou dur afin d'obtenir une procédure optimale en perte $\mathbb{L}^2$ sur des espaces de Besov $B^s_{\pi,r}([0,1])$. Ainsi, les systèmes duaux $(\boldsymbol{\psi}_\lambda)$ et $(\boldsymbol{\nu}_\lambda)$ possèdent une structure adaptée à la fois à l'analyse du signal $\boldsymbol{f}$ et de l'opérateur $\boldsymbol{K}$.

Une différence notable avec le cadre précédent est que le système de vaguelettes $(\boldsymbol{\nu}_\lambda)$ n'est pas une base (il n'est pas orthonormé). On voit donc que la notion de base n'est pas nécessaire à la mise en place d'une méthode de Galerkin. En particulier, la méthode WVD illustre l'utilisation d'une base de Riesz (voir [14]) adaptée à $\boldsymbol{K}$. Notons que cette méthode restreint inévitablement le champ d'applications aux opérateurs possédant une telle propriété, tels l'intégration, l'intégration fractionnaire ou bien la transformée de Radon.

Déconvolution en régime périodique

La présence de cet exemple ici se justifie par le fait que l'utilisation des needlets pour la déconvolution sphérique aveugle, au Chapitre 6, repose sur des arguments très similaires dans des cas plus complexes. Les principes de la méthode développée ont permis d'aborder similairement les problèmes inverses tels que l'inversion de la transformée de Radon ([50]) ou bien la déconvolution de Jacobi ([49]).
Dans le cas spécifique de la déconvolution sur $[0,1]$, Johnstone et al. [44] réconcilient l'efficacité de l'étape d'inversion grâce aux séries de Fourier avec la représentation de la fonction cible en ondelettes. Pour ce faire, ils se basent sur les ondelettes de Meyer périodisées, qui possèdent un support fréquentiel compact. En effet, on a, pour tout $j \geqslant 0$,

$$C_j \triangleq \{\ell \in \mathbb{Z}, \langle \boldsymbol{\psi}_{j,k}, e^{2i\pi\ell .}\rangle \neq 0\} \subset \frac{2\pi}{3}\Big([-2^{j+2}, -2^j]\bigcup[2^j, 2^{j+2}]\Big)\,, \tag{1.20}$$

de telle sorte que les coefficients d'ondelettes se calculent efficacement par la formule de Parseval. Plus précisément, supposons que l'on observe

$$d\boldsymbol{Y}_\varepsilon(t) = \boldsymbol{k} * \boldsymbol{f}(t)dt + \varepsilon d\boldsymbol{W}(t),\ t \in [0,1]\,,$$

où $\boldsymbol{k} \in \mathbb{L}^2([0,1])$. On notera $e_\ell(t) = e^{2i\pi\ell t}$. Par la formule de Parseval, on a

$$\langle \boldsymbol{f}, \boldsymbol{\psi}_{j,k}\rangle = \sum_{\ell\geqslant 0}\langle \boldsymbol{f}, e_\ell\rangle\langle \boldsymbol{\psi}_{j,k}, e_\ell\rangle = \sum_{\ell\in C_j}\frac{\langle \boldsymbol{f} * \boldsymbol{k}, e_\ell\rangle}{\langle \boldsymbol{k}, e_\ell\rangle}\langle \boldsymbol{\psi}_{j,k}, e_\ell\rangle$$

et la somme ci-dessus est finie. Un estimateur de $\langle \boldsymbol{f}, \boldsymbol{\psi}_{j,k}\rangle$ est donc

$$\widehat{\boldsymbol{\beta}}_{j,k} = \sum_{\ell\in C_j}\frac{\langle \boldsymbol{Y}_\varepsilon, e_\ell\rangle}{\langle \boldsymbol{k}, e_\ell\rangle}\langle \boldsymbol{\psi}_{j,k}, e_\ell\rangle\,.$$

Avec l'hypothèse de DIP (voir section 1.5) suivante :

$$\big(2^{-j}\sum_{|\ell|=2^j}^{2^{j+2}}|\langle \boldsymbol{k}, e_\ell\rangle|^{-2}\big)^{1/2} \sim 2^{j\nu}\,,$$

on peut calibrer le seuillage des coefficients obtenus et retrouver les vitesses d'estimation minimax sur les espaces de Besov (voir section A.3.2).

1.4.2 Décomposition biais-variance

Nous allons maintenant faire une hypothèse supplémentaire, vérifiée dans le cadre des Chapitre 3, 4, 5 et 6.

Assumption 1.4.1. *Pour tout* $\ell \geqslant 1$, $\boldsymbol{K}\boldsymbol{P}_{V_\ell} = \boldsymbol{P}_{W_\ell}\boldsymbol{K}$.

Sous Assumption 1.4.1, on a alors

$$\boldsymbol{G}^\ell = (\boldsymbol{K}^\ell)^{-1}\boldsymbol{K}\boldsymbol{P}_{V_\ell}\boldsymbol{P}_{V_\ell^\perp} = 0\,,$$

et par conséquent $\boldsymbol{f}_G = \boldsymbol{P}_{V_\ell}\boldsymbol{f}$, que nous assimilerons également à $\boldsymbol{f}^\ell$. Voyons comment s'articule le compromis biais-variance dans ce cas: en remplaçant $\boldsymbol{g}$ par $\boldsymbol{Y}_\varepsilon$ dans (1.12), l'erreur commise se décompose de la manière suivante:

$$\|\boldsymbol{f} - (\boldsymbol{K}^\ell)^{-1}(\boldsymbol{g}^\ell + \varepsilon\dot{\boldsymbol{W}}^\ell)\| \leqslant \|\boldsymbol{f} - \boldsymbol{f}^\ell\| + \varepsilon\|(\boldsymbol{K}^\ell)^{-1}\dot{\boldsymbol{W}}^\ell\|\,. \tag{1.21}$$

Le terme de biais $\|\boldsymbol{f} - \boldsymbol{f}^\ell\|$ décroît avec ℓ, tandis que, en raison du caractère mal posé du problème, le terme (aléatoire) de variance $\|(\boldsymbol{K}^\ell)^{-1}\dot{\boldsymbol{W}}^\ell\|$ a lui tendance à croître. Un choix judicieux de ℓ en fonction de ε réalise un bon compromis entre ces deux quantités.

1.5 Degree of ill-posedness, espaces de régularité et adaptativité.

A la lumière de (1.21), le caractère mal posé du problème est ainsi illustré lors de l'application d'un schéma de Galerkin par la croissance des normes $\|(\boldsymbol{K}^\ell)^{-1}\|_{\text{op}}$ au fur et à mesure que ℓ augmente. Par exemple, cette norme peut croître

- polynomialement, i.e.
$$\|(\boldsymbol{K}^\ell)^{-1}\|_{\text{op}} \leqslant C\ell^\nu\,, \tag{1.22}$$
auquel cas le problème est dit moyennement mal posé.
- exponentiellement auquel cas le problème est dit sévèrement mal posé.

Nous nous concentrerons sur le cas d'une croissance polynomiale. Le réel ν est appelé DIP (Degree of Ill-Posedness). Comme $\dot{\boldsymbol{W}}^\ell$ est un vecteur gaussien standard, $\|(\boldsymbol{K}^\ell)^{-1}\dot{\boldsymbol{W}}\|$ est une variable gaussienne de variance

$$\|{}^t\big[(\boldsymbol{K}^\ell)^{-1}\mathbf{1}\big](\boldsymbol{K}^\ell)^{-1}\mathbf{1}\| \leqslant \ell\|(\boldsymbol{K}^\ell)^{-1}\|_{\text{op}}^2\,,$$

où $\mathbf{1}$ est le vecteur de taille ℓ dont toutes les composantes valent 1.
D'autre part, la majoration du premier terme incite à considérer des espaces où la décroissance de $\|\boldsymbol{f}-\boldsymbol{f}^\ell\|$ est elle aussi polynomiale, c'est-à-dire qu'il existe $s>0, M\geqslant 0$ tel que $\|\boldsymbol{f}-\boldsymbol{f}^\ell\|^2 \leqslant M\ell^{-2s}$. Dans le cas où la base (u_ℓ) est constituée des fonctions propres de l'opérateur Laplacien sur $[0,1]$, on retrouve les espaces de Sobolev sur $[0,1]$, que nous noterons $\mathcal{W}^s$. Les espaces de Besov fournissent une généralisation de ce principe à une norme $\pi \geqslant 1$ quelconque (voir Appendix A).
Etant donné ν et s, le niveau de résolution optimal est $\ell(\varepsilon) \sim \varepsilon^{\frac{-1}{\nu+s+1/2}}$ et la perte associée sur la boule de Sobolev de rayon M, $\mathcal{W}^s(M)$, est

$$\sup_{\boldsymbol{f}\in\mathcal{W}^s(M)} \mathbb{E}\left[\|\boldsymbol{f} - (\boldsymbol{K}^\ell)^{-1}((\boldsymbol{K}\boldsymbol{f})^\ell + \varepsilon\dot{\boldsymbol{W}}^\ell)\|\right] \leqslant C\varepsilon^{\frac{2s}{2(s+\nu)+1}}\,. \tag{1.23}$$

On peut montrer (à l'aide des arguments présents dans Korostelev and Tsybakov [54, Chapitre 2]) que cette vitesse est optimale au sens minimax.
En pratique, la connaissance a priori de s (et de ν) n'est pas garantie, d'où la nécessité de construire des procédures indépendantes de ces paramètres, mais qui atteignent asymptotiquement le même ordre de convergence que dans le cas où ils sont connus. Souvent, cette adaptativité se paye au prix d'un facteur logarithmique dans les vitesses de convergence. En pratique, ce type de procédure recouvre par exemple la méthode de Lepski ([57], [5]), les stratégies de seuillage ([44]), ou de minimisation du risque empirique ([13]).

Remark 1.5.1. *On pourrait imaginer des décroissances exponentielles pour les deux termes considérés ci-dessus. Celles-ci ont par exemple été étudiées par Tsybakov [81].*

Afin d'illustrer la puissance des procédures de seuillage (que nous utiliserons de manière récurrente par la suite), nous rentrons en détail dans leur mise en place dans ce cadre spécifique. Choisissons donc pour niveau maximal

$$\ell(\varepsilon) \sim \left(\varepsilon\sqrt{|\log\varepsilon|}\right)^{\frac{-2}{2\nu+1}}.$$

Ce niveau surestime celui de la procédure linéaire. Cette surestimation est compensée par un traitement adéquat des résultats obtenus par méthode de Galerkin. Introduisons pour ce faire le seuillage défini pour $x \in \mathbb{R}$

$$\mathcal{T}_\ell(x) = x\mathbf{1}_{\left\{|x|>\tau\ell^\nu\varepsilon\sqrt{|\log\varepsilon|}\right\}},$$

et soit $\widetilde{\boldsymbol{f}}$ l'estimateur défini par

$$\langle\widetilde{\boldsymbol{f}}, u_\ell\rangle = \mathcal{T}_\ell\Big(\langle(\boldsymbol{K}^\ell)^{-1}\boldsymbol{Y}^\ell_\varepsilon, u_\ell\rangle\Big)\mathbf{1}_{\{\ell\leqslant\ell(\varepsilon)\}}.$$

Alors on peut montrer que cet estimateur atteint la même vitesse que (1.23), à un facteur logarithmique près. Plus précisément, pour $s, M > 0$,

$$\sup_{\boldsymbol{f}\in\mathcal{W}^s(M)} \mathbb{E}\,\|\widetilde{\boldsymbol{f}} - \boldsymbol{f}\| \leqslant C\left(\varepsilon\sqrt{|\log\varepsilon|}\right)^{\frac{2s}{2(s+\nu)+1}}.$$

Ainsi, le seuillage permet d'obtenir l'adaptativité. En fait, pour des pertes $\mathbb{L}^p$ plus générales, et dans certains espaces de Besov $B^s_{\pi,r}$, on peut montrer qu'aucune procédure linéaire n'atteint la vitesse minimax, et donc le seuillage (ou autre méthode non linéaire) devient essentiel (voir Theorem A.3.1).

1.6 Nécessité de considérer des opérateurs bruités

Afin d'introduire le chapitre suivant, revenons plus en détail sur le cas particulier de la déconvolution sphérique introduite en 1.3.2. Supposons que la fonction $\boldsymbol{f}$ vit dans l'espace de Sobolev

$$\mathcal{W}^s(M) = \{\boldsymbol{f} \in \mathbb{L}^2(\mathbb{S}^2),\ \sum_{\ell\geqslant 0}\ell^{2s}\|\boldsymbol{f}_\ell\|^2 \leqslant M^2\},$$

($s > 1/2$), et que les matrices $\boldsymbol{K}_\ell$ vérifient la condition de ill-posedness $\|\boldsymbol{K}_\ell^{-1}\|_{\mathrm{op}} \leqslant C\ell^\nu$. On introduit la procédure suivante: soit, pour tout $\ell \geqslant 0$,

$$\hat{\boldsymbol{f}}_\ell = \boldsymbol{K}_\ell^{-1}\boldsymbol{Y}_{\varepsilon,\ell}\,.$$

On définit alors l'estimateur

$$\tilde{\boldsymbol{f}} = \sum_{\ell \leqslant L}\sum_{|m|\leqslant \ell} \hat{\boldsymbol{f}}_{\ell,m}\mathbf{1}_{\left\{\|\hat{\boldsymbol{f}}_\ell\| \geqslant \kappa\ell^\nu\sqrt{2\ell+1}\varepsilon\sqrt{|\log\varepsilon|}\right\}} Y_{\ell,m}, \quad L \sim \left(\varepsilon\sqrt{|\log\varepsilon|}\right)^{\frac{-2}{2\nu+1}}. \tag{1.24}$$

On peut montrer par des arguments standards que cette procédure est quasi-optimale au sens minimax sur $\mathcal{W}^s(M)$. Cependant, en pratique, l'opérateur $\boldsymbol{K}$ est inconnu a priori. Cette difficulté est heureusement contournable car on sait que les coefficients $\langle \boldsymbol{K}Y_{\ell,m}, Y_{\ell,n}\rangle$ sont en réalité les coefficients de Fourier de la fonction $\boldsymbol{h} \in \mathbb{L}^2(\mathrm{SO}(3))$:

$$\langle \boldsymbol{K}Y_{\ell,m}, Y_{\ell,n}\rangle = \hat{\boldsymbol{h}}_{\ell,m,n} = \int_{\mathrm{SO}(3)} \boldsymbol{h}(r)\overline{R_{\ell,m,n}}(r)dr\,,$$

où les fonctions $R_{\ell,m,n}$ sont les fonctions propres du Laplacien sur SO(3) (voir Vilenkin [84]).
Dans le modèle de l'estimation de densité (1), $\boldsymbol{h}$ est une densité et on observe $\boldsymbol{\theta}_1, ..., \boldsymbol{\theta}_q$ q réalisations de la variable $\boldsymbol{\theta}$ à densité $\boldsymbol{h}$ sur SO(3). Un estimateur naturel de $\hat{\boldsymbol{h}}_{\ell,m,n}$ est alors

$$\frac{1}{q}\sum_{i=1}^{q}\overline{R_{\ell,m,n}(\boldsymbol{\theta}_i)}\,.$$

En remplaçant $\hat{\boldsymbol{h}}_{\ell,m,n}$ par sa version empirique, l'erreur commise sur $\boldsymbol{h}$ (et donc sur $\boldsymbol{K}$) affecte la procédure d'estimation 1.24. De manière similaire, dans un modèle de bruit blanc on n'observe non pas $\hat{\boldsymbol{h}}_{\ell,m,n}$ mais sa version bruitée

$$\hat{\boldsymbol{h}}_{\delta,\ell,m,n} = \hat{\boldsymbol{h}}_{\ell,m,n} + \delta\dot{\boldsymbol{B}}_{\ell,m,n}\,,$$

où les variables aléatoires $\dot{\boldsymbol{B}}_{\ell,m,n}$ sont i.i.d $\mathcal{N}(0,1)$. On note $\boldsymbol{K}_\delta$ (resp. $\dot{\boldsymbol{B}}$) l'opérateur constitué des coefficients de Fourier $\hat{\boldsymbol{h}}_{\delta,\ell,m,n}$ (resp. $\dot{\boldsymbol{B}}_{\ell,m,n}$). Afin de démontrer la nette influence de la pré-estimation des coefficients $\hat{\boldsymbol{h}}_{\ell,m,n}$ sur l'estimation de $\boldsymbol{f}$, nous comparons en Figure 1.2 les résultats obtenus par l'application de (1.24), d'abord en utilisant l'opérateur $\boldsymbol{K}$, puis en le remplaçant par sa version bruitée $\boldsymbol{K}_\delta$. Les paramètres sont les suivants:

- L'opérateur $\boldsymbol{K}$ est un opérateur de Laplace dont les coefficients de Fourier valent $\hat{h}_{\ell,m,n} = \left(1+\ell(\ell+1)\right)^{-1}\mathbf{1}_{\{m=n\}}$. $\boldsymbol{K}$ possède donc un DIP de $\nu = 2$.
- On définit $\boldsymbol{f}_0(\omega) = \exp(-2\|\omega - \omega_1\|_{\ell^1(\mathbb{R}^3)})$ où $\omega_1 = (0,1,0)$. La fonction cible $\boldsymbol{f}$ est la troncature de $\boldsymbol{f}_0$ au niveau $\ell = 16$:

$$\boldsymbol{f} = \sum_{\ell\leqslant 16}\sum_{|m|\leqslant\ell}\langle \boldsymbol{f}_0, Y_{\ell,m}\rangle Y_{\ell,m} \tag{1.25}$$

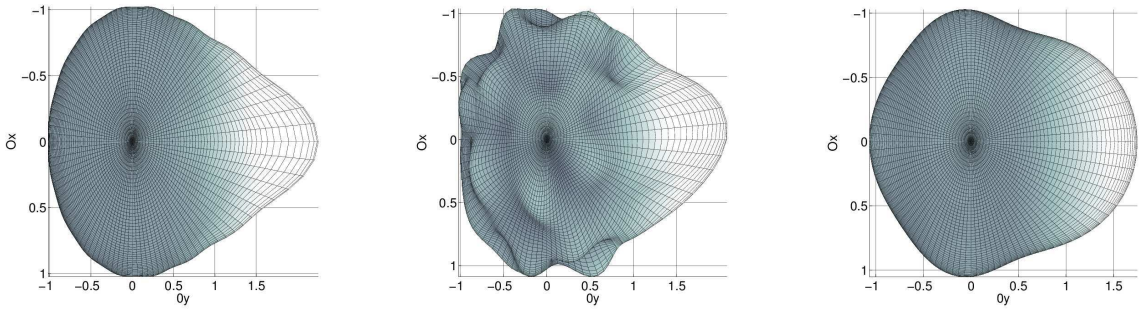

Figure 1.2: De gauche à droite : fonction cible, reconstruction $(\boldsymbol{K}_\delta)^{-1}\boldsymbol{Y}_\varepsilon$ ($E = 0.515$) et résultat de l'algorithme de Blockwise SVD ($E = 0.324$) à un niveau de bruit $\delta = 5.10^{-3}, \varepsilon = 0$.

- On a $(\delta, \varepsilon) = (5.10^{-3}, 0)$.

Le choix de ces données n'est pas innocent. D'une part, un DIP de 2 conduit déjà à des problèmes très mal posés en pratique par la croissance rapide des normes $\|\boldsymbol{K}_\ell^{-1}\|_{op}$ (ce qui signifie l'instabilité grandissante de l'inversion de $\boldsymbol{K}_\ell$). D'autre part, la présence d'un pic au point $\omega = \omega_1$ pour $\boldsymbol{f}_0$ assure une décroissance lente des coefficients de Fourier de $\boldsymbol{f}_0$. A titre de comparaison, on a également tracé le résultat obtenu par l'algorithme de Blockwise-SVD introduit en section 2.4, ou plus en détails au Chapitre 3. La perte E est la perte $\mathbb{L}^2$ renormalisée par $\|\boldsymbol{f}\|$. Comme on le voit, la présence d'erreur dans $\boldsymbol{K}_\delta$ impacte l'estimation de $\boldsymbol{f}$ de manière notoire dans les hautes fréquences. Ce phénomène n'est pas étonnant étant donné que la matrice $\boldsymbol{K}^{15}$ vaut environ $4.10^{-3}\boldsymbol{I}_{31}$, et qu'en vertu d'un argument classique sur les séries de Neumann, la matrice $\boldsymbol{K}_\delta$ n'est plus assurée de posséder des propriétés similaires à $\boldsymbol{K}$ si $\delta\|\dot{\boldsymbol{B}}_\ell\|_{op} > 4.10^{-3}$, soit $\|\dot{\boldsymbol{B}}_\ell\|_{op} > 4/5$, un évènement réalisé avec très forte probabilité comme on le verra par la suite (Lemma 2.1.3).
Cet exemple souligne la nécessité de traiter la nouvelle erreur induite par l'observation de $\boldsymbol{K}_\delta$ au lieu de $\boldsymbol{K}$. Ce sera l'objet des chapitres suivants.

Chapter 2

Problèmes inverses à opérateurs bruités. Principales contributions.

Dans ce chapitre, on introduit la notion de problème inverse à opérateur bruité (section 2.1). On étudie ensuite diverses approches de résolution en section 2.2. La fin de ce chapitre est dédié à la présentation de quatre exemples particuliers : la déconvolution aveugles par ondelettes (section 2.3) où l'on présente de manière succincte le travail de Hoffmann and Reiß [40], puis un résumé des travaux originaux effectués durant cette thèse, à savoir : la déconvolution dans le cas d'un opérateur diagonal par blocs dans un cadre $\mathbb{L}^2$ en section 2.4, l'extension de cette procédure à un cadre $\mathbb{L}^p$, $1 \leqslant p \leqslant \infty$ dans le cas de la déconvolution sphérique en section 2.6, et enfin la déconvolution de Volterra en section 2.5. Chacune de ces trois dernières section feront l'objet d'un chapitre plus détaillé dans la suite.

Contents

2.1 Modèle **27**

2.2 Schémas génériques de résolution **30**

2.3 Retour sur la déconvolution aveugle par ondelettes **35**

2.4 Traitement des opérateurs diagonaux par blocs **37**

2.5 Traitement des opérateurs intégraux de Volterra **41**

2.6 Opérateurs diagonaux par blocs : cas $\mathbb{L}^p$ **47**

2.1 Modèle

Nous avons jusqu'ici considéré le cas d'opérateurs $\boldsymbol{K}$ connus, et nous étendons maintenant notre étude au cas où $\boldsymbol{K}$ n'est pas connu a priori. Nous nous placerons durant tout ce chapitre dans le modèle de bruit blanc (3), c'est-à-dire que l'on observe

$$d\boldsymbol{Y}_\varepsilon(s) = \boldsymbol{K}\boldsymbol{f}(s)ds + \varepsilon d\boldsymbol{W}(s)\,.$$

Si $\boldsymbol{K}$ est inconnu, il est impossible de retrouver $\boldsymbol{f}$ en toute généralité. Il est donc nécessaire de disposer d'une information à priori sur $\boldsymbol{K}$. Dans notre cas, on supposera que nous avons accès à une version bruitée $\boldsymbol{K}_\delta$ modélisée par

$$\boldsymbol{K}_\delta = \boldsymbol{K} + \delta \dot{\boldsymbol{B}},\ 0 < \delta < 1\,.$$

Le processus $\dot{\boldsymbol{B}}$ est un bruit blanc gaussien sur les opérateurs linéaires de $\mathbb{H}$ dans $\mathbb{K}$, ce qui signifie que les quantités observables prennent la forme $\langle \dot{\boldsymbol{B}} u, v\rangle$ pour $u \in \mathbb{H}, v \in \mathbb{K}$. De plus, ces variables sont gaussiennes et on a

$$\mathrm{Cov}\big[\langle \dot{\boldsymbol{B}} u_1, v_1\rangle_{\mathbb{K}} \langle \dot{\boldsymbol{B}} u_2, v_2\rangle_{\mathbb{K}}\big] = \langle u_1, u_2\rangle_{\mathbb{H}} \langle v_1, v_2\rangle_{\mathbb{K}} \tag{2.1}$$

pour $u_1, u_2 \in \mathbb{H}$, $v_1, v_2 \in \mathbb{K}$. Par exemple, on peut supposer que l'opérateur $\boldsymbol{K}_\delta$ est le résultat d'une première inférence pratiquée sur l'opérateur $\boldsymbol{K}$ (voir section 1.6). Ou bien, un point de vue alternatif est de considérer que le 'vrai' opérateur $\boldsymbol{K}$ est une perturbation inconnue d'un opérateur connu $\boldsymbol{K}_\delta$. L'ampleur de la perturbation (ou bien la précision de l'inférence dans le premier cas) est quantifiée par le paramètre δ. On synthétise ces deux modèles sous la forme suivante

$$\begin{cases} \boldsymbol{Y}_\varepsilon &= \boldsymbol{K}\boldsymbol{f} + \varepsilon \dot{\boldsymbol{W}}\,, \\ \boldsymbol{K}_\delta &= \boldsymbol{K} + \delta \dot{\boldsymbol{B}}\,. \end{cases} \tag{2.2}$$

Cette modélisation, due à Efromovich and Koltchinskii [30], a depuis fait l'objet de plusieurs travaux ([40],[63],[23] par exemple). Avant de s'atteler à son traitement, présentons quelques exemples particuliers où la modélisation (2.2) est activement utilisée (d'autres exemples sont disponibles dans [30] et [40]).

Example 2.1.1 (Equation de la chaleur)**.** *Considérons l'équation d'évolution*

$$\frac{\partial u}{\partial t} + Lu = 0\,, \tag{2.3}$$

où $L = -\sum_{i,j=1}^{d} \frac{\partial}{\partial x_i}\{a_{ij}(x)\frac{\partial}{\partial x_j}\}$ *est un opérateur elliptique sur* G *un ouvert connexe borné de* $\mathbb{R}^d$*, avec conditions de Dirichlet. La solution de* (2.3) *avec condition initiale* $u(0,x) = \boldsymbol{f}(x)$ *s'écrit* $u(t,x) = e^{-Lt}\boldsymbol{f}(x)$ *où* e^{-Lt} *est un semi-groupe d'opérateurs avec noyau* $h_t(x,y)$*. On se pose le problème de déterminer la condition initiale* $\boldsymbol{f}$ *connaissant la solution* $u(t_0,x)$ *pour un certain* $t_0 > 0$*. Si* L *est inconnu, en notant* $\boldsymbol{H} = e^{-Lt_0}$ *on peut modéliser ce problème comme suit:*

$$d\boldsymbol{Y}_\varepsilon(x) = \boldsymbol{H}\boldsymbol{f}(x)dx + \varepsilon d\boldsymbol{W}(x)\,.$$

Pour tout $\boldsymbol{\varphi} \in \mathbb{L}^2(G)$*, on observe alors* $\langle \boldsymbol{Y}_\varepsilon, \boldsymbol{\varphi}\rangle = \langle \boldsymbol{H}\boldsymbol{f}, \boldsymbol{\varphi}\rangle + \varepsilon\langle \dot{\boldsymbol{W}}, \boldsymbol{\varphi}\rangle$*. Si* $\boldsymbol{H}$ *es inconnu, on peut conduire l'expérience avec une condition initiale* $\boldsymbol{f}'$ *connue, qui aboutit aux observations*

$$d\boldsymbol{Y}'_\varepsilon(x) = \boldsymbol{H}\boldsymbol{f}'(x)dx + \varepsilon d\boldsymbol{W}'(x)\,.$$

On retrouve donc le modèle 2.2 en supposant

$$\mathrm{Cov}\big[\langle \dot{\boldsymbol{W}}, \varphi_1\rangle\langle \dot{\boldsymbol{W}}', \varphi_2\rangle\big] = \langle \boldsymbol{f}, \boldsymbol{f}'\rangle\langle \varphi_1, \varphi_2\rangle \text{ et } \varepsilon = \delta\,.$$

Example 2.1.2 (Equation intégrale du premier type)**.** *On considère un opérateur intégral*

$$\boldsymbol{K}f(x) = \int_\Omega \boldsymbol{k}(x,y)f(y)dy\,,$$

où $\Omega \subset \mathbb{R}^d$. Un tel type d'opérateur apparaît par exemple en transformant le problème précédent en une formulation variationnelle équivalente. L'action de $\boldsymbol{K}$ est t-régularisante, c'est-à-dire que $\boldsymbol{K} : H^{-t/2}(\Omega) \to H^{t/2}(\Omega)$. De plus, $\boldsymbol{k}$ est typiquement singulier sur sa diagonale (par exemple $\boldsymbol{k} = b(x,y)/|x-y|^\beta$, $\|b\|_\infty < +\infty$, $\beta > 0$ pour l'opérateur d'Abel). Cependant, le noyau $\boldsymbol{k}$ est inconnu, ce qui motive l'introduction du modèle $\boldsymbol{k}_\delta(x,y) = \boldsymbol{k}(x,y) + \delta\dot{\boldsymbol{b}}(x,y)$ où $\dot{\boldsymbol{b}}$ est un processus gaussien et on aboutit au modèle (2.2)*.*

Afin d'obtenir une estimée de la fonction $\boldsymbol{f}$, Efromovich and Koltchinskii [30] eurent recours à une méthode de Galerkin sur deux bases orthonormales des espaces $\mathbb{H}$ et $\mathbb{K}$. Voyons donc comment s'articule cette méthode avec ce nouveau cadre : en projetant l'équation (3) sur les bases (u_ℓ) et (v_ℓ), on obtient de même que précédemment:

$$\boldsymbol{Y}_\varepsilon^\ell = \boldsymbol{K}^\ell \boldsymbol{f}_G^\ell + \varepsilon \dot{\boldsymbol{W}}^\ell\,.$$

$\boldsymbol{K}^\ell$ n'est ici pas connu, mais nous avons accès à la matrice

$$\boldsymbol{K}_\delta^\ell = \boldsymbol{P}_{W_\ell}\boldsymbol{K}\boldsymbol{P}_{V_\ell} + \delta\boldsymbol{P}_{W_\ell}\dot{\boldsymbol{B}}\boldsymbol{P}_{V_\ell} = \boldsymbol{K}^\ell + \delta\dot{\boldsymbol{B}}^\ell\,,$$

avec $\dot{\boldsymbol{B}}^\ell = (\langle \dot{\boldsymbol{B}}u_k, v_n\rangle)_{k,n\leqslant\ell}$. Une conséquence immédiate de (2.1) est que cette matrice est constituée d'entrées normales $\mathcal{N}(0,1)$ i.i.d.

2.1.1 Conséquence sur le compromis biais-variance

La présence d'un nouvel alea découlant du bruit blanc $\dot{\boldsymbol{B}}$ altère le compromis biais-variance (1.21). En supposant l'hypothèse 1.4.1 toujours valide, celui-ci devient:

$$(\boldsymbol{K}_\delta^\ell)^{-1}\boldsymbol{Y}_\varepsilon^\ell - \boldsymbol{f} = \boldsymbol{f}^\ell - \boldsymbol{f} - \delta(\boldsymbol{K}_\delta^\ell)^{-1}\dot{\boldsymbol{B}}^\ell\boldsymbol{f}^\ell + \varepsilon(\boldsymbol{K}_\delta^\ell)^{-1}\dot{\boldsymbol{W}}^\ell\,.$$

Remarquons que nous avons utilisé l'inversibilité de $\boldsymbol{K}_\delta^\ell$, propriété vérifiée presque sûrement. Ainsi la décomposition fait clairement apparaître trois termes :

- Un terme de biais $\boldsymbol{f}^\ell - \boldsymbol{f}$.
- Un terme de variance dû au bruit du signal $\varepsilon(\boldsymbol{K}_\delta^\ell)^{-1}\dot{\boldsymbol{W}}^\ell$ (la présence de bruit dans $(\boldsymbol{K}_\delta^\ell)^{-1}$ est secondaire, comme on le verra par la suite).

- Un terme de variance dû au bruit dans l'opérateur $\delta(\boldsymbol{K}_\delta^\ell)^{-1}\dot{\boldsymbol{B}}^\ell \boldsymbol{f}^\ell$.

Supposons pour un moment que $\boldsymbol{K}$ a un DIP ν, et que cette propriété se transmet à $\boldsymbol{K}_\delta$. Nous verrons dans les prochaines sections des traitements opérés sur l'opérateur $\boldsymbol{K}_\delta$ qui assurent ceci avec grande probabilité (voir par exemple le traitement du terme IV dans la preuve du Theorem 3.3.1). Alors on peut écrire

$$\|(\boldsymbol{K}_\delta^\ell)^{-1}\|_{op} \leqslant C\ell^\nu \,. \tag{2.4}$$

D'autre part, on dispose du lemme de concentration suivant, sur les variables $\|\dot{\boldsymbol{B}}^\ell\|_{op}$ (voir [22]),

Lemma 2.1.3. *Il existe des constantes universelles $\beta_0 > 0$ et $c_0 > 0$ tel que $\forall t \geqslant \beta_0$, $\ell \geqslant 1$,*

$$\mathbb{P}(\ell^{-1/2}\|\dot{\boldsymbol{B}}^\ell\|_{op} > t) \leqslant \exp(-c_0 t^2 \ell^2) \,.$$

Ce résultat de concentration entraîne en particulier la majoration des moments

$$\mathbb{E}\,\|\dot{\boldsymbol{B}}^\ell\|_{op}^p \leqslant C\ell^{p/2} \,.$$

La combinaison du Lemma 2.1.3 et de (2.4) implique

$$\mathbb{E}\,\|(\boldsymbol{K}_\delta^\ell)^{-1}\boldsymbol{Y}_\varepsilon^\ell - \boldsymbol{f}\|^2 \leqslant C\Big[(\delta \vee \varepsilon)\ell^{2\nu+1} + \ell^{-2s}\Big] \,.$$

En minimisant la quantité ci-dessus au point $\ell(\delta,\varepsilon) = (\delta \vee \varepsilon)^{-\frac{1}{2s+2\nu+1}}$, on obtient le risque

$$\mathbb{E}\,\|(\boldsymbol{K}_\delta^\ell)^{-1}\boldsymbol{Y}_\varepsilon^\ell - \boldsymbol{f}\| \leqslant C(\delta \vee \varepsilon)^{\frac{2s}{2s+2\nu+1}} \,, \tag{2.5}$$

dont on peut montrer qu'il est minimax lorsque $\boldsymbol{f}$ vit dans un espace de Sobolev et $\boldsymbol{K}$ vérifie la condition $\|(\boldsymbol{K}^\ell)^{-1}\|_{op} \leqslant C\ell^\nu$ (c.f. Appendix B). Encore une fois, l'accent est mis sur la nécessité de construire une procédure atteignant cette vitesse sans connaissance préalable de s. Pour la mise en place concrète d'une telle méthode ainsi que la preuve de la performance associée, on consultera la section 4.3.4.

2.2 Schémas génériques de résolution

Toute méthode raisonnable de résolution de (2.2) comporte deux opérations récurrentes : la régularisation du problème et son inversion. Toute la difficulté réside dans leur articulation. Tout d'abord, chaque méthode comporte invariablement une régularisation préliminaire $T_{\mathrm{op}}\big(\boldsymbol{K}_\delta^{-1}\big)$ (ou $T_{\mathrm{op}}\big(\boldsymbol{K}_\delta\big)$) de l'observation de l'opérateur, ceci afin de s'assurer de la stabilité de l'inversion future. Comme il est mentionné dans Hoffmann and Reiß [40], il se dégage ensuite deux grandes classes de procédures qui se distinguent par l'ordre dans lequel on effectue les opérations suivantes :

- Inversion puis régularisation du signal, que nous appellerons plus brièvement IR, où l'inversion du système précède la régularisation de $T_{\mathrm{op}}(\boldsymbol{K}_\delta^{-1})\boldsymbol{Y}_\varepsilon$.
- Régularisation du signal puis inversion que nous noterons RI, où l'on régularise d'abord les données $(\boldsymbol{Y}_\varepsilon, \boldsymbol{K}_\delta)$ avant d'effectuer l'étape d'inversion.

2.2.1 Régularisation de l'opérateur bruité

La première étape est la régularisation de $\boldsymbol{K}_\delta$, qui vise à se prémunir contre une trop grande instabilité de l'opérateur $\boldsymbol{K}_\delta^{-1}$. Dans la suite, cette méthode de régularisation sera toujours matérialisée par une procédure de seuillage. Cavalier and Hengartner [11] et Cavalier and Raimondo [12] procèdent eux par exemple par un choix adéquat du niveau maximal, indépendant de s, ν.
L'instabilité de la procédure étant intrinsèquement liée à l'inversion du système, il est nécessaire que cette régularisation soit compatible avec la structure du problème. Nous commençons donc par exposer celle de Efromovich and Koltchinskii [30] ainsi que sa motivation. Soit $\kappa > 0$. On définit le seuil $O_{\ell,\delta} = \ell^{1/2}\kappa\delta\sqrt{|\log\delta|}$ et on note

$$T_{\mathrm{op}}(\boldsymbol{K}_\delta^\ell)^{-1} = (\boldsymbol{K}_\delta^\ell)^{-1}\mathbf{1}_{\left\{\|(\boldsymbol{K}_\delta^\ell)^{-1}\|_{\mathrm{op}} < O_{\ell,\delta}^{-1}\right\}}\mathbf{1}_{\{\ell\leqslant L\}}\,, \tag{2.6}$$

où L est un niveau maximal. Supposons que la condition de DIP $\|(\boldsymbol{K}^\ell)^{-1}\| \leqslant Q\ell^\nu$ est vérifiée pour un certain $Q > 0$, et choisissons L tel que $L \leqslant (2Q\kappa\delta\sqrt{|\log\delta|})^{-\frac{1}{\nu+1/2}}$. Le seuillage opéré permet alors de détecter une valeur aberrante de $\boldsymbol{K}_\delta$. En effet, d'une part par un argument classique, $\boldsymbol{K}_\delta^\ell$ est inversible si $\delta\|(\boldsymbol{K}^\ell)^{-1}\dot{\boldsymbol{B}}^\ell\|_{\mathrm{op}} < 1$, qui est un évènement réalisé avec grande probabilité si $\ell \leqslant L$ d'après le Lemma 2.1.3. D'autre part, sous la condition $\|(\boldsymbol{K}^\ell)^{-1}\|_{op} \leqslant C\ell^\nu$ et selon le choix de L défini plus haut, l'évènement $\{\|(\boldsymbol{K}_\delta^\ell)^{-1}\|_{\mathrm{op}} < O_{\ell,\delta}^{-1}\}$ est réalisé avec très grande probabilité. Ceci découle du Lemma 2.2.1 ci-dessous, dont une preuve est donnée au Chapitre 3, Lemma 3.5.3:

Lemma 2.2.1. *Soient A et B deux opérateurs inversibles. Supposons que $\|B^{-1}\|_{op} > C^{-1}$ pour un certain $C > 0$. Alors soit $\|A^{-1}\|_{op} > C^{-1}/2$, soit $\|A - B\|_{op} > C$.*

En posant $A = \boldsymbol{K}^\ell$, $B = \boldsymbol{K}_\delta^\ell$, et $C = O_{\ell,\delta}$, le Lemma 3.5.3 implique donc

$$\left\{\|(\boldsymbol{K}_\delta^\ell)^{-1}\|_{\mathrm{op}} < O_{\ell,\delta}^{-1}\right\} \subset \left\{\|(\boldsymbol{K}^\ell)^{-1}\|_{\mathrm{op}} > O_{\ell,\delta}^{-1}/2\right\} \bigcup \left\{\|\delta\dot{\boldsymbol{B}}^\ell\|_{\mathrm{op}} > O_{\ell,\delta}\right\}$$

On vérifie alors que le choix du seuillage $O_{\ell,\delta}$ et du niveau maximal L impliquent

$$\{\|A\|_{\mathrm{op}} > C^{-1}/2\} \subset \varnothing \text{ et } \mathbb{P}(\|A - B\|_{\mathrm{op}} > C) \leqslant \delta^{c_0\kappa}\,.$$

Ce seuillage traite donc du cas où aucune structure a priori de la matrice $\boldsymbol{K}^\ell$ n'est connue. Aussi Efromovich and Koltchinskii [30] firent-ils remarquer que leur algorithme était substantiellement perfectible lorsque $\boldsymbol{K}^\ell$ possédait une structure diagonale.

Example 2.2.2 (Cas de la déconvolution 1D)**.** *Dans le modèle* (1.2)*, supposons désormais que l'on observe $\boldsymbol{k}_\delta$ selon le modèle*

$$\boldsymbol{k}_\delta = \boldsymbol{k} + \delta\dot{\boldsymbol{b}}\,,$$

où $\dot{\boldsymbol{b}}$ *est un bruit blanc gaussien sur* $\mathbb{L}^2([0,1])$*, indépendant de* $\dot{\boldsymbol{W}}$*. La projection de* $\boldsymbol{K}$ *sur les fonctions* $u_\ell : x \mapsto e^{2i\pi\ell x}$ *résulte en la projection de Galerkin*

$$\boldsymbol{K}_\delta^\ell = \mathrm{diag}(\boldsymbol{k}^\ell) + \delta \mathrm{diag}(\dot{\boldsymbol{b}}^\ell)$$

où $\boldsymbol{k}^\ell = \big(\langle \boldsymbol{k}, u_n\rangle\big)_{n\leqslant\ell}$ *est le vecteur constitué des coefficients de Fourier du noyau* $\boldsymbol{k}$*, et* $\dot{\boldsymbol{b}}^\ell = \big(\langle \dot{\boldsymbol{b}}, u_n\rangle\big)_{n\leqslant\ell}$ *est constitué de variables i.i.d gaussiennes centrées réduites. On a noté* $\mathrm{diag}(v)$ *la matrice diagonale constituée des éléments du vecteur* v*. D'autre part, on a*

$$\langle \boldsymbol{Y}_\varepsilon, u_n\rangle = \langle \boldsymbol{k}, u_n\rangle\langle \boldsymbol{f}, u_n\rangle + \varepsilon\mathcal{N}(0,1)\,,$$

de sorte que le problème est en fait une juxtaposition de problèmes indépendants sur chaque composante propre de l'opérateur. On voit que la méthodologie présentée ci-dessus est inadaptée car elle est totalement agnostique à cette structure séquentielle. Soit donc

$$\tilde{\boldsymbol{k}}_\delta^\ell = \sum_{n\leqslant\ell} \langle \boldsymbol{k}_\delta, u_n\rangle \mathbf{1}_{\left\{|\langle \boldsymbol{k}_\delta, u_n\rangle| > \kappa\delta\sqrt{|\log\delta|}\right\}} u_n\,.$$

On propose à la place le seuillage suivant, inspiré par Efromovich and Koltchinskii [30]:

$$\begin{aligned} T_{op}(\boldsymbol{K}_\delta^\ell) &= \mathrm{diag}(\tilde{\boldsymbol{k}}_\delta^\ell)\,,\\ \tilde{\boldsymbol{Y}}_\varepsilon^\ell &= \sum_{n\leqslant\ell} \langle \boldsymbol{Y}_\varepsilon, u_n\rangle \mathbf{1}_{\left\{|\langle \boldsymbol{Y}_\varepsilon, u_n\rangle| > \kappa\varepsilon\sqrt{|\log\varepsilon|}\right\}} u_n\,. \end{aligned}$$

Sous les conditions $\boldsymbol{f} \in \mathcal{W}^s(M)$ *et* $|\langle \boldsymbol{k}, u_\ell\rangle| \sim \ell^{-\nu}$*, et pour un niveau maximal adéquat, la perte devient (voir Chapitre 3)*

$$\sup_{\boldsymbol{f}\in\mathcal{W}^s(M)} \mathbb{E}\,\|T_{op}(\boldsymbol{K}_\delta^\ell)^{-1}\tilde{\boldsymbol{Y}}_\varepsilon^\ell - \boldsymbol{f}\| \lesssim \big(\delta\sqrt{|\log\delta|}\big)^{1\wedge\frac{s}{\nu}} \vee \big(\varepsilon\sqrt{|\log\varepsilon|}\big)^{\frac{2s}{2s+2\nu+1}}\,. \tag{2.7}$$

Cette perte est toujours inférieure à (2.5)*, et elle s'en démarque particulièrement dans les hauts niveaux de bruit en* δ*. On généralisera cette étude au Chapitre 3.*

Example 2.2.3 (Projection sur une base d'ondelettes)**.** *On considère l'opérateur l'opérateur à noyau* $\boldsymbol{K} : \mathbb{L}^2([0,1]) \to \mathbb{L}^2([0,1])$ *défini par*

$$\boldsymbol{K}\boldsymbol{f}(x) = \int_0^1 \boldsymbol{k}(x,y)\boldsymbol{f}(y)dy\,,$$

où $\boldsymbol{k} \in \mathbb{L}^2([0,1]^2)$*. Le caractère mal posé de ce problème se traduit par une singularité de* $\boldsymbol{k}$ *près de sa diagonale. Nous désirons élargir le cadre de la procédure précédente afin de considérer les pertes minimax sur des espaces de Besov. On discrétise donc l'opérateur* $\boldsymbol{K}$ *sur une base d'ondelettes* $(\psi_\lambda)_\lambda$*,* $\lambda = (j,k)$*. La singularité de* $\boldsymbol{k}$ *près de sa diagonale implique que les coefficients* $\boldsymbol{K}_{\lambda,\lambda'} = \langle \boldsymbol{K}\psi_\lambda, \psi_{\lambda'}\rangle$ *sont d'autant plus grands que les ondelettes ont un support proche. Par juxtaposition des ondelettes* ψ_λ*, on obtient donc une matrice 'soleil', comme présenté en Figure 2.1. La matrice est creuse, avec*

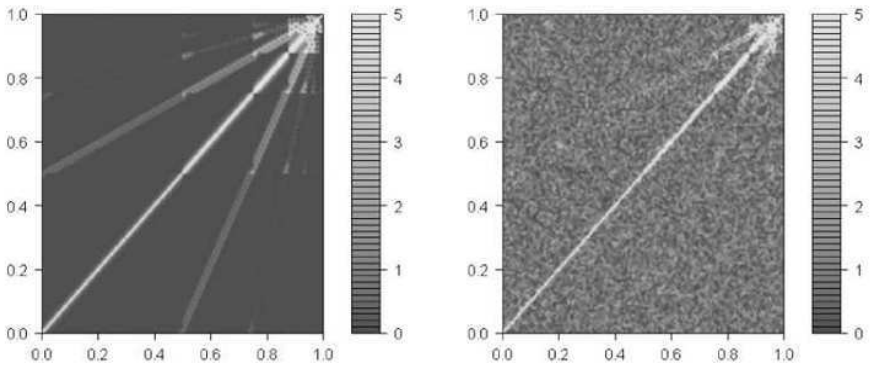

Figure 2.1: Structure de la matrice de Galerkin sur une base d'ondelette (à gauche), et matrice bruitée à $\delta = 0.001$ (à droite) pour le noyau $\boldsymbol{k}(x,y) = -\log\left(\frac{1}{2}|\sin(\pi(x-y))|\right)$. L'image est reprise de Hoffmann and Reiß [40].

peu de coefficients significatifs, ce qui invite à un seuillage composante par composante. Le seuillage de $\boldsymbol{K}_\delta$ proposé dans Hoffmann and Reiß [40] prend alors la forme

$$T_{op}(\boldsymbol{K}_\delta)_{\lambda,\lambda'} = (\boldsymbol{K}_\delta)_{\lambda,\lambda'} \mathbf{1}_{\left\{|(\boldsymbol{K}_\delta)_{\lambda,\lambda'}| > \kappa\delta\sqrt{|\log\delta|}\right\}}. \tag{2.8}$$

Nous réservons à plus tard l'étude spécifique des opérateurs qui constituent le corps de cette thèse, à savoir les opérateurs diagonaux par blocs, et les opérateurs de convolution de Volterra.

2.2.2 Procedures IR et RI

Les méthodes de résolution des problèmes inverses avec opérateur bruité se subdivisent en deux grandes catégories. Nous discutons maintenant de ces deux classes de méthodes dont la différence réside dans l'ordre dans lequel on effectue les étapes d'inversion et de régularisation du signal.
Les méthodes les plus naturelles sont sans doute les méthodes IR, car elles généralisent les méthodes d'inversion en cas d'opérateur connu sans changement profond du cadre sous-jacent: une fois l'opérateur seuillé, on pratique l'inversion $T_{\text{op}}(\boldsymbol{K}_\delta^{-1})\boldsymbol{Y}_\varepsilon$ avant de régulariser le résultat. Cette régularisation peut se faire via : une méthode de Lepski (Efromovich and Koltchinskii [30]), un seuillage (Hoffmann and Reiß [40], Chapitres 4 et 6), ou bien une minimisation d'un risque empirique (Marteau [63],Cavalier and Hengartner [11],Comte and Lacour [18]).
Les méthodes RI quant à elles comportent une régularisation préliminaire du signal observé et de l'opérateur avant l'inversion du système.

Example 2.2.4 (de méthode RI, en dimension finie, dans le cas '$n > p$')**.** *Supposons que l'on recherche $X \in \mathbb{R}^p$ solution du système $AX = B$ où $A \in M_{n,p}(\mathbb{R})$, $B \in \mathbb{R}^n$,*

Méthodes IR: Régularisation de $\boldsymbol{K}_\delta \Rightarrow$ Inversion $\Rightarrow$ Régularisation de $T_{op}(\boldsymbol{K}_\delta)^{-1}\boldsymbol{Y}_\varepsilon$
Méthodes RI: Régularisation de $\boldsymbol{K}_\delta$ et $\boldsymbol{Y}_\varepsilon \Rightarrow$ Inversion

Table 2.1: Schéma des deux méthodes principales de résolution

$n > p$, sachant qu'on observe deux versions bruitées $\tilde{A}$ et $\tilde{B}$. On note $[A|B]$ la matrice obtenue par adjonction de A et B. La méthode TLS (pour Total Least Square) cherche à résoudre

$$\text{argmin}_{X,\Delta A,\Delta b} \|[\Delta A|\Delta B]\|_{HS}^2 \text{ tel que } (\tilde{A}+\Delta A)X = \tilde{B}+\Delta B \text{ a une solution.} \quad (2.9)$$

La méthode RTLS (Regularized Total Least Squares) ajoute une condition de régularité $\|LX\| \leqslant S$ où S est un seuil fixé et $L \in M_{k,p}$, $k \leqslant p$.

Les méthodes RI présentent des vitesses de convergence potentiellement plus élevées sous couvert d'hypothèses additionnelles vérifiées par l'opérateur $\boldsymbol{K}$. En effet, il est nécessaire que la régularisation du signal observé $\boldsymbol{Y}_\varepsilon$ corresponde indirectement à une régularisation de la fonction cible $\boldsymbol{f}$. C'est pourquoi les méthodes IR nécessitent, en plus des hypothèses classiques de ill-posedness sur $\boldsymbol{K}^{-1}$, des hypothèses sur l'opérateur $\boldsymbol{K}$. Cette tendance se retrouve nettement dans les procédures de Hoffmann and Reiß [40], où la continuité de $\boldsymbol{K} : B^s_{p,p} \to B^{s+\nu}_{p,p}$ est requise, et au Chapitre 3, où l'on impose la condition $\|\boldsymbol{K}_\ell\|_{\text{op}} \leqslant C\ell^{-\nu}$.

Seuillage des données

Dans notre cas, l'étape de régularisation (de l'opérateur aussi bien que du signal) consistera en une procédure de seuillage, représentée génériquement par une fonction

$$T : x \mapsto x\mathbf{1}_{\{|x|>s\}},$$

où $|.|$ est une norme adéquate, et s un niveau de seuillage dépendant des données. Ainsi, par exemple, dans le cas du seuillage sur l'opérateur, on prendra $|.| = \|.\|_{\text{op}}$ la norme spectrale, et s de la forme $s = \kappa\ell^{1/2}\delta\sqrt{|\log\delta|}$ où κ est une constante à fixer. Le seuillage du signal lui prendra deux forme différentes selon le type (RI ou IR) de la procédure. Dans le cas d'une méthode RI, le seuillage sera de la forme $s = \tau\varepsilon\sqrt{|\log\varepsilon|}$, $\tau > 0$. Si au contraire une méthode IR est requise, alors le seuillage du signal inclura également un terme dépendant de δ, et se mettra sous la forme $s = \tau_{sig}h\varepsilon\sqrt{|\log\varepsilon|} \vee \tau_{op}h\delta\sqrt{|\log\delta|}$ où h est un facteur dépendant du niveau de résolution.
Derrière l'apparente simplicité de telles procédures se trouve la question hautement non triviale du choix des constantes $\kappa, \tau, \tau_{sig}, \tau_{op}$ en pratique (de manière générale, les théorèmes de convergence n'explicitent d'ailleurs pas la dépendance par rapport à ces constantes). Dans le cas direct ($\delta = 0$) Kerkyacharian et al. [51] proposent par exemple de travailler avec $\boldsymbol{f} = 0$, puis d'augmenter la constante de seuillage γ en jeu jusqu'à ce que tous les coefficients de Fourier du résultat soient tués (cette manière de procéder trouve elle même son inspiration dans [27]). Afin de généraliser cette dernière tout en respectant son principe, nous proposons la méthode suivante:

1. **Choix de κ**: nous nous basons sur le cas où $\boldsymbol{K} = 0$. Dans ce cas, on peut logiquement imposer que le seuillage de $\boldsymbol{K}_\delta^\ell$ retourne une matrice nulle pour tout ℓ. On fixe donc ℓ et δ assez grands, et, pour une certaine grille de valeurs G, on augmente la valeur de $\kappa \in G$ jusqu'à ce que tous les coefficients de $T_{op}(\boldsymbol{K}_\delta^\ell)$ soient nuls.

2. **Choix des constantes τ, τ_{sig} et τ_{op}**: le choix des constantes de seuillage du signal dépend bien évidemment du type de procédure en jeu. Nous proposons le choix suivant selon que l'on utilise une méthode RI ou bien IR.
   -Méthode RI, choix de τ: on se base cette fois-ci sur le cas où le signal à estimer est nul $\boldsymbol{f} = 0$. Si l'on avait accès à $\boldsymbol{K}$, alors il suffirait d'adapter la méthode ci-dessus. En l'absence de la connaissance $\boldsymbol{K}$, le substitut le plus pertinent est $T_{op}(\boldsymbol{K}_\delta)$ pour δ le plus petit possible (imposé par l'expérience). On adopte donc le protocole suivant: on observe $\boldsymbol{Y}_\varepsilon$ et $\boldsymbol{K}_\delta$ pour ε assez grand (et δ le plus petit possible). On choisit une grille H de valeurs pour τ et, en incorporant la valeur de κ précédemment calculée, on pose $\tau = \min\{\tau \in H,\ \widetilde{\boldsymbol{f}} = 0\}$.
   - Méthode IR, choix de τ_{sig} et τ_{op}: il est clair que le rôle de τ_{sig} et τ_{op} est de limiter l'influence d'une déviation (substantiellement plus grande que la variance de l'estimateur) due à l'erreur commise en ε (resp. en δ). On choisit donc les constantes séparément de la manière suivante: premièrement, on choisit $\varepsilon_{sig} > \delta_{sig} > 0$ et on pose $\tau_{op} = 0$ (resp. $\delta_{op} > \varepsilon_{op} > 0$ et on pose $\tau_{sig} = 0$). On se base encore sur le cas où le signal à estimer est nul $\boldsymbol{f} = 0$. Par conséquent, on doit retrouver $\widetilde{\boldsymbol{f}} = 0$. On choisit donc une grille G_{sig} (resp. G_{op}), puis, après avoir simulé $Y_{\varepsilon_{sig}}$ et $\boldsymbol{K}_{\delta_{sig}}$ (resp. $\boldsymbol{Y}_{\varepsilon_{op}}$ et $\boldsymbol{K}_{\delta_{op}}$) et intégré la valeur de κ précédemment déterminée, on pose $\tau_{sig} = \min\{\tau \in G_{sig},\ \widetilde{\boldsymbol{f}} = 0\}$ (resp. $\tau_{op} = \min\{\tau \in G_{op}\ \widetilde{\boldsymbol{f}} = 0\}$).

2.2.3 Détermination de bornes inférieures pour le risque minimax

Dans cette section nous présentons très brièvement les méthodes d'établissement des bornes inférieures pour le risque minimax. Premièrement, étant donné que les pertes sont croissantes en fonction de ε, δ, le risque minimax est borné inférieurement par le supremum des risques correspondant respectivement aux cas $\delta = 0$ et $\varepsilon = 0$. Pour cette raison, l'étude de bornes inférieures se découple en deux cas distincts. Le cas $\delta = 0$ correspond au cas régulier des problèmes inverses, et les bornes minimax ont en général déjà été établies. Par conséquent, l'étude des bornes inférieures se limite souvent à celle du cas $\varepsilon = 0$, c'est-à-dire que l'on observe $\boldsymbol{K}\boldsymbol{f}$ sans bruit, mais que seul $\boldsymbol{K}_\delta$ est accessible.
A la connaissance de l'auteur, on distingue ensuite deux stratégies particulières : soit perturber un opérateur connu $\boldsymbol{K}$ par un résidu $\delta\boldsymbol{H}$ de telle manière que $\boldsymbol{K} + \delta\boldsymbol{H}$ vérifie des conditions de DIP identiques, et appliquer les résultats de Korostelev and Tsybakov [54, Chap. 2] aux fonctions $\boldsymbol{f}_0$ (choisie préalablement) et $\boldsymbol{f}_1 = (\boldsymbol{K} + \delta\boldsymbol{H})^{-1}\boldsymbol{K}\boldsymbol{f}_0$. Cette

technique est appliquée dans Hoffmann and Reiß [40], ainsi que dans les Chapitre 3 et 4, et se généralise à plusieurs perturbations en vue de l'application du lemme d'Assouad ou de Fano (c.f. Appendix B). Soit perturber à la fois l'opérateur et la fonction cible, stratégie opérée dans [30].

2.3 Retour sur la déconvolution aveugle par ondelettes

Nous revenons ici aux méthodes développées dans Hoffmann and Reiß [40], car elles constituent en quelque sorte les avatars de celles présentes dans cette thèse. De plus, elles permettent d'illustrer les enjeux et performances des procédures IR ou RI. Pour un niveau de résolution J, on notera $\Lambda = \{(j,k),\, j \leqslant J, k \leqslant 2^j\}$. On rappelle que $\boldsymbol{f}$ est ici une fonction de $\mathbb{L}^2([0,1]^d)$. Supposons donc que l'opérateur $\boldsymbol{K}$ est symétrique, et possède un DIP ν, ce qui est matérialisé ici par la relation

$$\langle \boldsymbol{K}\boldsymbol{f}, \boldsymbol{f}\rangle \sim \|\boldsymbol{f}\|^2_{\mathcal{W}^{-\nu/2}}$$

Définissons le niveau de résolution maximal via $2^J \sim (\varepsilon \vee \delta)^{-1/\nu}$, et la procédure de reconstruction de type IR:

$$\tilde{\boldsymbol{f}} = \begin{cases} \displaystyle\sum_{j\leqslant J}\sum_{k\leqslant 2^j} \hat{\boldsymbol{\beta}}_{j,k} \mathbf{1}_{\left\{|\hat{\boldsymbol{\beta}}_{j,k}|>\tau 2^{j\nu}\left((\delta\sqrt{\log\delta})\vee(\varepsilon\sqrt{\log\varepsilon})\right)\right\}} \boldsymbol{\psi}_{j,k} \text{ si } \|(\boldsymbol{K}^\Lambda)^{-1}\|_{op} \leqslant \kappa 2^{J\nu}\,, \\ 0 \text{ sinon} \end{cases}$$

où $\hat{\boldsymbol{\beta}}_{j,k} = \langle \left(\boldsymbol{K}^\Lambda_\delta\right)^{-1}\boldsymbol{Y}^\Lambda_\varepsilon, \boldsymbol{\psi}_{j,k}\rangle$. Remarquons que nous n'avons défini ici qu'une simplification de la vraie procédure, qui comprend un terme additionnel dans le seuillage dans l'esprit de Delyon and Juditsky [24]. Alors on a, pour $\pi \geqslant 1$, $s > d/\pi - d/2$,

Theorem 2.3.1 (Hoffmann and Reiß [40], Theorem 5.1)**.**

$$\sup_{\boldsymbol{f}\in B^s_{\pi,\pi}(M)} \|\tilde{\boldsymbol{f}} - \boldsymbol{f}\| \lesssim \begin{cases} (\delta\vee\varepsilon)^{\frac{2s}{2(s+\nu)+d}} & si\ s > (2\nu+1)(1/\pi - 1/2)\,, \\ \left(\delta\sqrt{|\log\delta|}\vee\varepsilon\sqrt{|\log\varepsilon|}\right)^{\frac{s+d/2-d/\pi}{s+\nu+d/2-d/\pi}} & si\ s \leqslant (2\nu+1)(1/\pi-1/2)\,. \end{cases}$$

Dans le cas particulier où $p = 2$, on retrouve donc de manière adaptative en s le taux de convergence (2.5), et ces résultats le généralisent dans le cas où $\boldsymbol{f} \in B^s_{\pi,\pi}$, $\pi \geqslant 1$ pour le risque quadratique. Dans le cas où $\delta = 0$, ils coïncident avec ceux présentés dans le Theorem A.3.2 dans le cas de la déconvolution périodique par ondelettes. A notre connaissance, aucune étude systématique pour le risque $\mathbb{L}^p$, $p \geqslant 1$ n'a encore été effectuée lorsque $\delta \neq 0$ (cette étude peut être déduite du Chapitre 6).
On présente maintenant l'analogue RI de cette procédure. Le seuillage opéré sur l'opérateur a déjà été présenté dans l'exemple 2.2.3. Soit J le niveau de résolution maximal spécifié par

$$2^J \sim \varepsilon^{-1/\nu} \wedge (\delta\sqrt{|\log\delta|})^{-1/(\nu+d)}\,.$$

On note $T_{op}(\boldsymbol{K}_\delta^\Lambda)$ l'opérateur projeté sur l'espace des ondelettes de niveau $\leqslant J$, puis seuillé selon la procédure décrite en (2.2.3). Soit $\widehat{Y^\Lambda}$ la version seuillée de $\boldsymbol{Y}_\varepsilon$ définie par

$$\widehat{Y^\Lambda} = \sum_{j \leqslant J} \sum_{k \leqslant 2^j} \hat{\boldsymbol{\gamma}}_{j,k} \mathbf{1}_{\left\{|\hat{\boldsymbol{\gamma}}_{j,k}| > \tau\varepsilon\sqrt{\log \varepsilon}\right\}} \boldsymbol{\psi}_{j,k}\,,$$

où $\hat{\boldsymbol{\gamma}}_{j,k} = \langle \boldsymbol{Y}_\varepsilon^\Lambda, \boldsymbol{\psi}_{j,k} \rangle$. On définit l'estimateur

$$\tilde{\boldsymbol{f}} = \begin{cases} \left(T_{op}(\boldsymbol{K}_\delta^\Lambda)\right)^{-1} \widehat{Y^\Lambda} & \text{si } \left\| \left(T_{op}(\boldsymbol{K}_\delta^\Lambda)\right)^{-1} \right\|_{\mathcal{W}^\nu \to \mathbb{L}^2} \leqslant \kappa\,, \\ 0 \text{ sinon } . \end{cases}$$

Nous ne présentons pas en détail les résultats techniques de convergence de cette dernière procédure. Notons toutefois, comme mentionné précédemment, qu'ils nécessitent entre autres une hypothèse additionnelle vérifiée par l'opérateur $\boldsymbol{K}$, à savoir que $\boldsymbol{K} : B^s_{\pi,\pi} \to B^{s+\nu}_{\pi,\pi}$ est continu si $\boldsymbol{f} \in B^s_{\pi,\pi}$ (dans sa forme la plus simple), ainsi que la restriction des indices (s,π) à la région dense (voir Appendix A).

2.4 Traitement des opérateurs diagonaux par blocs dans un cadre RI

2.4.1 Modèle

L'exemple 2.2.2 montre que dans le cas où la matrice de Galerkin est diagonale, la procédure d'estimation peut être conduite séparément sur chacune des composantes propres, et appelle donc à une généralisation dans le cas d'une SVD par blocs. On se place dans le modèle (2.2), et on rappelle que la projection de la première équation sur l'espace $\mathbb{H}_\ell$ conduit à l'égalité

$$\boldsymbol{Y}_{\varepsilon,\ell} = \boldsymbol{K}_\ell \boldsymbol{f}_\ell + \varepsilon \dot{\boldsymbol{W}}_\ell, \ell \geqslant 1\,,$$

où $\boldsymbol{K}_\ell = \left(\langle \boldsymbol{K} u_{\ell,n}, v_{\ell,m} \rangle\right)_{m,n} \in M_{|\Lambda_\ell|}(\mathbb{C})$ et $(\dot{\boldsymbol{W}}_\ell)_\ell$ est une séquence de vecteurs gaussiens standards de taille $|\Lambda_\ell| = \dim \mathbb{H}_\ell$, indépendants entre eux. Les matrices $\boldsymbol{K}_\ell$ sont inconnues, cependant d'après l'exemple 2.2.2, on a accès aux variables

$$\langle \boldsymbol{K}_\delta u_{\ell,n}, v_{\ell,m} \rangle = \langle \boldsymbol{K} u_{\ell,n}, v_{\ell,m} \rangle + \delta \dot{\boldsymbol{B}}_{\ell,m,n}\,,$$

où $(\dot{\boldsymbol{B}}_{\ell,m,n})_{\ell,m,n}$ est une suite de variables normales $\mathcal{N}(0,1)$ i.i.d. On peut donc reformuler le modèle de la manière équivalente:

$$\forall \ell \geqslant 0, \quad \begin{cases} \boldsymbol{Y}_{\varepsilon,\ell} &= \boldsymbol{K}_\ell \boldsymbol{f}_\ell + \varepsilon \dot{\boldsymbol{W}}_\ell\,, \\ \boldsymbol{K}_{\delta,\ell} &= \boldsymbol{K}_\ell + \delta \dot{\boldsymbol{B}}_\ell\,. \end{cases} \tag{2.10}$$

où $\dot{\boldsymbol{B}}_\ell = \left(\dot{\boldsymbol{B}}_{\ell,m,n}\right)_{m,n\leqslant|\Lambda_\ell|} \in M_{|\Lambda_\ell|}(\mathbb{C})$. Par la suite, on supposera que la taille $|\Lambda_\ell|$ des espaces $\mathbb{H}_\ell$ vérifie

$$|\Lambda_\ell| \sim \ell^{d-1},\ d \in \mathbb{N}\,. \tag{2.11}$$

L'entier d jouera le rôle d'un paramètre de dimension. Cette exemple recoupe en particulier le cas de la déconvolution sphérique ($d = 2$) exposé en 1.3.2, mais également celui de la déconvolution de Fourier en dimension $d \geqslant 1$. Dans ce dernier cas, on observe

$$\boldsymbol{Y}_\varepsilon = \boldsymbol{k} * \boldsymbol{f} + \varepsilon\dot{\boldsymbol{W}}\,,$$

où $\boldsymbol{k}, \boldsymbol{f} \in \mathbb{L}^2([0,1]^d)$ et $\dot{\boldsymbol{W}}$ est un bruit blanc sur $\mathbb{L}^2([0,1]^d)$. En prenant pour bases $(u_\lambda)_{\ell\geqslant0} = (v_\lambda)_{\ell\geqslant0}$ les bases tensorisées :

$$u_\lambda(x_1,...,x_d) = \prod_{i=1}^{d} e^{2i\pi k_j x_j},\ \lambda = (k_1,...,k_d)\,.$$

Soit $|\lambda| = 1 + \sum_{j=1}^{d}|k_j|$ et $\mathbb{H}_\ell = \{u_\lambda,\ |\lambda| = \ell\}$. Alors on obtient une décomposition par blocs de tailles respectives

$$|\Lambda_\ell| = \binom{\ell+d-1}{d-1} \sim \ell^{d-1}\,.$$

En fait, cet exemple est quelque peu abusif, car $\boldsymbol{K}$ est directement diagonal dans la base des $(u_\lambda)_\lambda$, de sorte que la dimension réelle d'un bloc est 0 et non $d-1$. Nous verrons que notre algorithme se transcrit cependant aisément à ce cas.

2.4.2 Algorithme

On se place dans le cadre d'un problème moyennement mal posé, où

$$\boldsymbol{f} \in \mathcal{W}^s(M) := \{f \in \mathbb{H}, \sum_{\ell\geqslant0} \ell^{2s}\|\boldsymbol{P}_{\mathbb{H}_\ell} f\|^2 \leqslant M^2\}\,,$$

et $\boldsymbol{K}$ vérifie la condition de ill-posedness suivante:

$$\exists\, Q_1^{-1} \leqslant Q_2,\ \text{tel que } \forall\ell \geqslant 1,\ \|\boldsymbol{K}_\ell^{-1}\|_{\text{op}} \leqslant Q_2\ell^\nu \text{ et } \|\boldsymbol{K}_\ell\|_{\text{op}} \leqslant Q_1\ell^{-\nu}\,. \tag{2.12}$$

On notera $\mathcal{K}_\nu(Q)$ l'ensemble des opérateurs vérifiant (2.12), où $Q = (Q_1, Q_2)$. La condition (2.12) est typiquement une condition de type RI, car elle impose la continuité de $\boldsymbol{K}$ de $W^{-\nu/2}$ dans $W^{\nu/2}$, et assure par là l'efficacité d'une procédure de seuillage standard appliquée à $\boldsymbol{Y}_\varepsilon$. Soit donc $\kappa, \tau \geqslant 0$. Définissons comme précisé en section 2.2.2 le niveau de seuillage

$$O_{\ell,\delta} = \kappa|\Lambda_\ell|^{1/2}\delta\sqrt{|\log\delta|}\,, \tag{2.13}$$

ainsi que

$$\mathcal{E}_{\ell,\varepsilon} = \tau|\Lambda_\ell|^{1/2}\varepsilon\sqrt{|\log\varepsilon|}\,. \tag{2.14}$$

On définit maintenant la procédure d'estimation **BBD** (pour Blind Blockwise Deconvolution): soit

$$L = \delta^{-2/(\nu+(d-1))} \wedge \varepsilon^{-2/(\nu+d)},$$
$$\text{et } \widetilde{\boldsymbol{f}} = \sum_{\ell \leqslant L} \boldsymbol{K}_{\delta,\ell}^{-1} \mathbf{1}_{\left\{\|\boldsymbol{K}_{\delta,\ell}^{-1}\|_{\mathrm{op}} \leqslant O_{\ell,\delta}^{-1}\right\}} \boldsymbol{Y}_{\varepsilon,\ell} \mathbf{1}_{\left\{\|\boldsymbol{Y}_{\varepsilon,\ell}\| \geqslant \mathcal{E}_{\ell,\varepsilon}\right\}}.$$

Si $d \geqslant 2$, on vérifie (voir la preuve du Theorem 3.3.1) que poser $\nu = 0$ dans la définition de L donne les mêmes résultats que ci-dessous. Si $d = 1$, on ne peut pas poser $\nu = 0$, mais on peut remplacer L par $L = \delta^{-1/s_0} \wedge \varepsilon^{-2/d}$ où s_0 est un a priori sur la régularité de $\boldsymbol{f}$ (c'est-à-dire $\boldsymbol{f} \in \mathcal{W}^{s_0}$).
Remarquons que cette procédure utilise un seuillage par bloc ([38, 10, 9]), pratiqué sur l'opérateur et sur le signal, et opéré sur chaque espace $\mathbb{H}_\ell$. En cela, elle respecte la propriété de SVD par blocs.
Enfin, il est à noter que la procédure est entièrement adaptative, à la fois au signal $\boldsymbol{f}$ car elle ne requiert pas la connaissance préalable de s, M, mais également à l'opérateur $\boldsymbol{K}$ car elle ne dépend pas de ν, Q_1, Q_2.

Résultats de convergence

Etudions maintenant les vitesses de convergence de la procédure définie ci-dessus. Pour ce faire, nous adoptons le point de vue minimax exposé en 1.2.2.

Theorem 2.4.1. *Soit $s, M > 0$. Soit $\nu > 0$ et $Q = (Q_1, Q_2)$ avec $Q_1 > 0$ et $Q_1 Q_2 \geqslant 1$. Alors on a*

$$\sup_{\substack{\boldsymbol{f} \in \mathcal{W}^s(M) \\ \boldsymbol{K} \in \mathcal{K}(Q)}} \mathbb{E} \|\widetilde{\boldsymbol{f}} - \boldsymbol{f}\| \lesssim \left(\delta \sqrt{|\log \delta|}\right)^{1 \wedge \frac{2s}{2\nu+d-1}} \vee \left(\varepsilon \sqrt{|\log \varepsilon|}\right)^{\frac{2s}{2s+2\nu+d}}$$

où $\lesssim$ représente une inégalité à une constante multiplicative près, ne dépendant que de s, M, ν, Q, d.

Cette étude est complétée par celle de la borne inférieure du risque minimax. Le risque minimax pour $\delta = 0$ est classique, et le travail à effectuer se situe donc au niveau du premier terme ($\varepsilon = 0$), ce qui revient à observer $\boldsymbol{K}\boldsymbol{f}$ alors que $\boldsymbol{K}$ est inconnu. On a le

Theorem 2.4.2. *Sous les mêmes hypothèses que Theorem 2.4.1, avec de plus $Q_2 > 1/Q_1$, on a*

$$\inf_{\widetilde{\boldsymbol{f}}} \sup_{\substack{\boldsymbol{f} \in \mathcal{W}^s(M) \\ \boldsymbol{K} \in \mathcal{K}(Q)}} \mathbb{E} \|\widetilde{\boldsymbol{f}} - \boldsymbol{f}\| \gtrsim \delta^{1 \wedge \frac{2s}{2\nu+d-1}} \vee \varepsilon^{\frac{2s}{2s+2\nu+d}}$$

où l'infimum est pris sur tout les estimateurs $\widetilde{f}$ issus des observations (2.2).

Nous pouvons donc conclure que la procédure est optimale au sens minimax, à un facteur logarithmique près, sur les espaces de Sobolev $\mathcal{W}^s$, uniformément en $\boldsymbol{K} \in \mathcal{K}(Q)$.

Remarquons que le taux de convergence en δ fait intervenir l'entier $d-1$, caractéristique de la taille des blocs d'après (2.11).
Le résultat du Theorem 2.4.2 exclut le cas d'un opérateur diagonal, telle la déconvolution de Fourier sur $[0,1]^d$ mentionnée plus haut. Dans ce cas précis, il suffit de réadapter la procédure en adaptant le seuillage pratiqué sur l'opérateur afin de retrouver le taux de convergence

$$\left(\delta\sqrt{|\log\delta|}\right)^{1\wedge\frac{s}{\nu}} \vee \left(\varepsilon\sqrt{|\log\varepsilon|}\right)^{\frac{2s}{2s+2\nu+d}}.$$

Enfin, remarquons que le cas diagonal se distingue par le fait que les résultats restent valables si l'Assumption 2.12 est vérifiée pour $Q_1 = 0$ (c'est-à-dire que seule la borne supérieure compte). Un parcours de la preuve du Theorem 3.3.1 au chapitre 3 suffit à le démontrer.
Ces résultats très prometteurs montrent que l'effet de l'erreur en δ est minoritaire par rapport au niveau d'erreur dans le signal $\boldsymbol{Y}_\varepsilon$. De plus, ils explicitent la dépendance de l'erreur en ces deux paramètres de manière explicite. Bien sûr, la rapidité de ces vitesses a un prix, et ce prix est l'espace des opérateurs considérés. En effet, la condition de DIP (2.12) n'est satisfaite que par des opérateurs 'quasi-diagonaux', et dans le cas où seul un contrôle sur $\|\boldsymbol{K}_\ell^{-1}\|_{op}$ est disponible, les vitesses ne sont plus valables. Afin d'illustrer cette remarque, nous avons appliqué la procédure aux données suivantes:

- Les opérateurs $\boldsymbol{K}_\ell^{RI}$ et $\boldsymbol{K}_\ell^{IR}$ sont définis par

$$\boldsymbol{K}_\ell^{RI} = \ell^{-1}\boldsymbol{I}_{2\ell+1}\,, \tag{2.15}$$

$$\left(\boldsymbol{K}_\ell^{IR}\right)_{m,n} = m^{-1}\mathbf{1}_{\{m=n\}}\,. \tag{2.16}$$

  Ainsi, $\boldsymbol{K}_\ell^{RI}$ satisfait l'Assumption 2.12 alors que $\boldsymbol{K}_\ell^{IR}$ ne vérifie qu'une seule des deux inégalités.

- $\boldsymbol{f}$ est la troncature au niveau $\ell = 16$ de la fonction $\boldsymbol{f}_0(\omega) = 1/0.6729\exp(-2\|\omega - (0,1,0)\|_{\ell^1})$. La forme en pic de $\boldsymbol{f}_0$ assure une bonne répartition de ses coefficients de Fourier dans les hautes fréquences.

- Les constantes de seuillages, calculées à partir de la méthode présentée dans la section 2.2.2 sont $\kappa = 0.8$ et $\tau = 0.6$ pour les deux opérateurs.

Les résultats sont résumés dans le tableau 2.2, et on a tracé les estimations dans le cas où $(\delta,\varepsilon) = (10^{-3},10^{-3})$ en Figure 2.2. D'une part, ils confirment l'interaction entre les vitesses de convergence en δ et ε dans le cas de $\boldsymbol{K}^{RI}$. En effet, la perte en ε est clairement dominante par rapport à la perte en δ pour des niveaux de bruits comparables (et même pour $\delta > \varepsilon$ lorsque le différentiel n'est pas trop important). Une autre illustration de cet effet se trouve en Figure 3.6. D'autre part, ils montrent que la méthode ne s'adapte pas du tout à l'opérateur $\boldsymbol{K}^{RI}$, produisant des erreurs quadratiques très importantes en particulier lorsque ε est grand, ce qui indique que le seuillage du signal n'est plus du tout adapté. Nous verrons un moyen de corriger ce défaut en section 2.6 ou plus en détail au Chapitre 6.

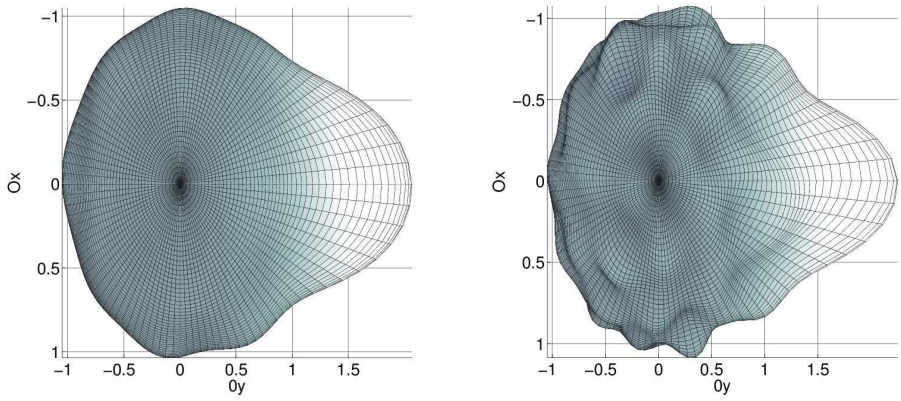

Figure 2.2: Comparaison graphique de la procédure pour les deux opérateurs $\boldsymbol{K}^{RI}$ (à gauche) et $\boldsymbol{K}^{IR}$ (à droite), au niveau de bruit $\delta = \varepsilon = 10^{-3}$.

	K^{RI}			K^{IR}		
δ \ ε	10^{-4}	10^{-3}	5.10^{-3}	10^{-4}	10^{-3}	5.10^{-3}
10^{-4}	0.037	0.147	0.491	0.042	0.349	0.989
10^{-3}	0.039	0.148	0.483	0.043	0.347	0.962
5.10^{-3}	0.142	0.171	0.480	0.216	0.230	0.736

Table 2.2: Comparaison des deux algorithmes pour les opérateurs $\boldsymbol{K}^{RI}$ et $\boldsymbol{K}^{RI}$. La perte considérée est l'espérance de la perte $\mathbb{L}^2$ renormalisée.

2.5 Traitement des opérateurs intégraux de Volterra du premier type

On s'intéresse ici à l'analogue causal du problème de déconvolution traité plus haut. Pour une fonction $\boldsymbol{k} \in \mathbb{L}^2(\mathbb{R}_+)$, on note

$$\begin{aligned} \boldsymbol{K} : \mathbb{L}^2(\mathbb{R}_+) &\to \mathbb{L}^2(\mathbb{R}_+) \\ f &\mapsto \left(g : t \mapsto \int_0^t \boldsymbol{k}(\tau) f(t-\tau) d\tau \right). \end{aligned} \tag{2.17}$$

L'opérateur $\boldsymbol{K}$ est une version canonique des problèmes causaux, c'est-à-dire tel que $\boldsymbol{K}\boldsymbol{f}(t)$ ne dépend de $\boldsymbol{f}(\tau)$ et $\boldsymbol{k}(\tau)$ que pour des temps τ antérieurs à t (voir Linz [59, Chap. 2]). La situation est différente de la section précédente, car **il n'existe pas de SVD indépendante du noyau $\boldsymbol{k}$** pour l'opérateur $\boldsymbol{K}$. Nous nous placerons ici spécifiquement dans le modèle de régression (2), c'est-à-dire qu'on observe

$$\boldsymbol{y}(t_i) = \int_0^{t_i} \boldsymbol{k}(\tau) \boldsymbol{f}(t_i - \tau) d\tau + \sigma \eta_i, \quad t_1, ..., t_n \in [0, T_n] \subset \mathbb{R}^+, \tag{2.18}$$

où $\sigma > 0$ est un facteur de précision, et (η_i) est une suite i.i.d de normales $\mathcal{N}(0,1)$. Cette modélisation est due à Abramovich et al. [3] et Comte et al. [19].
Un aspect particulier ici est la croissance des intervalles d'observations $[0, T_n]$ en fonction de n. Nous pourrions bien sûr utiliser une borne a priori $T_n \leqslant T$ (ce qui est fait le plus souvent en pratique) mais la restriction du problème à un intervalle $[0, T]$ créerait immanquablement plusieurs artefacts indésirables. La contrepartie de notre cadre est la restriction, imposée par la suite, sur la décroissance (exponentielle) des signaux en question vers l'infini. Remarquons tout de même que cette restriction n'est pas rédhibitoire, car les signaux observés en pratique (signaux physiques) la satisfont très souvent.
D'autre part, cette croissance d'intervalles interdit toute assimilation à un problème de déconvolution de Fourier (en posant par exemple $\boldsymbol{f}(t) = \boldsymbol{k}(t) = 0$ si $t < 0$) car ce dernier suppose une périodicité des signaux sur l'intervalle (variable!) $[0, T_n]$. Enfin, les méthodes de régularisation de Tikhonov sont souvent victimes d'un phénomène d'oversmoothing ([15]), en plus de ne pas respecter la nature causale de l'équation (2.18).
Les fonctions de Laguerre constituent un choix bien plus intéressant dans notre cas, comme nous allons le montrer. Rappelons qu'elles sont définies comme suit :

Definition 2.5.1. *Soit $a > 0$. Pour $\ell \geqslant 0$, on note*

$$\boldsymbol{\varphi}_\ell(t) = \sqrt{2a} e^{-at} L_\ell(2at)$$

la ℓ-ième fonction de Laguerre, où L_ℓ est le ℓ-ième polynôme de Laguerre, défini par

$$L_\ell(t) = \sum_{j=0}^{\ell} (-1)^\ell \binom{\ell}{j} \frac{t^j}{j!}.$$

Les fonctions de Laguerre forment une base hilbertienne de l'espace $\mathbb{L}^2(\mathbb{R}^+)$. On notera, pour une fonction $\boldsymbol{f} \in \mathbb{L}^2(\mathbb{R}^+)$, $\check{\boldsymbol{f}}_\ell = \langle \boldsymbol{f}, \boldsymbol{\varphi}_\ell \rangle$. Le paramètre a introduit ici joue le rôle d'un paramètre ajustable en fonction de la décroissance présupposée des signaux. Par souci de clarté, nous ne considèrerons désormais que le cas principal $a = 1/2$. Les résultats sont bien sûr directement généralisables.
Le rôle particulier joué par les fonctions de Laguerre dans ce contexte est explicité par la proposition suivante:

Proposition 2.5.2.

$$\forall k, \ell \geqslant 0,\ \forall t \geqslant 0, \int_0^t \boldsymbol{\varphi}_k(t)\boldsymbol{\varphi}_\ell(t-\tau)d\tau = \boldsymbol{\varphi}_{k+\ell}(t) - \boldsymbol{\varphi}_{k+\ell+1}(t)\,.$$

Soit V_ℓ l'espace vectoriel engendré par les fonctions de Laguerre de degré plus petit que ℓ. La proposition 2.5.2 aboutit aux deux conséquences suivantes sur l'élaboration d'une méthode de Galerkin couplée aux espaces V_ℓ: premièrement, l'Assumption 1.4.1 est satisfaite et donc $\boldsymbol{f}_G = \boldsymbol{P}_{V_\ell}\boldsymbol{f}$. Par la suite, on identifiera h^ℓ et $\boldsymbol{P}_{\mathbb{H}_\ell}h$ pour une fonction h quelconque. D'autre part, notons $\dot{\boldsymbol{k}}$ la fonction définie via ses coefficients de Fourier

$$\check{\dot{\boldsymbol{k}}}_\ell = \check{\boldsymbol{k}}_0\mathbf{1}_{\{\ell=0\}} + (\check{\boldsymbol{k}}_\ell - \check{\boldsymbol{k}}_{\ell-1})\mathbf{1}_{\{\ell\geqslant 1\}}\,.$$

Alors $\boldsymbol{K}^\ell$ est une matrice de Toeplitz triangulaire inférieure dont les coefficients sont donnés par les coefficients de Fourier de $\dot{\boldsymbol{k}}_\ell$:

$$\boldsymbol{K}^\ell = \begin{pmatrix} \check{\dot{\boldsymbol{k}}}_0 & 0 & \dots & 0 \\ \check{\dot{\boldsymbol{k}}}_1 & \check{\dot{\boldsymbol{k}}}_0 & \ddots & \vdots \\ \vdots & \ddots & \ddots & 0 \\ \check{\dot{\boldsymbol{k}}}_\ell & \dots & \check{\dot{\boldsymbol{k}}}_1 & \check{\dot{\boldsymbol{k}}}_0 \end{pmatrix} \tag{2.19}$$

La propriété de Toeplitz permet de dresser un parallèle intéressant entre l'inversion de (2.17) et l'inversion de séries entières définies sur le disque unité de $\mathbb{C}$. Si on note, pour une fonction $\boldsymbol{h} \in \mathbb{L}^2(\mathbb{R}^+)$, $\boldsymbol{h}(z) = \sum_{\ell\geqslant 0} \check{\boldsymbol{h}}_\ell z^\ell$ on a en effet $\boldsymbol{f}(z) = (1/\dot{\boldsymbol{k}})(z)(\boldsymbol{K}\boldsymbol{f})(z)$.
Il reste à prendre en compte la composante aléatoire du modèle (2.18). Pour ce faire, introduisons la matrice de taille $(\ell+1)\times n$, $\big(\boldsymbol{\Phi}_\ell\big)_{k,i} = \big(\boldsymbol{\varphi}_k(t_i)\big)$. Alors on a la relation suivante

$$\boldsymbol{y}^\ell = \boldsymbol{K}^\ell\boldsymbol{f}^\ell + \sigma\big({}^t\boldsymbol{\Phi}_\ell\boldsymbol{\Phi}_\ell\big)^{-1}{}^t\boldsymbol{\Phi}_\ell\boldsymbol{\eta}_n\,,$$

où $\boldsymbol{\eta}_n \sim \mathcal{N}(0, \boldsymbol{I}_n)$. Soit $P : [0, T_n] \to [0, T_n]$ une fonction strictement croissante et régulière tel que

$$P(0) = 0,\ \ P(T_n) = T_n \text{ et } P(t_i) = T_n\frac{i}{n}$$

Un calcul rapide montre alors que

$$\big({}^t\boldsymbol{\Phi}_\ell\boldsymbol{\Phi}_\ell\big)_{\ell,k} \sim \frac{n}{T_n}\int \boldsymbol{\varphi}_k(t)\boldsymbol{\varphi}_\ell(t)P'(t)dt\,,$$

de telle sorte que l'on peut reformuler (2.18) sous la forme suivante :

$$\boldsymbol{y}^\ell = \boldsymbol{K}^\ell \boldsymbol{f}^\ell + \sigma\sqrt{\frac{T_n}{n}}\boldsymbol{\xi}_\ell$$

où $\boldsymbol{\xi}_\ell \sim \mathcal{N}(0, \boldsymbol{\Omega}_\ell)$ et $\boldsymbol{\Omega}_\ell = nT_n^{-1}\left({}^t\boldsymbol{\Phi}_\ell\boldsymbol{\Phi}_\ell\right)^{-1}$. Dans un problème au design bien conditionné, on a $\boldsymbol{\Omega}_\ell \sim \boldsymbol{I}_{\ell+1}$.
Nous étendons de plus ce cadre à celui de la déconvolution aveugle en supposant que l'on n'observe non pas $\boldsymbol{k}$ mais une version bruitée $\dot{\boldsymbol{k}}_\delta = \dot{\boldsymbol{k}} + \delta\dot{\boldsymbol{b}}$ de $\dot{\boldsymbol{k}}$, où $\dot{\boldsymbol{b}}$ est un bruit blanc gaussien sur $\mathbb{L}^2(\mathbb{R}^+)$. Ces observations conduisent par projection sur l'espace des fonctions de Laguerre de degré inférieur à ℓ au modèle séquentiel suivant:

$$\begin{cases} \boldsymbol{y}^\ell & = \boldsymbol{K}^\ell \boldsymbol{f}^\ell + \sigma\sqrt{\frac{T_n}{n}}\boldsymbol{\xi}_\ell \\ \boldsymbol{K}_\delta^\ell & = \boldsymbol{K}^\ell + \delta\dot{\boldsymbol{B}}^\ell \end{cases} \tag{2.20}$$

Ici, $\dot{\boldsymbol{B}}^\ell$ est une matrice de Toeplitz triangulaire inférieure dont les entrées sont des normales $\mathcal{N}(0,1)$ i.i.d. Dans la suite, on notera $\varepsilon = \sigma\sqrt{T_n n^{-1}}$.

2.5.1 Hypothèses du modèle

En vue de la formulation d'algorithmes d'estimation, on considère les hypothèses suivantes sur le modèle:

Assumption 2.5.3 (Design). • *Il existe un entier n_0 tel que $nT_n^{-1} > \sigma$ pour tout $n \geqslant n_0$. De plus,*

$$\lim_{n\to\infty} T_n = \infty, \quad \textit{et} \lim_{n\to\infty} \frac{T_n}{n} = 0\,.$$

• *Pour un certain entier L (précisé ci-dessous), il existe $C \geqslant c > 0$, tel que*

$$\forall \ell \leqslant L,\ c \leqslant \|\boldsymbol{\Omega}_\ell\|_{op} \leqslant C\,.$$

Assumption 2.5.4 (Régularité de $\boldsymbol{f}$). *Il existe $s > 1/2$ tel que*

$$\boldsymbol{f} \in \mathcal{W}^s \triangleq \left\{ f \in \mathbb{L}^2(\mathbb{R}^+),\ \sum_{\ell\geqslant 0}(\ell+\frac{1}{2})^{2s}|\check{f}_\ell|^2 < \infty \right\}.$$

Assumption 2.5.5 (Degree of ill-posedness). *Soit $\boldsymbol{\gamma}_k = \langle(1/\dot{\boldsymbol{k}}), \boldsymbol{\varphi}_k\rangle$, de telle sorte que $(1/\dot{\boldsymbol{k}})(z) = \sum_{k\geqslant 0}\boldsymbol{\gamma}_k z^k$. Il existe $\nu > 0$, $Q_2, Q_1 > 0$, tel que pour tout $\ell \geqslant 0$,*

$$\sum_{k=0}^{\ell}\boldsymbol{\gamma}_k^2 \leqslant Q_2(\ell\vee 1)^{2\nu-1}\,, \tag{2.21}$$

$$\|(\boldsymbol{K}^\ell)^{-1}\|_{op} \geqslant Q_1(\ell\vee 1)^{\nu}\,. \tag{2.22}$$

On notera $\mathcal{K}_\nu(Q)$ l'ensemble des opérateurs vérifiant cette propriété.

2.5.2 Algorithme et vitesse de convergence

Nous allons mettre en place un algorithme IR afin d'estimer $\boldsymbol{f}$. On définit comme précédemment le niveau de résolution maximal

$$L = \lambda\Big(\varepsilon\sqrt{|\log\varepsilon|} \vee \delta|\log\delta|\Big)^{-1},$$

ainsi que les deux niveaux de seuillage

$$O_{\ell,\delta} = \kappa(\ell\log\ell \vee 1)\delta\sqrt{|\log\delta|}\,, \tag{2.23}$$

$$S_\ell = \begin{cases} \|(\boldsymbol{K}_\delta^\ell)^{-1}\|_{\mathrm{op}}(\ell\vee 1)^{-1/2}\Big(\tau_{sig}\varepsilon\sqrt{|\log\varepsilon|} \vee \tau_{\mathrm{op}}\delta|\log\delta|\Big) & \text{si } \|(\boldsymbol{K}_\delta^\ell)^{-1}\|_{\mathrm{op}} < O_{\ell,\delta}^{-1}\,, \\ +\infty & \text{si } \|(\boldsymbol{K}_\delta^\ell)^{-1}\|_{\mathrm{op}} \geqslant O_{\ell,\delta}^{-1}\,. \end{cases} \tag{2.24}$$

Pour $\ell \geqslant 0$, soit $\boldsymbol{\zeta}_\ell = \big\langle(\boldsymbol{K}_\delta^\ell)^{-1}\mathbf{1}_{\left\{\|(\boldsymbol{K}_\delta^\ell)^{-1}\|_{\mathrm{op}} < O_{\delta,l}^{-1}\right\}}\boldsymbol{y}^\ell, \boldsymbol{\varphi}_\ell\big\rangle$. L'estimateur $\widetilde{\boldsymbol{f}}$ de $\boldsymbol{f}$ est

$$\widetilde{\boldsymbol{f}} = \sum_{\ell\leqslant L} \boldsymbol{\zeta}_\ell \mathbf{1}_{\{|\boldsymbol{\zeta}_\ell| > S_\ell\}}\boldsymbol{\varphi}_\ell\,.$$

Ses performances sont résumées dans les deux théorèmes suivants.

Theorem 2.5.6 (Borne supérieure)**.** *Soit $M \geqslant 0$ et $s > 1/2$. Soit $\nu > 0$, $Q_2, Q_1 > 0$. Sous les conditions 2.5.3, pour κ, τ_{sig} et τ_{op} suffisamment grands,*

$$\sup_{\substack{\boldsymbol{f}\in\mathcal{W}^s(M)\\ \boldsymbol{K}\in\mathcal{K}_\nu(Q)}} \mathbb{E}\,\|\widetilde{\boldsymbol{f}} - \boldsymbol{f}\| \lesssim \Big(\delta|\log\delta|\Big)^{\frac{s}{s+\nu}} \vee \Big(\varepsilon\sqrt{|\log\varepsilon|}\Big)^{\frac{s}{s+\nu}}$$

où $\lesssim$ représente une inégalité à un facteur constant multiplicatif près, dépendant uniquement de $\lambda, \kappa, \tau_{sig}, \tau_{op}, s, M, \nu, Q_1, Q_2$.

Theorem 2.5.7 (Borne inférieure)**.** *Soit $s > 1/2$, $M \geqslant 0$, $\nu > 1/2$ et $Q_2 \geqslant c_\nu Q_1 > 0$. Ici c_ν est une constante dépendant de ν que nous ne chercherons pas à préciser. Alors*

$$\inf_{\tilde{f}} \sup_{\substack{f\in\mathcal{W}^s(M)\\ \boldsymbol{K}\in\mathcal{K}_\nu(Q)}} \mathbb{E}\,\|\tilde{\boldsymbol{f}} - \boldsymbol{f}\| \gtrsim \delta^{\frac{s}{s+\nu}}|\log\delta|^{-1} \vee \varepsilon^{\frac{s}{s+\nu}}|\log\varepsilon|^{-1}$$

où l'infimum est pris sur tout les estimateurs $\tilde{f}$ de f basés sur les observations (2.20)*.*

Ces deux théorèmes attestent donc de l'optimalité au sens minimax de la procédure pour une perte $\mathbb{L}^2$, à un facteur logarithmique près. Enfin, même si le cadre est dédié à la déconvolution de Volterra, les résultats se généralisent directement à n'importe quel problème inverse faisant intervenir une matrice de Galerkin triangulaire inférieure possédant la propriété de Toeplitz.

δ \ ε	0	10^{-3}	10^{-2}	3.10^{-2}
0	0	0.012	0.109	0.312
10^{-3}	0.005	0.012	0.108	0.301
10^{-2}	0.053	0.039	0.116	0.318
3.10^{-2}	0.118	0.109	0.145	0.324

Table 2.3: Erreur moyenne $\mathbb{L}^2$ renormalisée de la procédure.

2.5.3 Aspects pratiques

La mise en application du précédent algorithme requiert une précaution préliminaire. En effet, la bonne marche du Theorem 2.5.6 repose sur la validité de l'Assumption 2.5.3. De plus, la manipulation de polynômes de Laguerre de grand degré sur machine est sujette à une forte instabilité. Par conséquent, nous substituons au choix du niveau maximal le niveau maximal suivant, plus raisonnable en pratique

$$N = L \wedge \max\{\ell \geqslant 0 \text{ t.q. } \|\boldsymbol{\Omega}_\ell\|_{op} \leqslant \alpha\}\,,$$

où $\alpha > 1$ est un seuil préliminaire à fixer (ici fixé à 1.5). Etudions donc les performances pratiques de ce nouvel estimateur. On se propose dans un premier temps d'étudier l'interaction entre les deux types d'erreurs (en ε et en δ) dans le cas d'un design idéalement conditionné ($\boldsymbol{\Omega} = \boldsymbol{I}$), puis d'appliquer concrètement la procédure dans le cadre du problème de régression originel.
On ne considère donc dans un premier temps que l'influence de l'erreur en δ et ε sur la procédure, en imposant artificiellement $\boldsymbol{\Omega} = \boldsymbol{I}$. On applique la procédure aux données $\boldsymbol{f}_1(t) = (t - t^2)\exp(-t)$ et $\boldsymbol{k} = \boldsymbol{\varphi}_0$. Les constantes de seuillage sont $(\kappa, \tau_{sig}, \tau_{op}) = (0.3, 1, 0.1)$. On reporte les résultats dans le tableau 2.3, et on trace en Figure 2.3 le résultat de la procédure. Les résultats semblent indiquer que, même si les taux de convergence sont comparables dans le Theorem 2.5.6, en pratique l'erreur sur le signal a un effet plus prononcé que l'erreur sur l'opérateur.

Afin d'illustrer les performances de notre algorithme, on applique ensuite notre algorithme au problème initial 2.18. Nous avons représenté en Figure 2.4 le résultat de ce dernier, avec les paramètres suivants:

- Le design est constitué des points $t_i = \sum_{j=1}^{i}(\text{step} + |X_j|)$, $i \leqslant n$ où step est un pas fixe perturbé par la suite de variables gaussiennes $X_j \sim \mathcal{N}(0, 10^{-2})$. Les niveaux de bruit sont $\sigma = \delta = 5.10^{-2}$.

- La fonction $\boldsymbol{f}$ (resp. $\boldsymbol{k}$) est associée au polynôme $(1-z)^{1/2}$ (resp. $\boldsymbol{\varphi}_0$). Les valeurs observées sont donc les $\boldsymbol{y}(t_i) = \boldsymbol{g}(t_i) + \sigma\eta_i$ où $\boldsymbol{g}(z) = (1-z)^{3/2}$.

- Les paramètres utilisés, déterminés par la méthode présentée en section 2.2.2 sont $\kappa = 0.3$, $\tau_{sig} = 1$ et $\tau_{op} = 0.1$.

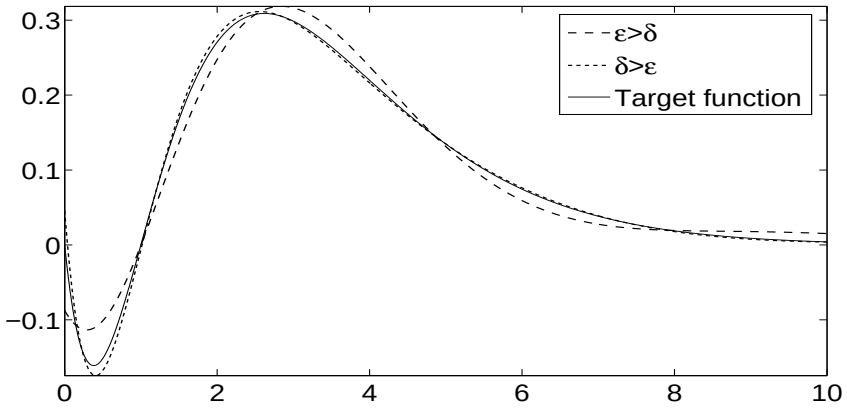

Figure 2.3: Estimation de $\boldsymbol{f}_1$ pour un bruit dans l'opérateur prédominant $(\delta, \varepsilon) = (10^{-2}, 10^{-3})$, puis pour un bruit dans le signal prédominant $(\delta, \varepsilon) = (10^{-3}, 10^{-2})$.

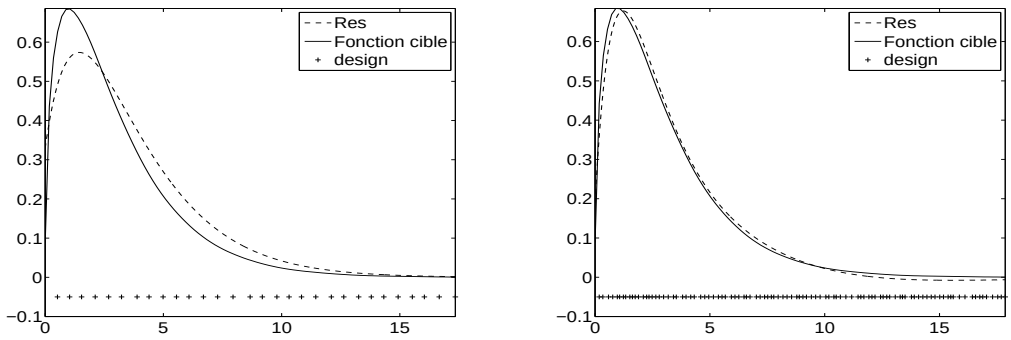

(a) $\begin{smallmatrix}\text{step}=5.10^{-1}; n=30\\ \text{Err}=0.177\end{smallmatrix}$ (b) $\begin{smallmatrix}\text{step}=10^{-1}; n=100\\ \text{Err}=0.133\end{smallmatrix}$

Figure 2.4: Résultat (Res) de la procédure appliquée au cadre de la régression. Ici, Err dénote l'erreur $\mathbb{L}^2$ renormalisée.

- Les coefficients de Fourier de $\boldsymbol{y}$ ont été estimés par une méthode des trapèzes.

La Figure 2.4 souligne l'influence de la qualité du design sur l'estimation de $\boldsymbol{f}$. En particulier, la concentration des points d'observations t_i autour de 0 a une influence prépondérante étant donnée la décroissance exponentielle des signaux observés.

2.6 Extension des opérateurs diagonaux par blocs au cas $\mathbb{L}^p$

Revenons au cas des opérateurs diagonaux par blocs, et plus précisément sur l'exemple de la déconvolution sphérique. Il est bien connu que qu'une perte de type $\mathbb{L}^2$, même

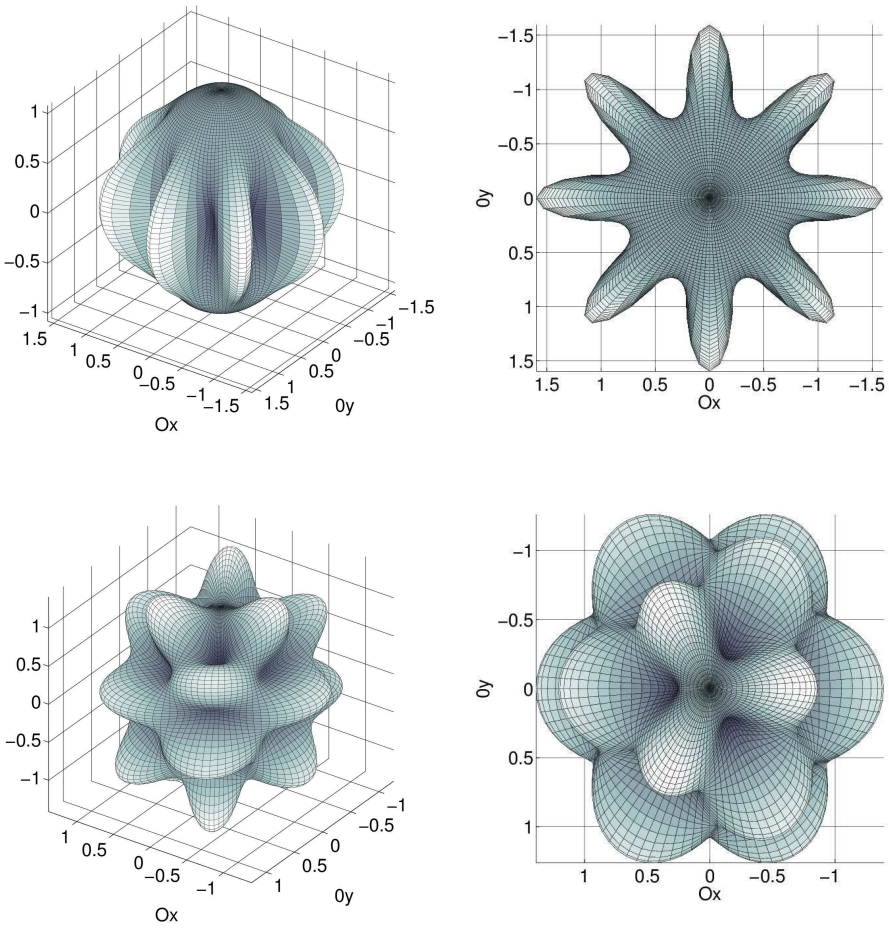

Figure 2.5: Vue de face et de haut des fonctions Y_1^8 (en haut) et Y_{12}^8 (en bas).

si elle constitue la perte la plus intuitive et la plus agréable à manipuler, ne rend pas efficacement compte de phénomènes spatiaux à l'échelle locale. En particulier, les harmoniques sphériques décrites en (1.10) présentent une localisation spatiale extrêmement pauvre, nous privant par là d'une analyse du type multi-résolution sur la sphère. Afin d'illustrer ces propos, nous avons disposé en Figure 2.5 les représentations graphiques des fonction Y_1^8 et Y_{12}^8.

D'autre part, le remède à ce phénomène compromettant est déjà connu dans le cas de la déconvolution 'directe' ($\delta = 0$). A partir d'une décomposition de Paley-Littlewood, Narcowich et al. [68] ont mis au point un système de fonctions sphériques, baptisées needlets pour leur forme en aiguille, et beaucoup plus aptes à représenter les signaux d'un point de vue local (voir Figure 2.6). De manière remarquable, ces fonctions conservent de surcroît les propriétés attrayantes des harmoniques sphériques dans le contexte des problèmes de déconvolution sphérique. Plus précisément, elles consistent en un réarrangement fréquentiel localisé de ces dernières, ce qui modifie

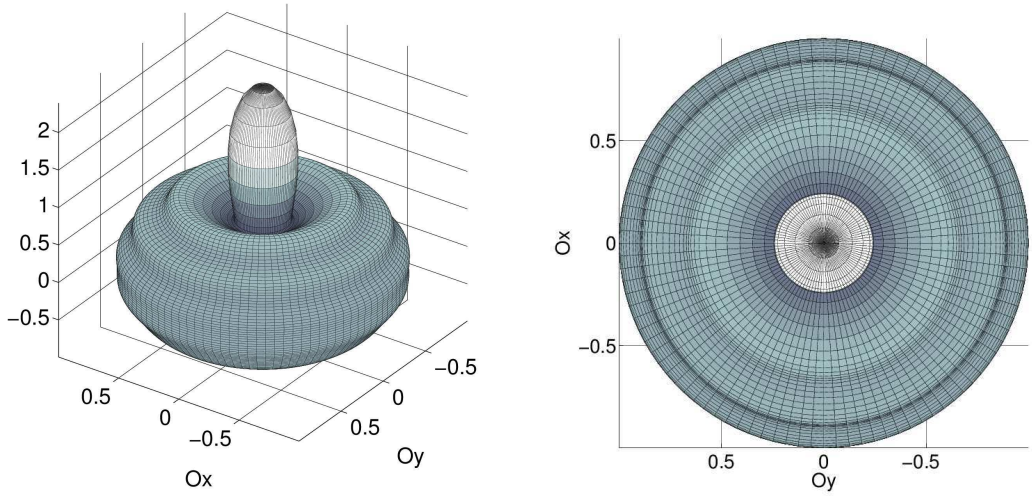

Figure 2.6: Vue de face et de haut d'une needlet de niveau 3 centrée autour du point $(0, 0, 1)$. La figure illustre la concentration de la needlet autour de son centre, ainsi que la propriété axisymétrique autour de l'axe Oz.

suffisamment peu la propriété de SVD par blocs pour les utiliser de manière efficace. Kerkyacharian et al. [51] ont donc tiré profit de ces avantages pour construire leur procédure d'estimation, optimale pour des pertes $\mathbb{L}^p$ sur des espaces de Besov $B^s_{\pi,q}$, dans le cas où $\boldsymbol{K}$ est connu.

Notre but est ici de tirer parti des needlets en adaptant la procédure précédente au cas d'un opérateur bruité. Le cadre défini en section 2.4 constitue un bon point de départ pour la prise en compte du bruit dans l'opérateur. Voyons ce que donne l'algorithme adapté: on définit

$$\hat{\boldsymbol{\beta}}_{j,\eta} = \langle \boldsymbol{Y}_\varepsilon, \boldsymbol{\psi}_{j,\eta} \rangle = \sum_{\ell=2^{j-1}}^{2^{j+1}} \langle \boldsymbol{Y}_{\varepsilon,\ell}, \boldsymbol{\psi}_{j,\eta,\ell} \rangle, \quad 2^J \sim \delta^{-1/(\nu+1/2)} \wedge \varepsilon^{-1/(\nu+1)} ,$$

$$\hat{\boldsymbol{Y}}_\varepsilon = \sum_{j=0}^{J} \sum_{\eta \in \mathcal{Z}_j} \hat{\boldsymbol{\beta}}_{j,\eta} \mathbf{1}_{\left\{|\hat{\boldsymbol{\beta}}_{j,\eta}| > \tau\varepsilon\sqrt{|\log\varepsilon|}\right\}} \boldsymbol{\psi}_{j,\eta}, \quad T_{op}(\boldsymbol{K}_\delta) = \sum_{\ell \leqslant 2^{J+1}} \boldsymbol{K}_{\delta,\ell} \mathbf{1}_{\left\{\|\boldsymbol{K}_{\delta,\ell}\|_{op} \leqslant O_{\ell,\delta}^{-1}\right\}} ,$$

et finalement

$$\tilde{\boldsymbol{f}} = T_{op}(\boldsymbol{K}_\delta)^{-1} \hat{\boldsymbol{Y}}_\varepsilon .$$

Malheureusement, cet algorithme possède de pauvres performances pratiques, même sur des cas très simples (opérateur diagonal). Nous listons ci-dessous plusieurs raisons qui nous ferons privilégier l'usage d'une procédure IR par rapport à une procédure RI.

- La raison principale de l'échec de cette procédure est l'incompatibilité du seuillage en aval sur $\boldsymbol{Y}_\varepsilon$ avec la régularisation $T_{op}(\boldsymbol{K}_\delta)$, contrairement au cas Fourier où la bonne marche de la procédure était garantie par la propriété de SVD par

blocs (voir le traitement du Term III dans la preuve du Theorem 3.3.1). En effet, là où un seuillage pratiqué sur $\|\boldsymbol{Y}_{\varepsilon,\ell}\|$ garantissait un seuillage en amont sur $\|\big(\boldsymbol{K}^{-1}\boldsymbol{Y}_{\varepsilon}\big)_{\ell}\|$, il n'y a aucune raison que cette propriété soit conservée au niveau des coefficients dans la base de needlets. En fait, chaque coefficient $\langle \boldsymbol{Y}_{\varepsilon}, \boldsymbol{\psi}_{j,\eta}\rangle$ fait intervenir tous les produits scalaires $\big(\langle \boldsymbol{K}^{-1}\boldsymbol{Y}_{\varepsilon}, \boldsymbol{\psi}_{h,\alpha}\rangle\big)_{\alpha\in\mathcal{Z}_h}$ pour $|h-j|\leqslant 1$.

- On pourrait donc être tenté d'utiliser également un seuillage par blocs dans l'idée de **BBD**, mais pratiqué dans la base de needlets à chaque niveau de résolution j. Ceci ne résout cependant pas le problème car la quantité $\sum_{\eta\in\mathcal{Z}_j}|\langle \boldsymbol{Y}_{\varepsilon}, \boldsymbol{\psi}_{j,\eta}\rangle|^2$ fait toujours intervenir les produits scalaires $\langle \boldsymbol{K}^{-1}\boldsymbol{Y}_{\varepsilon}, \boldsymbol{\psi}_{h,\alpha}\rangle$ pour $h=j-1, j+1$. De plus, l'efficacité d'un tel seuillage resterait confiné à une perte de type $\mathbb{L}^2$. L'une des propriétés remarquables des algorithmes d'estimation basés sur les needlets étant leur optimalité pour toute perte $\mathbb{L}^p$, $1\leqslant p\leqslant\infty$, nous ne voulons pas nous limiter à une seule d'entre elles.

- Comme nous l'avons déjà mentionné, les hypothèses nécessaires à la convergence d'un schéma de type IR sont moins contraignantes que pour une procédure RI. Nous allons voir que la procédure IR ne nécessite en effet qu'un contrôle (habituel) sur $\|\boldsymbol{K}_{\ell}^{-1}\|_{op}$.

- Ajoutons à cela que la procédure NEED-VD, décrite dans le Chapitre 5, et optimale dans le cas de la déconvolution sphérique avec opérateur connu, est une procédure de type IR. Il paraît donc naturel de requérir la même propriété pour l'algorithme de déconvolution avec opérateur bruité.

Nous nous tournons donc en conclusion vers un schéma de type IR avec un seuillage opéré coefficient par coefficient.

2.6.1 Needlets

Sans entrer dans les détails, rappelons les principales étapes de la construction des needlets. Une description plus détaillée est présentée au Chapitre 5. Tout d'abord, une décomposition de type Paley-Littlewood est appliquée aux noyaux des projecteurs $\boldsymbol{P}_{\mathbb{H}_\ell}$ sur les espaces $\mathbb{H}_\ell$. Ces noyaux étant eux même des polynômes, ils sont ensuite discrétisés (en espace) selon une formule de quadrature sur la sphère. Cette construction résulte en un système de fonctions $\boldsymbol{\psi}_{j,\eta}$ qui est 'presque' une base orthonormale (en particulier, deux needlets $\boldsymbol{\psi}_{j,\eta}$ et $\boldsymbol{\psi}_{h,\alpha}$ sont orthogonales si $|j-h|>1$), aux propriétés de concentration à la fois fréquentielles (par construction) mais également spatiales remarquables. En particulier, elles vérifient la propriété de type 'frame' suivante

$$\forall \boldsymbol{f}\in\mathbb{L}^2(\mathbb{S}^2),\ \|\boldsymbol{f}\|^2=\sum_{j\geqslant -1}\sum_{\eta\in\mathcal{Z}_j}\langle \boldsymbol{f}, \boldsymbol{\psi}_{j,\eta}\rangle^2\,,$$

ainsi que l'inégalité de concentration quasi-exponentielle

$$\forall k\geqslant 0, \exists C\geqslant 0 \text{ t.q. } \forall\omega\in\mathbb{S}^2,\ |\boldsymbol{\psi}_{j,\eta}(\omega)|\leqslant \frac{C2^{2j}}{\big(1+2^j d(\omega,\eta)\big)^k}\,, \tag{2.25}$$

où on a noté $d(.,.)$ la distance géodésique sur la sphère. Cette propriété en fait des outils adaptés à une analyse du type multi-résolution sur la sphère. Elles permettent également d'y introduire la notion d'espaces de Besov dans l'idée de ceux définis sur $\mathbb{R}^n$ (voir la section 5.2 ou de manière plus précise [68]).

2.6.2 Algorithme et résultats

Notre procédure est une schéma de type IR adapté à la base en question. Comme nous l'avons déjà mentionné, la matrice de $\boldsymbol{K}$ dans la base $\left(\boldsymbol{\psi}_{j,\eta}\right)_{j,\eta}$ est mal structurée (elle ressemble à la matrice dans la Figure 2.1, avec de plus des coefficients corrélés). De plus, les harmoniques sphériques, qui diagonalisent $\boldsymbol{K}$ par blocs, entrent naturellement dans l'expression des fonctions $\boldsymbol{\psi}_{j,\eta}$. Aussi, d'après l'égalité de Parseval et la propriété de SVD par blocs 1.11, le coefficient $\langle \boldsymbol{Kf}, \boldsymbol{\psi}_{j,\eta}\rangle$ se décompose de la manière suivante

$$\langle \boldsymbol{f}, \boldsymbol{\psi}_{j,\eta}\rangle = \sum_{\ell \in L_j} \langle \boldsymbol{K}_\ell^{-1}\left(\boldsymbol{Kf}\right)_\ell, \boldsymbol{\psi}_{j,\eta,\ell}\rangle_{\mathbb{R}^{2\ell+1}} ,$$

où on a noté L_j l'ensemble des entiers entre 2^{j-1} et 2^{j+1}. Il suffit alors d'introduire l'estimateur naturel de $\left(\boldsymbol{Kf}\right)_\ell$, à savoir $\boldsymbol{Y}_{\varepsilon,\ell}$, et l'estimateur naturel de $\boldsymbol{K}_\ell^{-1}$, à savoir $\boldsymbol{K}_{\ell,\delta}^{-1}$ combinés avec les procédures de seuillages adéquates.

Cadre de la procédure

Le cadre de la nouvelle procédure nécessite l'extension de la notion d'espace de Sobolev aux espaces de Besov, ainsi que la modification des hypothèses sur l'opérateur $\boldsymbol{K}$ afin d'opérer une méthode IR. On supposera donc que la fonction $\boldsymbol{f}$ vit dans un espace de Besov, dont une version plus détaillée est présente au Chapitre 5,

$$B^s_{\pi,r} = \left\{ \boldsymbol{f} \in L^\pi(\mathbb{S}^2),\ \left\| 2^{j(s+2(\frac{1}{2}-\frac{1}{\pi}))} \Big(\sum_{\eta \in \mathcal{Z}_j} |\langle \boldsymbol{f}, \boldsymbol{\psi}_{j,\eta}\rangle|^\pi \Big)^{1/\pi} \right\|_{\ell^r} < \infty \right\}.$$

Quant à l'opérateur $\boldsymbol{K}$, on supposera qu'il vérifie les conditions suivantes:

Assumption 2.6.1. *Il existe $\nu \geqslant 0$, $Q_1, Q_2 \geqslant 0$ tel que, pour tout $\ell \in \mathbb{N}$,*

$$Q_1(\ell \vee 1)^\nu \leqslant \|\boldsymbol{K}_\ell^{-1}\|_{op} \leqslant Q_2(\ell \vee 1)^\nu . \tag{2.26}$$

On notera $\mathcal{K}_\nu(Q_1, Q_2)$ l'ensemble des opérateurs satisfaisant à ces deux conditions.

Définition de la procédure BND

Supposons que Assumption 3.2.2 est vérifiée, et définissons le niveau maximal J par

$$2^J = \lambda \lfloor \left(\varepsilon \sqrt{|\log \varepsilon|}\right)^{-1} \wedge \left(\delta \sqrt{|\log \delta|}\right)^{-2} \rfloor , \tag{2.27}$$

pour un paramètre positif λ. On conserve la procédure de seuillage de l'opérateur de la section 2.4. Pour $j \in \mathbb{N}$, soit

$$\ell_j = \min\{\ell \in L_j,\ T_{op}\big(\boldsymbol{K}_{\delta,\ell}\big) \neq 0\}$$

(avec la convention $\min \varnothing = +\infty$), et, pour des constantes positives κ et τ_{sig}, τ_{op},

$$O_{\ell,\delta} = \kappa\sqrt{2\ell+1}\delta\sqrt{|\log\delta|}\,, \tag{2.28}$$

$$S_j(\delta,\varepsilon) = \begin{cases} \|\boldsymbol{K}_{\delta,\ell_j}^{-1}\|_{op}\Big(\tau_{sig}\varepsilon\sqrt{|\log\varepsilon|} \vee \tau_{op}2^{-j/2}\delta\sqrt{|\log\delta|}\Big) & \text{si } \ell_j < \infty\,, \\ +\infty & \text{si } \ell_j = +\infty\,. \end{cases} \tag{2.29}$$

Notre estimateur $\tilde{\boldsymbol{f}}$ de $\boldsymbol{f}$ est défini par

$$\tilde{\boldsymbol{f}} = \sum_{j\leqslant J}\sum_{\eta\in\mathcal{Z}_j} \hat{\boldsymbol{\beta}}_{j,\eta}\mathbf{1}_{\left\{|\hat{\boldsymbol{\beta}}_{j,\eta}|>S_j(\delta,\varepsilon)\right\}}\boldsymbol{\psi}_{j,\eta} \text{ où } \hat{\boldsymbol{\beta}}_{j,\eta} = \sum_{\ell=2^{j-1}}^{2^{j+1}} \big\langle (\boldsymbol{K}_{\delta,\ell})^{-1}\mathbf{1}_{\left\{\|(\boldsymbol{K}_{\delta,\ell})^{-1}\|\leqslant O_{\ell,\delta}^{-1}\right\}}\boldsymbol{Y}_{\varepsilon,\ell}, \boldsymbol{\psi}_{j,\eta,\ell}\big\rangle\,.$$

On appelle **BND** (pour Blind Deconvolution using Needlets) cette procédure.

Performances théoriques et pratiques

Theorem 2.6.2. *Soit $\pi \geqslant 1$, $s > 2/\pi$, $r \geqslant 1$ et $M > 0$. Soit $\nu \geqslant 0$, $Q_1 \geqslant Q_2 > 0$. Alors pour κ et τ_{sig}, τ_{op} suffisamment grands, pour tout $p \in [1, +\infty[$,*

$$\sup_{\boldsymbol{f}\in B^s_{\pi,r}(M),\boldsymbol{K}\in\mathcal{K}_\nu(Q_1,Q_2)} \mathbb{E}\,\|\tilde{\boldsymbol{f}} - \boldsymbol{f}\|_p^p \lesssim (|\log\varepsilon|)^{p-1}(\varepsilon\sqrt{|\log\varepsilon|})^{p\mu(2)} \vee (|\log\delta|)^{p-1}(\delta\sqrt{|\log\delta|})^{p\mu(1)} \tag{2.30}$$

où $\lesssim$ signifie inégalité à une constante multiplicative près ne dépendant que de $p, s, \pi, r, M, \nu, Q_1, Q_2, \lambda, \kappa, \tau_{sig}$ et τ_{op}, et où les éléments $\mu(d)$ sont définis pour $d \in \mathbb{N}$ par

$$\mu(d) = \begin{cases} \frac{s}{s+\nu+\frac{d}{2}} & si\ s > (\nu+\frac{d}{2})(\frac{p}{\pi}-1) \\ & ou\ s = (\nu+\frac{d}{2})(\frac{p}{\pi}-1)\ et\ r \leqslant \pi\,, \\ \frac{s-2/\pi+2/p}{s-2/\pi+\nu+\frac{d}{2}} & si\ \frac{2}{\pi} < s < (\nu+\frac{d}{2})(\frac{p}{\pi}-1)\,. \end{cases}$$

Theorem 2.6.3. *Sous les hypothèses du Theorem 2.6.2,*

$$\sup_{f\in B^s_{\pi,r}(M),\boldsymbol{K}\in\mathcal{K}_\nu(Q_1,Q_2)} \mathbb{E}\,\|\tilde{\boldsymbol{f}} - \boldsymbol{f}\|_\infty \lesssim \sqrt{|\log\varepsilon|}(\varepsilon\sqrt{|\log\varepsilon|})^{\mu'(2)} \vee \sqrt{|\log\delta|}(\delta\sqrt{|\log\delta|})^{\mu'(1)}\,, \tag{2.31}$$

où

$$\mu'(d) = \frac{s-2/\pi}{s-2/\pi+\nu+\frac{d}{2}}\,.$$

δ	ε	$E\|\tilde{\boldsymbol{f}} - \boldsymbol{f}\|_2$		$E\|\tilde{\boldsymbol{f}} - \boldsymbol{f}\|_\infty$	
		BBD	**BND**	**BBD**	**BND**
3.10^{-3}	10^{-3}	0.2210	0.1695	0.3867	0.3464
	10^{-4}	0.1013	0.1603	0.2146	0.3374
10^{-3}	10^{-3}	0.2195	0.1242	0.3870	0.2204
	10^{-4}	0.0839	0.0594	0.1931	0.1569
10^{-4}	10^{-3}	0.2194	0.1267	0.3863	0.2257
	10^{-4}	0.0825	0.0584	0.1924	0.1571

Table 2.4: Average normalized $\mathbb{L}^2$ and $\mathbb{L}^\infty$ loss of **BBD** and **BND**.

Nous avons ainsi généralisé les résultats de Kerkyacharian et al. [51] au cas de la déconvolution aveugle. Dans le cas où l'opérateur est connu, la procédure, ainsi que le théorème de convergence, sont en effet identiques. Cela n'aurait pas été le cas si nous avions voulu appliquer une procédure RI.
Remarquons également que l'on retrouve dans les taux de convergence en δ et ε le même différentiel dimensionnel que celui observé dans le Chapitre 3. En effet, l'erreur en ε correspond à un problème en dimension 2, alors que l'erreur en δ correspond elle à un problème en dimension 1 (la 'dimension' d'un bloc).
Enfin, cet algorithme et ses résultats se transcrivent au cas générique d'une SVD par blocs, lorsque le système de needlets construit à l'aide de la décomposition de Paley-Littlewood sur les fonctions propres de l'opérateur jouit de propriétés similaires à (2.25). Dans ce cas, l'entier intervenant dans le taux de convergence en δ est remplacé par la dimension des blocs (c'est-à-dire l'entier k tel que $|\Lambda_\ell| \sim \ell^k$). Plusieurs exemples d'applications sont mentionnés en section 6.2.1.
Nous avons comparé les performances pratiques de cette procédure (que nous noterons **BND**) avec celle développée dans le Chapitre 3 (que nous noterons **BBD**). En particulier, les paramètres choisis sont les suivants:

- La fonction cible est la fonction en pic $\boldsymbol{f}(\omega) = \exp(-2\|\omega - \omega_1\|_{\ell^1(\mathbb{R}^3)})$ où $\omega_1 = (0,1,0)$.
- L'opérateur est un opérateur de Rosenthal (voir Chapitre 6 pour une définition) de DIP $\nu = 1$.
- Les constantes de seuillage, déterminées par la méthode décrite en 2.2.2 sont : $\kappa = 0.8$ puis, pour **BBD**, $(\tau_{sig}, \tau_{op}) = (0.6, 0.1)$ et pour **BND**, $(\tau_{sig}, \tau_{op}) = (0.9, 0.2)$.

On reporte dans le tableau 2.4 les pertes moyennes quadratiques ainsi qu'en norme infinie (calculées sur une grille de 4096 points, à partir d'une méthode de Monte-Carlo à 200 observations) pour certaines valeurs de (δ, ε) et on représente en Figure 2.7 les résultats des deux algorithmes pour $(\delta, \varepsilon) = (10^{-3}, 10^{-4})$.

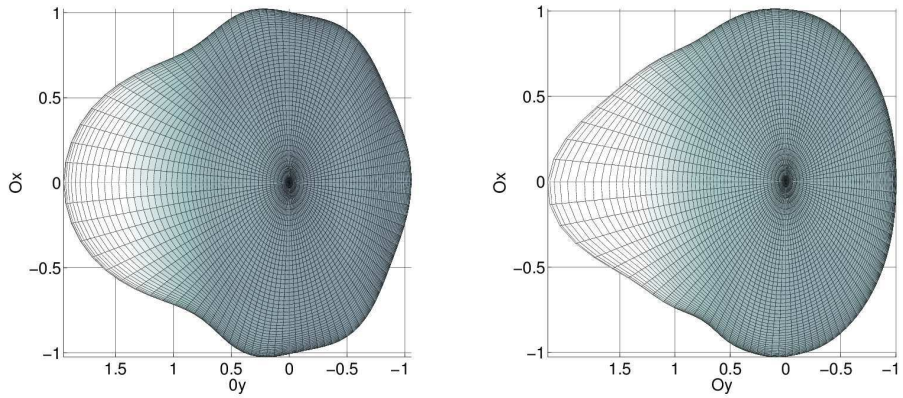

(a) **BBD** (b) **BND**

Figure 2.7: Résultats des deux algorithmes pour $(\delta, \varepsilon) = (10^{-3}, 10^{-4})$.

Les résultats confirment clairement nos attentes : lorsque $\varepsilon > \delta$, les performances des needlets surpassent celles de la base de Fourier, que ce soit en norme $\mathbb{L}^2$ ou $\mathbb{L}^\infty$, alors que dans le cas où $\delta \gg \varepsilon$, **BBD** l'emporte sur **BND**. Ceci est dû au fait que l'opérateur de Rosenthal $\boldsymbol{K}$ satisfait également la condition (2.12), et par conséquent les résultats de convergence établis en section 2.4.2 s'appliquent. Le choix $\boldsymbol{K} = \boldsymbol{K}^{IR}$ aurait évidemment accentué ces différences de performances.

Chapter 3

Blockwise SVD with error in the operator and application to blind deconvolution

This chapter is the replica of an article written in collaboration with Sylvain Delattre, Marc Hoffmann and Dominique Picard, and submitted to a scientific review. It can be read independently from the rest of the manuscript.

Abstract: We consider linear inverse problems in a nonparametric statistical framework. Both the signal and the operator are unknown and subject to error measurements. We establish minimax rates of convergence under squared error loss when the operator admits a blockwise singular value decomposition (blockwise SVD) and the smoothness of the signal is measured in a Sobolev sense. We construct a nonlinear procedure adapting simultaneously to the unknown smoothness of both the signal and the operator and achieving the optimal rate of convergence to within logarithmic terms. When the noise level in the operator is dominant, by taking full advantage of the blockwise SVD property, we demonstrate that the block SVD procedure overperforms classical methods based on Galerkin projection [30] or nonlinear wavelet thresholding [40]. We subsequently apply our abstract framework to the specific case of blind deconvolution on the torus and on the sphere.

Contents

3.1 Introduction **56**

3.2 Estimation by blockwise SVD **58**

3.3 Main results **60**

3.4 Application to blind deconvolution **64**

3.5 Proofs **71**

3.1 Introduction

3.1.1 Motivation

Consider the following idealised statistical problem: estimate a function f (a signal, an image) from data

$$y_n = Kf + n^{-1/2}\dot{W}, \tag{3.1}$$

where

$$K : \mathbb{H} \to \mathbb{G}$$

is a linear operator between two Hilbert spaces $\mathbb{H}$ and $\mathbb{G}$. The observation of the unknown $f \in \mathbb{H}$ is challenged by the action of the linear degradation K as well as contaminated by an experimental Gaussian white noise $\dot{W}$ on $\mathbb{G}$ with vanishing noise level $n^{-1/2}$ as $n \to \infty$. Alternatively, in a density estimation setting, we observe a random sample $(Z_1, \ldots, Z_n)$ drawn from a probability distribution[1] with density Kf. In each case, we do not know the operator K exactly, but we have access to

$$K_\delta = K + \delta\dot{B}, \tag{3.2}$$

where $\dot{B}$ is a Gaussian white noise on $\mathbb{H} \times \mathbb{G}$ thanks to preliminary experiments or calibration through trial functions. This setting has been discussed in details in [30, 40]. In this paper, we are interested in operators K admitting a singular value decomposition (SVD) or a blockwise SVD. In essence, we know the typical eigenfunctions of K but not the eigenvalues. We cover two specific examples of interest: spherical and circular deconvolution.

Spherical deconvolution. Used for the analysis of data distributed on the celestial sphere, see Section 3.4.1 below. One observes a random sample $(Z_1, \ldots, Z_n)$ with

$$Z_i = \varepsilon_i X_i, \quad i = 1, \ldots, n$$

where the ε_i are random elements in SO(3), the group of 3×3 rotation matrices, and the X_i are independent and identically distributed on the sphere $\mathbb{S}^2$, with common density f with respect to the uniform probability distribution μ on $\mathbb{S}^2$. In this setting, if the ε_i have common density g with respect to the Haar measure du on SO(3), we have

$$Kf(x) = g \star f(x) = \int_{\mathrm{SO}(3)} g(u) f(u^{-1}x) du, \quad x \in \mathbb{S}^2.$$

We are interested in the case where the exact form g is unknown. However, K is block-diagonal in the spherical harmonic basis. □

[1] In that setting, Kf must therefore also be a probability density .

Circular deconvolution. Used for restoring signal or images, see Section 3.4.2 below. We take $\mathbb{H} = \mathbb{G} = \mathbb{L}^2(\mathbb{T})$ the space of square integrable functions on the torus $\mathbb{T} = [0,1]$ (or $[0,1]^d$) appended with periodic boundary conditions. We have

$$Kf(x) = g \star f(x) = \int_{\mathbb{T}} g(u) f(x-u) du, \quad x \in \mathbb{T}.$$

The degradation process $K = g \star \cdot$ is characterised by the impulse response function g which we do not know exactly. However, K is diagonal in the Fourier basis. □

Although the problem of estimating f is fairly classical and well understood when K is known (a selected literature is [81, 13, 26, 2, 17, 44, 50] and the references therein), only moderate attention has been paid in the case of an unknown K despite its relevance in practice. When the eigenfunctions of K are known solely, we have the results of Cavalier and Hengartner [11], Cavalier and Raimondo [12] but they are confined to the case where the error in the operator is negligible $\delta \ll n^{-1/2}$. In a general setting with error in the operator, Efromovitch and Kolchinskii [30] and later Hoffmann and Reiß [40] studied the recovery of f when the eigenfunctions and eigenvalues of K are unknown. In both contributions, a marginal attention is paid to the case of sparse or diagonal operators, but it is showed in both papers that unusual rates of convergence can be obtained when $n^{-1/2} \ll \delta$. In a univariate setting, Neumann [70] and Comte and Lacour [18] consider the case of deconvolution with an error density, known only through an auxiliary set of m learning data. This formally corresponds to having $\delta = m^{-1/2}$ in our setting. Minimax rates and adaptive estimators are derived in both regimes $m \ll n$ and $n \ll m$. We address in the paper the following program:

i) Construction of a feasible procedure $\widehat{f}_{n,\delta}$ estimating f from data (3.1) and (3.2) that achieves optimal rates of convergence (up to inessential logarithmic terms). We require $\widehat{f}_{n,\delta}$ to be adaptive with respect to smoothness constraints on f and K.

ii) Identification of best achievable accuracy for f under smoothness constraints on f and K so that the interplay between $n^{-1/2}$ and δ can be explicitly related in the asymptotic $\delta \to 0$ and $n \to \infty$; this includes the comparison with earlier results of [70, 30, 40] in the context of blockwise SVD.

iii) Application to spherical deconvolution on $\mathbb{S}^2$ or circular deconvolution on the torus; this includes the discussion of our findings in terms of the existing literature on the topic [12, 51, 52] and some practical aspects of numerical implementation.

3.1.2 Main results and organisation of the paper

In Section 3.2, we present an abstract framework that allows for operators K to admit a so-called blockwise SVD. This property is simply turned into the existence of pairs of increasing finite dimensional spaces $(H_\ell,\ G_\ell)$ that are stable under the action of K. The

blockwise SVD property is further appended with a smoothness condition quantified by the arithmetic decay of the operator norm of K and its inverse on H_ℓ (resp. G_ℓ) (the so-called *ordinary smooth* assumption, see *e.g.* [81]). By means of a reconstruction formula, we obtain in Section 3.2.2 an estimator $\widehat{f}_{n,\delta}$ of f by first inverting K_δ on H_ℓ with a thresholding tuned with δ and then filter the resulting signal by a block thresholding tuned with $n^{-1/2}$. As for i) and ii), we establish in Theorems 3.3.1 and 3.12 of Section 3.3 the minimax rates of convergence for Sobolev constraints on f under squared error loss and we demonstrate that $\widehat{f}_{n,\delta}$ is optimal and adaptive to within logarithmic terms. The explicit interplay between δ and $n^{-1/2}$ is revealed and discussed in the case of sparse operator when $n^{-1/2} \ll \delta$, completing earlier findings in [30, 40] and to some extent [70] in the univariate case for density deconvolution. In particular, we demonstrate that a certain parametric regime dominates when the smoothness of the signal dominates the smoothing properties of the operator. Concerning iii), the method is applied to the case of spherical and circular deconvolution in Section 3.4 where harmonic Fourier analysis enables to provide explicit blockwise SVD for the convolution operator. We illustrate the numerical feasability of $\widehat{f}_{n,\delta}$ and the phenomena that appear in the case $n^{-1/2} \ll \delta$. Section 3.5 is devoted to the proofs.

We choose to state and prove our results in the white Gaussian model generated by the observation of y_n and K_δ defined by (3.1) and (3.2). The extension to the case of density estimation, when y_n is replaced by the observation of a random sample of size n drawn from the distribution Kf, like for instance in [70, 18] is a bit more involved, due to the intrinsic heteroscedasticity that appears when enforcing a formal analogy with the Gaussian setting (3.1). It is briefly addressed in the discussion Section 3.3.2

3.2 Estimation by blockwise SVD

3.2.1 The blockwise SVD property

Let $\mathcal{G}$ denote a family of linear operators

$$K : \mathbb{H} \to \mathbb{G}$$

between two Hilbert spaces $\mathbb{H}$ and $\mathbb{G}$ that shall represent our parameter set of unknown K.

A fundamental property (Assumption 3.2.1 below) is that an explicit singular value decomposition (SVD) or blockwise SVD is known for all $K \in \mathcal{G}$ simultaneously. More specifically, we suppose that there exist two explicitly known bases $(e_\lambda,\ \lambda \in \Lambda)$ of $\mathbb{H}$ and $(g_\lambda,\ \lambda \in \Lambda)$ of $\mathbb{G}$, as well as a partition of $\Lambda = \cup_{\ell \geqslant 1} \Lambda_\ell$ with $\Lambda_\ell \cap \Lambda_{\ell'} = \varnothing$ if $\ell \neq \ell'$, and a constant $d \geqslant 1$ such that:

$$\ell^{d-1} \lesssim |\Lambda_\ell| \lesssim \ell^{d-1},$$

where $\lesssim$ means inequality up to a multiplicative constant that does not depend on ℓ. Here $|\Lambda_\ell| = \mathrm{Card}(\Lambda_\ell)$.

It is worthwhile to notice that in our examples as well as in the rates of convergence that we will exhibit later, d plays the role of a dimension. In particular, $d = 1$ corresponds to a 'standard SVD', whereas $d > 1$ creates blocks and deserves the name of 'blockwise' SVD. However, there is no need in the paper to assume that d is in $\mathbb{N}$. Set

$$H_\ell = \mathrm{Span}\{e_\lambda, \lambda \in \Lambda_\ell\} \text{ and } G_\ell = \mathrm{Span}\{g_\lambda, \lambda \in \Lambda_\ell\}.$$

The Galerkin projection of an operator $T : \mathbb{H} \to \mathbb{G}$ onto (H_ℓ, G_ℓ) is defined by $T_\ell = P_\ell T_{|H_\ell}$, where P_ℓ is the orthogonal projector onto G_ℓ.

Assumption 3.2.1 (Blockwise SVD)**.**

$$K_{|H_\ell} = K_\ell \quad \textit{for every } K \in \mathcal{G}, \ell \geqslant 1.$$

We further need to quantify the action of K on H_ℓ. We denote by $\|T_\ell\|_{H_\ell \to G_\ell} = \sup_{v \in H_\ell, \|v\|_{\mathbb{H}}=1} \|T_\ell v\|_{\mathbb{G}}$ the operator norm of T_ℓ.

Assumption 3.2.2 (Spectral behaviour of $K_{|H_\ell}$)**.** *For every $\ell \geqslant 1$, K_ℓ is invertible and there exists $\nu \geqslant 0$ such that*

$$Q_1(K) = \sup_{\ell \geqslant 1} \ell^{-\nu} \|(K_\ell)^{-1}\|_{G_\ell \to H_\ell} < \infty$$

and

$$Q_2(K) = \sup_{\ell \geqslant 1} \ell^{\nu} \|K_\ell\|_{H_\ell \to G_\ell} < \infty$$

for every $K \in \mathcal{G}$.

We associate with the bases $(e_\lambda, \lambda \in \Lambda)$ and $(g_\lambda, \lambda \in \Lambda)$ the following decompositions

$$f = \sum_{\ell \geqslant 1} \sum_{\lambda \in \Lambda_\ell} \langle f, e_\lambda \rangle e_\lambda, \quad g = \sum_{\ell \geqslant 1} \sum_{\lambda \in \Lambda_\ell} \langle g, g_\lambda \rangle g_\lambda \quad \text{for every } \ f \in \mathbb{H}, \ g \in \mathbb{G},$$

where $\langle \cdot, \cdot \rangle$ denotes the inner product either in $\mathbb{H}$ or $\mathbb{G}$ and the scale of Sobolev spaces

$$\mathcal{W}^s = \Big\{ f \in \mathbb{H}, \ \ \|f\|^2_{\mathcal{W}^s} = \sum_{\ell \geqslant 1} \ell^{2s} \sum_{\lambda \in \Lambda_\ell} \langle f, e_\lambda \rangle^2 < \infty \Big\}, \ \ s \in \mathbb{R}, \tag{3.3}$$

$$\tilde{\mathcal{W}}^s = \Big\{ g \in \mathbb{G}, \ \ \|g\|^2_{\tilde{\mathcal{W}}^s} = \sum_{\ell \geqslant 1} \ell^{2s} \sum_{\lambda \in \Lambda_\ell} \langle g, g_\lambda \rangle^2 < \infty \Big\}, \ \ s \in \mathbb{R}\,.$$

For $\nu \geqslant 0$, Assumption 3.2.2 implies that $K : \mathcal{W}^{-\nu/2} \to \tilde{\mathcal{W}}^{\nu/2}$ is continuous. In particular, when $\nu > 0$, the operator K is ill-posed with degree ν, see for instance [71].

3.2.2 Blockwise SVD reconstruction with noisy data

Under Assumption 3.2.1 and 3.2.2, we have the reconstruction formula

$$f = \sum_{\ell \geqslant 0} (K_\ell)^{-1} \sum_{\lambda \in \Lambda_\ell} \langle Kf, g_\lambda \rangle \, e_\lambda. \tag{3.4}$$

By the observed blurred version K_δ of K in (3.2), we obtain a family of estimators of $(K_\ell)^{-1}$ from data (3.2) by considering the operator

$$\mathbf{1}_{\left\{ \|(K_{\delta,\ell})^{-1}\|_{G_\ell \to H_\ell} \leqslant \kappa \right\}} (K_{\delta,\ell})^{-1}, \tag{3.5}$$

where $\kappa > 0$ is a cutoff level, possibly depending on ℓ. Likewise, the coefficient $\langle Kf, g_\lambda \rangle$ can be estimated by

$$z_{n,\lambda} := \langle y_n, g_\lambda \rangle. \tag{3.6}$$

Mimicking the reconstruction formula (3.4) with the estimates (3.6) and (3.5), we finally obtain a (family of) estimator(s) of f by setting

$$\widehat{f}_{n,\delta} = \sum_{0 \leqslant \ell \leqslant L} \big(K_{\delta,\ell}\big)^{-1} \Big(\sum_{\lambda \in \Lambda_\ell} z_{n,\lambda} e_\lambda \mathbf{1}_{\left\{ \sum_{\lambda \in \Lambda_\ell} z_{n,\lambda}^2 \geqslant \tau_\ell^2 \right\}} \Big) \mathbf{1}_{\mathcal{E}_{\delta,\ell}(\kappa_\ell)}$$

where

$$\mathcal{E}_{\delta,\ell}(\kappa_\ell) = \big\{ \|(K_{\delta,\ell})^{-1}\|_{G_\ell \to H_\ell} \leqslant \kappa_\ell \big\}.$$

The procedure is specified by the maximal frequency level L and the threshold levels

$$\kappa_\ell = \Big(\lambda_0 |\Lambda_\ell|^{-1/2} \big(\delta^2 |\log \delta| \big)^{-1/2} \Big) \bigwedge n^{1/2} \tag{3.7}$$

and

$$\tau_\ell = \mu_0 |\Lambda_\ell|^{1/2} \big(n^{-1} \log n \big)^{1/2}, \tag{3.8}$$

for some prefactors $\lambda_0, \mu_0 > 0$. The threshold rule we introduce in both the signal (with level τ_ℓ) and the operator (with level κ_ℓ) is inspired by classical block thresholding [38, 10, 9] and will enable to adapt with respect to the smoothness properties of both the signal f and the operator K, see below.

3.3 Main results

3.3.1 Minimax rates of convergence

We assess the performance of the estimator $\widehat{f}_{n,\delta}$ defined in Section 3.2.2 over the Sobolev spaces linked to the basis $(e_\lambda, \lambda \in \Lambda)$ defined in (3.3). Define the Sobolev balls $\mathcal{W}^s(M) = \{f \in \mathcal{W}^s, \ \|f\|_{\mathcal{W}^s} \leqslant M\}$ for $M > 0$ and let

$$\mathcal{G}^\nu(Q) = \big\{ K \in \mathcal{G}, \ \ Q_i(K) \leqslant Q_i, i = 1, 2 \big\}. \tag{3.9}$$

for $Q = (Q_1, Q_2)$ with $Q_1 > 0$, $Q_1 Q_2 \geqslant 1$, where the mapping constants $Q_i(K)$ are defined in Assumption 3.2.2.

Theorem 3.3.1 (Upper bounds). *Let $\mathcal{G}$ be a class of operators satisfying Assumptions 3.2.1 and 3.2.2. Assume we observe (y_n, K_δ) given by (3.1) and (3.2), with $n \geqslant 1$ and $\delta \leqslant \delta_0 < 1$. Specify $\widehat{f}_{n,\delta}$ with*

$$L = \lfloor (\delta^2)^{-1/(2\nu+d-1)} \rfloor \bigwedge \lfloor n^{1/(2\nu+d)} \rfloor \tag{3.10}$$

and κ_ℓ, τ_ℓ as in (3.7) and (3.8). For sufficiently small λ_0 and sufficiently large μ_0, for every $s, M > 0$, $Q = (Q_1, Q_2)$ with $Q_1 > 0$ and such that $Q_1 Q_2 \geqslant 1$, we have

$$\begin{aligned} &\sup_{f \in \mathcal{W}^s(M), K \in \mathcal{G}^\nu(Q)} \mathbb{E}\left[\left\| \widehat{f}_{n,\delta} - f \right\|_{\mathbb{H}}^2 \right] \\ &\lesssim \left(\delta^2 |\log \delta|\right)^{1 \bigwedge 2s/(2\nu+d-1)} \bigvee \left(n^{-1} \log n\right)^{2s/(2(s+\nu)+d)} \end{aligned} \tag{3.11}$$

where $\lesssim$ means inequality up to a multiplicative constant that depends on d, s, ν, M, Q and μ_0, λ_0 only.

The bounds for μ_0 and λ_0 are explicitly computable. In the model generated by y_n in (3.1) and K_δ in (3.2), they depend on the dimension d and on the absolute constants c_0 and c_1 of the concentration lemmas 3.21 and 3.24 below. However, they are in practice much too conservative, as is well known in the signal detection case [29] or the classical inverse problem case [2], see the numerical implementation Section 3.4.

Our next result shows that the rate achieved by $\widehat{f}_{n,\delta}$ is indeed optimal, up to logarithmic terms. The lower bound in the case $\delta = 0$ is classical (Nussbaum and Pereverzev [71]) and will not decrease for increasing noise levels δ or $n^{-1/2}$ whence it suffices to provide the case which formally corresponds to observing Kf without noise while K remains unknown.

Theorem 3.3.2 (Lower bounds). *In the same setting as Theorem 3.3.1, with in addition $Q_2 > 1/Q_1$, assume we observe Kf exactly and K_δ given by (3.2). For sufficiently small δ, we have*

$$\inf_{\widehat{f}} \sup_{f \in \mathcal{W}^s(M), K \in \mathcal{G}^\nu(Q)} \mathbb{E}\left[\left\| \widehat{f} - f \right\|_{\mathbb{H}}^2 \right] \gtrsim \left(\delta^2\right)^{1 \bigwedge 2s/(2\nu+d-1)} \tag{3.12}$$

where $\gtrsim$ means inequality up to a positive multiplicative constant that depends on d, s, ν, M and Q only.

Combining (3.11) together with (3.12) and the results of [71], we conclude that $\widehat{f}_{n,\delta}$ is minimax over $\mathcal{W}^s(M)$ to within logarithmic terms in n and δ, and that this result is uniform over the nuisance parameter $K \in \mathcal{G}^\nu(Q)$.

3.3.2 Discussion

The case of diagonal operators

It is interesting to notice that the condition $Q_2 > 1/Q_1$ in Theorem 3.3.2 excludes the case where K is diagonal. In this particular case, considered especially in the

deconvolution example of Section 3.4.2 below, a closer inspection of the proof of the upper bound shows that the rate

$$n^{-s/(2(s+\nu)+d)} \bigvee \delta^{1 \wedge s/\nu}$$

can be obtained (up to some extra logarithmic factors) as in the case where $d = 1$, which improves on the rate

$$n^{-s/(2(s+\nu)+d)} \bigvee \delta^{1 \wedge 2s/(2\nu+d-1)}$$

provided by Theorem 3.3.1. This sheds some light on the role of the number d. It is in fact twofolds: it acts as a 'dimension' in the term $n^{-2s/(2(s+\nu)+d)}$; in the term involving error in the operator δ, it reflects the distance to the diagonal case expanding from $\delta^{1 \wedge s/\nu}$ in the diagonal case, to $\delta^{1 \wedge 2s/(2\nu+d-1)}$ in the case $Q_2 > 1/Q_1$. It is very plausible, though beyond the scope of this paper, to express conditions on K leading to rates of the form $2s/(2\nu + \alpha)$, with α continuously varying from 0 to $d - 1$. Note that in the case $d = 1$, we recover the minimax rate of density deconvolution with unknown error as proved by Neumann [70], see also [18].

Relation to other works in the case of sparse operators

For an unknown signal f with smoothness $s > 0$ and unknown operator with degree of ill-posedness $\nu \geqslant 0$, the optimal rates of convergence are

$$n^{-\alpha(s,\nu)/2} \bigvee \delta^{\beta(s,\nu)}, \tag{3.13}$$

up to inessential logarithmic terms. The exponents $\alpha(s, \nu)$ and $\beta(s, \nu)$ are linked respectively to the error in the signal y_n and the error in the operator K_δ. Efromovitch and Kolchinskii [30] established that under fairly general conditions on the operator K, the optimal exponents are given by

$$\alpha(s, \nu) = \beta(s, \nu) = \frac{2s}{2(s + \nu) + d}.$$

They noted however that if certain sparsity properties on K are moreover assumed (and that we shall not describe here, for instance if K is diagonal in an appropriate basis) then the exponent $\beta(s, \nu) = \frac{2s}{2(s+\nu)+d}$ is no longer optimal, while $\alpha(s, \nu)$ remains unchanged.

In the related context of operators acting on Besov spaces $B^s_{p,p}([0, 1]^d)$ of functions with smoothness s measured in L^p-norm, Hoffmann and Reiß [40] introduce an *ad hoc* hypothesis on the sparsity of the unknown operator (that we shall not describe here either), expressed in terms of the wavelet discretization of K. They subsequently obtain new rates of convergence for a certain nonlinear wavelet procedure, and these rates overperform (3.13) as expected from the results by [30]. In particular, if one

considers the estimation of $f \in B^s_{2,2}$, in the extreme case where the operator K is diagonal in a wavelet basis, the procedure in [40] achieves the rate

$$n^{-\alpha(s,\nu)/2} \bigvee (\delta^2)^{1 \wedge (s-d/2)/\nu} \tag{3.14}$$

up to extra logarithmic terms. We may compare our results with the rate (3.14). In our setting, if we pick $(e_\lambda, \lambda \in \Lambda)$ as the Fourier basis described in Section 3.4.2, then we have $\mathcal{W}^s = B^s_{2,2}([0,1]^d)$. Assuming K to be diagonal in the basis $(e_\lambda, \lambda \in \Lambda)$ which is the exact counterpart of the approach of Hoffmann and Reiß with K being diagonal in a wavelet basis, then by Theorem 3.3.1, our estimator $\widehat{f}_{n,\delta}$ (nearly) achieves the rate

$$n^{-\alpha(s,\nu)/2} \bigvee (\delta^2)^{1 \wedge 2s/(2\nu+d-1)}$$

which already outperforms the rate (3.14) whenever the error in the signal y_n is dominated by the error in the operator and s is small compared to ν, as follows from the elementary inequality

$$2s/(2\nu + d - 1) > (s - d/2)/\nu \text{ for } 2\nu + d - 1 \geqslant 2s.$$

The superiority of the blockwise SVD in this setting is explained by the fact that the wavelet procedure in [40] is agnostic to the diagonal structure of K in the wavelet basis, in contrast to $\widehat{f}_{n,\delta}$ that takes full advantage of the block structure of K. As already explained in the preceding section, one could actually improve further this result in the specific case of K being diagonal in $(e_\lambda, \lambda \in \Lambda)$ and show that $\widehat{f}_{n,\delta}$ (nearly) achieves the rate $n^{-\alpha(s,\nu)/2} \bigvee (\delta^2)^{1 \wedge s/\nu}$, thus deleting the 'dimensional effect' of d for the error in the operator.

Adaptation over the scales $\{\mathcal{W}^s, s > 0\}$ and $\{\mathcal{G}^\nu, \nu \geqslant 0\}$

The estimator $\widehat{f}_{n,\delta}$ is fully adaptive over the family of Sobolev balls $\{W^s(M), s > 0, M > 0\}$ (in the sense that $\widehat{f}_{n,\delta}$ does not require the knowledge of s nor M). However, the knowledge of the degree of ill-posedness ν of K is required through the choice of the maximal frequency L in (3.10). This restriction can actually be relaxed further in dimension $d \geqslant 2$. Indeed, setting formally $\nu = 0$ in (3.10), one readily checks that $\widehat{f}_{n,\delta}$ becomes adaptive over $\{\mathcal{W}^s(M), s > 0, M > 0\}$ and $\{\mathcal{G}^\nu(Q), \nu \geqslant 0, Q = (Q_1, Q_2), Q_1 Q_2 \geqslant 1\}$ simultaneously. In dimension $d = 1$ however, setting $\nu = 0$ in (3.10) is forbidden, but an alternative adaptivity result can be obtained by taking $L = \lfloor (\delta^2)^{-1/s_0} \rfloor \wedge n$ for some $s_0 > 0$, in which case $\widehat{f}_{n,\delta}$ is fully adaptive over the scale $\{\mathcal{G}^\nu(Q), \nu \geqslant 0, Q = (Q_1, Q_2), Q_1 Q_2 \geqslant 1\}$ and the restricted family $\{W^s(M), s \geqslant s_0, M > 0\}$.

Extension to density estimation

We briefly show a line of proof for extending Theorem 3.3.1 to the framework of density estimation. Suppose that instead of y_n we observe a random sample $Z_1, \ldots, Z_n$ drawn

from Kf assumed to a probability density. By analogy to (3.6), we have an estimator of $\mathbb{P}(g_\lambda) = \langle Kf, g_\lambda \rangle$ replacing $\langle y_n, g_\lambda \rangle$ with

$$\mathbb{P}_n(g_\lambda) = n^{-1} \sum_{i=1}^{n} g_\lambda(Z_i).$$

Writing

$$\mathbb{P}_n(g_\lambda) = \langle Kf, g_\lambda \rangle + n^{-1/2} \eta_{n,\lambda},$$

with $\eta_{n,\lambda} = n^{1/2}\big(\mathbb{P}_n(g_\lambda) - \mathbb{P}(g_\lambda)\big)$, an inspection of the proof of Theorem 3.3.1 reveals that an extension to the density estimation setting carries over as soon as the vector $(\eta_{n,\lambda}, \lambda \in \Lambda_\ell)$ satisfies a concentration inequality, namely

$$\exists \beta_1 > 0, c_1 > 0, \ \forall \beta \geqslant \beta_0, \ \ \mathbb{P}\left(|\Lambda_\lambda|^{-1} \sum_{\lambda \in \Lambda} \eta_{n,\lambda}^2 \geqslant \beta^2 \right) \leqslant \exp\big(- c\beta^2 |\Lambda_\ell| \big),$$

see (3.24) in Lemma 3.5.2. To that end, we may apply a concentration inequality by Bousquet [8] as developed for instance in Massart [64], Eq (5.51) p. 171. The precise control of this extension requires further properties on the basis $(g_\lambda, \lambda \in \Lambda)$ and on the density Kf via the behaviour of $\sum_{\lambda \in \Lambda_\ell} \mathrm{Var}\big(g_\lambda(Z_1)\big)$, see Eq. (5.52) p. 171 in [64]. We do not pursue that here.

3.4 Application to blind deconvolution

3.4.1 Spherical deconvolution

Scientific context. A common challenge in astrophysics is the analysis of complex data sets consisting of a number of objects or events such as galaxies of a particular type or ultra high energy cosmic rays (UHECR) and that are genuinely distributed over the celestial sphere. Such objects or events are distributed according to a probability density distribution f on the sphere, depending itself on the physics that governs the production of these objects or events. For instance, UHECR are particles of unknown nature arriving at the earth from apparently random directions of the sky. They could originate from long-lived relic particles from the Big Bang. Alternatively, they could be generated by the acceleration of standard particles, such as protons, in extremely violent astrophysical phenomena. They could also originate from Active Galactic Nuclei (AGN), or from neutron stars surrounded by extremely high magnetic fields. As a consequence, in some hypotheses, the underlying probability distribution for observed UHECRs would be a finite sum of point-like sources. In other hypotheses, the distribution could be uniform, or smooth and correlated with the local distribution of matter in the universe. The distribution could also be a superposition of the above. Identifying between these hypotheses is of primordial importance for understanding the origin and mechanism of production of UHECRs. The observations, denoted by X_i, are often perturbated by an experimental noise, say ε_i, that lead to the deconvolution problem

described in Section 3.1.1. Following van Rooj and Ruymgart [83], Healy *et al.* [39], Kim and Koo [52] and Kerkyacharian *et al.* [51], we assume the following model: we observe an n-sample $(Z_1, \ldots, Z_n)$ with

$$Z_i = \varepsilon_i X_i, \quad i = 1, \ldots, n$$

where the X_i are distributed on the sphere $\mathbb{S}^2$, with common density f with respect to the uniform probability distribution $\mu(d\omega)$ on $\mathbb{S}^2$ and independent of the ε_i that have a common density g with respect to the Haar probability measure dr on the group SO(3) of 3×3 rotation matrices. One proves in [39, 52] that the density of the Z_i is

$$Kf(\omega) = g \star f(\omega) := \int_{\mathrm{SO}(3)} g(r) f(r^{-1}x) dr, \quad \omega \in \mathbb{S}^2 \tag{3.15}$$

and we are interested in the case where the exact form g of the convolution operator $K = g \star \cdot$ is unknown, due for instance to insufficient knowledge of the device that is used to measure the observations. However, we assume approximate knowledge of g through K_δ as defined in (3.2). □

Checking the blockwise SVD Assumptions 3.2.1 and 3.2.1. We closely follow the exposition of [39, 52, 51] for an overview of Fourier theory on $\mathbb{S}^2$ and SO(3) in order to establish rigorously the connection to Theorem 3.3.1 and 3.12. Define

$$u(\varphi) = \begin{pmatrix} \cos\varphi & -\sin\varphi & 0 \\ \sin\varphi & \cos\varphi & 0 \\ 0 & 0 & 1 \end{pmatrix} \text{ and } a(\theta) = \begin{pmatrix} \cos\theta & 0 & \sin\theta \\ 0 & 1 & 0 \\ -\sin\theta & 0 & \cos\theta \end{pmatrix}$$

where $\varphi \in [0, 2\pi)$, $\theta \in [0, \pi)$. Every rotation $r \in \mathrm{SO}(3)$ has representation $r = u(\varphi)a(\theta)u(\psi)$ for some $\varphi, \psi \in [0, 2\pi), \theta \in [0, \pi)$. Define the rotational harmonics

$$D^l_{mn}(r) = D^l_{mn}(\varphi, \theta, \psi) = e^{-i(m\varphi + n\psi)} P^l_{mn}\big(\cos(\theta)\big)$$

for $l \in \mathbb{N}$, $-l \leqslant m, n \leqslant l$ where P^l_{mn} are the second type Legendre functions described in details in [84]. The D^l_{mn} are the eigenfunctions of the Laplace-Beltrami operator on SO(3) hence the family $(\sqrt{2l+1} D^l_{mn})$ forms a complete orthonormal basis of $\mathbb{L}^2(dr)$ on SO(3), where dr is the Haar probability measure. Every $h \in \mathbb{L}^2(dr)$ has a rotational Fourier transform

$$\mathcal{F}(h)^l_{mn} = \int_{\mathrm{SO}(3)} h(u) D^l_{mn}(u) du, \quad l \in \mathbb{N}, -l \leqslant m, n \leqslant l,$$

and for every $h \in \mathbb{L}^2(dr)$ we have a reconstruction formula

$$\begin{aligned} h &= \sum_{l \in \mathbb{N}} \sum_{-l \leqslant m,n \leqslant l} \mathcal{F}(h)^l_{mn} \overline{D^l_{mn}} \\ &= \sum_{l \in \mathbb{N}} \sum_{-l \leqslant m,n \leqslant l} \mathcal{F}(h)^l_{mn} D^l_{mn}(\cdot^{-1}) \end{aligned}$$

An analogous analysis is available on $\mathbb{S}^2$. Any point $\omega \in \mathbb{S}^2$ is determined by its spherical coordinates $\omega = \big(\sin(\theta)\cos(\varphi), \sin(\theta)\sin(\varphi), \cos(\theta)\big)$ for some $\theta \in [0, \pi), \varphi \in [0, 2\pi)$. Define

$$Y_m^l(\omega) = Y_l^m(\theta, \varphi) = (-1)^m \sqrt{\tfrac{2l+1}{4\pi} \tfrac{(l-m)!}{(l+m)!}} P_m^l\big(\cos(\theta)\big) e^{im\varphi} \tag{3.16}$$

for $l \in \mathbb{N}, -l \leqslant m \leqslant l$ where P_m^l are the Legendre functions. We have $Y_{-m}^l = (-1)^m Y_m^l$ and the (Y_m^l) constitute an orthonormal basis of $\mathbb{L}^2(\mu)$ on $\mathbb{S}^2$, generally referred to as the spherical harmonic basis. Any $f \in \mathbb{L}^2(\mu)$ has a spherical Fourier transform

$$\mathcal{F}(f)_m^l = \int_{\mathbb{S}^2} f(\omega) \overline{Y_m^l(\omega)} \mu(d\omega)$$

and a reconstruction formula

$$f = \sum_{\ell \in \mathbb{N}} \sum_{-l \leqslant m \leqslant l} \mathcal{F}(f)_m^l Y_m^l.$$

If $g \in \mathbb{L}^2\big(\mathrm{SO}(3)\big)$ the spherical convolution operator $Kf = g \star f$ defined in (3.15) satisfies

$$\mathcal{F}(g \star f)_m^l = \sum_{n=-l}^{l} \mathcal{F}(g)_{mn}^l \mathcal{F}(f)_n^l \tag{3.17}$$

and we retrieve the blockwise SVD formalism of Section 3.2.1 in dimension $d = 2$ by setting $\mathbb{H} = \mathbb{G} = \mathbb{L}^2(\mathbb{S}^2, \mu)$, where μ the probability Haar measure on $\mathbb{S}^2$ and

$$e_\lambda = g_\lambda = Y_m^\ell \text{ with } \lambda = (m, \ell), \quad \Lambda_\ell = \{(m, \ell), \quad -\ell \leqslant m \leqslant \ell\}.$$

We have $|\Lambda_\ell| = 2\ell + 1$ and by (3.17), K_ℓ is the finite dimension operator stable on $\mathrm{Span}\{e_\lambda, \lambda \in \Lambda_\ell\}$ with matrix having entries

$$(K_\ell)_{mn} = \mathcal{F}(g)_{mn}^\ell.$$

Hence Assumption 3.2.1 is satisfied. Notice also that in this case K_ℓ is generally not diagonal. Assumption 3.2.2 is satisfied as we assume that g is *ordinary smooth* in the terminology of Kim and Koo [52]. Our Assumption 3.2.2 exactly matches the constraint (3.6) in their paper with examples given by the Laplace distribution on the sphere ($\nu = 2$) or the Rosenthal distribution ($\nu > 0$ arbitrary). □

Numerical implementation. Following Kerkyacharian, Pham Ngoc and Picard [51] in their Example 2, we take $f(\omega) = C \exp(-4\|\omega - \omega_1\|^2)$ with $\omega_1 = (0, 1, 0)$ and $C = 1/0.7854$. We have $\|f\|_{\mathbb{L}^2(\mu)} = 0.7469$.
g is the density of a Laplace distribution on SO(3), defined through $\mathcal{F}(g)_{mn}^\ell = \delta_{mn}\big(1 + \ell(\ell+1)\big)^{-1}$. Hence, the matrices $(K_\ell)_{mn}$ are homotheties whose ratios behave as ℓ^{-2}. We have $\nu = 2$.
We plot in Figures 3.1 a 1000-sample of X_i with density f on the sphere, and the action by ε_i on the X_i, where the ε_i are distributed according to g in Figure 3.2. Note that for the estimation of g, we have access to a noisy version of g with noise level δ only.

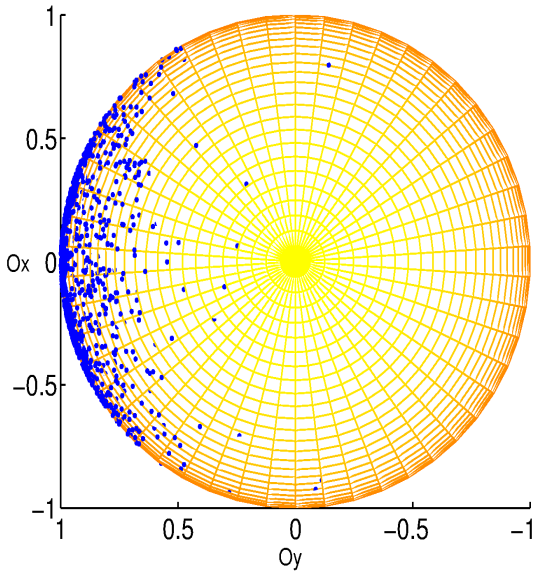

Figure 3.1: **Data from f.** Plot of $n = 1000$ data with common distribution f on the sphere $\mathbb{S}$ (planar representation).

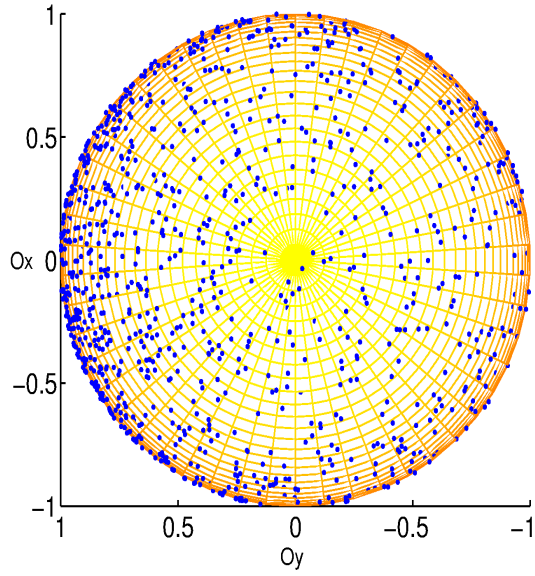

Figure 3.2: **Data from $f \star g$.** Plot of $n = 1000$ data $\varepsilon_i X_i$ on the sphere $\mathbb{S}$ with common distribution $Kf = f \star g$. The X_i are the data pictured in Figure 3.1 and the ε_i are sampled according to g (planar representation).

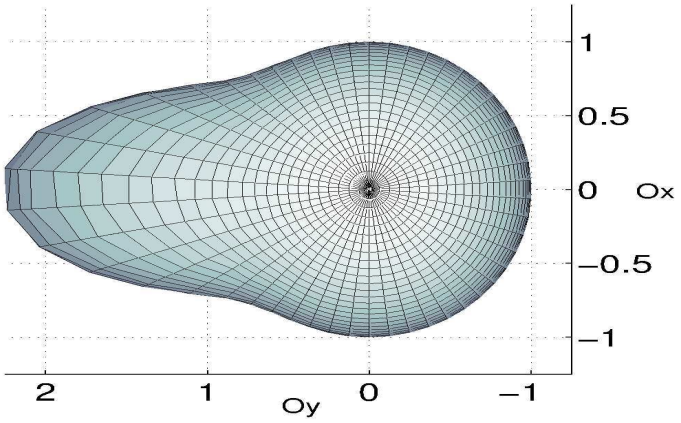

Figure 3.3: **Target density f.** The representation is simplified through a view from above the sphere through the Oz-axis.

We display below the (renormalised) empirical squared error of $\widehat{f}_{10^8,\delta}$ (oracle choice $\lambda_0 = 1, \mu_0 = 1$) for 1000 Monte-Carlo for several values of δ. The noise level δ is to to be compared with the noise level $n^{-1/2} = 10^{-4}$. The latter is chosen non-negative, in order to show the interaction between the two types of error, and sufficiently small to emphasize the influence of δ on the process of estimation.

Noise level δ	0	10^{-3}	$3\,10^{-3}$	$5\,10^{-3}$	10^{-2}
Mean error	0.0466	0.0542	0.1732	0.2784	0.4335
Standard dev.	0.0011	0.0022	0.0126	0.0355	0.0466

Finally, on a specific sample of $n = 10^8$ data, we plot the target density f (Figure 3.3) and its reconstruction for $n = 10^8$ data with $\delta = 0$ (Figure 3.4) and $\delta = 3\,10^{-3}$ (Figure 3.5). At a visual level, we oversimplify the representation by plotting f and its reconstruction with a view from above the sphere through the Oz axis. We see that the contour in Figure 3.5 is not well recovered in the regions where f is small (on the right side of the graph in Figure 3.5). The choice of λ_0, μ_0 remains unchanged. □

3.4.2 Circular deconvolution

Scientific context. In many engineering problems, the observation of a signal f or image is distorted by the action of a linear operator K. We assume for simplicity that f lives on the torus $\mathbb{T} = [0,1]$ (or $[0,1]^d$) appended with periodic boundary conditions. In many instances, the restoration of f from the noisy observation of Kf is challenged by the additional uncertainty about the operator K. This is the case for instance in electronic microscopy [72] for the restoration of fluorescence Confocal Laser Scanning Microscope (CLSM) images. In other words, the quality of the image suffers from two

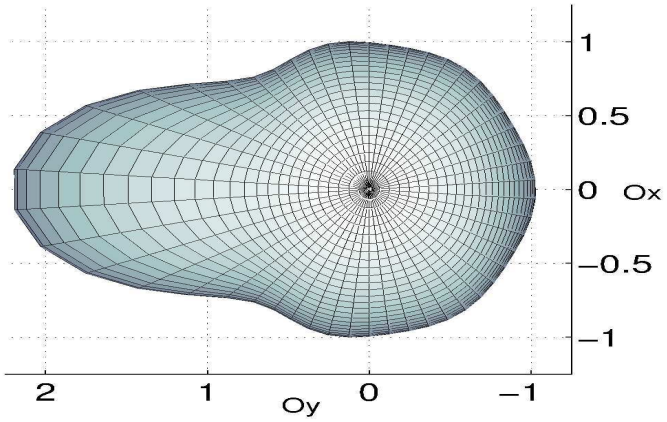

Figure 3.4: **Reconstruction for** $n = 10^8$ **and** $\delta = 0$.

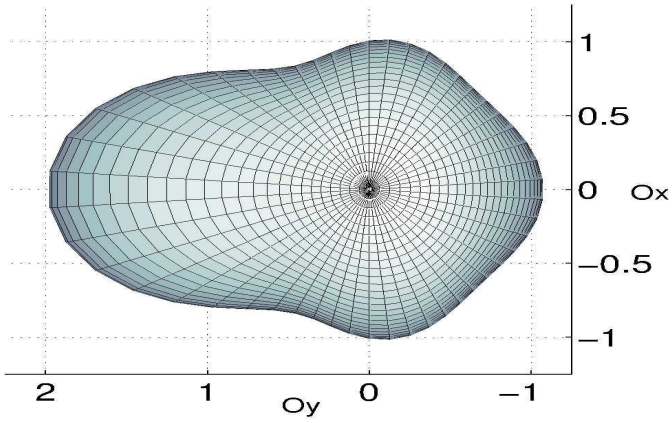

Figure 3.5: **Reconstruction for** $n = 10^8$ **and** $\delta = 3\,10^{-3}$. The reconstruction is polluted simultaneously by the limited number of observations n and the noise level δ in the blurring g.

physical limitations: error measurements or limited accuracy, and the fact that the exact PSF (the incoherent point spread function) that accounts for the blurring of f (mathematically the action of K) is not precisely known. This is a classical issue that goes back to [78, 33]. An idealised additive Gaussian model for the noise contamination yields the observation (3.1) with

$$Kf(x) = g \star f(x) := \int_{\mathbb{T}^d} g(u) f(x-u) du, \quad x \in \mathcal{D} = \mathbb{T}^d.$$

The degradation process $K = g \star \cdot$ is characterised by the impulse response function g. In most cases of interest, we do not know the exact form of g. In a condensed idealised statistical setup, we have access to

$$g_\delta = g + \delta \dot{W}', \tag{3.18}$$

where $\dot{W}'$ is another Gaussian white noise defined on $\mathbb{L}^2(\mu)$ and independent of $\dot{W}$. Experimental approaches that justify representation (3.18) are described in [20, 47, 76]. □

Checking Assumptions 3.2.1 and 3.2.1. We obviously have $\mathbb{H} = \mathbb{G} = \mathbb{L}^2(\mathbb{T}^d)$ and the bases (e_λ) and (g_λ) will coincide with the d-dimensional extension of the circular trigonometric basis $(e^{2i\pi kx}, k \in \mathbb{Z})$ if we set:

$$e_\lambda(x_1, \ldots, x_d) = \prod_{j=1}^{d} e^{2i\pi k_j x_j}, \quad (x_1, \ldots, x_d) \in \mathbb{T}^d,$$

where we put

$$\lambda = (k_1, \ldots, k_d), \quad \ell = |\lambda| = 1 + \sum_{j=1}^{d} |k_j|, \quad \text{and} \quad \ell \geqslant 1.$$

Any $f \in \mathbb{L}^2(\mu)$ has a Fourier transform $\mathcal{F}(f)_\lambda = \int_{\mathbb{T}^d} f(x)\overline{e_\lambda(x)}\mu(dx)$ and moreover, if $g \in \mathbb{L}^2(\mu)$, we have

$$\mathcal{F}(f \star g)_\lambda = \mathcal{F}_\lambda(f)\mathcal{F}_\lambda(g).$$

Therefore, K is diagonal in the basis $(e_\lambda, \lambda \in \Lambda)$ henceforth stable. Moreover, with $\Lambda_\ell = \{\lambda, |\lambda| = \ell\}$, we have $|\Lambda_\ell| = \binom{\ell - 1 + d}{d-1} \sim \ell^{d-1}$. Moreover $K_\ell = \mathrm{Diag}\big(\mathcal{F}_\lambda(g), \lambda \in \Lambda_\ell\big)$ and Assumption 3.2.1 follows. Assuming that g satisfies $c|\lambda|^{-\nu} \leqslant \big|\mathcal{F}(g)_\lambda\big| \leqslant c'|\lambda|^{-\nu}$ for some $\nu \geqslant 0$ and constants $c, c' > 0$, we readily obtain Assumption 3.2.2. Note also that since K is diagonal in the basis $(e_\lambda, \lambda \in \Lambda)$ observing g_δ in the representation (3.18) is equivalent to observing K_δ in (3.2). □

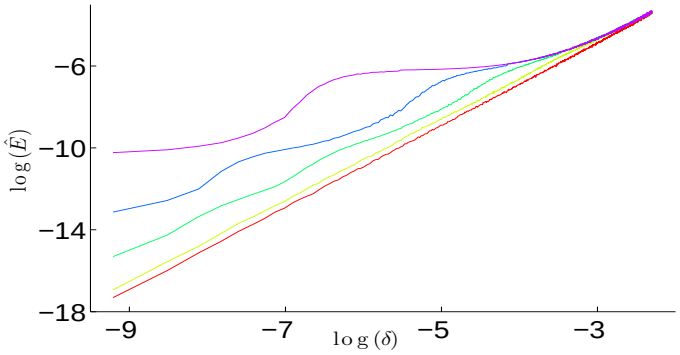

Figure 3.6: **Estimation of the rate exponent when** $n^{-1/2} \ll \delta$**.** Empirical squared-error $\hat{E}$ versus δ in log-log scale. Top-to-bottom: $\nu = 8, 6, 5, 4, 1$. The target function has smoothness $s = 5 - \alpha$ for all $\alpha > 1/2$. For $\nu < 4.5$, the slope of the curve is constant and close to 2, confirming the parametric rate predicted by the theory when the smoothess of the signal dominates the degree of ill-posedness of the operator. The empirical errors were computed using 1000 Monte-Carlo simulations.

Numerical implementation. We numerically implement $\widehat{f}_{n,\delta}$ in dimension $d = 1$ in the case where there is no noise in the signal (formally $n^{-1/2} = 0$) in order to illustrate the parametric effect that dominates in the optimal rate of convergence in Theorems 3.3.1 and 3.12 that becomes $\left(\delta^2\right)^{s/\nu \wedge 1}$ in that case. We take as target function $f : \mathbb{T} \to \mathbb{R}$ belonging to $\mathcal{W}^{5-\alpha}$ for all $\alpha > 1/2$ and defined by its Fourier coefficients

$$\mathcal{F}(f)_\lambda = |\lambda|^{-5}, \quad \lambda \in \{-1000, \dots, 1000\}.$$

We pick a family of blurring functions g_ν defined in the same manner by the formula

$$\mathcal{F}(g_\nu)_\lambda = |\lambda|^{-\nu}, \quad \lambda \in \{-1000, \dots, 1000\}, \quad \nu \in \{1, 4, 5, 6, 8\}.$$

We show in Figure 3.6 in a log-log plot the mean-squared error of $\widehat{f}_{\infty,\delta}$ for the oracle choice $\mu_0 = 0, \lambda_0 = 1$ over 1000 Monte-Carlo simulations for $\nu \in \{1, 4, 5, 6, 8\}$ and $\delta \in [10^{-4}, 10^{-1}]$. For small values of δ the predicted slope of the curve gives a rough estimate of the rate of convergence. We visually see that for the critical case $\nu \leqslant s = 5 - \alpha$ with $\alpha > 1/2$ and below, the slope is close to 2 confirming the parametric rate that is obtained whenever $\nu \leqslant s$. □

3.5 Proofs

3.5.1 Preliminary estimates

Preparation. Recall that $H_\ell = \mathrm{Span}\{e_\lambda, \lambda \in \Lambda_\ell\}$, $G_\ell = \mathrm{Span}\{g_\lambda, \lambda \in \Lambda_\ell\}$ and that P_ℓ (resp. Q_ℓ) denotes the orthogonal projector onto G_ℓ (resp. H_ℓ). For $h \in \mathbb{H}$, we have

$$P_\ell K h = P_\ell K Q_\ell h + P_\ell K (\mathrm{Id} - Q_\ell) h.$$

Using Assumption 3.2.1, we have $K(\mathrm{Id} - Q_\ell)h \in G_\ell^\perp$ and therefore $P_\ell K(\mathrm{Id} - Q_\ell)h = 0$. As a consequence

$$P_\ell K = K_\ell Q_\ell. \tag{3.19}$$

In turn, we have a convenient description of the observation K_δ defined in (3.2) and y_n defined in (3.1) and in terms of a sequence space model that we shall now describe. □

Notation. If $h \in \mathbb{G}$, we denote by $\boldsymbol{h}_\ell$ the (column) vector of coordinates of $P_\ell h$ in the basis $(g_\lambda, \lambda \in \Lambda_\ell)$. If $T : \mathbb{H} \to \mathbb{G}$ is a linear operator, we write $\boldsymbol{T}_\ell$ for the matrix of the Galerkin projection $T_\ell = P_\ell T_{|H_\ell}$ of T. □

Sequence model for error in the operator. The observation of K_δ in (3.2) leads to the representation $K_{\delta,\ell} = K_\ell + \delta \dot{B}_\ell$, or equivalently, in matrix notation

$$\boldsymbol{K}_{\delta,\ell} = \boldsymbol{K}_\ell + \delta \dot{\boldsymbol{B}}_\ell, \quad \ell \geqslant 1, \tag{3.20}$$

where $\dot{\boldsymbol{B}}_\ell$ is a $|\Lambda_\ell| \times |\Lambda_\ell|$ matrix with entries that are independent centred Gaussian random variables, with unit variance. The following estimate is a classical concentration property of random matrices. For $\ell \leqslant L$, $\|\cdot\|_{\mathrm{op}}$ denotes the operator norm for $|\Lambda_\ell| \times |\Lambda_\ell|$ matrices (we shall skip the dependence upon ℓ in the notation).

Lemma 3.5.1 ([22], Theorem II.4)**.** *There are positive constants β_0, c_0 such that*

$$\textit{For all } \beta \geqslant \beta_0, \ \mathbb{P}\big(|\Lambda_\ell|^{-1/2}\|\dot{\boldsymbol{B}}_\ell\|_{op} \geqslant \beta\big) \leqslant \exp\big(-c_0\beta^2|\Lambda_\ell|^2\big). \tag{3.21}$$

An immediate consequence of Lemma 3.5.1 is the following moment bound:

$$\text{For every } \ p > 0, \ \ \mathbb{E}\big[\|\dot{\boldsymbol{B}}_\ell\|_{\mathrm{op}}^p\big] \lesssim |\Lambda_\ell|^{p/2}. \tag{3.22}$$

□

Sequence model for error in the signal. From (3.1), we observe the Gaussian measure y_n, or equivalently, thanks to (3.19)

$$P_\ell y_n = P_\ell K f + n^{-1/2} P_\ell \dot{W} = K_\ell Q_\ell f + n^{-1/2}\boldsymbol{\eta}_\ell, \quad \ell \geqslant 1$$

or, using the notation introduced in (3.6), in matrix notation

$$\boldsymbol{z}_{n,\ell} = \boldsymbol{K}_\ell \boldsymbol{f}_\ell + n^{-1/2}\boldsymbol{\eta}_\ell, \quad \ell \geqslant 1 \tag{3.23}$$

where we used (3.19), with $\boldsymbol{\eta}_\ell$ denoting a vector of $|\Lambda_\ell|$ independent centred Gaussian random variables with unit variance.

The following result is a direct consequence of the fact that $\boldsymbol{\eta}_\ell$ has a χ-square distribution with $|\Lambda_\ell|$ degrees of freedom. The proof is standard

Lemma 3.5.2. *There are positive constant β_1, c_1 such that*

$$\textit{For all } \beta \geqslant \beta_1, \ \mathbb{P}\big(|\Lambda_\ell|^{-1/2}\|\boldsymbol{\eta}_\ell\| \geqslant \beta\big) \leqslant \exp\big(-c_1\beta^2|\Lambda_\ell|\big), \tag{3.24}$$

□

3.5.2 Proof of Theorem 3.3.1

We have

$$\|\widehat{f}_n - f\|_{\mathbb{H}}^2 = \sum_{\ell \geqslant 1} \|\widehat{\boldsymbol{f}}_{n,\ell} - \boldsymbol{f}_\ell\|^2 = \sum_{\ell=1}^{L} \|\widehat{\boldsymbol{f}}_{n,\ell} - \boldsymbol{f}_\ell\|^2 + \sum_{\ell > L} \|\boldsymbol{f}_\ell\|^2$$

where $\|\cdot\|$ denotes the Euclidean norm on $\mathbb{R}^{|\Lambda_\ell|}$ (we shall omit any reference to ℓ when no confusion is possible). Concerning the bias term, we have

$$\sum_{\ell > L} \|\boldsymbol{f}_\ell\|^2 \leqslant \|f\|_{\mathcal{W}^s}^2 L^{-2s} \tag{3.25}$$

and this term has the right order by definition of L in (3.10). Concerning the stochastic term, thanks to our preliminary analysis, we may write

$$\widehat{\boldsymbol{f}}_{n,\ell} = (\boldsymbol{K}_{\delta,\ell})^{-1} \boldsymbol{z}_{n,\ell} \mathbf{1}_{\{\|(\boldsymbol{K}_{\delta,\ell})^{-1}\|_{\mathrm{op}} \leqslant \kappa_\ell\}} \mathbf{1}_{\{\|\boldsymbol{z}_{n,\ell}\| \geqslant \tau_\ell\}},$$

We set

$$\mathcal{A}_\ell = \{\|(\boldsymbol{K}_{\delta,\ell})^{-1}\|_{\mathrm{op}} \leqslant \kappa_\ell\} \text{ and } \mathcal{B}_\ell = \{\|\boldsymbol{z}_{n,\ell}\| \geqslant \tau_\ell\}.$$

We thus obtain the decomposion of the variance term as

$$\sum_{\ell=1}^{L} \|\widehat{\boldsymbol{f}}_{n,\ell} - \boldsymbol{f}_\ell\|^2 \leqslant I + II + III,$$

with

$$\begin{aligned} I &= \sum_{\ell=1}^{L} \|(\boldsymbol{K}_{\delta,\ell})^{-1} \boldsymbol{z}_{n,\ell} - \boldsymbol{f}_\ell\|^2 \mathbf{1}_{\mathcal{A}_\ell} \mathbf{1}_{\mathcal{B}_\ell} \\ II &= \sum_{\ell=1}^{L} \|\boldsymbol{f}_\ell\|^2 \mathbf{1}_{\mathcal{A}_\ell^c}, \\ III &= \sum_{\ell=1}^{L} \|\boldsymbol{f}_\ell\|^2 \mathbf{1}_{\mathcal{B}_\ell^c}. \end{aligned}$$

We shall successively bound each term I, II and III.

- *The term I, preliminary decomposition.* Writing

$$\boldsymbol{z}_{n,\ell} = \big(\boldsymbol{K}_{\delta,\ell} - \delta \dot{\boldsymbol{B}}_\ell\big) \boldsymbol{f}_\ell + n^{-1/2} \boldsymbol{\eta}_\ell,$$

we obtain

$$(\boldsymbol{K}_{\delta,\ell})^{-1} \boldsymbol{z}_{n,\ell} - \boldsymbol{f}_\ell = -\delta (\boldsymbol{K}_{\delta,\ell})^{-1} \dot{\boldsymbol{B}}_\ell \boldsymbol{f}_\ell + n^{-1/2} (\boldsymbol{K}_{\delta,\ell})^{-1} \boldsymbol{\eta}_\ell.$$

We introduce further the event $\{\|\delta \dot{\boldsymbol{B}}_\ell\|_{\mathrm{op}} \leqslant a_\ell\}$ with $a_\ell = \frac{\rho}{\kappa_\ell}$ for some $0 < \rho < \frac{1}{2}$ and the condition $\{\|\boldsymbol{K}_\ell \boldsymbol{f}_\ell\| \geqslant \frac{\tau_\ell}{2}\}$. We thus have

$$I \lesssim IV + V + VI + VII,$$

with

$$
\begin{aligned}
IV &= \sum_{\ell=1}^{L} \|\delta(\boldsymbol{K}_{\delta,\ell})^{-1}\dot{\boldsymbol{B}}_\ell \boldsymbol{f}_\ell\|^2 \mathbf{1}_{\mathcal{A}_\ell \cap \mathcal{B}_\ell} \mathbf{1}_{\left\{\|\delta\dot{\boldsymbol{B}}_\ell\|_{\mathrm{op}} \leqslant a_\ell\right\}} \mathbf{1}_{\left\{\|\boldsymbol{K}_\ell \boldsymbol{f}_\ell\| \geqslant \frac{\tau_\ell}{2}\right\}},\\
V &= \sum_{\ell=1}^{L} \|n^{-1/2}(\boldsymbol{K}_{\delta,\ell})^{-1}\boldsymbol{\eta}_\ell\|^2 \mathbf{1}_{\mathcal{A}_\ell \cap \mathcal{B}_\ell} \mathbf{1}_{\left\{\|\delta\dot{\boldsymbol{B}}_\ell\|_{\mathrm{op}} \leqslant a_\ell\right\}} \mathbf{1}_{\left\{\|\boldsymbol{K}_\ell \boldsymbol{f}_\ell\| \geqslant \frac{\tau_\ell}{2}\right\}},\\
VI &= \sum_{\ell=1}^{L} \|\delta(\boldsymbol{K}_{\delta,\ell})^{-1}\dot{\boldsymbol{B}}_\ell \boldsymbol{f}_\ell\|^2 \mathbf{1}_{\mathcal{A}_\ell \cap \mathcal{B}_\ell} \Big(\mathbf{1}_{\left\{\|\delta\dot{\boldsymbol{B}}_\ell\|_{\mathrm{op}} > a_\ell\right\}} + \mathbf{1}_{\left\{\|\boldsymbol{K}_\ell \boldsymbol{f}_\ell\| < \frac{\tau_\ell}{2}\right\}}\Big),\\
VII &= \sum_{\ell=1}^{L} \|n^{-1/2}(\boldsymbol{K}_{\delta,\ell})^{-1}\boldsymbol{\eta}_\ell\|^2 \mathbf{1}_{\mathcal{A}_\ell \cap \mathcal{B}_\ell} \Big(\mathbf{1}_{\left\{\|\delta\dot{\boldsymbol{B}}_\ell\|_{\mathrm{op}} > a_\ell\right\}} + \mathbf{1}_{\left\{\|\boldsymbol{K}_\ell \boldsymbol{f}_\ell\| < \frac{\tau_\ell}{2}\right\}}\Big).
\end{aligned}
$$

We shall next successively bound each term IV, V, VI and VII □

• *The term IV.* First, we have

$$
\begin{aligned}
(\boldsymbol{K}_\ell)^{-1} &= (\boldsymbol{K}_{\delta,\ell} - \delta\dot{\boldsymbol{B}}_\ell)^{-1}\\
&= (\boldsymbol{I} - \delta\boldsymbol{K}_{\delta,\ell}^{-1}\dot{\boldsymbol{B}})^{-1}(\boldsymbol{K}_{\delta,\ell})^{-1}.
\end{aligned}
$$

On $\mathcal{A}_\ell = \{\|(\boldsymbol{K}_{\delta,\ell})^{-1}\|_{\mathrm{op}} \leqslant \kappa_\ell\}$ and $\{\|\delta\dot{\boldsymbol{B}}_\ell\|_{\mathrm{op}} \leqslant a_\ell\}$, since a_ℓ satisfies $\kappa_\ell\, a_\ell = \rho < \frac{1}{2}$, by a usual Neumann series argument,

$$
\begin{aligned}
\|\big(\boldsymbol{I} - \delta(\boldsymbol{K}_{\delta,\ell})^{-1}\dot{\boldsymbol{B}}\big)^{-1}\|_{\mathrm{op}} &= \|\sum_{i\geqslant 0}(-\boldsymbol{K}_{\delta,\ell})^i(\delta\dot{\boldsymbol{B}})^i\|_{\mathrm{op}}\\
&\leqslant \sum_{i\geqslant 0}\|\boldsymbol{K}_{\delta,\ell}\|_{\mathrm{op}}^i\|\delta\dot{\boldsymbol{B}}\|_{\mathrm{op}}^i\\
&\leqslant \sum_{i\geqslant 0}\rho^i = (1-\rho)^{-1}.
\end{aligned}
$$

Therefore, on $\mathcal{A}_\ell$ and $\{\|\delta\dot{\boldsymbol{B}}_\ell\|_{\mathrm{op}} \leqslant a_\ell\}$, we have

$$
\|(\boldsymbol{K}_\ell)^{-1}\|_{\mathrm{op}} \leqslant (1-\rho)^{-1}\|(\boldsymbol{K}_{\delta,\ell})^{-1}\|_{\mathrm{op}} \leqslant (1-\rho)^{-1}\kappa_\ell. \tag{3.26}
$$

Second, we now write

$$
(\boldsymbol{K}_{\delta,\ell})^{-1} = \big(\boldsymbol{I} - (\boldsymbol{K}_\ell)^{-1}\delta\dot{\boldsymbol{B}}_\ell\big)^{-1}(\boldsymbol{K}_\ell)^{-1},
$$

hence, on $\mathcal{A}_\ell$ and $\{\|\delta\dot{\boldsymbol{B}}_\ell\|_{\mathrm{op}} \leqslant a_\ell\}$, we have by (3.26)

$$
\|(\boldsymbol{K}_\ell)^{-1}\delta\dot{\boldsymbol{B}}_\ell\|_{\mathrm{op}} \leqslant (1-\rho)^{-1}\kappa_\ell a_\ell \leqslant \frac{\rho}{1-\rho} < 1
$$

since $\rho < \frac{1}{2}$ by assumption. The same Neumann series argument now entails

$$
\|(\boldsymbol{K}_{\delta,\ell})^{-1}\|_{\mathrm{op}} \leqslant \frac{\rho}{1-\rho}\|(\boldsymbol{K}_\ell)^{-1}\|_{\mathrm{op}}. \tag{3.27}
$$

We are ready to bound the term IV itself. We have

$$\begin{aligned}
&\|\delta(\boldsymbol{K}_{\delta,\ell})^{-1}\dot{\boldsymbol{B}}_\ell \boldsymbol{f}_\ell\|^2 \mathbf{1}_{\mathcal{A}_\ell}\mathbf{1}_{\left\{\|\delta\dot{\boldsymbol{B}}_\ell\|_{\mathrm{op}}\leqslant a_\ell\right\}}\\
&\leqslant \|(\boldsymbol{K}_{\delta,\ell})^{-1}\|_{\mathrm{op}}^2\|\delta\dot{\boldsymbol{B}}_\ell\|_{\mathrm{op}}^2\|\boldsymbol{f}_\ell\|^2\,\mathbf{1}_{\mathcal{A}_\ell}\mathbf{1}_{\left\{\|\delta\dot{\boldsymbol{B}}_\ell\|_{\mathrm{op}}\leqslant a_\ell\right\}}\\
&\lesssim \|(\boldsymbol{K}_\ell)^{-1}\|_{\mathrm{op}}^2\kappa_\ell^{-2}\|\boldsymbol{f}_\ell\|^2\,\mathbf{1}_{\left\{\|(\boldsymbol{K}_\ell)^{-1}\|_{\mathrm{op}}\leqslant(1-\rho)^{-1}\kappa_\ell\right\}},
\end{aligned}$$

where we successively used (3.26) and (3.27). It follows that

$$\begin{aligned}
\mathbb{E}\left[IV\right] &\lesssim \sum_{\ell=1}^{L}\|(\boldsymbol{K}_\ell)^{-1}\|_{\mathrm{op}}^2\kappa_\ell^{-2}\|\boldsymbol{f}_\ell\|^2\,\mathbf{1}_{\left\{\|(\boldsymbol{K}_\ell)^{-1}\|_{\mathrm{op}}\leqslant(1-\rho)^{-1}\kappa_\ell\right\}}\\
&\lesssim \sum_{\ell=1}^{L}\ell^{2\nu}\kappa_\ell^{-2}\|\boldsymbol{f}_\ell\|^2
\end{aligned}$$

where we used Assumption 3.2.2. The bound is uniform in $K\in\mathcal{G}^\nu(Q)$. By definition of κ_ℓ and using that $|\Lambda_\ell|$ is of order ℓ^{d-1}, we derive

$$\mathbb{E}[IV]\lesssim\left((\delta^2|\log\delta|)\bigvee n^{-1}\right)\sum_{\ell=1}^{L}\ell^{2\nu+d-1}\|\boldsymbol{f}_\ell\|^2.$$

If $2\nu+d-1\leqslant 2s$, we have

$$\sum_{\ell=1}^{L}\ell^{2\nu+d-1}\|\boldsymbol{f}_\ell\|^2\leqslant\|f\|_{\mathcal{W}^s}^2,$$

therefore

$$\begin{aligned}
\mathbb{E}\left[IV\right] &\lesssim \delta^2|\log\delta| + L^{-2s}\\
&\lesssim \left(\delta^2|\log\delta|\right)^{1\wedge 2s/(2\nu+d-1)}\bigvee n^{-2s/(2\nu+d)} \qquad (3.28)
\end{aligned}$$

by definition of L in (3.10), and this result is uniform in $f\in\mathcal{W}^s(M)$. If $2\nu+d-1\geqslant 2s$, we have

$$\begin{aligned}
\sum_{\ell=1}^{L}\ell^{2\nu+d-1}\|\boldsymbol{f}_\ell\|^2 &\leqslant L^{2(\nu-s)+d-1}\sum_{\ell=1}^{L}\ell^{2s}\|\boldsymbol{f}_\ell\|^2\\
&\leqslant L^{2(\nu-s)+d-1}\|f\|_{\mathcal{W}^s}^2.
\end{aligned}$$

By definition of L again we derive

$$\begin{aligned}
\mathbb{E}\left[IV\right] &\lesssim L^{-2s}L^{2\nu+d-1}(n^{-1}\bigvee\delta^2|\log\delta|)\\
&\lesssim L^{-2s}(n^{-1/(2\nu+d)}\bigvee 1)\leqslant L^{-2s} \qquad (3.29)
\end{aligned}$$

and this bound is uniform in $f\in\mathcal{W}^s(M)$. Putting together (3.28) and (3.29), we finally obtain

$$\mathbb{E}\left[IV\right]\lesssim\left(\delta^2|\log\delta|\right)^{1\wedge 2s/(2\nu+d-1)}\bigvee n^{-2s/(1\nu+d)} \qquad (3.30)$$

uniformly in $f\in\mathcal{W}^s(M), K\in\mathcal{G}^\nu(Q)$. □

• *The term V.* We have

$$\begin{aligned}
&\|n^{-1/2}(\boldsymbol{K}_{\delta,\ell})^{-1}\boldsymbol{\eta}_\ell\|^2\mathbf{1}_{\mathcal{A}_\ell}\mathbf{1}_{\left\{\|\delta\dot{\boldsymbol{B}}_\ell\|_{\mathrm{op}}\leqslant a_\ell\right\}}\mathbf{1}_{\left\{\|\boldsymbol{K}_\ell\boldsymbol{f}_\ell\|\geqslant\frac{\tau_\ell}{2}\right\}}\\
\leqslant\, & n^{-1}\|(\boldsymbol{K}_{\delta,\ell})^{-1}\|_{\mathrm{op}}^2\|\boldsymbol{\eta}_\ell\|^2\mathbf{1}_{\mathcal{A}_\ell}\mathbf{1}_{\left\{\|\delta\dot{\boldsymbol{B}}_\ell\|_{\mathrm{op}}\leqslant a_\ell\right\}}\mathbf{1}_{\left\{\|\boldsymbol{K}_\ell\boldsymbol{f}_\ell\|\geqslant\frac{\tau_\ell}{2}\right\}}\\
\lesssim\, & n^{-1}\|(\boldsymbol{K}_\ell)^{-1}\|_{\mathrm{op}}^2\|\boldsymbol{\eta}_\ell\|^2\mathbf{1}_{\mathcal{A}_\ell}\mathbf{1}_{\left\{\|\delta\dot{\boldsymbol{B}}_\ell\|_{\mathrm{op}}\leqslant a_\ell\right\}}\mathbf{1}_{\left\{\|\boldsymbol{K}_\ell\boldsymbol{f}_\ell\|\geqslant\frac{\tau_\ell}{2}\right\}}\\
\lesssim\, & n^{-1}\ell^{2\nu}\|\boldsymbol{\eta}_\ell\|^2\mathbf{1}_{\left\{\|\boldsymbol{K}_\ell\boldsymbol{f}_\ell\|\geqslant\frac{\tau_\ell}{2}\right\}}
\end{aligned}$$

where we successively used (3.26) and (3.27) in the same way as for the term IV, the last inequality being obtained thanks to Assumption 3.2.2. By Assumption 3.2.2 again, since

$$\|\boldsymbol{K}_\ell\boldsymbol{f}_\ell\| \leqslant \|\boldsymbol{K}_\ell\|_{\mathrm{op}}\|\boldsymbol{f}_\ell\| \leqslant Q_1(K)\ell^\nu\|\boldsymbol{f}_\ell\|$$

we derive

$$\mathbf{1}_{\left\{\|\boldsymbol{K}_\ell\boldsymbol{f}_\ell\|\geqslant\frac{\tau_\ell}{2}\right\}} \leqslant \mathbf{1}_{\left\{\|\boldsymbol{f}_\ell\|\geqslant Q_1(K)^{-1}\frac{\tau_\ell}{2}\ell^\nu\right\}} = \mathbf{1}_{\left\{\|\boldsymbol{f}_\ell\|\geqslant c\ell^{\nu+(d-1)/2}n^{-1/2}(\log n)^{1/2}\right\}}$$

for some constant c that depends on $Q_1(K)$ and the pre-factor μ_0 in the choice of τ_ℓ only. Since $\mathbb{E}[\|\boldsymbol{\eta}_\ell\|^2] = |\Lambda_\ell| \lesssim \ell^{d-1}$, we infer, for any $1 \leqslant k \leqslant L$

$$\begin{aligned}
\mathbb{E}[V] &\lesssim n^{-1}\sum_{\ell=1}^{L}\ell^{2\nu+d-1}\mathbf{1}_{\left\{\|\boldsymbol{f}_\ell\|\geqslant c\ell^{\nu+(d-1)/2}n^{-1/2}(\log n)^{1/2}\right\}}\\
&\lesssim n^{-1}\Big(\sum_{\ell=1}^{k}\ell^{2\nu+d-1} + \sum_{\ell=k+1}^{L} n(\log n)^{-1}\|\boldsymbol{f}_\ell\|^2\Big)\\
&\leqslant n^{-1}k^{2\nu+d} + (\log n)^{-1}\sum_{\ell>k}\|\boldsymbol{f}_\ell\|^2\\
&\lesssim n^{-1}k^{2\nu+d} + (\log n)^{-1}\|f\|_{\mathcal{W}^s}^2 k^{-2s}.
\end{aligned}$$

The admissible choice $k = \big\lfloor\big(n(\log n)^{-1/2}\big)^{1/(2(s+\nu)+d)}\big\rfloor \wedge (\delta^2)^{-1/(2\nu+d-1)}$ yields

$$\begin{aligned}
\mathbb{E}[V] &\lesssim n^{-1}k^{\nu+d} + k^{-2s}\\
&\lesssim \big(n^{-1}\log n\big)^{2s/(2(s+\nu)+d)} + k^{-2s}\\
&\lesssim \big(n^{-1}\log n\big)^{2s/(2(s+\nu)+d)} \bigvee (\delta^2)^{2s/(2\nu+d-1)}
\end{aligned} \tag{3.31}$$

uniformly in $f \in \mathcal{W}^s(M), K \in \mathcal{G}^\nu(Q)$. □

• *The term VI.* We further bound the term VI via

$$VI \leqslant VIII + IX,$$

with

$$VIII = \sum_{\ell=1}^{L} \|\delta(\boldsymbol{K}_{\delta,\ell})^{-1}\dot{\boldsymbol{B}}_\ell \boldsymbol{f}_\ell\|^2 \mathbf{1}_{\mathcal{A}_\ell} \mathbf{1}_{\left\{\|\delta\dot{\boldsymbol{B}}_\ell\|_{\mathrm{op}} > a_\ell\right\}},$$

$$IX = \sum_{\ell=1}^{L} \|\delta(\boldsymbol{K}_{\delta,\ell})^{-1}\dot{\boldsymbol{B}}_\ell \boldsymbol{f}_\ell\|^2 \mathbf{1}_{\mathcal{A}_\ell \cap \mathcal{B}_\ell} \mathbf{1}_{\left\{\|\boldsymbol{K}_\ell \boldsymbol{f}_\ell\| < \frac{\tau_\ell}{2}\right\}}.$$

On $\mathcal{A}_\ell$, we have

$$\|\delta(\boldsymbol{K}_{\delta,\ell})^{-1}\dot{\boldsymbol{B}}_\ell \boldsymbol{f}_\ell\|^2 \lesssim \delta^2\, \kappa_\ell^2 \|\dot{\boldsymbol{B}}_\ell\|_{\mathrm{op}}^2 \|\boldsymbol{f}_\ell\|^2$$

hence

$$\begin{aligned}
\mathbb{E}\left[VIII\right] &\lesssim \delta^2 \sum_{\ell=1}^{L} \kappa_\ell^2 \|\boldsymbol{f}_\ell\|^2\, \mathbb{E}\left[\|\dot{\boldsymbol{B}}_\ell\|_{\mathrm{op}}^2 \mathbf{1}_{\left\{\|\delta\dot{\boldsymbol{B}}_\ell\|_{\mathrm{op}} > a_\ell\right\}}\right] \\
&\leqslant \delta^2 \sum_{\ell=1}^{L} \kappa_\ell^2 \|\boldsymbol{f}_\ell\|^2\, \mathbb{E}\left[\|\dot{\boldsymbol{B}}_\ell\|_{\mathrm{op}}^4\right]^{1/2} \mathbb{P}\left(\|\delta\dot{\boldsymbol{B}}_\ell\|_{\mathrm{op}} > a_\ell\right)^{1/2} \\
&\lesssim \delta^2 \sum_{\ell=1}^{L} \kappa_\ell^2 \|\boldsymbol{f}_\ell\|^2 |\Lambda_\ell| \delta^{\,c_0\rho^2|\Lambda_\ell|^2/2\lambda_0^2} \\
&\lesssim |\log\delta| \max_{1\leqslant\ell\leqslant L} \delta^{\,c_0\rho^2|\Lambda_\ell|^2/2\lambda_0^2} \|f\|_{\mathbb{H}}^2
\end{aligned}$$

applying successively Cauchy-Schwarz, the moment bound (3.22) and Lemma 3.5.1. Indeed, since $a_\ell = \rho/\kappa_\ell$, by definition of κ_ℓ in (3.7), we infer

$$\begin{aligned}
\mathbb{P}\left(\|\delta\dot{\boldsymbol{B}}_\ell\|_{\mathrm{op}} > a_\ell\right) &\leqslant \mathbb{P}\left(|\Lambda_\ell|^{-1/2}\|\dot{\boldsymbol{B}}_\ell\|_{\mathrm{op}} > |\Lambda_\ell|^{-1/2}\tfrac{\rho}{\kappa_\ell}\delta^{-1}\right) \\
&= \mathbb{P}\left(|\Lambda_\ell|^{-1/2}\|\dot{\boldsymbol{B}}_\ell\|_{\mathrm{op}} > \tfrac{\rho}{\lambda_0}|\log\delta|^{1/2}\right) \\
&\leqslant \exp\left(-c_0\tfrac{\rho^2}{\lambda_0^2}|\log\delta||\Lambda_\ell|^2\right) = \delta^{\,c_0\rho^2|\Lambda_\ell|^2/\lambda_0^2}
\end{aligned} \tag{3.32}$$

by (3.24) of Lemma 3.5.2 since $\frac{\rho}{\lambda_0}|\log\delta|^{1/2} \geqslant \beta_0$ for sufficiently small λ_0 thanks to the assumption $\delta \leqslant \delta_0 < 1$. Finally, since Λ_ℓ is non-empty, by taking λ_0 sufficiently small, we conclude

$$\mathbb{E}\left[VIII\right] \lesssim \delta^2 \tag{3.33}$$

uniformly in $f \in \mathcal{W}^s(M)$. We now turn to the term IX. Observe first that

$$\mathbf{1}_{\mathcal{B}_\ell} \mathbf{1}_{\left\{\|\boldsymbol{K}_\ell \boldsymbol{f}_\ell\| < \frac{\tau_\ell}{2}\right\}} \leqslant \mathbf{1}_{\left\{n^{-1/2}\|\boldsymbol{\eta}_\ell\| \geqslant \frac{\tau_\ell}{2}\right\}}. \tag{3.34}$$

We reproduce the steps we used for the term $VIII$, replacing the event $\{\|\delta\dot{\boldsymbol{B}}_\ell\|_{\mathrm{op}} > a_\ell\}$ by $\{n^{-1/2}\|\boldsymbol{\eta}_\ell\| \geqslant \frac{\tau_\ell}{2}\}$. We obtain

$$\mathbb{E}\left[IX\right] \lesssim \delta^2 \sum_{\ell=1}^{L} \kappa_\ell^2 \|\boldsymbol{f}_\ell\|^2 |\Lambda_\ell|\, \mathbb{P}\left(n^{-1/2}\|\boldsymbol{\eta}_\ell\| \geqslant \tfrac{\tau_\ell}{2}\right)^{1/2}.$$

By definition of τ_ℓ in (3.8) and Lemma 3.24, we have

$$\begin{aligned}\mathbb{P}\left(n^{-1/2}\|\boldsymbol{\eta}_\ell\| > \tfrac{\tau_\ell}{2}\right) &= \mathbb{P}\left(|\Lambda_\ell|^{-1/2}\|\boldsymbol{\eta}_\ell\| > \tfrac{\mu_0}{2}(\log n)^{1/2}\right)\\ &\leqslant \exp\big(-c_1\tfrac{\mu_0^2}{4}\log n\big) = n^{-c_1\mu_0^2/4} \end{aligned} \tag{3.35}$$

since $\frac{\mu_0}{2}(\log n)^{1/2} \geqslant \beta_1$ for large enough μ_0. It follows that

$$\mathbb{E}\big[IX\big] \lesssim |\log\delta|\|f\|_{\mathbb{H}}^2\, n^{-c_1\mu_0^2/4} \lesssim n^{-1}|\log\delta| \tag{3.36}$$

by taking μ_0 sufficiently large. The bound is uniform in $f \in \mathcal{W}^s(M)$. Putting together the estimates (3.33) and (3.36), we derive

$$\mathbb{E}\big[VI\big] \lesssim \delta^2 + n^{-1}|\log\delta| \tag{3.37}$$

for large enough n, uniformly in $f \in \mathcal{W}^s(M)$. □

• *The term VII.* . The arguments needed here are quite similar to those we used for the term VI. On $\mathcal{A}_\ell$, we have

$$\|n^{-1/2}(\boldsymbol{K}_{\delta,\ell})^{-1}\boldsymbol{\eta}_\ell\|^2 \leqslant n^{-1}\kappa_\ell^2\|\boldsymbol{\eta}_\ell\|^2,$$

hence, using (3.34), the fact that $\mathbb{E}\big[\|\boldsymbol{\eta}_\ell\|^2\big] = |\Lambda_\ell| \lesssim \ell^{d-1}$ together with $\kappa_\ell \leqslant n^{1/2}$ by definition (3.7), we successively obtain

$$\begin{aligned}\mathbb{E}\big[VII\big] &\leqslant n^{-1}\sum_{\ell=1}^{L}\kappa_\ell^2\,\mathbb{E}\big[\|\boldsymbol{\eta}_\ell\|^2\big]\Big(\mathbb{P}\left(\|\delta\dot{\boldsymbol{B}}_\ell\|_{\mathrm{op}} > a_\ell\right) + \mathbb{P}\left(n^{-1/2}\|\boldsymbol{\eta}_\ell\| > \tfrac{\tau_\ell}{2}\right)\Big)\\ &\lesssim \max_{1\leqslant\ell\leqslant L}\Big\{\mathbb{P}\left(\|\delta\dot{\boldsymbol{B}}_\ell\|_{\mathrm{op}} > a_\ell\right) + \mathbb{P}\left(n^{-1/2}\|\boldsymbol{\eta}_\ell\| > \tfrac{\tau_\ell}{2}\right)\Big\}\sum_{\ell=1}^{L}\ell^{d-1}\\ &\lesssim L^{d-1}\big(\delta^{c_0\rho^2/\lambda_0^2} + n^{-c_1\mu_0^2/4}\big)\end{aligned}$$

where we applied (3.32) and (3.35) to obtain the last inequality. The choice of L in (3.10) leads to

$$\mathbb{E}\big[VII\big] \lesssim (\delta^2)^{-\frac{d-1}{2\nu+d-1}+\frac{c_0\rho^2}{\lambda_0^2}} + n^{\frac{1}{2\nu+d}-\frac{c_1\mu_0^2}{4}} \lesssim \delta^2 \bigvee n^{-1} \tag{3.38}$$

by taking λ_0 sufficiently small and μ_0 sufficiently large. □

• *The term I, conclusion.* We put together the estimates (3.30), (3.31), (3.37) and (3.38). We obtain

$$\mathbb{E}\big[I\big] \lesssim \big(\delta^2|\log\delta|\big)^{1\wedge 2s/(2\nu+d-1)} \bigvee \big(n^{-1}\log n\big)^{2s/(2(s+\nu)+d)} \tag{3.39}$$

uniformly in $f \in \mathcal{W}^s(M)$. □

• *The term II.* We claim the following inequality

$$\mathbf{1}_{\mathcal{A}^c} \leqslant \mathbf{1}_{\left\{\|(\boldsymbol{K}_\ell)^{-1}\|_{\mathrm{op}} \geqslant \frac{\kappa_\ell}{2}\right\}} + \mathbf{1}_{\left\{\|\boldsymbol{K}_{\delta,\ell} - \boldsymbol{K}_\ell\|_{\mathrm{op}} \geqslant \kappa_\ell^{-1}\right\}}, \tag{3.40}$$

a consequence of the following elementary lemma

Lemma 3.5.3. *Let A and B be two bounded operators with bounded inverse. If $\|B^{-1}\| \geqslant \kappa$ for some $\kappa > 0$, then either $\|A^{-1}\| \geqslant \kappa/2$ or $\|A - B\| \geqslant 1/\kappa$.*

Proof of Lemma 3.5.3. Write $B = A + \xi$. Assume that $\|A^{-1}\| < \kappa/2$. By the triangle inequality, $\|(A+\xi)^{-1} - A^{-1}\| \geqslant \kappa/2$. We proceed by contradiction: suppose that $\|\xi\| \leqslant 1/\kappa$. Then we have $\|A^{-1}\xi\| \leqslant \|A^{-1}\|\|\xi\| \leqslant 1/2 < 1$ and a standard Neumann series argument entails

$$\begin{aligned}
\|(A+\xi)^{-1} - A^{-1}\| =& \|(I + A^{-1}\xi)^{-1}A^{-1} - A^{-1}\| \\
=& \|\sum_{i\geqslant 1}(-1)^i (A^{-1})^{i+1}\xi^i\| \\
\leqslant& \sum_{i\geqslant 1}\|A^{-1}\|^{i+1}\|\xi\|^i \\
<& \frac{\kappa}{2}\sum_{i\geqslant 1}\Big(\frac{\kappa}{2}\Big)^i\Big(\frac{1}{\kappa}\Big)^i = \frac{\kappa}{2},
\end{aligned}$$

a contradiction. □

By Assumption (3.2.2), we have $\|(\boldsymbol{K}_\ell)^{-1}\|_{\mathrm{op}} \leqslant Q_2(K)\ell^\nu$. Therefore

$$\mathbf{1}_{\left\{\|(\boldsymbol{K}_\ell)^{-1}\|_{\mathrm{op}} \geqslant \frac{\kappa_\ell}{2}\right\}} \leqslant \mathbf{1}_{\left\{\ell \geqslant c\left(\delta^2|\log\delta|\right)^{1/(2\nu+d-1)} \wedge n^{1/(2\nu)}\right\}}$$

for some constant c that depends on $Q_2(K)$ and λ_0 only. For the second term in the right-hand side of (3.40), we apply by Lemma 3.5.1 in the same way as we obtained (3.33) for the term $VIII$. We derive

$$\begin{aligned}
\mathbb{P}\left(\|\delta\dot{\boldsymbol{B}}_\ell\|_{\mathrm{op}} \geqslant \kappa_\ell^{-1}\right) &= \mathbb{P}\left(|\Lambda_\ell|^{-1/2}\|\dot{\boldsymbol{B}}_\ell\|_{\mathrm{op}} \geqslant \mu_0^{-1}|\log\delta|^{1/2}\right) \\
&\leqslant \exp\Big(-\tfrac{c_0}{\mu_0^2}|\log\delta||\Lambda_n|^2\Big) = \delta^{\,c_0|\Lambda_\ell|^2/\mu_0} \leqslant \delta^{\,c_0/\mu_0}
\end{aligned}$$

for large enough μ_0. Therefore

$$\begin{aligned}
\mathbb{E}\left[II\right] &\leqslant \sum_{\ell=1}^{L}\|\boldsymbol{f}_\ell\|^2\Big(\mathbf{1}_{\left\{\ell\geqslant c\left(\delta^2|\log\delta|\right)^{1/(2\nu+d-1)} \wedge n^{1/(2\nu)}\right\}} + \mathbb{P}\left(\|\delta\dot{\boldsymbol{B}}_\ell\|_{\mathrm{op}} \geqslant \kappa_\ell^{-1}\right)\Big) \\
&\lesssim \big(n^{-s/\nu} \bigvee \left(\delta^2|\log\delta|\right)^{2s/(2\nu+d-1)}\big)\|f\|_{\mathcal{W}^s}^2 + \|f\|_{\mathbb{H}}^2\,\delta^{\,c_0/\mu_0}.
\end{aligned}$$

We finally obtain

$$\begin{aligned}
\mathbb{E}\left[II\right] &\lesssim \left(\delta^2\log\delta^{-1}\right)^{2s/(2\nu+d-1)} + \delta^2 + n^{-s/\nu} \\
&\lesssim \left(\delta^2|\log\delta|\right)^{1\wedge 2s/(2\nu+d-1)} \bigvee \left(n^{-1}\log n\right)^{2s/(2(s+\nu)+d)}
\end{aligned} \tag{3.41}$$

uniformly in $f \in \mathcal{W}^s(M), K \in \mathcal{G}^\nu(Q)$. □

• *The term III.* Obviously, the decomposition (3.23) entails

$$\mathbf{1}_{\mathcal{B}^c} = \mathbf{1}_{\left\{\|\boldsymbol{K}_\ell \boldsymbol{f}_\ell + n^{-1/2}\boldsymbol{\eta}_\ell\| < \tau_\ell\right\}} \leqslant \mathbf{1}_{\left\{\|\boldsymbol{K}_\ell \boldsymbol{f}_\ell\| \leqslant 2\tau_\ell\right\}} + \mathbf{1}_{\left\{n^{-1/2}\|\boldsymbol{\eta}_\ell\| > \tau_\ell\right\}}.$$

On the one hand, we have

$$\|\boldsymbol{K}_\ell \boldsymbol{f}_\ell\| \geqslant \|(\boldsymbol{K}_\ell)^{-1}\|_{\mathrm{op}}^{-1}\|\boldsymbol{f}_\ell\| \geqslant Q_2(K)^{-1}\ell^{-\nu}\|\boldsymbol{f}_\ell\|$$

by Assumption 3.2.2. By definition of τ_ℓ in (3.8) it follows that, for any $1 \leqslant k \leqslant L$,

$$\begin{aligned}
\sum_{\ell=1}^{L} \|\boldsymbol{f}_\ell\|^2 \mathbf{1}_{\left\{\|\boldsymbol{K}_\ell \boldsymbol{f}_\ell\| \leqslant 2\tau_\ell\right\}} &\leqslant \sum_{\ell=1}^{L} \|\boldsymbol{f}_\ell\|^2 \mathbf{1}_{\left\{\|\boldsymbol{f}_\ell\| \leqslant 2Q_2(K)^{-1}\ell^{\nu}\tau_\ell\right\}} \\
&\lesssim \sum_{\ell=1}^{k} \ell^{2\nu}\tau_\ell^2 + \sum_{\ell=k+1}^{L} \|\boldsymbol{f}_\ell\|^2 \\
&\lesssim (n^{-1}\log n) \sum_{\ell=1}^{k} \ell^{2\nu+d-1} + \|f\|_{\mathcal{W}^s}^2 k^{-2s} \\
&\lesssim (n^{-1}\log n)\, k^{2\nu+d} + \|f\|_{\mathcal{W}^s}^2 k^{-2s}.
\end{aligned}$$

The choice $k = \lfloor \left(n^{1/2}(\log n)^{-1/2}\right)^{1/(2(s+\nu)+d)} \rfloor$ yields

$$\sum_{\ell=1}^{L} \|\boldsymbol{f}_\ell\|^2 \mathbf{1}_{\left\{\|\boldsymbol{K}_\ell \boldsymbol{f}_\ell\| \leqslant 2\tau_\ell\right\}} \lesssim \left(n^{-1}\log n\right)^{2s/(2(s+\nu)+d)} \tag{3.42}$$

uniformly in $f \in \mathcal{W}^s(M), K \in \mathcal{G}^\nu(Q)$. On the other hand, by (3.35), we have

$$\sum_{\ell=1}^{L} \|\boldsymbol{f}_\ell\|^2 \, \mathbb{P}\left(n^{-1/2}\|\boldsymbol{\eta}_\ell\| > \tau_\ell\right\}\right) \lesssim \|f\|_{\mathbb{H}}^2 \, n^{-c_1\mu_0^2/4} \lesssim n^{-1}$$

by taking μ_0 large enough, uniformly in $f \in \mathcal{W}^s(M)$. Combining this last estimate with (3.42) we infer

$$\mathbb{E}\left[III\right] \lesssim \left(n^{-1}\log n\right)^{2s/(2(s+\nu)+d)} + n^{-1} \tag{3.43}$$

uniformly in $f \in \mathcal{W}^s(M), K \in \mathcal{G}^\nu(Q)$. □

Proof of Theorem 3.3.1, completion. It remains to piece together the estimates (3.25), (3.39), (3.41) and (3.43). □

3.5.3 Proof of Theorem 3.3.2

Preliminaries: a Bayesian inequality

For every $\ell \geqslant 1$, denote by $\mathcal{M}_\ell$ the set of $|\Lambda_\ell| \times |\Lambda_\ell|$ matrices. We denote by $\mathcal{M}_\ell^\nu(Q)$ the subset of $\mathcal{M}_\ell$ of matrices $\boldsymbol{K}_\ell$ such that

$$\|\boldsymbol{K}_\ell\|_{\mathrm{op}} \leqslant Q_2\ell^{-\nu} \;\text{ and }\; \|(\boldsymbol{K}_\ell)^{-1}\|_{\mathrm{op}} \leqslant Q_1\ell^{\nu}.$$

Define

$$\boldsymbol{K}_\ell^0 = c_1 \ell^{-\nu} \boldsymbol{I}_\ell \tag{3.44}$$

where $\boldsymbol{I}_\ell$ denotes the identity in $\mathcal{M}_\ell$ and $c_1 > 0$ is such that

$$1/Q_1 < c_1 < Q_2$$

so that $\boldsymbol{K}_\ell^0 \in \mathcal{M}_\ell^\nu(Q)$. We assume a Bayesian approach and pick $\boldsymbol{K}_\ell$ at random, with

$$\boldsymbol{K}_\ell = \boldsymbol{K}_\ell^0 + c_2\, \delta \dot{\boldsymbol{W}}_\ell,$$

for some $c_2 > 0$ and where $\dot{\boldsymbol{W}}_\ell$ is an independent copy of $\dot{\boldsymbol{B}}_\ell$. Define $\boldsymbol{g}_\ell = (1\ 0\ \ldots\ 0)^T$ as the first canonical (column) vector in $\mathbb{R}^{|\Lambda_\ell|}$. Define also

$$\boldsymbol{\vartheta} = -(\boldsymbol{K}_\ell^0)^{-1}(\boldsymbol{K}_\ell - \boldsymbol{K}_\ell^0)(\boldsymbol{K}_\ell^0)^{-1}\boldsymbol{g}_\ell \tag{3.45}$$

and

$$\boldsymbol{X} = -(\boldsymbol{K}_\ell^0)^{-1}(\boldsymbol{K}_{\delta,\ell} - \boldsymbol{K}_\ell^0)(\boldsymbol{K}_\ell^0)^{-1}\boldsymbol{g}_\ell. \tag{3.46}$$

Lemma 3.5.4. *There exists a constant c_3 depending on ν, Q and c_2 only such that*

$$\inf_T \mathbb{P}\left(\delta^{-2}\ell^{-4\nu}|\Lambda_\ell|^{-1}\|T(\boldsymbol{X}) - \boldsymbol{\vartheta}\|^2 \geqslant c_3\right) \geqslant \tfrac{1}{2}, \tag{3.47}$$

where the infimum is taken among all estimators T based on the observation $\boldsymbol{X}$.

Proof of Lemma 3.5.4. We have $\boldsymbol{X} = \boldsymbol{\vartheta} + \boldsymbol{\varepsilon}$, with

$$\boldsymbol{\vartheta} = -(\boldsymbol{K}_\ell^0)^{-1} c_2 \delta \dot{\boldsymbol{W}} (\boldsymbol{K}_\ell^0)^{-1}\boldsymbol{g}_\ell \ \text{ and } \ \boldsymbol{\varepsilon} = -(\boldsymbol{K}_\ell^0)^{-1}\delta\dot{\boldsymbol{B}}(\boldsymbol{K}_\ell^0)^{-1}\boldsymbol{g}_\ell.$$

By construction, $\boldsymbol{\vartheta}$ and $\boldsymbol{\varepsilon}$ are two independent Gaussian random vectors. More precisely, by definition of $\boldsymbol{g}_\ell$ and with obvious notation, we have

$$\boldsymbol{\vartheta} \sim \mathcal{N}\big(0, \delta^2 c_2^2 c_1^{-4}\ell^{4\nu}\boldsymbol{I}_\ell\big) \ \text{ and } \ \boldsymbol{\varepsilon} \sim \mathcal{N}\big(0, \delta^2 c_1^{-4}\ell^{4\nu}\boldsymbol{I}_\ell\big).$$

It readily follows that the posterior law of $\boldsymbol{\vartheta}$ given $\boldsymbol{X}$ is

$$\mathcal{L}(\boldsymbol{\vartheta} \,|\, \boldsymbol{X}) = \mathcal{N}\Big(\frac{c_2^2}{1+c_2^2}\boldsymbol{X}, \delta^2\frac{c_2^2}{1+c_2^2}c_1^{-4}\ell^{4\nu}\boldsymbol{I}_\ell\Big).$$

Now, for $c_3 > 0$, define

$$H_\delta(c_3, \boldsymbol{x}) = \mathbf{1}_{\{\delta^{-2}\ell^{-4\nu}|\Lambda_\ell|^{-1}\|\boldsymbol{x}\|^2 \geqslant c_3\}} \ \text{ for } \ \boldsymbol{x} \in \mathbb{R}^{|\Lambda_\ell|}.$$

Setting $z(\boldsymbol{X}) = T(\boldsymbol{X}) - \mathbb{E}[\boldsymbol{\vartheta} \,|\, \boldsymbol{X}]$, we have

$$\begin{aligned}\mathbb{E}\left[H_\delta\big(c_3, T(\boldsymbol{X}) - \boldsymbol{\vartheta}\big) \,|\, \boldsymbol{X}\right] &= \mathbb{E}\left[H_\delta\big(c_3, z(\boldsymbol{X}) + \mathbb{E}[\boldsymbol{\vartheta} \,|\, \boldsymbol{X}] - \boldsymbol{\vartheta}\big) \,|\, \boldsymbol{X}\right] \\ &\geqslant \mathbb{E}\left[H_\delta\big(c_3, \mathbb{E}[\boldsymbol{\vartheta} \,|\, \boldsymbol{X}] - \boldsymbol{\vartheta}\big) \,|\, \boldsymbol{X}\right]\end{aligned}$$

where we used a version of Anderson's Lemma given in Lemma 10.2 in [42] p. 157. Indeed, the law of $\mathbb{E}[\boldsymbol{\vartheta} \,|\, \boldsymbol{X}] - \vartheta$ has a centrally symmetric density and the function H_δ is nonnegative, centrally symmetric, satisfies $H_\delta(0) = 0$ and the sets $\{\boldsymbol{x},\ H_\delta(c_3, \boldsymbol{x}) < c\}$ are convex for any $c > 0$.

Now, $\| \mathbb{E}[\boldsymbol{\vartheta} \,|\, \boldsymbol{X}] - \boldsymbol{\vartheta}\|^2$ has a χ^2-distribution with $|\Lambda_\ell|$ degrees of freedom, up to a scaling factor of order $\delta^2 \ell^{4\nu}$. This means that the sequence of random variables $\delta^{-2}\ell^{-4\nu}|\Lambda_\ell|^{-1}\| \mathbb{E}[\boldsymbol{\vartheta} \,|\, \boldsymbol{X}] - \boldsymbol{\vartheta}\|^2$ is bounded below in probability in $\ell \geqslant 1$ and $\delta > 0$. Since $\mathbb{E}[\boldsymbol{\vartheta} \,|\, \boldsymbol{X}] - \boldsymbol{\vartheta}$ is moreover independent of $\boldsymbol{X}$, it follows that there exists c_3 independent of δ and ℓ such that

$$\mathbb{E}\left[H_\delta\big(c_3, \mathbb{E}[\boldsymbol{\vartheta} \,|\, \boldsymbol{X}] - \boldsymbol{\vartheta}\big) \,|\, \boldsymbol{X}\right] \geqslant \tfrac{1}{2}.$$

Integrating with respect to $\boldsymbol{X}$, we obtain (3.47) and the result follows. □

Proof of Theorem 3.3.2

We assume with no loss of generality that $2\nu + d - 1 \geqslant 2s$. (Otherwise, the lower bound δ trivially follows from the parametric case.) Let $\Pi^{s,\nu}(M, Q_1)$ denote the set of sequences $\pi = (\pi_\ell)_{\ell \geqslant 1}$ satisfying

$$\sum_{\ell \geqslant 1} \pi_\ell^2 \ell^{2(s+\nu)} \leqslant \frac{M^2}{Q_1^2}. \tag{3.48}$$

For $\pi \in \Pi^{s,\nu}(M, Q_1)$ and $K \in \mathcal{G}^\nu(Q)$, define f via its coordinates in H_ℓ by

$$\boldsymbol{f}_\ell = \pi_\ell \boldsymbol{K}_\ell^{-1} \boldsymbol{g}_\ell, \quad \ell \geqslant 1,$$

where $\boldsymbol{g}_\ell$ is an arbitrary vector in $\mathbb{R}^{|\Lambda_\ell|}$ with $\|\boldsymbol{g}_\ell\| = 1$ (fixed in the sequel). Then

$$\sum_{\ell \geqslant 1} \ell^{2s} \|\pi_\ell \boldsymbol{K}_\ell^{-1} \boldsymbol{g}_\ell\|^2 \leqslant \sum_{\ell \geqslant 1} \pi_\ell^2 \|\boldsymbol{K}_\ell^{-1}\|_{\mathrm{op}}^2 \|\boldsymbol{g}_\ell\|^2 \leqslant Q_1^2 \sum_{\ell \geqslant 1} \pi_\ell^2 \ell^{2(s+\nu)} \leqslant M^2$$

since $\pi \in \Pi^{s,\nu}(M, Q_1)$. Therefore $f \in \mathcal{W}^s(M)$. It follows that for an arbitrary estimator $\widehat{f}$, we have

$$\begin{aligned}
&\sup_{f \in \mathcal{W}^s(M), K \in \mathcal{G}^\nu(Q)} \mathbb{E}\left[\big\|\widehat{f} - f\big\|_{\mathbb{H}}^2\right] \\
&= \sup_{f \in \mathcal{W}^s(M), K \in \mathcal{G}^\nu(Q)} \sum_{\ell \geqslant 1} \mathbb{E}\left[\big\|\widehat{\boldsymbol{f}}_\ell - \boldsymbol{f}_\ell\big\|^2\right] \\
&\geqslant \sup_{\pi \in \Pi^{s,\nu}(M,Q_1), K \in \mathcal{G}^\nu(Q)} \sum_{\ell \geqslant 1} \mathbb{E}\left[\big\|\widehat{\boldsymbol{f}}_\ell - \pi_\ell \boldsymbol{K}_\ell^{-1} \boldsymbol{g}_\ell\big\|^2\right].
\end{aligned}$$

Lemma 3.5.5. *There exist a choice of $\boldsymbol{g}_\ell$ with $\|\boldsymbol{g}_\ell\| = 1$ and constants c_4, c_5 (depending on s, ν, M, Q) such that for any $\pi \in \Pi^{s,\nu}(M, Q_1)$, if $|\Lambda_\ell|^{1/2}\delta \leqslant c_4\, \ell^{-\nu}$, we have*

$$\inf_{\widehat{\boldsymbol{f}}_\ell} \sup_{K \in \mathcal{G}^\nu(Q)} \mathbb{E}\left[\|\widehat{\boldsymbol{f}}_\ell - \pi_\ell \boldsymbol{K}_\ell^{-1} \boldsymbol{g}_\ell\|^2\right] \geqslant c_5\, \delta^2 \ell^{4\nu + d - 1} \pi_\ell^2 \tag{3.49}$$

where the infimum is taken over all estimators and provided $\delta > 0$ is sufficiently small.

With (3.49), we easily conclude: Define $L = \lfloor c_6 \delta^{-2/(2\nu+d-1)} \rfloor$ with $c_6 > 0$. For $1 \leqslant \ell \leqslant L$, the assumption $|\Lambda|^{1/2}\delta \leqslant c_4\, \ell^{-\nu}$ of Lemma 3.5.5 is satisfied by picking $c_6 > 0$ sufficiently small and we have

$$\begin{aligned}
&\sup_{\pi \in \Pi^{s,\nu}(M,Q_1), K \in \mathcal{G}^\nu(Q)} \sum_{\ell \geqslant 1} \mathbb{E}\left[\big\| \widehat{\boldsymbol{f}}_\ell - \pi_\ell \boldsymbol{K}_\ell^{-1} \boldsymbol{g}_\ell \big\|^2 \right] \\
&\geqslant c_5 \delta^2 \sup_{\pi \in \Pi^{s,\nu}(M,Q_1)} \sum_{\ell=1}^{L} \ell^{4\nu+d-1} \pi_\ell^2 \\
&\geqslant c_5 \delta^2 \frac{M^2}{Q_1^2} L^{2\nu+d-1-2s} \geqslant\ c_5 c_6^{2\nu+d-1-2s} \frac{M^2}{Q_1^2} \delta^{2s/(2\nu+d-1)}
\end{aligned}$$

thanks to the admissible choice π specified by $\pi_\ell^2 = \ell^{-2(\nu+s)} M^2/Q_1^2$ if $\ell = L$ and 0 otherwise. Theorem 3.3.2 follows. It remains to prove Lemma 3.5.5.

Proof of Lemma 3.5.5. In view of (3.49), we may (and will) assume that $\pi_\ell = 1$. We rely on the notation and definition of the preliminaries. Observe first that

$$\begin{aligned}
&\inf_{\widehat{\boldsymbol{f}}_\ell} \sup_{K \in \mathcal{G}^\nu(Q)} \mathbb{E}\left[\| \widehat{\boldsymbol{f}}_\ell - \boldsymbol{K}_\ell^{-1} \boldsymbol{g}_\ell \|^2 \right] \\
&= \inf_{\widehat{\boldsymbol{f}}_\ell} \sup_{K \in \mathcal{G}^\nu(Q)} \mathbb{E}\left[\| \widehat{\boldsymbol{f}}_\ell - \big(\boldsymbol{K}_\ell^{-1} - (\boldsymbol{K}_\ell^0)^{-1} \big) \boldsymbol{g}_\ell \|^2 \right].
\end{aligned}$$

where $\boldsymbol{K}^0$ is defined in (3.44). Put $v_{\delta,\ell} = \delta^2 \ell^{4\nu+d-1}$. For any $c > 0$, by Chebyshev inequality, we have

$$\begin{aligned}
&c^2 v_{\delta,\ell}^{-2} \inf_{\widehat{\boldsymbol{f}}_\ell} \sup_{K \in \mathcal{G}^\nu(Q)} \mathbb{E}\left[\| \widehat{\boldsymbol{f}}_\ell - \big(\boldsymbol{K}_\ell^{-1} - (\boldsymbol{K}_\ell^0)^{-1} \big) \boldsymbol{g}_\ell \|^2 \right] \\
&\geqslant \inf_{\widehat{\boldsymbol{f}}_\ell} \sup_{K \in \mathcal{G}^\nu(Q)} \mathbb{P}\left(\| \widehat{\boldsymbol{f}}_\ell - \big(\boldsymbol{K}_\ell^{-1} - (\boldsymbol{K}_\ell^0)^{-1} \big) \boldsymbol{g}_\ell \| \geqslant c\, v_{\delta,\ell} \right). \qquad (3.50)
\end{aligned}$$

We adopt the same Bayesian approach as in the preliminaries and consider $\boldsymbol{K}_\ell$ as a random matrix with distribution such that

$$\boldsymbol{K}_\ell = \boldsymbol{K}_\ell^0 + c_2\, \delta \dot{\boldsymbol{W}}_\ell, \qquad (3.51)$$

where $\dot{\boldsymbol{W}}_\ell$ is an independent copy of $\dot{\boldsymbol{B}}_\ell$ and $c_2 > 0$ is to be specified later. Using the randomisation (3.51) on $\boldsymbol{K}_\ell$, the right-hand side in (3.50) is now bigger than

$$\inf_{\widehat{\boldsymbol{f}}_\ell} \mathbb{P}\left(\| \widehat{\boldsymbol{f}}_\ell - \big(\boldsymbol{K}_\ell^{-1} - (\boldsymbol{K}_\ell^0)^{-1} \big) \boldsymbol{g}_\ell \| \geqslant c\, v_{\delta,\ell} \right) - \mathbb{P}\left(\boldsymbol{K}_\ell \notin \mathcal{M}_\ell^\nu(Q) \right). \qquad (3.52)$$

Let us first show that

$$\inf_{\widehat{\boldsymbol{f}}_\ell} \mathbb{P}\left(\| \widehat{\boldsymbol{f}}_\ell - \big(\boldsymbol{K}_\ell^{-1} - (\boldsymbol{K}_\ell^0)^{-1} \big) \boldsymbol{g}_\ell \| \geqslant c\, v_{\delta,\ell} \right) \qquad (3.53)$$

is bounded below for an appropriate choice of $c > 0$. Introduce the event

$$\mathcal{A}_\delta = \left\{ Q_1 \ell^\nu c_2 \delta \| \dot{\boldsymbol{W}}_\ell \|_{\mathrm{op}} \leqslant \rho \right\}$$

for some $0 < \rho < 1$. Observe that $\|(\boldsymbol{K}_\ell^0)^{-1} c_2 \delta \dot{\boldsymbol{W}}_\ell\|_{\mathrm{op}} \leqslant \rho$ on $\mathcal{A}_\delta$, therefore, by an usual Neuman series argument, we have the decomposition

$$\begin{aligned}&\boldsymbol{K}_\ell^{-1} - (\boldsymbol{K}_\ell^0)^{-1} \\ =& -(\boldsymbol{K}_\ell^0)^{-1}(c_2\delta\dot{\boldsymbol{W}}_\ell)(\boldsymbol{K}_\ell^0)^{-1} + \sum_{n\geqslant 2}(-1)^n\big((\boldsymbol{K}_\ell^0)^{-1}c_2\dot{\boldsymbol{W}}_\ell\big)^n(\boldsymbol{K}_\ell^0)^{-1}\end{aligned}$$

Applying the vector $\boldsymbol{g}_\ell = (1, 0, \ldots, 0)$ and setting

$$\boldsymbol{\zeta}_{\delta,\ell} = \sum_{n\geqslant 2}(-1)^n\big((\boldsymbol{K}_\ell^0)^{-1}c_2\dot{\boldsymbol{W}}_\ell\big)^n(\boldsymbol{K}_\ell^0)^{-1}\boldsymbol{g}_\ell,$$

we obtain the decomposition

$$\begin{aligned}\big(\boldsymbol{K}_\ell^{-1} - (\boldsymbol{K}_\ell^0)^{-1}\big)\boldsymbol{g}_\ell &= -(\boldsymbol{K}_\ell^0)^{-1}(c_2\delta\dot{\boldsymbol{W}}_\ell)(\boldsymbol{K}_\ell^0)^{-1}\boldsymbol{g}_\ell + \boldsymbol{\zeta}_{\delta,\ell} \\ &= \boldsymbol{\vartheta} + \boldsymbol{\zeta}_{\delta,\ell},\end{aligned}$$

where $\boldsymbol{\vartheta}$ is defined in (3.45). We derive, for any $c > 0$

$$\begin{aligned}&\mathbb{P}\left(\|\widehat{\boldsymbol{f}}_\ell - \big(\boldsymbol{K}_\ell^{-1} - (\boldsymbol{K}_\ell^0)^{-1}\big)\boldsymbol{g}_\ell\| \geqslant c\, v_{\delta,\ell}\right) \\ \geqslant\ &\mathbb{P}\left(\|\widehat{\boldsymbol{f}}_\ell - (\boldsymbol{\vartheta} + \boldsymbol{\zeta}_{\delta,\ell})\| \geqslant c\, v_{\delta,\ell} \text{ and } \mathcal{A}_\delta\right) \\ \geqslant\ &\mathbb{P}\left(\|\widehat{\boldsymbol{f}}_\ell - \boldsymbol{\vartheta}\| \geqslant \tfrac{1}{2}c\, v_{\delta,\ell} \text{ and } \mathcal{A}_\delta \text{ and } \|\boldsymbol{\zeta}_{\delta,\ell}\| \leqslant \tfrac{1}{2}c\, v_{\delta,\ell}\right)\end{aligned}$$

by the triangle inequality. We claim that for any $\varepsilon > 0$, there exists a choice of sufficiently small c_2 such that for any $c > 0$:

$$\limsup_{\delta\to 0}\mathbb{P}\left(\mathcal{A}_\delta \text{ and } \|\boldsymbol{\zeta}_{\delta,\ell}\| \leqslant \tfrac{1}{2}c\, v_{\delta,\ell}\right) \geqslant 1 - \varepsilon. \tag{3.54}$$

Let us admit temporarily (3.54). For such a choice, we thus have

$$\begin{aligned}&\mathbb{P}\left(\|\widehat{\boldsymbol{f}}_\ell - \big(\boldsymbol{K}_\ell^{-1} - (\boldsymbol{K}_\ell^0)^{-1}\big)\boldsymbol{g}_\ell\| \geqslant c\, v_{\delta,\ell}\right) \\ \geqslant &\mathbb{P}\left(\|\widehat{\boldsymbol{f}}_\ell - \boldsymbol{\vartheta}\| \geqslant \tfrac{1}{2}c\, v_{\delta,\ell}\right) - \varepsilon.\end{aligned}$$

Let us now look at an apparently different problem: we want to estimate $\boldsymbol{\vartheta}$ from our observation $\boldsymbol{K}_{\delta,\ell}$, or equivalently, from the observation

$$-(\boldsymbol{K}_\ell^0)^{-1}(\boldsymbol{K}_{\delta,\ell} - \boldsymbol{K}_\ell^0)(\boldsymbol{K}_\ell^0)^{-1}.$$

The choice $\boldsymbol{g}_\ell = (1, 0, \ldots, 0)^T$ entails that $-(\boldsymbol{K}_\ell^0)^{-1}(\boldsymbol{K}_{\delta,\ell} - \boldsymbol{K}_\ell^0)(\boldsymbol{K}_\ell^0)^{-1}\boldsymbol{g}_\ell$ is a sufficient statistic, but this last quantity is precisely $\boldsymbol{X}$ defined in (3.46). Thus, without loss of generality, $\widehat{\boldsymbol{f}}_\delta$ can be taken as an estimator of the form $T(\boldsymbol{X})$. By Lemma 3.5.4, we know that $v_{\delta,\ell}$ is a lower bound for estimating $\boldsymbol{\vartheta}$.

More specifically, by taking c such that $c \leqslant 2\sqrt{c_3}$, we have

$$\mathbb{P}\left(\|\widehat{\boldsymbol{f}}_\ell - \boldsymbol{\vartheta}\| \geqslant \tfrac{1}{2}c\, v_{\delta,\ell}\right) - \varepsilon \geqslant \tfrac{1}{2} - \varepsilon \geqslant \tfrac{1}{4}$$

say, since the choice of ε is arbitrary, and (3.53) follows. It remains to prove (3.54).

First, we have that $|\Lambda_\ell|^{-1/2}\|\dot{\boldsymbol{W}}_\ell\|_{\mathrm{op}}$ is bounded in probability by Lemma 3.5.1 in $\ell \geqslant 1$. Since $|\Lambda_\ell|^{1/2}\delta \leqslant c_4\ell^\nu$ by assumption, we also have that $\ell^\nu\delta\|\dot{\boldsymbol{W}}_\ell\|_{\mathrm{op}}$ is bounded in probability, hence the probability of $\mathcal{A}_\delta$ can be taken arbitrarily close to 1 by taking c_2 sufficiently small. Moreover, on $\mathcal{A}_\delta$, we have

$$\begin{aligned}\|\zeta_{\delta,\ell}\| &\leqslant Q_1\ell^\nu \sum_{n\geqslant 2} \big(Q_1\ell^\nu c_2\delta\|\dot{\boldsymbol{W}}_\ell\|_{\mathrm{op}}\big)^n \\ &\leqslant (1-\rho)^{-1}c_2^2\,Q_1^3\delta^2\ell^{3\nu}\|\dot{\boldsymbol{W}}_\ell\|_{\mathrm{op}}^2 \\ &\leqslant (1-\rho)^{-1}c_2^2\,Q_1^3\delta\ell^{2\nu}|\Lambda_\ell|^{1/2}c_4|\Lambda_\ell|^{-1}\|\dot{\boldsymbol{W}}_\ell\|_{\mathrm{op}}^2\end{aligned}$$

where we again used the fact that $|\Lambda_\ell|^{1/2}\delta \leqslant c_4\ell^{-\nu}$ by assumption. The claim follows from the fact that $|\Lambda_\ell|^{-1/2}\|\dot{\boldsymbol{W}}_\ell\|_{\mathrm{op}}$ is bounded in probability. Hence (3.54) and (3.53) is proved.

In order to complete the proof of Lemma 3.5.5, we need to check that the term $\mathbb{P}\big(\boldsymbol{K}_\ell \notin \mathcal{M}_\ell^\nu(Q)\big)$ can be taken arbitrarily small when bounding (3.50) below by (3.52). We have

$$\begin{aligned}&\mathbb{P}\big(\boldsymbol{K}_\ell \notin \mathcal{M}_\ell^\nu(Q)\big) \\ &\leqslant \mathbb{P}\big(\|\boldsymbol{K}_\ell\|_{\mathrm{op}} > Q_2\ell^{-\nu}\big) + \mathbb{P}\big(\|\boldsymbol{K}_\ell^{-1}\|_{\mathrm{op}} > Q_1\ell^\nu\big).\end{aligned} \tag{3.55}$$

For the first term in the right-hand side of (3.55), we have

$$\begin{aligned}\mathbb{P}\big(\|\boldsymbol{K}_\ell\|_{\mathrm{op}} > Q_2\ell^{-\nu}\big) &\leqslant \mathbb{P}\big(\|c_2\delta\dot{\boldsymbol{W}}_\ell\|_{\mathrm{op}} > Q_2\ell^{-\nu} - \|\boldsymbol{K}_\ell^0\|_{\mathrm{op}}\big) \\ &\leqslant \mathbb{P}\big(\|c_2\delta\dot{\boldsymbol{W}}_\ell\|_{\mathrm{op}} > (Q_2 - c_1)\ell^{-\nu}\big).\end{aligned}$$

The last term can be rewritten as

$$\mathbb{P}\big(|\Lambda_\ell|^{-1/2}\|\dot{\boldsymbol{W}}_\ell\|_{\mathrm{op}} > (Q_2 - c_1)c_2^{-1}\ell^{-\nu}|\Lambda_\ell|^{-1/2}\delta^{-1}\big).$$

For the second term in the right-hand side of (3.55), thanks to the property $\|\boldsymbol{K}_\ell^{-1}\|_{\mathrm{op}} \leqslant \big(c_1\ell^{-\nu} - \|c_2\delta\dot{\boldsymbol{W}}_\ell\|_{\mathrm{op}}\big)^{-1}$ we derive

$$\begin{aligned}&\mathbb{P}\big(\|\boldsymbol{K}_\ell^{-1}\|_{\mathrm{op}} > Q_1\ell^\nu\big) \\ &\leqslant \mathbb{P}\big(|\Lambda_\ell|^{-1/2}\|\dot{\boldsymbol{W}}_\ell\|_{\mathrm{op}} > (c_1 - Q_1^{-1})c_2^{-1}\ell^{-\nu}|\Lambda_\ell|^{-1/2}\delta^{-1}\big).\end{aligned}$$

By assumption, we have that $\ell^{-\nu}|\Lambda_\ell|^{-1/2}\delta^{-1}$ is bounded away from zero. Since $|\Lambda_\ell|^{-1/2}\|\dot{\boldsymbol{W}}_\ell\|_{\mathrm{op}}$ is tight in $\ell \geqslant 1$, we can conclude by taking c_2 sufficiently small. The proof of Lemma 3.5.5 is complete.

□

Acknowledgements

The research of M. Hoffmann is partly supported by the French Agence Nationale de la Recherche (Blanc SIMI 1 2011 project CALIBRATION). The research of D. Picard is partly supported by the French Agence Nationale de la Recherche (ANR-09-BLAN-0128 PARCIMONIE). We are grateful to J. Rousseau for helpful comments.

Chapter 4

Noisy Laplace deconvolution with error in the operator

This chapter is the replica of an article submitted to a scientific review. It can be read independently from the rest of the manuscript.

Abstract: We address the problem of Laplace deconvolution with random noise in a regression framework. The time set is not considered to be fixed, but grows with the number of observation points. Moreover, the convolution kernel is unknown, and accessible only through experimental noise. We make use of a recent procedure of estimation based on a Galerkin projection of the operator on Laguerre functions ([19]), and couple it with a threshold performed both on the operator and the observed signal. We establish the minimax optimality of our procedure under the squared loss error, when the smoothness of the signal is measured in a Laguerre-Sobolev sense and the kernel satisfies fair blurring assumptions. It is important to stress that the resulting process is adaptive with regard both to the target function's smoothness and to the kernel's blurring properties. We end this paper with a numerical study emphasizing the good practical performances of the procedure on concrete examples.

Contents

4.1 Introduction **88**

4.2 Discretization of Laplace deconvolution **90**

4.3 Features of the target function and the kernel **93**

4.4 Adaptation to the standard framework **97**

4.5 Practical performances **99**

4.6 Proofs **104**

4.1 Introduction

Laplace deconvolution is motivated by a wide set of practical applications, ranging from population dynamics or physics to computational tomography or fluorescence spectroscopy (Linz [59, Chap. 2], Ameloot et al. [4], Comte et al. [19]). In the corresponding setting we observe $\boldsymbol{q}$, the result of the action of a kernel $\boldsymbol{g}$ on the function of interest $\boldsymbol{f}$, according to the following equation

$$\boldsymbol{q}(t) = \int_0^t \boldsymbol{g}(t-\tau)\boldsymbol{f}(\tau)d\tau,\ t \geqslant 0\,. \tag{4.1}$$

Equation (4.1) is also referred to as Volterra integral equation. One of its main features is its causal property, since $\boldsymbol{q}(t)$ is affected only by the values of $\boldsymbol{f}$ and $\boldsymbol{g}$ at times anterior to t. Of course, only finite samples of $\boldsymbol{q}(t)$ are accessible in practice. Moreover, the presence of additional noise justifies the empirical modelization of (4.1) by the classical regression model, inspired by Abramovich et al. [3]

$$\boldsymbol{y}(t_i) = \int_0^{t_i} \boldsymbol{g}(t_i-\tau)\boldsymbol{f}(\tau)d\tau + \sigma\eta_i,\ i = 1, ..., n\,, \tag{4.2}$$

where $0 \leqslant t_1 \leqslant ... \leqslant t_n \leqslant T_n$ are the points of observation, $(\eta_i)_{i=1,...,n}$ are independent standard Gaussian variables, and σ is a fixed factor accounting for the precision of the observations. T_n is supposed to grow with the number of observations n.
As pointed out in Abramovich et al. [3] and Comte et al. [19], in spite of its apparent similarity with the Fourier deconvolution problem, the theoretical features of equation (4.1), as well as the practical problems raised during its resolution are deeply different. More precisely, setting artificially $\boldsymbol{g}(t) = \boldsymbol{f}(t) = 0$ for $t < 0$ amounts to solving the classical Fourier deconvolution problem

$$\boldsymbol{y}(t_i) = \int_0^{T_n} \boldsymbol{g}(t_i-\tau)\boldsymbol{f}(\tau)d\tau + \sigma\eta_i,\ i = 1, ..., n\,. \tag{4.3}$$

A first notable objection is that the framework of classical Fourier deconvolution assumes periodicity of the function $\boldsymbol{f}$ and the kernel $\boldsymbol{g}$ on $[0, T]$, a meaningless notion when applied to a varying time set $[0, T_n]$. Even more problematic is the fact that this modelization totally ignores the causal feature of Laplace convolution, creating unwanted interferences between different time sets. To finish, the manipulation consisting in artificially expanding $\boldsymbol{q}$ and $\boldsymbol{g}$ for $t < 0$ creates artifacts on the estimated function at times $t < 0$ as well.
Another approach is to treat equation (4.2) as a general ill-posed problem and apply a Tikhonov regularization (Golubev [34]). However the direct implementation of this method also destroys the causal nature of equation (4.1), and tends to oversmooth the

solution (Cinzori and Lamm [15]). Subsequent adaptations which remedy these shortcomings are present in Lamm [56] and Cinzori and Lamm [15]. However in these works the time set is considered to be fixed.
A more suitable theoretical tool in solving (4.1) is the use of Laplace transform, which allows to derive a closed form of the solution. However, its direct implementation is compromised by numerical problems, since the generic expression of the inverse Laplace transform is not easily computable in general. This motivates the widespread use of inversion tables, unfortunately irrelevant when the image function is not known exactly but approximated via a numerical scheme.
In this paper, following Comte et al. [19], we will exploit the properties of Laguerre functions, which can be used either to compute the inverse Laplace transform (Abate et al. [1], Lien et al. [58]), or to solve directly equation (4.1) (Keilson and Nunn [46]). More precisely, a Galerkin method applied to (4.2) shows that, even if their role is not entirely symmetric to the role played by harmonics in the framework of Fourier deconvolution, they allow a sparse analysis of equation (4.1).
All the previous mentioned works only concerned the case of a deterministic noise at best. The presence of random noise requires an additional treatment, and calls for specific statistical tools. In the setting of random noise, Dey et al. [25] considered a kernel of the form e^{-at} and used a regularized inversion of the inverse Laplace transform. More recently, Abramovich et al. [3] conceived an optimal procedure in the minimax sense on Hölder spaces $\boldsymbol{H}^s(\mathbb{R}_+)$. This procedure used an exact expression of the solution involving the derivatives of $\boldsymbol{q}$, which were then estimated via Lepski's method. However a shortcoming of the procedure is its strong dependence on the kernel $\boldsymbol{g}$, in the sense that a small error in $\boldsymbol{g}$ can translate into a wide difference in the result. In other words there seems to be a trade off between the closed form of the solution, and the instability with regard to the kernel. Moreover, the fact that $\boldsymbol{g}$ is seldom observed directly in practice, but is usually subject to experimental noise should prompt us to privilege stability over exactitude.
In that spirit, Comte et al. [19] took advantage of the algebraic properties of Laguerre functions in the context of (4.2). With an adequate penalty term, they proposed an estimator which mimics the oracle risk to within logarithmic terms. This modelization has the non negligible advantage of practical simplicity and efficiency, since solving equation (4.1) amounts to the inversion of a lower triangular Toeplitz matrix.
Even if this latter procedure proves to be more stable with regard to $\boldsymbol{g}$ experimentally, no systematic study has been conducted on the subject yet. In this paper we attempt to fill in this gap: we suppose that the observation of $\boldsymbol{g}$ is contaminated by a Gaussian white noise, and show how Laguerre functions allow to handle this issue. We place ourselves under the minimax point of view and suppose that $\boldsymbol{f}$ belongs to a Laguerre-Sobolev space and that $\boldsymbol{g}$ satisfies standard blurring assumptions. We apply recent techniques for the treatment of noisy operators in the context of inverse problems (Hoffmann and Reiß [40],Delattre et al. [23]), which consist in a preliminary processing of the operator $\boldsymbol{K}$ coupled with a classical thresholding procedure applied to $\boldsymbol{y}$.

4.2 Discretization of Laplace deconvolution

4.2.1 Laguerre functions

Suppose that the target function $\boldsymbol{f}$ and the kernel $\boldsymbol{g}$ are elements of $\mathbb{L}^2(\mathbb{R}_+)$. Define the Laguerre polynomials (see Gradshteyn and Ryzhik [35])

$$L_\ell(t) = \sum_{j=0}^{\ell} (-1)^j \binom{\ell}{j} \frac{t^j}{j!}, \tag{4.4}$$

and, following Comte et al. [19], the ensuing Laguerre functions, depending on the parameter $\alpha > 0$,

$$\boldsymbol{\varphi}_\ell(t) = \sqrt{2\alpha} e^{-\alpha t} L_\ell(2\alpha t),\ \ell \in \mathbb{N}. \tag{4.5}$$

The parameter a is a tuning parameter used to fit experimental curves. The Laguerre functions constitute a Hilbert basis of $\mathbb{L}^2(\mathbb{R}_+)$. Any function $f \in \mathbb{L}^2(\mathbb{R}_+)$ satisfies

$$f = \sum_{\ell \geqslant 0} \check{f}_\ell \boldsymbol{\varphi}_\ell(t),\ \check{f}_\ell \triangleq \int_0^\infty f(\tau)\boldsymbol{\varphi}_\ell(\tau)d\tau. \tag{4.6}$$

The following proposition illustrates the convenience of Laguerre functions in the framework of equation (4.1).

Proposition 4.2.1 (Gradshteyn and Ryzhik [35], Formula 7.411.4)**.**

$$\forall \alpha > 0,\ \forall t \geqslant 0,\ \int_0^t \boldsymbol{\varphi}_k(x)\boldsymbol{\varphi}_\ell(t-x)dx = (2\alpha)^{-1/2}\big(\boldsymbol{\varphi}_{\ell+k}(t) - \boldsymbol{\varphi}_{\ell+k+1}(t)\big). \tag{4.7}$$

From now on, except if explicitly mentionned, we will suppose $\alpha = 1/2$.

4.2.2 Galerkin method

Proposition 4.2.1 prompted Comte et al. [19] to apply a Galerkin scheme to equation (4.1). Galerkin schemes rely on the choice of a set of functions which discretize the inverse problem at stake in a convenient way. They were beneficially applied in the context of inverse problems (Cohen et al. [17]), and blind deconvolution (Efromovich and Koltchinskii [30], Hoffmann and Reiß [40] and Delattre et al. [23]). To this end we will remind briefly the underlying methodology of a Galerkin scheme and show how it conveniently applies to equation (4.1).
Let $f \in \mathbb{L}^2(\mathbb{R}_+)$ and K an operator of $\mathbb{L}^2(\mathbb{R}_+)$, and suppose we want to recover f from the observation $q = Kf$. Note $\boldsymbol{V}_\ell$ the finite dimensional space spanned by the orthogonal set of Laguerre functions $\{\boldsymbol{\varphi}_k\}_{k \leqslant \ell}$. The Galerkin approximation f_G of f on $\boldsymbol{V}_\ell$ is the solution of the equation

$$\begin{aligned} &\langle Kf_G, v\rangle = \langle q, v\rangle,\ \forall v \in \boldsymbol{V}_\ell, \\ \Leftrightarrow &\sum_{k \leqslant \ell} \langle K\boldsymbol{\varphi}_k, \boldsymbol{\varphi}_k'\rangle\langle f_G, \boldsymbol{\varphi}_k\rangle = \langle q, \boldsymbol{\varphi}_k\rangle,\ \forall k' \leqslant \ell. \end{aligned} \tag{4.8}$$

We shall note K^ℓ the Galerkin matrix $(K^\ell)_{i,j} = \langle K\boldsymbol{\varphi}_j, \boldsymbol{\varphi}_i\rangle$, $i,j \leqslant \ell$, and, for a function $h \in \mathbb{L}^2(\mathbb{R}_+)$, h^ℓ the vector $(\check{h}_i)_{i\leqslant\ell}$. Note hence $\boldsymbol{K}$ the operator of $\mathbb{L}^2(\mathbb{R}_+)$ mapping f onto $t \mapsto \int_0^t f(t-\tau)\boldsymbol{g}(\tau)d\tau$. Proposition 4.2.1 has two consequences : first, the equality $\boldsymbol{f}_G^\ell = \boldsymbol{f}^\ell$, which entails

$$\boldsymbol{q}^\ell = \boldsymbol{K}^\ell \boldsymbol{f}^\ell . \tag{4.9}$$

Secondly, it implies the following proposition:

Proposition 4.2.2 (Comte et al. [19], Lemma 1)**.** *The Galerkin matrix $\boldsymbol{K}^\ell$ is lower triangular, Toeplitz. More precisely, note $\dot{\boldsymbol{g}}$ the function with Laguerre coefficients*

$$\check{\dot{\boldsymbol{g}}}_\ell = \check{\boldsymbol{g}}_0 \mathbf{1}_{\{\ell=0\}} + \big(\check{\boldsymbol{g}}_\ell - \check{\boldsymbol{g}}_{\ell-1}\big)\mathbf{1}_{\{\ell\geqslant 1\}}, \quad \ell \in \mathbb{N}.$$

Then

$$\boldsymbol{K}^\ell = \begin{pmatrix} \check{\dot{\boldsymbol{g}}}_0 & 0 & \dots & 0 \\ \check{\dot{\boldsymbol{g}}}_1 & \check{\dot{\boldsymbol{g}}}_0 & \ddots & \vdots \\ \vdots & \ddots & \ddots & 0 \\ \check{\dot{\boldsymbol{g}}}_\ell & \dots & \check{\dot{\boldsymbol{g}}}_1 & \check{\dot{\boldsymbol{g}}}_0 \end{pmatrix}$$

In the sequel, for any function $f \in \mathbb{L}^2(\mathbb{R}_+)$, we will note $T(f)$ the infinite Toeplitz matrix such that $T(f)_{i,1} = \check{f}_{i+1}$ for all $i \geqslant 0$, and $T_\ell(f)$ the extracted matrix defined by $T_\ell(f)_{i,1} = T(f)_{i,1}$, $i \leqslant \ell+1$. In particular,

$$\boldsymbol{K}^\ell = T_\ell(\dot{\boldsymbol{g}})$$

The resolution of the linear system (4.8) is now very convenient, provided that $\boldsymbol{K}^\ell$ is invertible. This is equivalent to $\check{\boldsymbol{g}}_0 \neq 0$, an assumption we will make in the sequel.

4.2.3 Application to the regression model with irregular design

It remains to incorporate two supplementary features of equation (4.2) in the inversion of (4.9). First, the presence of the random noise $\boldsymbol{\eta}$ and secondly, the possible irregularity of the design points $t_1, ..., t_n$. This construction is due to Comte et al. [19]. Due to the fact that the observation points t_i are imposed by the problem, the estimation of the Laguerre coefficients $\check{\boldsymbol{q}}_\ell$ of the function $\boldsymbol{q}$ suffers from two potential drawbacks. First, the infinite support of the Laguerre polynomials as well as the function $\boldsymbol{q}$ which should not be too problematic, provided that T_n is large enough and that the functions decrease sufficiently to infinity. More problematic is the fact that the observation points t_i are sometimes subject to experimental constraints, which affect their distribution on $\mathbb{R}_+$. The consistency of the estimation of $\check{\boldsymbol{q}}_\ell$ is hereby deteriorated.
We will hence suppose that the following conditions are fulfilled:

- There exists an integer n_0 such that $\frac{n}{T_n} > \sigma$ for all $n \geqslant n_0$.

- $\lim_{n\to\infty} T_n = \infty$, and $\lim_{n\to\infty} \frac{T_n}{n} = 0$.

To take into account the irregularity of the design, we follow Comte et al. [19] and define $P_n : [0; T_n] \to [0; T_n]$ a regular non decreasing function such that

$$P_n(0) = 0,\ P_n(T_n) = T_n,\ P_n(t_i) = \frac{i}{n} T_n \text{ for } i \leqslant n\,. \tag{4.10}$$

Note $\boldsymbol{\Phi}_\ell$ the $(\ell+1)\times n$ matrix with entries $(\boldsymbol{\Phi}_\ell)_{k,i} = \boldsymbol{\varphi}_k(t_i)$. For any function $h \in \mathbb{L}^2(\mathbb{R})$, we have

$$\begin{aligned} \boldsymbol{P}_\ell h(t_i) &= \sum_{k\leqslant \ell} \boldsymbol{\varphi}_k(t_i)\check{h}_k = \boldsymbol{\Phi}_\ell h^\ell\,, \\ \Leftrightarrow h^\ell &= \big({}^{\boldsymbol{t}}\boldsymbol{\Phi}_\ell\boldsymbol{\Phi}_\ell\big)^{-1}{}^{\boldsymbol{t}}\boldsymbol{\Phi}_\ell \boldsymbol{P}_\ell h(t_i)\,. \end{aligned}$$

where $\boldsymbol{P}_\ell$ is the orthogonal projector onto $\boldsymbol{V}_\ell$. We deduce that

$$\boldsymbol{y}^\ell = \big({}^{\boldsymbol{t}}\boldsymbol{\Phi}_\ell\boldsymbol{\Phi}_\ell\big)^{-1}{}^{\boldsymbol{t}}\boldsymbol{\Phi}_\ell \boldsymbol{P}_\ell\big[\boldsymbol{q} + \sigma\boldsymbol{\eta}\big](t_i) = \boldsymbol{K}^\ell \boldsymbol{f}^\ell + \sigma\big({}^{\boldsymbol{t}}\boldsymbol{\Phi}_\ell\boldsymbol{\Phi}_\ell\big)^{-1}{}^{\boldsymbol{t}}\boldsymbol{\Phi}_\ell\boldsymbol{\eta}_n\,, \tag{4.11}$$

where $\boldsymbol{\eta}_\ell \sim \mathcal{N}(0, \boldsymbol{I}_n)$. Let us take a closer look to the matrix $\big({}^{\boldsymbol{t}}\boldsymbol{\Phi}_\ell\boldsymbol{\Phi}_\ell\big)$. Its general term is

$$\begin{aligned} ({}^{\boldsymbol{t}}\boldsymbol{\Phi}_\ell\boldsymbol{\Phi}_\ell)_{\ell,k} =& \sum_{i=1}^{n} \boldsymbol{\varphi}_k(P^{-1}(\frac{i}{n}T_n))\boldsymbol{\varphi}_\ell(P^{-1}(\frac{i}{n}T_n)) \\ \sim& \frac{n}{T_n}\int_0^{T_n} \boldsymbol{\varphi}_k(P^{-1}(\tau))\boldsymbol{\varphi}_\ell(P^{-1}(\tau))d\tau \\ =& \frac{n}{T_n}\int_0^{T_n} \boldsymbol{\varphi}_k(\tau)\boldsymbol{\varphi}_\ell(\tau)P'(\tau)d\tau \end{aligned}$$

for n, T_n large enough. If the points t_i are equispaced, taking $P(\tau) = \tau$ in (4.10) entails that $T_n n^{-1}\big({}^{\boldsymbol{t}}\boldsymbol{\Phi}_\ell\boldsymbol{\Phi}_\ell\big)$ is close to the identity provided that T_n is large enough. As in Comte et al. [19], we hence reformulate (4.11) as the sequential model

$$\boldsymbol{y}^\ell = \boldsymbol{K}^\ell \boldsymbol{f}^\ell + \sigma\sqrt{\frac{T_n}{n}}\boldsymbol{\xi}_\ell\,,$$

where $\boldsymbol{\xi}_\ell \sim \mathcal{N}(0, \boldsymbol{\Omega}_\ell)$ and $\boldsymbol{\Omega}_\ell = nT_n^{-1}\big({}^{\boldsymbol{t}}\boldsymbol{\Phi}_\ell\boldsymbol{\Phi}_\ell\big)^{-1}$. In general, $\boldsymbol{\Omega}_\ell$ somehow quantifies the distance to the uniform design case. To ensure that the design is not too ill-conditioned, we will suppose that the following assumption is fulfilled.

Assumption 4.2.3. *Let $L \in \mathbb{N}$. There exists $C \geqslant c > 0$, such that for all $\ell \leqslant L$, for all $\lambda \in Sp(\boldsymbol{\Omega}_\ell)$, $c \leqslant \lambda \leqslant C$.*

This assumption is dependent on the integer L, which plays the role of a maximal resolution level, and will be adapted to the case of interest later. The inversion of (4.11) now requires controls of the variable $(\boldsymbol{K}^\ell)^{-1}\boldsymbol{\xi}_\ell$. Under suitable properties of $\boldsymbol{f}$ and $\boldsymbol{g}$, we shall be able to apply a classical inverse/thresholding procedure, and derive rates of convergence over specific regularity spaces. These properties are the subject of Part 4.3.

4.2.4 Error in the operator

We already mentionned the fact that the resolution of (4.1) is usually unstable with respect to $\boldsymbol{g}$ (Abramovich et al. [3]). Furthermore, in practice, inference on the kernel $\boldsymbol{g}$ is possible only through experimental noise, and requires a preliminary step of estimation giving way to imprecision. This additional error might significantly contaminate the result of any procedure of estimation if not properly treated. Let us see how Laguerre functions $\boldsymbol{\varphi}_\ell$ allow to handle this issue: in section 4.2.2, we established that the discretization of (4.13) with Laguerre functions involved a Toeplitz matrix with entries constituted of the Laguerre coefficients of $\dot{\boldsymbol{g}}$. We can thus consider $\dot{\boldsymbol{g}}$ as the finite impulse response of the operator $\boldsymbol{K}$ when applied to the system $(\boldsymbol{\varphi}_\ell)_{\ell\geqslant 0}$. To take into account the imprecision in the observations of $\dot{\boldsymbol{g}}$, we adopt the framework of blind deconvolution and suppose that $\dot{\boldsymbol{g}}$ is not known exactly, but that we have access to the noisy version

$$\dot{\boldsymbol{g}}_\delta = \dot{\boldsymbol{g}} + \delta \boldsymbol{b}\,, \tag{4.12}$$

where $\boldsymbol{b}$ is a Gaussian white noise on $\mathbb{L}^2(\mathbb{R}_+)$. The generic problem of blind deconvolution is motivated by numerous scientific fields, including for example electronic microscopy or astrophysics, where the corresponding kernel is seldom known nor directly observed. It was adequately discussed in Efromovich and Koltchinskii [30] and Hoffmann and Reiß [40].
Taking into account the observations (4.12), the projection $\dot{\boldsymbol{g}}^\ell$ is changed to $\dot{\boldsymbol{g}}^\ell_\delta = \dot{\boldsymbol{g}}^\ell + \delta \boldsymbol{b}^\ell$ where $\boldsymbol{b}^\ell$ is a Gaussian vector with covariance $\boldsymbol{I}_\ell$. The new model, adjusted from (4.11) becomes

$$\begin{cases} \boldsymbol{y}^\ell & = \boldsymbol{K}^\ell \boldsymbol{f}^\ell + \sigma\sqrt{\frac{T_n}{n}}\boldsymbol{\xi}_\ell\,, \\ \boldsymbol{K}^\ell_\delta & = \boldsymbol{K}^\ell + \delta \boldsymbol{B}^\ell\,, \end{cases} \tag{4.13}$$

where $\boldsymbol{B}^\ell = T_\ell(\boldsymbol{b})$ is a random Toeplitz matrix. In the sequel, for the sake of clarity, we note $\varepsilon = \sigma\sqrt{\frac{T_n}{n}}$.

Remark 4.2.4. *We could as well suppose that we observe $\boldsymbol{g}_\delta = \boldsymbol{g} + \delta\boldsymbol{b}$, yet it is more convenient to work with $\dot{\boldsymbol{g}}$ (the entries of the noisy Toeplitz matrix $\boldsymbol{B}$ are directly i.i.d standard Gaussian variables). In the former case, the rest of the paper however adapts with no change in the algorithms, since inequality* (4.27) *is satisfied as well. A modification of the proof of Theorem 4.4.6 should also provide the lower bound for the second procedure.*

4.3 Features of the target function and the kernel

4.3.1 Sobolev spaces associated to Laguerre functions

We proceed to the description of regularity spaces associated with the resolution of (4.13). The following material is classical, we refer to Bongioanni and Torrea [6] or

Rathnakumar [74] for example.
Since $f \mapsto \sqrt{2\alpha} f(2\alpha .)$ is an isometry of $\mathbb{L}^2(\mathbb{R}_+)$, the structures defined for different values of α are equivalent. Hence we shall only concentrate on the mainstream case where $\alpha = 1/2$. Define the operator $\mathfrak{L}$ on $\mathbb{L}^2(\mathbb{R}_+, dx)$ by

$$\mathfrak{L} = -\Big[x\frac{d^2}{dx^2} + \frac{d}{dx} - \frac{x}{4}\Big]. \tag{4.14}$$

The functions $\boldsymbol{\varphi}_\ell$ are the eigenfunctions of $\mathfrak{L}$ associated with eigenvalues $(\ell + \frac{1}{2})$. We hence define the Sobolev space $\mathcal{W}^s$ associated with Laguerre functions as

$$\mathcal{W}^s = \{f \in \mathbb{L}^2(\mathbb{R}_+, dx) \text{ s.t. } \mathfrak{L}^s f \in \mathbb{L}^2(\mathbb{R}_+, dx)\}.$$

For a function $f \in \mathbb{L}^2(\mathbb{R}_+, dx)$, we have the straightforward equivalence

$$f \in \mathcal{W}^s \Leftrightarrow \sum_{\ell \geqslant 0} \big|\big(\ell + \frac{1}{2}\big)^s \langle f, \boldsymbol{\varphi}_\ell\rangle\big|^2 < \infty,$$

and the associated norm

$$\|f\|^2_{\mathcal{W}^s} = \sum_{\ell \geqslant 0} \big|\big(\ell + \frac{1}{2}\big)^s \langle f, \boldsymbol{\varphi}_\ell\rangle\big|^2.$$

For $M \geqslant 0$, we shall note $\mathcal{W}^s(M)$ the Sobolev ball of radius M. Finally, we remind that, as $\|\boldsymbol{\varphi}_\ell\|_\infty \leqslant 1$ for all $\ell \geqslant 0$, we have $s > 1/2 \Rightarrow \mathcal{W}^s \subset \mathcal{C}^0(\mathbb{R}_+)$. From now on, we will hence suppose that there exists $s > 1/2$ such that $\boldsymbol{f} \in \mathcal{W}^s$.

4.3.2 Banded Toeplitz matrices

Before entering into details about the kernel features, we introduce basic material on Toeplitz matrices. Most of it is inspired by Böttcher and Grudsky [7] and Comte et al. [19].
Let $a = (a_\ell) \in \ell^1(\mathbb{Z})$ be a sequence of real numbers. We remind from section 4.2.2 that we note $T(a)$ the infinite Toeplitz matrix defined by

$$T(a) = \begin{pmatrix} a_0 & a_{-1} & a_{-2} & \dots & \dots \\ a_1 & a_0 & a_{-1} & \dots & \dots \\ a_2 & a_1 & a_0 & \dots & \dots \\ \vdots & \ddots & \ddots & \ddots & \dots \end{pmatrix}$$

and $T_\ell(a) \in M_\ell(\mathbb{R})$ the truncated Toeplitz matrix defined as

$$(T_\ell(a))_{i,j} = (T(a))_{i,j},\ i,j \leqslant \ell + 1.$$

The Toeplitz matrices $T(a)$ and $T_\ell(a)$ are naturally linked to the two respective Laurent series

$$\bar{a}(z) = \sum_{k=-\infty}^{\infty} a_k z^k \text{ and } a_\ell(z) = \sum_{k=-\ell}^{\ell} a_k z^k$$

We will indifferently refer to the vector a or the corresponding Laurent series. The spectral norm of $T(a)$ is related to the behavior of $a(z)$, as illustrated in the following proposition.

Proposition 4.3.1. *Let $a \in \ell^1(\mathbb{Z})$. Let $\mathcal{C}$ stand for the complex unit circle. We have*

$$\|T(a)\|_{op} = \|a(z)\|_{circ}\,,$$

where $\|a(z)\|_{circ} \triangleq \sup_{z\in\mathcal{C}} \left| \sum_{\ell=-\infty}^{\infty} a_\ell z^\ell \right|$. A simple corollary is the following inequality

$$\|T(a)\|_{op} \leqslant \sum_{\ell=-\infty}^{\infty} |a_\ell|\,.$$

In particular, Proposition 4.3.1 applies to the case of truncated Toeplitz matrices $T_\ell(a)$. Moreover, if a has no zero on the complex unit circle, we have

$$\limsup_{\ell\to\infty} \|T_\ell(a)\|_{\text{op}} < \infty \text{ and } \lim_{\ell\to\infty} \|T_\ell(a)\|_{\text{op}} = \|T(a)\|_{\text{op}} \tag{4.15}$$

Now suppose that a and a' both generate lower triangular Toeplitz matrices (i.e. $a_k = a'_k = 0$ if $k < 0$). Then the following equalities hold for all $\ell \geqslant 0$:

$$T_\ell(a)T_\ell(a') = T_\ell(a')T_\ell(a) = T_\ell(aa') \text{ and } T_\ell(a)^{-1} = T_\ell(1/a)\,. \tag{4.16}$$

In other words, the matrix multiplication (resp. inversion) is equivalent to a power series multiplication (resp. inversion).

4.3.3 Degree of ill posedness

We now need to precise the properties of $\boldsymbol{K}$ as a blurring operator of $\mathbb{L}^2(\mathbb{R}_+)$. Usually the operator $\boldsymbol{K}$ is not compact, and the problem (4.1) is ill-posed. This results in practical instabilities when trying to invert equation (4.11) from discrete observations. The quantification of the ill-posedness of the problem is specified by the introduction of a constant, called degree of ill-posedness (DIP) of the problem (see Nussbaum and Pereverzev [71], Mathe and Pereverzev [65] for a generic review). We adapt this concept to our framework, and make the following assumption.

Assumption 4.3.2 (Degree of ill-posedness of $\boldsymbol{g}$)**.** *There exists $\nu \geqslant 0$, $Q \geqslant 0$ such that, for all $\ell \geqslant 0$,*

$$\|(\boldsymbol{K}^\ell)^{-1}\|_{op} \leqslant Q(\ell \vee 1)^\nu\,.$$

ν is called degree of ill-posedness of $\boldsymbol{g}$ (or equivalently of $\boldsymbol{K}$). We note $\mathcal{K}_\nu(Q)$ the set of functions which satisfy this assumption.

We shall see examples of kernels satisfying this assumption further. For the moment, we concentrate on the treatment of observations (4.13) in the context we just described.

4.3.4 A first algorithm of estimation

The main challenge which remains to be treated now is to articulate the two critical steps of inversion and regularization, via adapted procedures. For example, let us give a brief overview of the methodology in Comte et al. [19]: Let $\ell \in \mathbb{N}$, and let Λ be the following contrast function, defined on $\mathbb{R}^\ell$ by

$$\Lambda : t \mapsto \|t\|^2 - 2\langle t, (\boldsymbol{K}^\ell)^{-1}\boldsymbol{y}^\ell\rangle .$$

Note $\|.\|_{\mathrm{op}}$ the spectral norm and $\|.\|_{\mathrm{HS}}$ the Hilbert Schmidt norm. A model selection is performed on the maximal level L, by introducing the following penalizing factor ($B > 0$ is an arbitrary constant):

$$\mathrm{pen}(\ell) = 4\sigma^2 T_n n^{-1}\Big((1+B)\|\sqrt{\boldsymbol{Q}^\ell}\|^2_{\mathrm{HS}} + (1+B)^{-1}(\nu+1)\|\sqrt{\boldsymbol{Q}^\ell}\|^2_{\mathrm{op}}\log\ell\Big) ,$$

where $\boldsymbol{Q}^\ell = (\boldsymbol{K}^\ell)^{-1}\boldsymbol{\Omega}_\ell{}^{\boldsymbol{t}}(\boldsymbol{K}^\ell)^{-1}$ and $\sqrt{\boldsymbol{Q}^\ell}$ is a lower triangular matrix satisfying $\sqrt{\boldsymbol{Q}^\ell}{}^{\boldsymbol{t}}\sqrt{\boldsymbol{Q}^\ell} = \boldsymbol{Q}^\ell$. The maximal level $\tilde{L}$ is hence chosen as

$$\tilde{L} = \underset{\ell\leqslant\ell(n)}{\mathrm{argmin}}\{\Lambda^2\big((\boldsymbol{K}^\ell)^{-1}\boldsymbol{y}^\ell\big) + \mathrm{pen}(\ell)\} ,$$

where $\ell(n)$ is a large enough resolution level, possibly depending on n, and the ensuing estimator of $\boldsymbol{f}$ is

$$(\boldsymbol{K}^{\tilde{L}})^{-1}\boldsymbol{y}^{\tilde{L}} .$$

We follow here a different path: we suppose that the target function belongs to a Sobolev-Laguerre space, and perform thresholding techniques in a minimax framework. Furthermore, our results are asymptotic with regard to ε, δ. Would $\boldsymbol{g}$ be known, the estimation of $\boldsymbol{f}$ from observations (4.13) amounts to solving a standard inverse problem with signal noise. To this end, a prolific literature is at disposal (a selected list is Donoho [26], Abramovich and Silverman [2], Cohen et al. [17]). In order to take into account the presence of noise in the operator, we shall hence apply a preliminary regularizing thresholding procedure to the noisy operator $\boldsymbol{K}_\delta$ in order to ensure the stability of the further inversion step. To that end, define the maximal level as

$$L^{\mathbf{I}} = \lambda\Big(\varepsilon\sqrt{|\log\varepsilon|} \vee \delta|\log\delta|\Big)^{\frac{-1}{\nu+1}} , \tag{4.17}$$

with λ a positive constant. Define also the two thresholding levels

$$O_{\ell,\delta} = \kappa\big((\ell\vee 1)\log(\ell\vee 2)\big)^{1/2}\delta\sqrt{|\log\delta|} , \tag{4.18}$$

$$S^{\mathbf{I}}_{\ell,n} = (\ell\vee 1)^\nu\Big(\tau_{sig}\varepsilon\sqrt{|\log\varepsilon|} \vee \tau_{\mathrm{op}}\delta|\log\delta|\Big) . \tag{4.19}$$

For $\ell \geqslant 0$, note $\boldsymbol{\zeta}_\ell = \langle (\boldsymbol{K}_\delta^\ell)^{-1} \mathbf{1}_{\left\{\|(\boldsymbol{K}_\delta^\ell)^{-1}\|_{\mathrm{op}} < O_{\delta,l}^{-1}\right\}} \boldsymbol{y}^\ell, \boldsymbol{\varphi}_\ell \rangle$. The estimator $\widetilde{\boldsymbol{f}}^{\mathbf{I}}$ of $\boldsymbol{f}$ is defined by

$$\widetilde{\boldsymbol{f}}^{\mathbf{I}} = \sum_{\ell \leqslant L^{\mathbf{I}}} \boldsymbol{\zeta}_\ell \mathbf{1}_{\{|\boldsymbol{\zeta}_\ell| > S_\ell\}} \boldsymbol{\varphi}_\ell \,.$$

We call this procedure **Algorithm I**. The preliminary threshold performed on $(\boldsymbol{K}_\delta^\ell)^{-1}$ ensures its proximity with $(\boldsymbol{K}^\ell)^{-1}$ with high probability (see Lemma 4.6.2). We now study the squared loss performance of the procedure.

Theorem 4.3.3. *Let $M \geqslant 0$, $s > 1/2$. Let $\nu \geqslant 0$, $Q \geqslant 0$. Suppose that Assumption 4.2.3 holds for $L = L^{\boldsymbol{I}}$. Then for sufficiently large thresholding constants κ, τ_{sig} and τ_{op},*

$$\sup_{\substack{\boldsymbol{f} \in \mathcal{W}^s(M) \\ \boldsymbol{g} \in \mathcal{K}_\nu(Q)}} \mathbb{E} \|\widetilde{\boldsymbol{f}}^{\boldsymbol{I}} - \boldsymbol{f}\| \lesssim \left(\delta |\log \delta|\right)^{\frac{2s}{2(s+\nu)+1}} \vee \left(\varepsilon \sqrt{|\log \varepsilon|}\right)^{\frac{2s}{2(s+\nu)+1}},$$

where $\lesssim$ means inequality up to a constant depending only on $\lambda, \kappa, \tau_{sig}, \tau_{op}, s, M, \nu, Q$.

The rates in Theorem 4.3.3 reveal two components, accounting respectively for the imprecision in the observation of the operator and the signal. The latter is fairly classic in non parametric statistics (Nussbaum and Pereverzev [71], Johnstone et al. [44]) where it is also optimal, while the former is standard (and optimal too) in blind deconvolution on Hilbert spaces (Efromovich and Koltchinskii [30], Hoffmann and Reiß [40]). Thus, we do not study the optimality of these rates in this paper, but rather concentrate on a more specific framework related to the problem of interest.

4.4 Adaptation to the standard framework of Laplace deconvolution

We now discuss the adaptation of our algorithm to the mainstream framework of Laplace deconvolution, as exposed in Abramovich et al. [3] or Comte et al. [19]. As we shall see, this more restrictive framework allows to treat observations (4.13) more efficiently. To this end, we first define a more restrictive version of the degree of ill-posedness.

Assumption 4.4.1 (Second kind degree of ill-posedness)**.** *Note $\boldsymbol{\gamma}_k = \langle (1/\dot{\boldsymbol{g}}), \boldsymbol{\varphi}_k \rangle$, so that $(1/\dot{\boldsymbol{g}})(z) = \sum_{k \geqslant 0} \boldsymbol{\gamma}_k z^k$. There exists $\nu > 0$, there exists $Q_2, Q_1 > 0$, such that for all $\ell \geqslant 0$,*

$$\sum_{k=0}^{\ell} \boldsymbol{\gamma}_k^2 \leqslant Q_2 (\ell \vee 1)^{2\nu - 1}, \tag{4.20}$$

$$\|(\boldsymbol{K}^\ell)^{-1}\|_{op} \geqslant Q_1 (\ell \vee 1)^\nu. \tag{4.21}$$

For $Q = (Q_1, Q_2)$, we note $\mathcal{G}_\nu(Q)$ the set of functions $\boldsymbol{g} \in \mathbb{L}^2(\mathbb{R}_+)$ such that Assumption 4.4.1 holds. Assumption 4.4.1 is clearly more restrictive that Assumption 4.3.2. However, it is satisfied by a natural class of functions $\boldsymbol{g}$:

Proposition 4.4.2 (Comte et al. [19], Lemma 3/ Lemma 5)**.** *Suppose that there exists $C, \nu > 1/2$, $\mu \in \mathcal{C}$ and $w(z) = \prod_{i=1}^{N}(z - \mu_i)$, $|\mu_i| > 1$ a polynomial function with no pole inside of the complex unit disc, such that*

$$\dot{\boldsymbol{g}}(z) = Cw(z)(\mu - z)^\nu . \tag{4.22}$$

Then Assumption 4.4.1 is satisfied. Furthermore, if $w \equiv 1$ and $\nu \geqslant 0$, then $|\boldsymbol{\gamma}_\ell| \sim \frac{\ell^{\nu-1}}{\Gamma(\nu)}$.

For completeness, we give a proof of Proposition 4.4.2 in section 4.6. We now turn to the standard framework of Laplace deconvolution, as exposed in Abramovich et al. [3] and Comte et al. [19]. To this end, we define the following assumptions concerning the kernel $\boldsymbol{g}$.

Assumption 4.4.3.

(A1) There exists an integer $r \geqslant 1$ such that

$$\frac{d^j \boldsymbol{g}}{dt^j}\Big|_{t=0} = \begin{cases} 0 & \text{if } j = 0, 1, ..., r-2 \\ B_r \neq 0 & \text{if } j = r-1 \end{cases}$$

(A2) $\boldsymbol{g} \in L^1\big([0, +\infty)\big)$ is r times differentiable and $\boldsymbol{g}^{(r)} \in L^1\big([0, +\infty)\big)$.

(A3) The Laplace transform of $\boldsymbol{g}$ has no zeros with non negative real parts except for the zeros of the form $\infty + ib$.

The consequences of these assumptions are well formulated in the terms of the preceding framework:

Proposition 4.4.4 (Comte et al. [19], Lemma 3)**.** *Suppose that Assumptions (A1), (A2) and (A3) hold. Then the hypotheses of Proposition 4.4.2 are satisfied with $\mu = 1$, $\nu = r$.*

Hence, Assumption 4.4.1 is verified with $\nu = r$ and **Algorithm I** applies. However, Assumption 4.4.1 provides additional information on the behavior of $(1/\dot{\boldsymbol{g}})$. We adapt **Algorithm I** to this new framework, by operating the following changes:

- Set the maximal level to

$$L^{\mathbf{II}} = \lambda\Big(\varepsilon\sqrt{|\log\varepsilon|} \vee \delta|\log\delta|\Big)^{-1} .$$

- Set the signal thresholding level to

$$S^{\mathbf{II}}_{\ell,n} = \begin{cases} \|(\boldsymbol{K}^\ell_\delta)^{-1}\|_{\mathrm{op}}(\ell \vee 1)^{-1/2}\Big(\tau_{sig}\varepsilon\sqrt{|\log\varepsilon|} \vee \tau_{\mathrm{op}}\delta|\log\delta|\Big) & \text{if } \|(\boldsymbol{K}^\ell_\delta)^{-1}\|_{\mathrm{op}} < O^{-1}_{\ell,\delta} , \\ +\infty & \text{if } \|(\boldsymbol{K}^\ell_\delta)^{-1}\|_{\mathrm{op}} \geqslant O^{-1}_{\ell,\delta} , \end{cases} \tag{4.23}$$

where $\|A\|_{\mathrm{HS}} = \sqrt{\mathrm{Tr}({}^tAA)}$ is the Hilbert-Schmidt norm. We call the modified procedure **Algorithm II** and note $\widetilde{\boldsymbol{f}}^{\mathbf{II}}$ the corresponding estimated function. A notable gain of this new algorithm is its independence with regard to the parameter ν. Indeed, Assumption 4.4.1 allows us to use $\|(\boldsymbol{K}_\delta^\ell)^{-1}\|_{\mathrm{HS}}$ in (4.19) as a substitute of ℓ^ν, and to overestimate the 'true' maximal level $L^{\mathbf{I}}$. Its performances are exposed in the next theorem:

Theorem 4.4.5. *Let $M \geqslant 0$. Let $\nu > 0$, $Q_2, Q_1 > 0$ and $s > 1/2$. Suppose that Assumption 4.2.3 holds with $L = L^{\boldsymbol{II}}$. Then for sufficiently large thresholding constants κ, τ_{sig} and τ_{op},*

$$\sup_{\substack{\boldsymbol{f}\in\mathcal{W}^s(M)\\ \boldsymbol{K}\in\mathcal{G}_\nu(Q)}} \mathbb{E}\,\|\widetilde{\boldsymbol{f}}^{\boldsymbol{II}} - \boldsymbol{f}\| \lesssim \left(\delta|\log\delta|\right)^{\frac{s}{s+\nu}} \vee \left(\varepsilon\sqrt{|\log\varepsilon|}\right)^{\frac{s}{s+\nu}},$$

where $\lesssim$ means inequality up to a constant depending only on $\lambda, \kappa, \tau_{sig}, \tau_{op}, s, M, \nu, Q_1, Q_2$.

Thus, in addition to the adaptivity over the parameter ν, the strengthening of Assumption 4.3.2 via (4.20) and (4.21) allows to improve on the rates of Theorem 4.3.3 with regard both to the operator and signal noise. Our next result shows that the rate achieved in Theorem 4.4.5 is indeed optimal, up to logarithmic terms. The lower bound will not decrease for increasing noise levels δ and ε, whence it suffices to provide separately the cases $\delta = 0$ and $\varepsilon = 0$.

Theorem 4.4.6. *Let $s > 1/2$, let $M \geqslant 0$ $\nu > 1/2$ and $Q_2 \geqslant c_\nu Q_1 > 0$. Here c_ν is a constant depending only on ν which will will not seek to precise. We have*

$$\inf_{\tilde f} \sup_{\substack{f\in\mathcal{W}^s(M)\\ \boldsymbol{g}\in\mathcal{G}_\nu(Q)}} \mathbb{E}\,\|\tilde{\boldsymbol{f}} - \boldsymbol{f}\| \gtrsim \delta^{\frac{s}{s+\nu}}|\log\delta|^{-1} \vee \varepsilon^{\frac{s}{s+\nu}}|\log\varepsilon|^{-1},$$

where the infimum is taken among all estimators $\tilde f$ of f based on observations (4.13).

Combining Theorem 4.3.3 together with Theorem 4.4.6, we conclude that our algorithm is minimax over $\mathcal{W}^s(M)$ to within logarithmic terms in ε and δ, uniformly with regard to the blurring kernel $\boldsymbol{g} \in \mathcal{G}_\nu(Q)$.

4.5 Practical performances

In this section we study the practical performances of the two procedures developed above. Note that three potential sources of errors may contaminate the quality of the observations in (4.13) : the signal precision $\sigma\sqrt{T_n/n}$, the operator precision δ and the design quality $\|\boldsymbol{\Omega}_{\boldsymbol{\ell}}\|_{\mathrm{op}}$. We shall hence emphasize their influence in the estimation of $\boldsymbol{f}$, as well as their respective interactions.
Our first aim is to study the interaction between the effect of signal and kernel noise in the two procedures of reconstruction. To this end, we will isolate them from the effect

κ	0.1	0.2	0.3
N	3	1	0

Table 4.1: Choosing of κ. N is the average number, computed on a basis of 10 realizations, of levels $\ell \leqslant 10$ such that $\|(\boldsymbol{K}_\delta^\ell)^{-1}\|_{\mathrm{op}} < O_{\delta,l}^{-1}(\kappa)$. We have $\delta = 10^{-2}$.

τ_{sig}	0.3	0.4	0.5	0.6	0.7	0.8	0.9	1
$N_{\mathbf{I}}$	1	1	0	0	0	0	0	0
$N_{\mathbf{II}}$	7	5	4	3	2	1	1	0

τ_{op}	0.1
$N_{\mathbf{I}}$	0
$N_{\mathbf{II}}$	0

Table 4.2: Choosing of τ. For $(\delta_{sig}, \varepsilon_{sig}) = (\varepsilon_{\mathrm{op}}, \delta_{\mathrm{op}}) = (10^{-2}, 10^{-1})$ and each value of τ, we computed 10 times the described procedure and reported N_i the average number of remaining Laguerre coefficients for **Algorithm** i.

of the design, and suppose that the latter is ideally conditioned by setting $\boldsymbol{\Omega}_\ell = \boldsymbol{I}_\ell$. Let us start by a few precision concerning the tuning parameters of **Algorithm I** and **II**. The setting up of these procedures requires the preliminary definition of $\lambda, \kappa, \tau_{sig}$ and τ_{op}.

Tuning parameters: for the definition of the maximal level of resolution, we set $\lambda = 1$ for both algorithms. The concrete choice of adequate thresholding constants κ and τ is a complex issue. Our practical choices will be based on the following remark, inspired by Donoho and Johnstone [27]: in the case of direct estimation on real line, the universal threshold which is both efficient and simple to implement, takes the form $2\sqrt{|\log \varepsilon|}$. A consistent interpretation is to consider that this threshold should kill any pure noise signal. We will adapt this reasoning to the case of interest.

Choice of κ : we use as a benchmark the case where $\boldsymbol{g} \equiv 0$. Given δ large enough, we define κ as the smallest value κ_δ such that , for all $\ell \leqslant 10$, $\mathbf{1}_{\left\{\|(\boldsymbol{K}_\delta^\ell)^{-1}\|_{\mathrm{op}} < O_{\delta,l}^{-1}\right\}} = 0$. The results are reported in Table 4.1 and give $\kappa = 0.3$.

Choice of τ_{sig} and τ_{op}: It is clear that the role of τ_{sig} and τ_{op} is to control the influence of the signal (resp. the operator) error. To choose τ_{sig} (resp. τ_{op}), we therefore set $\varepsilon_{sig} > \delta_{sig} > 0$ (resp. $\delta_{op} > \varepsilon_{op} > 0$) large enough. We resort to the case $\boldsymbol{f} \equiv 0$ as a benchmark: we have $\langle \boldsymbol{f}, \boldsymbol{\varphi}_\ell \rangle = 0$ for $\ell \geqslant 1$, consequently the observations $\langle \boldsymbol{g}_{\varepsilon_{sig}}, \boldsymbol{\varphi}_\ell \rangle$, $\ell \geqslant 0$ are pure noise. We hence simulate $\boldsymbol{K}_{\delta_{sig}}$ and, integrating the previously computed value of κ, apply the procedure for increasing values of τ_{sig} (resp. τ_{op}) until all the computed coefficients $\langle \tilde{\boldsymbol{f}}^i, \boldsymbol{\varphi}_\ell \rangle$ (i =**I**,**II**) are killed for $\ell \leqslant 10$. The results are reported in Table 4.2.

We now apply the two procedures to the case where $\boldsymbol{f}_1(t) = (t^2 - t)\exp(-t)$ and $\boldsymbol{g} = \boldsymbol{\varphi}_0$ (a graphical representation of these two functions is presented in Figure 4.1). We have

$$\big(1/\dot{\boldsymbol{g}}\big)(z) = (1-z)^{-1} = \sum_{\ell \geqslant 0} z^\ell \,,$$

hence Assumptions 4.3.2 and 4.4.1 are both satisfied taking $\nu = 1$. For several values

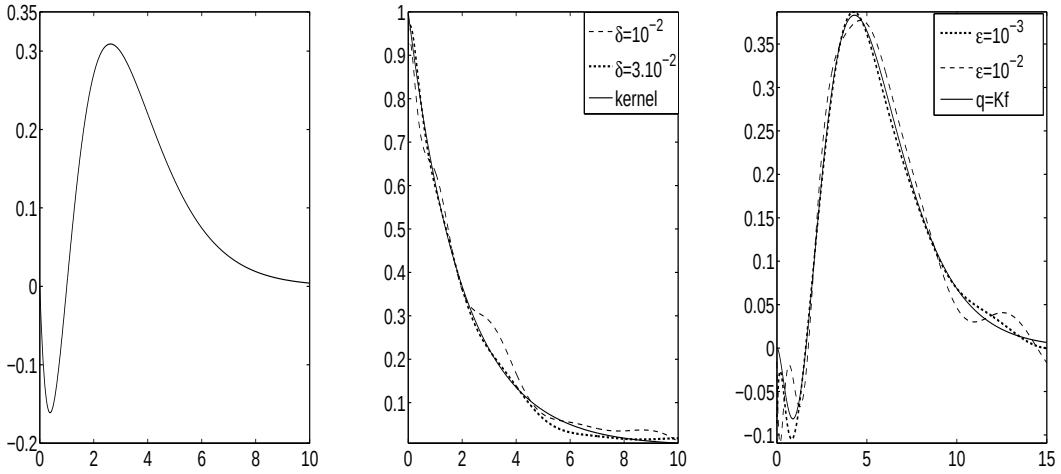

(a) **Target function f_1** (b) **Kernel g** (c) $q = Kf$

Figure 4.1: Datas and noisy observations of g and q

	Algorithm I				**Algorithm II**			
δ \ ε	0	10^{-3}	10^{-2}	3.10^{-2}	0	10^{-3}	10^{-2}	3.10^{-2}
0	0	0.020	0.141	0.348	0	0.012	0.109	0.312
10^{-3}	0.004	0.020	0.141	0.352	0.005	0.012	0.108	0.301
10^{-2}	0.047	0.054	0.143	0.344	0.053	0.039	0.116	0.318
3.10^{-2}	0.170	0.169	0.190	0.348	0.118	0.109	0.145	0.324

Table 4.3: Normalized mean squared error of the two procedures applied to the functions f_1 and g. The computations were performed using a Monte-Carlo method on 500 realizations.

of ε and δ, we report the corresponding squared loss, computed on a basis of 500 realizations with the use of Parseval's identity, in Table 4.3. The corresponding results are presented in Figure 4.2 for one particular realization of $\boldsymbol{\xi}, \boldsymbol{b}$. The results indicate that the transition on the two types of errors occur when δ is higher than ε, translating a prevailing effect of the signal noise ε over the operator error δ in practice. As Theorems 4.3.3 and 4.4.5 suggest, the second Algorithm overperforms the first in (almost) every case.

Discussion on the design irregularity: to control the squared risk of the two procedures, one needs condition 4.2.3 to be fulfilled. If not, the eigenvalues of the matrix $\boldsymbol{\Omega}_L$ become potentially too large, and observations (4.11) are not conveniently treatable. In this case, it is preferable to lower the maximal level down to a point where $\|\boldsymbol{\Omega}_L\|_{op}$ remains under control. To this end, we change the maximal level of the two

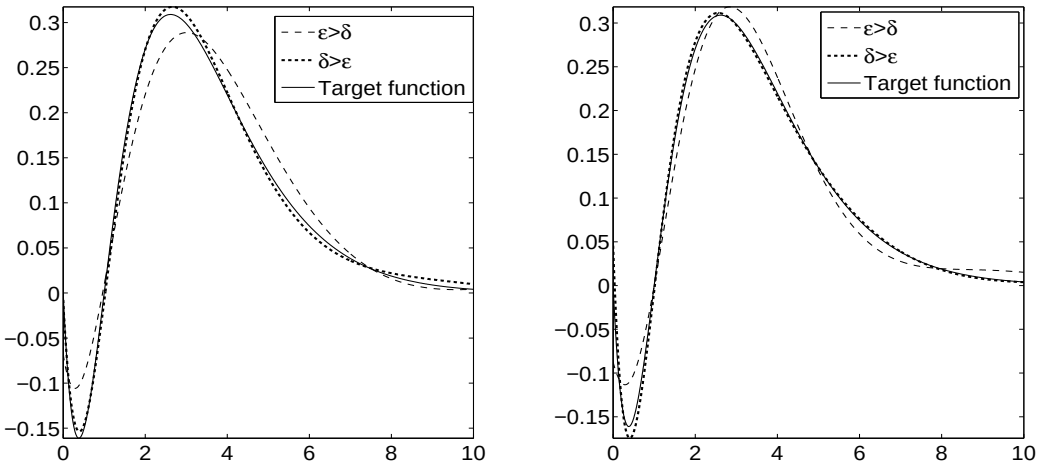

(a) **Algorithm I** (b) **Algorithm II**

Figure 4.2: Estimation of $\boldsymbol{f}_1$ for predominant signal noise $(\varepsilon, \delta) = (10^{-2}, 10^{-3})$ and predominant operator noise $(\delta, \varepsilon) = (10^{-3}, 10^{-2})$.

respective procedures to

$$N^i = L^i \wedge \max\{\ell \geqslant 0 \text{ s.t. } \|\boldsymbol{\Omega}_\ell\|_{op} \leqslant c\}, \quad i = \mathbf{I}, \mathbf{II}\,,$$

where c is an arbitrary thresholding constant, set to 1.5 in the sequel. We now fix $\sigma = \delta = 10^{-2}$ and chose the design points t_i as $t_i = 100i/n$ for $n = 200, 250, 750$ and 1000. Taking the same kernel $\boldsymbol{g} = \boldsymbol{\varphi}_0$, and setting $\boldsymbol{f}_2(t) = (t^{1/2} - t)\exp(-t)$, we compare the performances of the new choice N^i to the previous one L^i, by computing the respective mean squared losses on a basis of 500 observations and report the result in Table 4.4. The results show a minor effect of the design ill-posedness on **Algorithm I**, since L^i is usually already smaller than N^i. However, the gain is notable for **Algorithm II** when $n \leqslant 250$. To illustrate this point, we plot in Figure 4.3 the corresponding results when $n = 200$.

Back to the regression model

We now turn back to the original model (4.2) to apply the two procedures. It is well known that this model is asymptotically equivalent to (4.11), in the sense that a fine enough design will provide an estimation of the Laguerre coefficients with a negligible error when $n \to \infty$. We work with $\boldsymbol{f}_3(z) = (1-z)^{1/2}$, $\boldsymbol{g} = \boldsymbol{\varphi}_0$, $\delta = 10^{-2}$, and suppose that the design is constituted of the points $t_i = \sum_{j=1}^{i} (\text{step} + |X_j|)$ where $(X_j)_{j \leqslant n}$ is an i.i.d sequence of $\mathcal{N}(0, 10^{-2})$ variables. We observe the noisy values $\boldsymbol{y}(t_i) = \boldsymbol{q}(t_i) + \sigma\eta_i$ where

	$n =$	200	250	500	750
Algorithm I	$(L^{\mathbf{I}}, N^{\mathbf{I}})$	(6,6)	(6,6)	(6,6)	(6,6)
	MSE, $L^{\mathbf{I}}$	0.273	0.270	0.264	0.258
	MSE, $N^{\mathbf{I}}$	0.275	0.272	0.264	0.257
Algorithm II	$(L^{\mathbf{II}}, N^{\mathbf{II}})$	(37,12)	(37,15)	(37,27)	(37,27)
	MSE, $L^{\mathbf{II}}$	1.336	0.559	0.289	0.253
	MSE, $N^{\mathbf{II}}$	0.294	0.291	0.284	0.256

Table 4.4: Normalized mean squared error of the two procedures when the design is constituted of 200 equispaced points on the interval $[0; 100]$. We compare the performances of the two maximal resolution levels L^i and N^i for the parameters $\sigma = \delta = 10^{-2}$, $\boldsymbol{g} = \boldsymbol{\varphi}_0$ and $\boldsymbol{f}_2(t) = (t^{1/2} - t)\exp(-t)$.

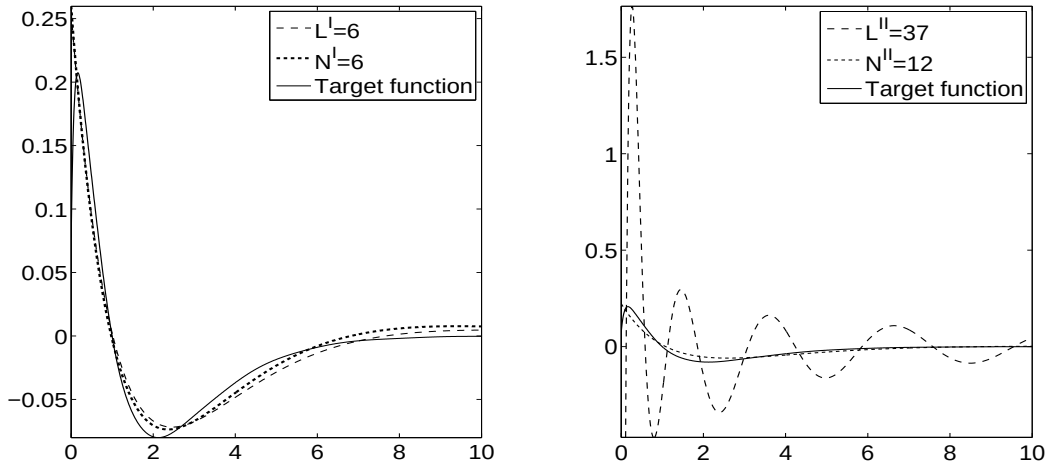

(a) **Algorithm I** (b) **Algorithm II**

Figure 4.3: Result of the two different maximal levels L^i and N^i to estimate $\boldsymbol{f}_2$, for a particular realization of $\boldsymbol{b}$ and $\boldsymbol{\xi}$. The design is constituted of 200 equidistant points of observations in $[0; 100]$. The noise levels are $\sigma = \delta = 10^{-2}$.

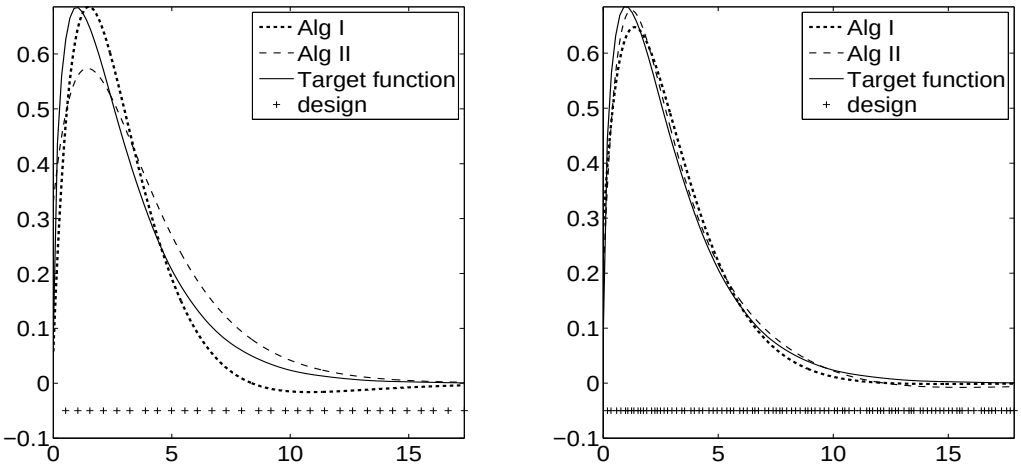

(a) $\substack{\text{step}=5.10^{-1};\, n=30 \\ (\text{MSE}\mathbf{I},\text{MSE}\mathbf{II})=(0.166,0.177)}$ (b) $\substack{\text{step}=10^{-1};\, n=100 \\ (\text{MSE}\mathbf{I},\text{MSE}\mathbf{II})=(0.118,0.133)}$

Figure 4.4: Adaptation of the procedures to the regression framework. Here, MSE denotes the normalized mean squared error for each algorithm (computed with 500 realizations). The target function is $\boldsymbol{f}_3$ and the noise levels are $\sigma = \delta = 5.10^{-2}$.

$\boldsymbol{q}(z) = (1-z)^{3/2}$, and compute the Laguerre coefficients $\check{\boldsymbol{q}}_\ell$ via the approximation

$$\check{\boldsymbol{q}}_\ell \sim \sum_{i=1}^{n-1} \frac{\boldsymbol{q}(t_i)\boldsymbol{\varphi}_\ell(t_i) + \boldsymbol{q}(t_{i+1})\boldsymbol{\varphi}_\ell(t_{i+1})}{2}(t_{i+1} - t_i)\,.$$

We apply the two procedures and present the results on Figure 4.4.

4.6 Proofs

In the sequel, for the sake of clarity, we suppose that $\tau_{sig} = \tau_{\text{op}} \stackrel{\Delta}{=} \tau$.

4.6.1 Proof of Proposition 4.4.2

Proof. We can restrict ourselves to the case where $\mu = 1$. Proposition 4.16 applied to equality (4.22) entails

$$\begin{aligned} \forall \ell \geqslant 0,\ T_\ell\big((1/\dot{\boldsymbol{g}})\big) &= C^{-1} T_\ell\big(w^{-1}\big) T_\ell\big((1-z)^{-\nu}\big) \\ T_\ell\big((1-z)^{-\nu}\big) &= C T_\ell\big(w\big) T_\ell\big((1/\dot{\boldsymbol{g}})\big)\,. \end{aligned}$$

As a consequence,

$$\sum_{k=0}^{\ell} \boldsymbol{\gamma}_k^2 = \|(1/\dot{\boldsymbol{g}})^\ell\|^2 \leqslant C^{-1}\|T_\ell(w^{-1})\|_{\mathrm{op}}\|(1-z)_\ell^{-\nu}\|^2 \tag{4.24}$$

$$\text{and} \quad \|(\boldsymbol{K}^\ell)^{-1}\|_{\mathrm{HS}} \geqslant C^{-1}\|T_\ell\big(w\big)\|_{\mathrm{op}}^{-1}\|T_\ell\big((1-z)^{-\nu}\big)\|_{\mathrm{HS}}\,. \tag{4.25}$$

Since w is assumed to have no zeros on $\mathcal{C}$, we deduce from Proposition 4.3.1 that both $\|w^{-1}\|_{circ}$ and $\|w\|_{circ}$ are finite, and from (4.15) that

$$\|T_\ell\big(w^{-1}\big)\|_{\mathrm{op}} \asymp 1 \text{ and } \|T_\ell\big(w\big)\|_{\mathrm{op}} \asymp 1\,.$$

It remains to treat the binomial series $(1-z)^{-\nu}$. This series can be expanded as

$$(1-z)^{-\nu} = \sum_{\ell \geqslant 0} (-1)^\ell \binom{-\nu}{\ell} z^\ell\,,$$

where $\binom{-\nu}{\ell} \triangleq \frac{\Gamma(-\nu+1)}{\Gamma(\ell+1)\Gamma(-\nu-\ell+1)}$ is the generalized binomial coefficient. Furthermore, we have

$$\binom{-\nu}{\ell} \underset{\ell\to\infty}{\sim} \frac{(-1)^\ell}{\Gamma(\nu)\ell^{-\nu+1}}\,, \tag{4.26}$$

which is a direct consequence of Euler's definition of the Gamma function $\Gamma(z) = \lim_{k\to\infty} \frac{k!k^z}{\Pi_{i=0}^k(z+i)}$. Since $\nu > 1/2$, the series $\sum_k \binom{-\nu}{k}^2$ is hence divergent, and there exists $\widetilde{Q}_2, \widetilde{Q}_1 > 0$ such that, for all $\ell \geqslant 0$,

$$\sum_{k=0}^{\ell} \binom{-\nu}{k}^2 \leqslant \widetilde{Q}_1(\ell \vee 1)^{2\nu-1} \quad \text{and}$$

Otherwise, it is readily seen that condition (4.21) is satisfied. The proof is complete thanks to (4.24) and (4.25). □

4.6.2 Proofs of theorems 4.3.3 and 4.4.5

Preliminary lemmas

We begin with the following lemmas. Lemma 4.6.1 is a concentration inequality on the variable $\|\boldsymbol{B}^\ell\|_{\mathrm{op}}$, which results from a concentration inequality on subgaussian processes. Lemma 4.6.2 states that $\|(\boldsymbol{K}_\delta^\ell)^{-1}\|_{\mathrm{op}}$ behaves as $\|(\boldsymbol{K}^\ell)^{-1}\|_{\mathrm{op}}$ on a set with large probability. Finally, Lemma 4.6.3 establishes deviations bounds on the variables $\boldsymbol{\zeta}_\ell - \check{\boldsymbol{f}}_\ell$ which will be useful throughout the proofs of Theorem 4.3.3 and Theorem 4.4.5.

Lemma 4.6.1. *There exists β_0, c_0 independent from $\ell \geqslant 0$, such that, for all $\ell \geqslant 0$, for all $t \geqslant \beta_0$,*

$$\mathbb{P}\Big(\frac{1}{\sqrt{(\ell \vee 1)\log(\ell \vee 2)}}\|\boldsymbol{B}^\ell\|_{op} > t\Big) \leqslant \exp(-c_0 t^2)\,.$$

This readily entails the following moments control, available for all $\ell \geqslant 0$, $p \geqslant 1$

$$\mathbb{E}\,\|\boldsymbol{B}^\ell\|_{op}^p \lesssim \big(\ell \log \ell\big)^{p/2} \vee 1\,.$$

Proof. The proof is a slight modification of Meckes [66, Theorem 1], to which we refer for a complete study. Lemma 4.6.1 is trivially satisfied if $\ell = 0, 1$, hence we will suppose that $\ell \geqslant 2$. From Proposition 4.3.1, we derive that

$$\mathbb{E}\,\|\boldsymbol{B}^\ell\|_{\mathrm{op}} \leqslant \mathbb{E}\,\|T\big((\boldsymbol{b})_k\big)\|_{\mathrm{op}} = \mathbb{E}\sup_{x\in[0,1]}|Y_x|, \qquad Y_x \triangleq \sum_{k=0}^{\ell} \boldsymbol{b}_\ell e^{2i\pi kx}\,.$$

We claim the two following facts:

- Let $a_0, ..., a_\ell \in \mathbb{R}$. There exists $c \geqslant 0$ such that for all $t > 0$,

$$\mathbb{P}\Big(\Big|\sum_{k=0}^{\ell} a_k \boldsymbol{b}_k\Big| > t\Big) \leqslant \exp\Big(\frac{-ct^2}{\sum_{k=0}^{\ell} a_k^2}\Big)\,. \tag{4.27}$$

- $d(x,y) \triangleq \sqrt{\mathbb{E}\,|Y_x - Y_y|^2} \leqslant 4\ell^{3/2}|x-y| \wedge 2\sqrt{\ell}$.

The first point is readily verified since $(\boldsymbol{b}_k)_{k\leqslant\ell}$ is a standard Gaussian vector, while the second point directly results from the bound

$$\big|e^{2i\pi kx} - e^{2i\pi ky}\big| \leqslant 2 \wedge 2\pi k|x-y| \text{ for all } x, y \in [0,1],\ k \geqslant 0$$

A direct application of Dudley's entropy bound (Talagrand [79, Proposition 2.1]) now entails

$$\mathbb{E}\sup_{x\in[0,1]}|Y_x| \lesssim (\ell \log \ell)^{1/2}$$

(see Meckes [66] for the rest of the proof). The deviation bound is now a consequence of Talagrand [79, Lemma 5.3]. Indeed, for all $x \in [0,1]$,

$$E|Y_x|^2 = \mathbb{E}\,\Big|\sum_{k=0}^{\ell} \boldsymbol{b}_k e^{2i\pi kx}\Big|^2 \lesssim \ell$$

which ends the proof. □

Lemma 4.6.2. *Let $\ell \geqslant 0$, $a_\ell = \rho O_{\ell,\delta}$ for some $0 < \rho < \frac{1}{2}$. Note $\boldsymbol{\gamma}_\delta(z) = \sum_{\ell \geqslant 0} \boldsymbol{\gamma}_{k,\delta} z^k$ the power series associated to $(\boldsymbol{K}_\delta^\ell)^{-1}$. On $\boldsymbol{A}_\ell \stackrel{\Delta}{=} \{\|(\boldsymbol{K}_\delta^\ell)^{-1}\|_{op} \leqslant O_{\ell,\delta}^{-1}\}$ and $\boldsymbol{B}_\ell \stackrel{\Delta}{=} \{\|\delta \boldsymbol{B}^{\boldsymbol{\ell}}\|_{op} \leqslant a_\ell\}$, the following inequalities hold*

$$\|(\boldsymbol{K}_\delta^\ell)^{-1}\|_{op} \leqslant \frac{\rho}{1-\rho}\|(\boldsymbol{K}^\ell)^{-1}\|_{op} \text{ and } \|(\boldsymbol{K}^\ell)^{-1}\|_{op} \leqslant (1-\rho)^{-1}\|(\boldsymbol{K}_\delta^\ell)^{-1}\|_{op}\,, \tag{4.28}$$

$$\sum_{k=0}^{\ell} \boldsymbol{\gamma}_{k,\delta}^2 \leqslant \frac{\rho}{1-\rho}\sum_{k=0}^{\ell} \boldsymbol{\gamma}_k^2 \tag{4.29}$$

Proof. First, we have

$$\big(\boldsymbol{K}^\ell\big)^{-1} = \big(\boldsymbol{K}_\delta^\ell - \delta \boldsymbol{B}^\ell\big)^{-1} = \big(\boldsymbol{I} - \delta(\boldsymbol{K}_\delta^\ell)^{-1}\boldsymbol{B}^\ell\big)^{-1}\big(\boldsymbol{K}_\delta^\ell\big)^{-1}\,.$$

On $\boldsymbol{A}_\ell \cap \boldsymbol{B}_\ell$, since a_ℓ satisfies $O_{\ell,\delta}^{-1}\, a_\ell = \rho < \frac{1}{2}$, by a usual Neumann series argument, we have

$$\begin{aligned}
\|\big(\boldsymbol{K}^\ell\big)^{-1}\|_{\mathrm{op}} &= \Big\|\Big[\sum_{k\geqslant 0}\big(-\delta(\boldsymbol{K}_\delta^\ell)^{-1}\boldsymbol{B}^\ell\big)^k\Big]\big(\boldsymbol{K}_\delta^\ell\big)^{-1}\Big\|_{\mathrm{op}} \\
&\leqslant \Big[\sum_{k\geqslant 0}\delta^k\|\big(\boldsymbol{K}_\delta^\ell\big)^{-1}\|_{\mathrm{op}}^k\|\boldsymbol{B}^\ell\|_{\mathrm{op}}^k\Big]\|\big(\boldsymbol{K}_\delta^\ell\big)^{-1}\|_{\mathrm{op}} \\
&\leqslant \Big[\sum_{k\geqslant 0}\rho^k\Big]\|\big(\boldsymbol{K}_\delta^\ell\big)^{-1}\|_{\mathrm{op}} \\
&\leqslant (1-\rho)^{-1}\|\big(\boldsymbol{K}_\delta^\ell\big)^{-1}\|_{\mathrm{op}}\,.
\end{aligned} \tag{4.30}$$

Secondly, we have

$$\big(\boldsymbol{K}_\delta^\ell\big)^{-1} = \big(\boldsymbol{K}^\ell + \delta \boldsymbol{B}^\ell\big)^{-1} = \big(\boldsymbol{I} + \delta(\boldsymbol{K}^\ell)^{-1}\boldsymbol{B}^\ell\big)^{-1}\big(\boldsymbol{K}^\ell\big)^{-1}\,.$$

Moreover, thanks to (4.30), on $\boldsymbol{A}_\ell \cap \boldsymbol{B}_\ell$, we have

$$\|\delta(\boldsymbol{K}^\ell)^{-1}\boldsymbol{B}^\ell\|_{\mathrm{op}} \leqslant (1-\rho)^{-1}O_{\ell,\delta}^{-1}\, a_\ell \leqslant \frac{\rho}{1-\rho} < 1\,. \tag{4.31}$$

So that we can now similarly derive

$$\|\big(\boldsymbol{K}_\delta^\ell\big)^{-1}\|_{\mathrm{op}} \leqslant \frac{\rho}{1-\rho}\|\big(\boldsymbol{K}^\ell\big)^{-1}\|_{\mathrm{op}}\,.$$

This proves (4.28). The proof of (4.29) follows the same lines, since $\|Ab\| \leqslant \|A\|_{\mathrm{op}}\|b\|$. □

Proof of theorem 4.3.3

Lemma 4.6.3. *Under Assumption 4.3.2, we have, for all $\ell \geqslant 0$,*

$$\mathbb{E}\Big[\Big|\big\langle(\boldsymbol{K}_\delta^\ell)^{-1}\mathbf{1}_{\boldsymbol{A}_\ell}\mathbf{1}_{\boldsymbol{B}_\ell}\big(-\delta\boldsymbol{B}^\ell\boldsymbol{f}^\ell + \varepsilon\boldsymbol{\xi}_{L^{\boldsymbol{I}}}\big), \boldsymbol{\varphi}_\ell\big\rangle\Big|^q\Big] \lesssim (\ell\vee 1)^{q\nu}(\varepsilon\vee\delta)^q \tag{4.32}$$

$$\mathbb{P}\left(\Big|\big\langle(\boldsymbol{K}_\delta^\ell)^{-1}\mathbf{1}_{\boldsymbol{A}_\ell}\mathbf{1}_{\boldsymbol{B}_\ell}\big(-\delta\boldsymbol{B}^\ell\boldsymbol{f}^\ell + \varepsilon\boldsymbol{\xi}_{L^{\boldsymbol{I}}}\big), \boldsymbol{\varphi}_\ell\big\rangle\Big| > S_{\ell,\varepsilon}^{\boldsymbol{I}}\right) \lesssim \varepsilon^{\tau^2}\vee\delta^\tau\,. \tag{4.33}$$

Proof. In order to prove Inequalities (4.32) and (4.33), it suffices to study the tails of the random variables $\left|\langle (\boldsymbol{K}_\delta^\ell)^{-1}\mathbf{1}_{\boldsymbol{A}_\ell}\mathbf{1}_{\boldsymbol{B}_\ell}\big(-\delta\boldsymbol{B}^\ell\boldsymbol{f}^\ell+\varepsilon\boldsymbol{\xi}_{L^{\mathrm{I}}}\big),\boldsymbol{\varphi}_\ell\rangle\right|$. For convenience we will only treat the case where $\ell\geqslant 2$, otherwise the result follows by identical arguments. To this end, we study each term apart. On $\boldsymbol{A}_\ell\cap\boldsymbol{B}_\ell$, Lemma 4.6.2 and Assumption 4.3.2 entail

$$\|(\boldsymbol{K}_\delta^\ell)^{-1}\|_{\mathrm{op}}\leqslant\frac{Q\rho}{1-\rho}\ell^\nu\,.$$

Thus, combining Assumption 4.2.3 with the latter inequality, a brief conditioning argument readily yields

$$\mathbb{P}\left(\left|\langle(\boldsymbol{K}_\delta^\ell)^{-1}\mathbf{1}_{\boldsymbol{A}_\ell}\mathbf{1}_{\boldsymbol{B}_\ell}\varepsilon\boldsymbol{\xi}_{L^{\mathrm{I}}},\boldsymbol{\varphi}_\ell\rangle\right|>t\right)\lesssim\exp\big(-\frac{t^2}{\varepsilon^2\ell^{2\nu}}\big)\,.$$

Let us study the second term. On $\boldsymbol{A}_\ell\cap\boldsymbol{B}_\ell$, we have

$$\delta(\boldsymbol{K}_\delta^\ell)^{-1}\boldsymbol{B}^\ell=\sum_{k\geqslant1}\big(\delta(\boldsymbol{K}^\ell)^{-1}\boldsymbol{B}^\ell\big)^k=\delta(\boldsymbol{K}^\ell)^{-1}\boldsymbol{B}^\ell+\sum_{k\geqslant2}\big(\delta(\boldsymbol{K}^\ell)^{-1}\boldsymbol{B}^\ell\big)^k\,.$$

Hence,

$$\delta(\boldsymbol{K}_\delta^\ell)^{-1}\mathbf{1}_{\boldsymbol{A}_\ell}\mathbf{1}_{\boldsymbol{B}_\ell}\boldsymbol{B}^\ell\boldsymbol{f}^\ell=r_1+r_2\,,\tag{4.34}$$

where

$$\begin{cases}r_1&=\langle\delta(\boldsymbol{K}^\ell)^{-1}\boldsymbol{B}^\ell\boldsymbol{f}^\ell,\boldsymbol{\varphi}_\ell\rangle\,,\\ r_2&=\big\langle\big(\delta(\boldsymbol{K}^\ell)^{-1}\boldsymbol{B}^\ell\big)^2\big(\boldsymbol{I}+\delta(\boldsymbol{K}^\ell)^{-1}\boldsymbol{B}^\ell\big)^{-1}\boldsymbol{f}^\ell,\boldsymbol{\varphi}_\ell\big\rangle\,.\end{cases}\tag{4.35}$$

Let's now bound separately r_1 and r_2. We first apply equality (4.16) to get

$$\begin{aligned}\langle(\boldsymbol{K}^\ell)^{-1}\boldsymbol{B}^\ell\boldsymbol{f}^\ell,\boldsymbol{\varphi}_\ell\rangle&=\langle(\boldsymbol{K}^\ell)^{-1}\boldsymbol{f}^\ell,{}^{\mathrm{t}}\boldsymbol{B}^\ell\boldsymbol{\varphi}_\ell\rangle\\&=\langle(\boldsymbol{K}^\ell)^{-1}\boldsymbol{f}^\ell,(\boldsymbol{b}^\ell)'\rangle\,,\end{aligned}$$

where $(\boldsymbol{b}^\ell)'_k=(\boldsymbol{b}^\ell)_{\ell-k}$. The result is a centered Gaussian variable with variance

$$\|\delta(\boldsymbol{K}^\ell)^{-1}\boldsymbol{f}^\ell\|^2\leqslant\delta^2Q^2M^2\ell^{2\nu}\,,$$

which hence satisfies

$$\mathbb{P}(|r_1|>t)\lesssim\exp\big(\frac{-t^2}{\delta^2\ell^{2\nu}}\big)\,.$$

Let us study the term r_2. Since the maximal level L verifies $L\leqslant\lambda(\delta|\log\delta|)^{-\frac{1}{\nu+1}}$, we have, for all $\ell\leqslant L$, $\delta\ell^{\nu+1}\log\ell\lesssim1$. We deduce that

$$\begin{aligned}\mathbb{P}(|r_2|>t)&\leqslant\mathbb{P}(\delta^2\ell^{2\nu}\|\boldsymbol{B}^\ell\|_{\mathrm{op}}^2>t)\\&\leqslant\mathbb{P}(\frac{1}{\ell\log\ell}\|\boldsymbol{B}^\ell\|_{\mathrm{op}}^2>\delta^{-2}\ell^{-2\nu-1}(\log\ell)^{-1}t)\\&\lesssim\mathbb{P}(\frac{1}{\ell\log\ell}\|\boldsymbol{B}^\ell\|_{\mathrm{op}}^2>\delta^{-1}\ell^{-\nu}t)\\&\lesssim\exp(-t\big(\delta\ell^\nu\big)^{-1})\mathbf{1}_{\{t>\beta_0\delta\ell^\nu\}}+\mathbf{1}_{\{t\leqslant\beta_0\delta\ell^\nu\}}\,.\end{aligned}$$

Inequality (4.33) directly follows, and inequality (4.32) is now a direct application of the well known formula

$$\mathbb{E}[X^2] = \int_{t>0} 2t\,\mathbb{P}(|X| > t)dt\,.$$

□

Proof of theorem 4.3.3. We apply Parseval's formula to derive

$$\mathbb{E}\,\|\tilde{\boldsymbol{f}}^{\mathbf{I}} - \boldsymbol{f}\|_2^2 = \sum_{\ell \leqslant L^{\mathbf{I}}} \mathbb{E}\langle \tilde{\boldsymbol{f}} - \boldsymbol{f}, \boldsymbol{\varphi}_\ell\rangle^2 + \sum_{\ell > L^{\mathbf{I}}} \check{\boldsymbol{f}}_\ell^2\,.$$

The second term is easily handled. Remark first that, since $s > 1/2$, we have $\frac{2s}{\nu+1} > \frac{2s}{s+\nu+1/2}$ and we can write

$$\begin{aligned}\sum_{\ell > L^{\mathbf{I}}} \check{\boldsymbol{f}}_\ell^2 &\leqslant \big(L^{\mathbf{I}}\big)^{-2s} \\ &\leqslant \big(\varepsilon\sqrt{|\log\varepsilon|}\big)^{\frac{2s}{\nu+1}} \vee \big(\delta|\log\delta|\big)^{\frac{2s}{\nu+1}} \\ &\leqslant \big(\varepsilon\sqrt{|\log\varepsilon|}\big)^{\frac{4s}{2(s+\nu)+1}} \vee \big(\delta|\log\delta|\big)^{\frac{4s}{2(s+\nu)+1}}\,.\end{aligned}$$

In order to lighten the notations, we will only consider the indexes $\ell \geqslant 2$ in the first term. This is of course not problematic, since an identical reasoning allows to bound the two remaining summands by the desired rates of convergence. We hence write the following decomposition

$$\begin{aligned}\sum_{\ell \leqslant L^{\mathbf{I}}} \mathbb{E}\langle \tilde{\boldsymbol{f}} - \boldsymbol{f}, \boldsymbol{\varphi}_\ell\rangle^2 &= \sum_{\ell \leqslant L^{\mathbf{I}}} \mathbb{E}(\boldsymbol{\zeta}_\ell - \check{\boldsymbol{f}}_\ell)^2 \mathbf{1}_{\{|\boldsymbol{\zeta}_\ell| > S^{\mathbf{I}}_{\ell,\varepsilon}\}} + \mathbb{E}\sum_{\ell \leqslant L^{\mathbf{I}}} \check{\boldsymbol{f}}_\ell^2 \mathbf{1}_{\{|\boldsymbol{\zeta}_\ell| \leqslant S^{\mathbf{I}}_{\ell,\varepsilon}\}}\,, \\ &\lesssim I + II + III + IV\,,\end{aligned}$$

where

$$\begin{aligned} I &= \sum_{\ell \leqslant L^{\mathbf{I}}} \mathbb{E}\left(\boldsymbol{\zeta}_\ell - \check{\boldsymbol{f}}_\ell\right)^2 \mathbf{1}_{\boldsymbol{A}_\ell} \mathbf{1}_{\boldsymbol{B}_\ell} \mathbf{1}_{\{|\boldsymbol{\zeta}_\ell| > S^{\mathbf{I}}_{\ell,\varepsilon}\}}\,, \\ II &= \sum_{\ell \leqslant L^{\mathbf{I}}} \mathbb{E}\,\check{\boldsymbol{f}}_\ell^2 \mathbf{1}_{\{|\boldsymbol{\zeta}_\ell| \leqslant S^{\mathbf{I}}_{\ell,\varepsilon}\}} \mathbf{1}_{\boldsymbol{A}_\ell} \mathbf{1}_{\boldsymbol{B}_\ell}\,, \\ III &= \sum_{\ell \leqslant L^{\mathbf{I}}} \mathbb{E}\left(\boldsymbol{\zeta}_\ell - \check{\boldsymbol{f}}_\ell\right)^2 \mathbf{1}_{\boldsymbol{A}_\ell} \mathbf{1}_{\boldsymbol{B}_\ell^c} \mathbf{1}_{\{|\boldsymbol{\zeta}_\ell| > S^{\mathbf{I}}_{\ell,\varepsilon}\}} + \sum_{\ell \leqslant L^{\mathbf{I}}} \mathbb{E}\,\check{\boldsymbol{f}}_\ell^2 \mathbf{1}_{\{|\boldsymbol{\zeta}_\ell| \leqslant S^{\mathbf{I}}_{\ell,\varepsilon}\}} \mathbf{1}_{\boldsymbol{B}_\ell^c}\,, \\ IV &= \sum_{\ell \leqslant L^{\mathbf{I}}} \mathbb{E}\,\check{\boldsymbol{f}}_\ell^2 \mathbf{1}_{\boldsymbol{A}_\ell^c} \mathbf{1}_{\{|\boldsymbol{\zeta}_\ell| \leqslant S^{\mathbf{I}}_{\ell,\varepsilon}\}}\,. \end{aligned}$$

- ***Term I and II.*** On $\boldsymbol{A}_\ell$, we have

$$\boldsymbol{\zeta}_\ell - \check{\boldsymbol{f}}_\ell = \big\langle (\boldsymbol{K}_\delta^\ell)^{-1}\big(-\delta \boldsymbol{B}^\ell \boldsymbol{f}^\ell + \varepsilon \boldsymbol{\xi}\big), \boldsymbol{\varphi}_\ell\big\rangle\,. \tag{4.36}$$

Hence we can decompose further I as

$$\begin{aligned} I &\lesssim \sum_{\ell\leqslant L^{\mathrm{I}}} \mathbb{E}\langle (\boldsymbol{K}_\delta^\ell)^{-1}\mathbf{1}_{\boldsymbol{A}_\ell}\mathbf{1}_{\boldsymbol{B}_\ell}\big(-\delta\boldsymbol{B}^\ell\boldsymbol{f}^\ell+\varepsilon\boldsymbol{\xi}\big),\boldsymbol{\varphi}_\ell\rangle^2\mathbf{1}_{\{|\zeta_\ell|>S^{\mathrm{I}}_{\ell,\varepsilon}\}} \\ &\lesssim \sum_{\ell\leqslant L^{\mathrm{I}}} \mathbb{E}\langle (\boldsymbol{K}_\delta^\ell)^{-1}\mathbf{1}_{\boldsymbol{A}_\ell}\mathbf{1}_{\boldsymbol{B}_\ell}\big(-\delta\boldsymbol{B}^\ell\boldsymbol{f}^\ell+\varepsilon\boldsymbol{\xi}\big),\boldsymbol{\varphi}_\ell\rangle^2\mathbf{1}_{\{|\zeta_\ell|>S^{\mathrm{I}}_{\ell,\varepsilon}\}}\mathbf{1}_{\{|\check{\boldsymbol{f}}_\ell|\geqslant S^{\mathrm{I}}_{\ell,\varepsilon}/2\}} \\ &\quad+\sum_{\ell\leqslant L^{\mathrm{I}}} \mathbb{E}\langle (\boldsymbol{K}_\delta^\ell)^{-1}\mathbf{1}_{\boldsymbol{A}_\ell}\mathbf{1}_{\boldsymbol{B}_\ell}\big(-\delta\boldsymbol{B}^\ell\boldsymbol{f}^\ell+\varepsilon\boldsymbol{\xi}\big),\boldsymbol{\varphi}_\ell\rangle^2\mathbf{1}_{\{|\zeta_\ell|>S^{\mathrm{I}}_{\ell,\varepsilon}\}}\mathbf{1}_{\{|\check{\boldsymbol{f}}_\ell|< S^{\mathrm{I}}_{\ell,\varepsilon}/2\}}, \\ &\triangleq V+VI. \end{aligned}$$

Let us first treat the term VI. From Lemmas 4.6.2 and 4.6.3 and Cauchy-Schwarz inequality, we derive

$$\begin{aligned} VI &\leqslant \sum_{\ell\leqslant L^{\mathrm{I}}} \mathbb{E}\Big[\langle (\boldsymbol{K}_\delta^\ell)^{-1}\mathbf{1}_{\boldsymbol{A}_\ell}\mathbf{1}_{\boldsymbol{B}_\ell}\big(\delta\boldsymbol{B}^\ell\boldsymbol{f}^\ell+\varepsilon\boldsymbol{\xi}\big),\boldsymbol{\varphi}_\ell\rangle^4\Big]^{1/2} \\ &\qquad\qquad .\,\mathbb{P}(|\boldsymbol{\zeta}_\ell-\check{\boldsymbol{f}}_\ell|>S^{\mathrm{I}}_{\ell,\varepsilon})^{1/2} \\ &\lesssim \sum_{\ell\leqslant L^{\mathrm{I}}}\big[(\delta\vee\varepsilon)^4\ell^{4\nu}\big]^{1/2}\big(\delta^{\tau/2}\vee\varepsilon^{\tau^2/2}\big), \end{aligned}$$

which is less than the desired bound for τ large enough. As for term V, we split it in two and write

$$\begin{aligned} V &\leqslant \sum_{\ell\leqslant L^{\mathrm{I}}} \mathbb{E}\langle (\boldsymbol{K}_\delta^\ell)^{-1}\mathbf{1}_{\boldsymbol{A}_\ell}\mathbf{1}_{\boldsymbol{B}_\ell}\big(\delta\boldsymbol{B}^\ell\boldsymbol{f}^\ell+\varepsilon\boldsymbol{\xi}\big),\boldsymbol{\varphi}_\ell\rangle^2\mathbf{1}_{\{|\check{\boldsymbol{f}}_\ell|\geqslant S^{\mathrm{I}}_{\ell,\varepsilon}/2\}} \\ &\leqslant \sum_{\ell\leqslant L^{\mathrm{I}}} \mathbb{E}\langle (\boldsymbol{K}_\delta^\ell)^{-1}\mathbf{1}_{\boldsymbol{A}_\ell}\mathbf{1}_{\boldsymbol{B}_\ell}\delta\boldsymbol{B}^\ell\boldsymbol{f}^\ell,\boldsymbol{\varphi}_\ell\rangle^2\mathbf{1}_{\{|\check{\boldsymbol{f}}_\ell|\geqslant \ell^\nu\delta|\log\delta|/2\}} \\ &\quad+\sum_{\ell\leqslant L^{\mathrm{I}}} \mathbb{E}\langle (\boldsymbol{K}_\delta^\ell)^{-1}\mathbf{1}_{\boldsymbol{A}_\ell}\mathbf{1}_{\boldsymbol{B}_\ell}\varepsilon\boldsymbol{\xi},\boldsymbol{\varphi}_\ell\rangle^2\mathbf{1}_{\{|\check{\boldsymbol{f}}_\ell|\geqslant \ell^\nu\varepsilon\sqrt{|\log\varepsilon|}/2\}} \\ &\leqslant \sum_{\ell\leqslant L^{\mathrm{I}}} \delta^2\ell^{2\nu}\big(\check{\boldsymbol{f}}_\ell^2\big(\ell^\nu\,\delta|\log\delta|\big)^{-2}\wedge 1\big) \\ &\qquad\qquad\vee\sum_{\ell\leqslant L^{\mathrm{I}}} \varepsilon^2\ell^{2\nu}\big(\check{\boldsymbol{f}}_\ell^2\big(\ell^\nu\varepsilon\sqrt{|\log\varepsilon|}\big)^{-2}\wedge 1\big). \end{aligned}$$

Note $\ell_\delta=\big(\delta|\log\delta|\big)^{\frac{-2}{2(s+\nu)+1}}$ and write

$$\begin{aligned} \sum_{\ell\leqslant L^{\mathrm{I}}} \delta^2\ell^{2\nu}\big(\check{\boldsymbol{f}}_\ell^2\big(\ell^\nu\delta|\log\delta|\big)^{-2}\wedge 1\big) &\leqslant \sum_{\ell\leqslant\ell_\delta}\delta^2\ell^{2\nu}+\sum_{\ell>\ell_\delta}\check{\boldsymbol{f}}_\ell^2|\log\delta|^{-2} \\ &\lesssim \big(\delta|\log\delta|\big)^{\frac{4s}{2(s+\nu)+1}}. \end{aligned}$$

The ε-term is treated similarly by taking $\ell_\varepsilon=\big(\varepsilon\sqrt{|\log\varepsilon|}\big)^{\frac{-2}{2s+2\nu+1}}$ and leads to the desired convergence rate. As for the term II, a similar reasoning leads to

$$\begin{aligned} II &\leqslant \sum_{\ell\leqslant L^{\mathrm{I}}}\mathbb{E}\,\check{\boldsymbol{f}}_\ell^2\mathbf{1}_{\{|\zeta_\ell|\leqslant S^{\mathrm{I}}_{\ell,\varepsilon}\}}\mathbf{1}_{\{|\check{\boldsymbol{f}}_\ell|\leqslant 2S^{\mathrm{I}}_{\ell,\varepsilon}\}}+\sum_{\ell\leqslant L^{\mathrm{I}}}\mathbb{E}\,\check{\boldsymbol{f}}_\ell^2\mathbf{1}_{\{|\zeta_\ell|\leqslant S^{\mathrm{I}}_{\ell,\varepsilon}\}}\mathbf{1}_{\{|\check{\boldsymbol{f}}_\ell|>2S^{\mathrm{I}}_{\ell,\varepsilon}\}}, \\ &\triangleq VII+VIII. \end{aligned}$$

The term $VIII$ is handled as the term VI. Indeed,

$$VIII \leqslant \sum_{\ell \leqslant L^{\mathbf{I}}} \check{\boldsymbol{f}}_\ell^2 \, \mathbb{P}\left(|\boldsymbol{\zeta}_\ell - \check{\boldsymbol{f}}_\ell| > S^{\mathbf{I}}_{\ell,\varepsilon}\right) \leqslant \sum_{\ell \leqslant L^{\mathbf{I}}} \check{\boldsymbol{f}}_\ell^2 (\varepsilon^{\tau^2} \vee \delta^\tau) \,,$$

which is less than the desired rate for τ large enough. Finally, we have

$$\begin{aligned} VII &\leqslant \sum_{\ell \leqslant L^{\mathbf{I}}} \mathbb{E}\, \check{\boldsymbol{f}}_\ell^2 \mathbf{1}_{\left\{|\check{\boldsymbol{f}}_\ell| \leqslant 2 S^{\mathbf{I}}_{\ell,\varepsilon}\right\}} \\ &\leqslant \sum_{\ell \leqslant L^{\mathbf{I}}} \mathbb{E}\, \check{\boldsymbol{f}}_\ell^2 \mathbf{1}_{\left\{|\check{\boldsymbol{f}}_\ell| \leqslant 2\tau \ell^\nu \varepsilon \sqrt{|\log \varepsilon|}\right\}} + \sum_{\ell \leqslant L^{\mathbf{I}}} \mathbb{E}\, \check{\boldsymbol{f}}_\ell^2 \mathbf{1}_{\left\{|\check{\boldsymbol{f}}_\ell| \leqslant 2\tau \ell^\nu \delta |\log \delta|\right\}} \\ &\lesssim \sum_{\ell \leqslant \ell_\varepsilon} \ell^{2\nu} \varepsilon^2 |\log \varepsilon| + \sum_{\ell > \ell_\varepsilon} \check{\boldsymbol{f}}_\ell^2 + \sum_{\ell \leqslant \ell_\delta} \ell^{2\nu} \delta^2 |\log \delta| + \sum_{\ell > \ell_\delta} \check{\boldsymbol{f}}_\ell^2 \\ &\lesssim \left(\varepsilon \sqrt{|\log \varepsilon|}\right)^{\frac{4s}{2(s+\nu)+1}} \vee \left(\delta |\log \delta|^2\right)^{\frac{4s}{2(s+\nu)+1}} . \end{aligned}$$

□

- ***Term III***. We have

$$\begin{aligned} III &\leqslant \sum_{\ell \leqslant L^{\mathbf{I}}} \mathbb{E}\left(\left(\boldsymbol{\zeta}_\ell - \check{\boldsymbol{f}}_\ell\right)^2 \mathbf{1}_{\boldsymbol{A}_\ell} + \check{\boldsymbol{f}}_\ell^2\right) \mathbf{1}_{\boldsymbol{B}_\ell^c} \\ &\leqslant \sum_{\ell \leqslant L^{\mathbf{I}}} \mathbb{E}\left[\left(\boldsymbol{\zeta}_\ell - \check{\boldsymbol{f}}_\ell\right)^4 \mathbf{1}_{\boldsymbol{A}_\ell}\right]^{1/2} \mathbb{P}\left(\boldsymbol{B}_\ell^c\right)^{1/2} + \sum_{\ell \leqslant L^{\mathbf{I}}} \check{\boldsymbol{f}}_\ell^2 \, \mathbb{P}(\boldsymbol{B}_\ell^c) \,. \end{aligned}$$

Moreover, Lemma 4.6.1 entails

$$\mathbb{P}\left(\boldsymbol{B}_\ell^c\right) \leqslant \delta^{\kappa^2 \rho^2}$$

for all $\ell \geqslant 1$. It is hence clear that for κ large enough, the term III is less than the announced rate. □

- ***Term IV***. We claim that

$$\mathbf{1}_{\left\{\boldsymbol{A}_\ell^c\right\}} \leqslant \mathbf{1}_{\left\{\|(\boldsymbol{K}^\ell)^{-1}\|_{\mathrm{op}} \geqslant O_{\ell,\delta}^{-1}/2\right\}} + \mathbf{1}_{\left\{\|\delta \boldsymbol{B}^\ell\|_{\mathrm{op}} \geqslant O_{\ell,\delta}\right\}}$$

for all $\ell \geqslant 0$ (see Delattre et al. [23], Lemma 5.3). Hence,

$$\begin{aligned} IV &\leqslant \sum_{\ell \leqslant L^{\mathbf{I}}} \mathbb{E}\, \check{\boldsymbol{f}}_\ell^2 \left(\mathbf{1}_{\left\{\|(\boldsymbol{K}^\ell)^{-1}\|_{\mathrm{op}} \geqslant O_{\ell,\delta}^{-1}/2\right\}} + \mathbf{1}_{\left\{\|\delta \boldsymbol{B}^\ell\|_{\mathrm{op}} \geqslant O_{\ell,\delta}\right\}}\right) , \\ &\triangleq VIII + IX \,. \end{aligned}$$

Since $\|(\boldsymbol{K}^\ell)^{-1}\|_{\mathrm{op}} \leqslant Q_2 \ell^\nu$, we have $\{\|(\boldsymbol{K}^\ell)^{-1}\|_{\mathrm{op}} \geqslant O_{\ell,\delta}^{-1}/2\} \subset \{\ell^{\nu+1/2}\sqrt{\log \ell} \geqslant c\big(\delta |\log \delta|\big)^{-1}\}$ where c is a constant depending only on Q_2 and κ. Hence

$$\begin{aligned} VIII &\leqslant \sum_{\ell \geqslant c\left(\delta |\log \delta|^{3/2}\right)^{-\frac{2}{2\nu+1}}} \check{\boldsymbol{f}}_\ell^2 \\ &\lesssim \left(\delta |\log \delta|\right)^{\frac{4s}{2\nu+2s+1}} . \end{aligned}$$

As for IX, a quick application of 4.6.1 entails

$$\mathbb{P}(\|\delta \boldsymbol{B}^\ell\|_{\rm op} \geqslant O_{\ell,\delta}) \leqslant \delta^{\kappa^2}\,,$$

so that

$$IX \leqslant \sum_{\ell \leqslant L^{\rm I}} \check{\boldsymbol{f}}_\ell^2 \delta^{\kappa^2} \lesssim \delta^{\kappa^2}\,,$$

which is less than the announced rate for κ large enough. □

It remains to put together the bounds of the four terms above to get the desired rates of convergence in theorem 4.3.3. □

Proof of theorem 4.4.5

Lemma 4.6.4. *Note, for $\ell \geqslant 0$, $\overline{S^{\boldsymbol{II}}_{\ell,\varepsilon}} \triangleq (\ell \vee 1)^{\nu-1/2}\big(\tau_{sig}\varepsilon\sqrt{|\log\varepsilon|} \vee \tau_{op}\delta|\log\delta|\big)$. Under Assumption 4.4.1, we have, for all $\ell \geqslant 0$, for all $q \geqslant 0$,*

$$\mathbb{E}\Big[\big|\langle (\boldsymbol{K}_\delta^\ell)^{-1}\mathbf{1}_{\boldsymbol{A}_\ell}\mathbf{1}_{\boldsymbol{B}_\ell}(-\delta\boldsymbol{B}^\ell\boldsymbol{f}^\ell + \varepsilon\boldsymbol{\xi}_{L^{\rm II}}), \boldsymbol{\varphi}_\ell\rangle\big|^q\Big] \lesssim (\ell\vee 1)^{q(\nu-1/2)}(\varepsilon\vee\delta)^q\,, \quad (4.37)$$

$$\mathbb{P}\left(\big|\langle (\boldsymbol{K}_\delta^\ell)^{-1}\mathbf{1}_{\boldsymbol{A}_\ell}\mathbf{1}_{\boldsymbol{B}_\ell}(-\delta\boldsymbol{B}^\ell\boldsymbol{f}^\ell + \varepsilon\boldsymbol{\xi}_{L^{\rm II}}), \boldsymbol{\varphi}_\ell\rangle\big| > \overline{S^{\boldsymbol{II}}_{\ell,\varepsilon}}\right) \lesssim \varepsilon^{\tau^2} \vee \delta^\tau\,. \quad (4.38)$$

Proof. The proof is very similar to Lemma 4.6.3, whence we will just mention the notable changes compared to it. Once more, we shall only treat the case $\ell \geqslant 2$. First, we have

$$\langle (\boldsymbol{K}_\delta^\ell)^{-1}\mathbf{1}_{\boldsymbol{A}_\ell}\mathbf{1}_{\boldsymbol{B}_\ell}\varepsilon\boldsymbol{\xi}, \boldsymbol{\varphi}_\ell\rangle = \langle \varepsilon\boldsymbol{\xi}_{L^{\rm II}}, {}^t(\boldsymbol{K}_\delta^\ell)^{-1}\mathbf{1}_{\boldsymbol{A}_\ell}\mathbf{1}_{\boldsymbol{B}_\ell}\boldsymbol{\varphi}_\ell\rangle = \varepsilon\langle \boldsymbol{\xi}_{L^{\rm II}}, ((1/\dot{\boldsymbol{g}}_\delta)^\ell)'\rangle\,,$$

so that a brief conditioning argument, combined with (4.29) and Assumption 4.2.3 entails

$$\mathbb{P}(|\langle (\boldsymbol{K}_\delta^\ell)^{-1}\mathbf{1}_{\boldsymbol{A}_\ell}\mathbf{1}_{\boldsymbol{B}_\ell}\varepsilon\boldsymbol{\xi}_{L^{\rm II}}, \boldsymbol{\varphi}_\ell\rangle| > t) \lesssim \exp(\frac{-t^2}{\varepsilon^2\ell^{2\nu-1}})\,.$$

In order to treat the term $\mathbb{P}(|\langle (\boldsymbol{K}_\delta^\ell)^{-1}\mathbf{1}_{\boldsymbol{A}_\ell}\mathbf{1}_{\boldsymbol{B}_\ell}\delta\boldsymbol{B}^\ell\boldsymbol{f}^\ell, \boldsymbol{\varphi}_\ell\rangle| > t)$, we first establish a useful result for the sequel: if $\boldsymbol{g}$ satisfies (4.20), then

$$\|(\boldsymbol{K}^\ell)^{-1}\boldsymbol{f}^\ell\| = \|T_\ell(\boldsymbol{f})(1/\dot{\boldsymbol{g}})^\ell\| \leqslant \|T_\ell(\boldsymbol{f})\|_{\rm op}\|(1/\dot{\boldsymbol{g}})^\ell\|\,.$$

Furthermore, thanks to Proposition 4.3.1 we have

$$\|T_\ell(\boldsymbol{f})\|_{\rm op} \leqslant \sum_{\ell\geqslant 0}|\check{\boldsymbol{f}}_\ell| \leqslant \sum_{\ell\geqslant 0}\ell^{2s}|\check{\boldsymbol{f}}_\ell|^2\sum_{\ell\geqslant 0}\ell^{-2s} \lesssim 1\,,$$

since $\boldsymbol{f} \in \mathcal{W}^s(M)$ and $s > 1/2$. We derive that

$$\|(\boldsymbol{K}^\ell)^{-1}\boldsymbol{f}^\ell\|^2 \lesssim \ell^{2\nu-1}\,. \quad (4.39)$$

Let us now bound the term of interest. Once more, we decompose it as $r_1 + r_2$ where r_1 and r_2 are defined in (4.35). We now apply Proposition 4.16 and (4.31) and derive

$$\begin{aligned}\mathbb{P}\left(|r_1| > t\right) &= \mathbb{P}\left(|\langle \delta(\boldsymbol{K}^\ell)^{-1}\boldsymbol{B}^\ell \mathbf{1}_{\boldsymbol{A}_\ell}\mathbf{1}_{\boldsymbol{B}_\ell}\boldsymbol{f}^\ell, \boldsymbol{\varphi}_\ell\rangle| > t\right)\\ &\leqslant \mathbb{P}\left(|\langle \delta(\boldsymbol{K}^\ell)^{-1}\boldsymbol{f}^\ell, {}^t\boldsymbol{B}^\ell\boldsymbol{\varphi}_\ell\rangle| > t\right).\end{aligned}$$

The latter is a Gaussian random variable with variance $\delta^2\|(\boldsymbol{K}^\ell)^{-1}\boldsymbol{f}^\ell\|^2 \lesssim \delta^2\ell^{2\nu-1}$ where we used (4.39). Turning to the term r_2, we apply Proposition 4.16 to derive

$$\begin{aligned}\mathbb{P}\left(|r_2| > t\right) &= \mathbb{P}\left(\left|\langle \delta\big(\boldsymbol{B}^\ell\big)^2(\boldsymbol{K}^\ell_\delta)^{-1}\mathbf{1}_{\boldsymbol{A}_\ell}\mathbf{1}_{\boldsymbol{B}_\ell}\boldsymbol{f}^\ell, {}^t(\boldsymbol{K}^\ell)^{-1}\boldsymbol{\varphi}_\ell\rangle\right| > t\right)\\ &\lesssim \mathbb{P}\left(\delta\|\boldsymbol{B}^\ell\|^2_{\mathrm{op}}\|(\boldsymbol{K}^\ell_\delta)^{-1}\boldsymbol{f}^\ell\|\|^t(\boldsymbol{K}^\ell)^{-1}\boldsymbol{\varphi}_\ell\|\mathbf{1}_{\boldsymbol{A}_\ell}\mathbf{1}_{\boldsymbol{B}_\ell} > t\right).\end{aligned}$$

We now apply (4.29) and (4.39) to get

$$\|(\boldsymbol{K}^\ell_\delta)^{-1}\boldsymbol{f}^\ell\|\|^t(\boldsymbol{K}^\ell)^{-1}\boldsymbol{\varphi}_\ell\| \lesssim \ell^{2\nu-1}.$$

Hence,

$$\begin{aligned}\mathbb{P}\left(|r_2| > t\right) &\lesssim \mathbb{P}\left(\delta^2\ell^{2\nu-1}\|\boldsymbol{B}^\ell\|^2_{\mathrm{op}}\mathbf{1}_{\boldsymbol{A}_\ell}\mathbf{1}_{\boldsymbol{B}_\ell} > t\right)\\ &\lesssim \mathbb{P}\left(\frac{1}{\ell\log\ell}\|\boldsymbol{B}^\ell\|^2_{\mathrm{op}}\mathbf{1}_{\boldsymbol{A}_\ell}\mathbf{1}_{\boldsymbol{B}_\ell} > t(\delta^2\ell^{2\nu}\log\ell)^{-1}\right)\end{aligned}$$

Let us take a look back to Lemma 4.6.2. On $\boldsymbol{A}_\ell \cap \boldsymbol{B}_\ell$ we have proved that

$$\|(\boldsymbol{K}^\ell_\delta)^{-1}\|_{op} \geqslant (1-\rho)Q_1\ell^\nu,$$

so that $\boldsymbol{A}_\ell \cap \boldsymbol{B}_\ell \subset \left\{\delta\ell^{\nu+1/2}\log\ell \lesssim 1\right\}$. We deduce

$$\begin{aligned}\mathbb{P}(|r_2| > t) &\lesssim \mathbb{P}\left(\frac{1}{\ell\log\ell}\|\boldsymbol{B}^\ell\|^2_{\mathrm{op}} > t(\delta\ell^{\nu-1/2})^{-1}\right)\\ &\lesssim \exp\left(\frac{-t}{\delta\ell^{\nu-1/2}}\right)\mathbf{1}_{\left\{t>\beta_0^2\delta\ell^{\nu-1/2}\right\}} + \mathbf{1}_{\left\{t\leqslant\beta_0^2\delta\ell^{\nu-1/2}\right\}}.\end{aligned}$$

The end of the proof is identical to Lemma 4.6.3. □

Proof of Theorem 4.4.5. The proof is very similar to Theorem 4.3.3, whence we will just emphasize the notable changes compared to it. First, we apply Parseval's formula to derive

$$\mathbb{E}\,\|\tilde{\boldsymbol{f}}^{\mathbf{II}} - \boldsymbol{f}\|_2^2 = \sum_{\ell\leqslant L^{\mathbf{II}}}\mathbb{E}\langle\tilde{\boldsymbol{f}}^{\mathbf{II}} - \boldsymbol{f}, \boldsymbol{\varphi}_\ell\rangle^2 + \sum_{\ell > L^{\mathbf{II}}}\check{\boldsymbol{f}}_\ell^2.$$

The second term is easily handled, since

$$\begin{aligned}\sum_{\ell>L^{\mathbf{II}}} \check{\boldsymbol{f}}_\ell^2 &\leqslant (L^{\mathbf{II}})^{-2s} \\ &\leqslant \left(\varepsilon\sqrt{|\log\varepsilon|} \vee \delta|\log\delta|\right)^{2s} \\ &\leqslant \left(\varepsilon\sqrt{|\log\varepsilon|}\right)^{\frac{2s}{s+\nu}} \vee \left(\delta|\log\delta|\right)^{\frac{2s}{s+\nu}}.\end{aligned}$$

To bound the first sum, we write the following decomposition

$$\begin{aligned}\sum_{\ell\leqslant L^{\mathbf{II}}} \mathbb{E}\,\|\widetilde{\boldsymbol{f}}^{\mathbf{II}} - \boldsymbol{f}\|^2 &= \sum_{\ell\leqslant L^{\mathbf{II}}} \mathbb{E}\left(\boldsymbol{\zeta}_\ell - \check{\boldsymbol{f}}_\ell\right)^2 \mathbf{1}_{\left\{|\boldsymbol{\zeta}_\ell|>S^{\mathbf{II}}_{\ell,\varepsilon}\right\}} + \mathbb{E}\sum_{\ell\leqslant L} \check{\boldsymbol{f}}_\ell^2 \mathbf{1}_{\left\{|\boldsymbol{\zeta}_\ell|\leqslant S^{\mathbf{II}}_{\ell,\varepsilon}\right\}}, \\ &\lesssim I + II + III + IV,\end{aligned}$$

where

$$\begin{aligned}I &= \sum_{\ell\leqslant L^{\mathbf{II}}} \mathbb{E}\left(\boldsymbol{\zeta}_\ell - \check{\boldsymbol{f}}_\ell\right)^2 \mathbf{1}_{\boldsymbol{A}_\ell}\mathbf{1}_{\boldsymbol{B}_\ell}\mathbf{1}_{\left\{|\boldsymbol{\zeta}_\ell|>S^{\mathbf{II}}_{\ell,\varepsilon}\right\}}, \\ II &= \sum_{\ell\leqslant L^{\mathbf{II}}} \mathbb{E}\,\check{\boldsymbol{f}}_\ell^2 \mathbf{1}_{\left\{|\boldsymbol{\zeta}_\ell|\leqslant S^{\mathbf{II}}_{\ell,\varepsilon}\right\}}\mathbf{1}_{\boldsymbol{A}_\ell}\mathbf{1}_{\boldsymbol{B}_\ell}, \\ III &= \sum_{\ell\leqslant L^{\mathbf{II}}} \mathbb{E}\left(\boldsymbol{\zeta}_\ell - \check{\boldsymbol{f}}_\ell\right)^2 \mathbf{1}_{\boldsymbol{A}_\ell}\mathbf{1}_{\boldsymbol{B}_\ell^c}\mathbf{1}_{\left\{|\boldsymbol{\zeta}_\ell|>S^{\mathbf{II}}_{\ell,\varepsilon}\right\}} + \sum_{\ell\leqslant L^{\mathbf{II}}} \mathbb{E}\,\check{\boldsymbol{f}}_\ell^2 \mathbf{1}_{\left\{|\boldsymbol{\zeta}_\ell|\leqslant S^{\mathbf{II}}_{\ell,\varepsilon}\right\}}\mathbf{1}_{\boldsymbol{B}_\ell^c}, \\ IV &= \sum_{\ell\leqslant L^{\mathbf{II}}} \mathbb{E}\,\check{\boldsymbol{f}}_\ell^2 \mathbf{1}_{\boldsymbol{A}_\ell^c}\mathbf{1}_{\left\{|\boldsymbol{\zeta}_\ell|\leqslant S^{\mathbf{II}}_{\ell,\varepsilon}\right\}}.\end{aligned}$$

Thanks to Lemma 4.6.2 and the definition of $S^{\mathbf{II}}_{\ell,\varepsilon}$, we have

$$\frac{Q_1}{1-\rho}\overline{S^{\mathbf{II}}_{\ell,\varepsilon}} \leqslant S^{\mathbf{II}}_{\ell,\varepsilon} \leqslant \frac{Q_2\rho}{1-\rho}\overline{S^{\mathbf{II}}_{\ell,\varepsilon}}$$

on $\boldsymbol{A}_\ell \cap \boldsymbol{B}_\ell$. Thus, the Terms I and II can be treated identically to the preceding proof and yield the desired rates of convergence. The terms III and IV are treated exactly as in the preceding proof. □

4.6.3 Proof of theorem 4.4.6

Proof. The lower bound will not decrease for increasing noise levels δ and ε, whence it suffices to provide the case $\delta = 0$ and the case $\varepsilon = 0$ separately. In the sequel, c_i will denote a positive constant to be adjusted later and L will play the role of a maximal level. Also, we will note $\dot{\boldsymbol{g}}_\nu$ the function associated with the Laurent series $(1-z)_L^\nu$ (i.e. $(1-z)_L^\nu = \sum_{\ell\geqslant 0}\left(\int_{\mathbb{R}_+}\dot{\boldsymbol{g}}_\nu\boldsymbol{\varphi}_\ell\right)z^\ell$), and $\boldsymbol{K}_\nu$ the operator with kernel $\boldsymbol{g}_\nu$. The function $\dot{\boldsymbol{g}}_{-1/2}$ will play an essential role in the sequel. Unfortunately it is not square integrable. We thus begin with a preliminary lemma, which states that a minor modification corrects this defect.

Lemma 4.6.5. *Let $\boldsymbol{h}$ be the function associated to the Laurent series $\sum_{\ell\geqslant 0}\frac{(-1)^\ell}{\log(\ell\vee 2)}\binom{-1/2}{\ell}z^\ell$. Then $\boldsymbol{h}$ is square integrable. Furthermore, for all $\nu\geqslant 0$, for all $\ell\leqslant L$,*

$$\frac{(\ell\vee 1)^{\nu-1/2}}{\log(\ell\vee 2)}\lesssim|\langle\boldsymbol{K}_{-\nu}\boldsymbol{h},\boldsymbol{\varphi}_\ell\rangle|\lesssim(\ell\vee 1)^{\nu-1/2}\,.$$

Proof of Lemma 4.6.5. $\boldsymbol{h}$ is trivially squared integrable thanks to (4.26) and Parseval's formula. Now, we have

$$\langle\boldsymbol{K}_{-\nu}\boldsymbol{h},\boldsymbol{\varphi}_\ell\rangle=(-1)^\ell\sum_{k=0}^{\ell}\binom{-\nu}{k}\binom{-1/2}{\ell-k}\log^{-1}\big((\ell-k)\vee 2\big)\,.$$

Moreover, since the product $\binom{-\nu}{k}\binom{-1/2}{\ell-k}$ has a constant sign for all $k\leqslant\ell$, we derive

$$\log^{-1}(\ell\vee 2)\Big|\sum_{k=0}^{\ell}\binom{-\nu}{k}\binom{-1/2}{\ell-k}\Big|\leqslant|\langle\boldsymbol{K}_{-\nu}\boldsymbol{h},\boldsymbol{\varphi}_\ell\rangle|\leqslant\Big|\sum_{k=0}^{\ell}\binom{-\nu}{k}\binom{-1/2}{\ell-k}\Big|\,,$$

but $(-1)^\ell\sum_{k=0}^{\ell}\binom{-\nu}{k}\binom{-1/2}{\ell-k}$ is precisely the ℓ^{th} coefficient of the power series $(1-z)^{-\nu}(1-z)^{-1/2}=(1-z)^{-\nu-1/2}$ which satisfies, thanks to (4.26),

$$\Big|(-1)^\ell\sum_{k=0}^{\ell}\binom{-\nu}{k}\binom{-1/2}{\ell-k}\Big|\sim\frac{\ell^{\nu-1/2}}{\Gamma(\nu+1/2)}\,.$$

This entails the result. □

• *Case $\delta=0$.* For more clarity, we will suppose that $\boldsymbol{\xi}$ is a white noise (the proof readily adapts otherwise). Let hence $\boldsymbol{K}^0=c_1\boldsymbol{K}_\nu$. Then $\boldsymbol{K}^0\in\mathcal{G}_\nu(Q)$ for an appropriate constant c_1, thanks to Proposition 4.4.2. Following the arguments of Willer [85], it suffices to find $\boldsymbol{f}_0$, $\boldsymbol{f}_1$ such that

i) $\boldsymbol{f}_0,\boldsymbol{f}_1\in\mathcal{W}^s(M)$.

ii) $\|\boldsymbol{f}_0-\boldsymbol{f}_1\|^2\gtrsim\varepsilon^{\frac{2s}{s+\nu}}|\log\varepsilon|^{-2}$.

iii) $K(\mathbb{P}_1,\mathbb{P}_2)\lesssim 1$ where $\mathbb{P}_i$ is the law of $\boldsymbol{y}$ under the hypothesis $\boldsymbol{f}_i$, and K is the Kullback-Leibler divergence.

Let $L=c_2\varepsilon^{\frac{-1}{s+\nu}}$. Set $\boldsymbol{f}_0=0$ and define $\boldsymbol{f}_1=c_3\boldsymbol{K}_{-\nu}\boldsymbol{h}$.
Point i): $\boldsymbol{f}_0$ trivially belongs to the considered set. Moreover, Lemma 4.6.5 entails

$$\|\boldsymbol{f}_1\|^2_{\mathcal{W}^s}\lesssim\varepsilon^2\sum_{\ell=0}^{L}\ell^{2s}\ell^{2\nu-1}\lesssim 1\,.$$

Point ii): again, thanks to Lemma 4.6.5, we have

$$\|\boldsymbol{f}_0 - \boldsymbol{f}_1\|^2 \gtrsim \varepsilon^2 \sum_{\ell \leqslant L} \frac{\ell^{2\nu-1}}{\log^2(\ell \vee 2)} \gtrsim \varepsilon^2 L^{2\nu} (\log L)^{-2} \gtrsim \varepsilon^{\frac{2s}{s+\nu}} |\log \varepsilon|^{-2} .$$

Point iii): the expression of the Kullback-Leibler divergence in this case is

$$K(\mathbb{P}_1, \mathbb{P}_2) = \frac{1}{2} \|\varepsilon^{-1} \boldsymbol{K}^0 (\boldsymbol{f}_0 - \boldsymbol{f}_1)\|^2 = \frac{c_3}{2} \|\boldsymbol{h}\|^2 \lesssim 1 ,$$

thanks to Lemma 4.6.5. The choice of appropriate constants c_i clearly yields the result and the proof is complete. □

• *Case* $\varepsilon = 0$. Let $L = c_1 \delta^{\frac{-1}{s+\nu}}$. Following the lines of Hoffmann and Reiß [40], we set $\boldsymbol{f}_0 = c_2 \varphi_0$, $\boldsymbol{K}^0 = c_3 \boldsymbol{K}_\nu$ and we only consider couples $(\boldsymbol{K}, \boldsymbol{f})$ such that $\boldsymbol{K}\boldsymbol{f} = \boldsymbol{q}_0$ for a fixed $\boldsymbol{q}_0 = \boldsymbol{K}^0 \boldsymbol{f}_0$. It is clear that, for well chosen c_2 and c_3, we have $\boldsymbol{f}_0 \in \mathcal{W}^s(M)$ and $\boldsymbol{K}^0 \in \mathcal{G}_\nu(Q)$. We thus define $\boldsymbol{H}$ the operator associated to the kernel $\boldsymbol{h}$ and introduce $\boldsymbol{K}^\delta = \boldsymbol{K}_\nu + c_4 \delta \boldsymbol{H}$ a perturbation of $\boldsymbol{K}_\nu$. We shall refer to $\dot{\boldsymbol{g}}^\delta$ for the corresponding kernel. Remark that we have

$$\boldsymbol{f}_1 - \boldsymbol{f}_0 = c_4 \delta (\boldsymbol{K}^\delta)^{-1} \boldsymbol{H} \boldsymbol{f}_0 = c_4 \delta (\boldsymbol{K}^\delta)^{-1} \boldsymbol{h} . \tag{4.40}$$

Furthermore, for c_4 small enough, we have thanks to Lemma 4.6.5 and Proposition 4.4.2,

$$\|\delta \boldsymbol{K}_\nu^{-1} \boldsymbol{H}\|_{\mathrm{op}} \lesssim \delta L^{\nu+1/2} \lesssim \delta^{\frac{2s-1}{2(s+\nu)}} < \frac{1}{2} ,$$

since $s > 1/2$. Hence, the same Neumann series argument as in Lemma 4.6.2 entail that $\boldsymbol{K}^\delta$ belongs to $\mathcal{G}_\nu(Q)$. We now need to check that i), ii) and iii) are satisfied, replacing ε with δ.
Point i) : (4.40) and the preceding remark entail

$$\|\boldsymbol{f}_1 - \boldsymbol{f}_0\|_{\mathcal{W}^s}^2 = c_4^2 \delta^2 \sum_{\ell \leqslant L} \ell^{2s} \langle (\boldsymbol{K}^\delta)^{-1} \boldsymbol{h}, \boldsymbol{\varphi}_\ell \rangle \lesssim \delta^2 \sum_{\ell \leqslant L} \ell^{2s+2\nu-1} \lesssim 1 .$$

Point ii) : we precise (4.40) and write

$$\boldsymbol{f}_1 - \boldsymbol{f}_0 = c_4 \delta \boldsymbol{K}^{-1} \boldsymbol{h} + c_4^2 \delta^2 (\boldsymbol{K}^\delta)^{-1} \boldsymbol{K}^{-1} \boldsymbol{H} \boldsymbol{h} .$$

Moreover, Lemma 4.6.5 and the preceding remark entail

$$\|\delta \boldsymbol{K}^{-1} \boldsymbol{H} \boldsymbol{f}_0\|^2 = \|\delta \boldsymbol{K}^{-1} \boldsymbol{h}\|^2 \gtrsim \delta^2 \sum_{\ell \leqslant L} \frac{\ell^{2\nu-1}}{\log(\ell \vee 2)} \gtrsim \delta^2 L^{2\nu} (\log L)^{-2} \gtrsim \delta^{\frac{2s}{s+\nu}} |\log \delta|^{-2} ,$$

$$\|\delta^2 (\boldsymbol{K}^\delta)^{-1} \boldsymbol{K}^{-1} \boldsymbol{H}^2 \boldsymbol{f}_0\|^2 \lesssim \delta^4 \|(\boldsymbol{K}^\delta)^{-1}\|_{\mathrm{HS}} \|\boldsymbol{K}^{-1} \boldsymbol{H}\|_{\mathrm{HS}} \|\boldsymbol{h}\| \lesssim \delta^4 L^{4\nu+1} \lesssim \delta^{\frac{2s-1}{\nu+s}} \delta^2 L^{2\nu} .$$

Since $s > 1/2$, the second term is negligible with respect to the first. This proves the point ii).
Point iii) : Since we work with couples $(\boldsymbol{K}, \boldsymbol{f})$ such that $\boldsymbol{Kf}$ is fixed, we have

$$K(\mathbb{P}_0, \mathbb{P}_1) = \frac{1}{2}\delta^{-2}\|\dot{\boldsymbol{g}}^{\delta} - \dot{\boldsymbol{g}}_{\nu}\|^2 = \frac{c_4}{2}\|\boldsymbol{h}\|^2 \lesssim 1\,,$$

thanks to Lemma 4.6.5 and the proof is complete. □

It remains to piece together the two cases $\delta = 0$ and $\varepsilon = 0$ to get the desired result. □

Acknowledgements

The author would like to thank his advisor Dominique Picard for her help and her support.

Chapter 5

Needlets on $\mathbb{S}^2$ and the NEED-VD procedure

This chapter's role is to serve as a link between Chapter 3 and Chapter 6. Since Chapter 6 only concerns blind spherical deconvolution on $\mathbb{S}^2$, we shall restrict ourselves to this case.
The first part of this chapter is devoted to bringing technical material about needlets which will serve in the next chapter as well. These are tackled through the notion of frame (section 5.1), followed by the theoretical construction of needlets (section 5.2), and the definition of Besov spaces on the sphere.
In a second part (section 5.3) we proceed to the description of the so-called 'NEED-VD procedure' ([49]) in the context of spherical deconvolution.

Contents

5.1 A brief introduction to frame theory 119
5.2 Needlets 121
5.3 The NEED-VD procedure 126

5.1 A brief introduction to frame theory

In view of the construction of needlets, we will first explain why the concept of Hilbert basis is too restrictive in the context of noise reduction, and then present the natural generalization of the notion to more flexible sets of functions. Most of the material presented here originates from [14] and [60].
A crippling defect of orthonormal bases in the context of noise reduction is their lack of flexibility. Namely,

- It is often impossible to construct a basis with specific properties.
- The basis property is not stable with regard to the addition of new elements.

For example, the addition of a linear combination of elements in a basis destroys its basis property. However, the new set is entirely capable of representing any vector (though not in a unique way). In other words, the uniqueness of representation of a vector in a basis is not fundamental in the context of noise reduction. What matters is the existence of an explicit process allowing to compute **one** representation.
One could ask why it is more convenient to add vectors in system of functions enjoying the uniqueness property. This is because, in the context of estimation, the addition of new elements has a noise reduction effect. Let us begin by the definition of operators which play a central role in frame theory.

Definition 5.1.1. *Let $(u_\ell)_{\ell\geqslant 0}$ be a set of vectors of $\mathbb{H}$. The synthesis operator T is defined by*

$$\begin{aligned} T : \ell^2(\mathbb{N}) &\to \mathbb{H} \\ (c_k) &\mapsto \sum_{\ell\geqslant 0} c_\ell u_\ell \,. \end{aligned}$$

Its adjoint T^*, called the analysis operator, satisfies

$$\begin{aligned} T^* : \mathbb{H} &\to \ell^2(\mathbb{N}) \\ f &\mapsto (\langle f, u_\ell\rangle) \,. \end{aligned}$$

Finally, the frame operator is the operator $S = TT^*$, which satisfies

$$\begin{aligned} S : \mathbb{H} &\to \mathbb{H} \\ f &\mapsto \sum_{\ell\geqslant 0} \langle f, u_\ell\rangle u_\ell \,. \end{aligned}$$

Those three operators clearly characterize the performance of a given set of functions to represent any element in $\mathbb{H}$. For example, $(u_\ell)_{\ell\geqslant 0}$ is a Hilbert basis if and only if $T^* = T^{-1}$ and $S = \boldsymbol{I}_{\mathbb{H}}$.

Definition 5.1.2. *The set $(u_\ell)_{\ell\geqslant 0}$ is a frame if there exists $0 < B \leqslant A$ such that, for all $f \in \mathbb{H}$,*

$$B\|f\|^2 \leqslant \sum_{\ell\geqslant 0} \langle f, u_\ell\rangle^2 \leqslant A\|f\|^2 \,.$$

Proposition 5.1.3. *Let $(u_\ell)_{\ell\geqslant 0}$ be a frame in $\mathbb{H}$. Then the frame operator S is invertible, self-adjoint and positive.*
Moreover, any vector $f \in \mathbb{H}$ is decomposed in the following way :

$$f = \sum_{\ell\geqslant 0} \langle f, S^{-1}u_\ell\rangle u_\ell = \sum_{\ell\geqslant 0} \langle f, u_\ell\rangle S^{-1}u_\ell \,. \tag{5.1}$$

The system $(S^{-1}u_\ell)_{\ell\geqslant 0}$ is itself a frame, called the canonical dual frame of $(u_\ell)_{\ell\geqslant 0}$.

If moreover $A = B$, the frame is said 'tight'. In this case, the dual frame satisfies

$$S^{-1}u_\ell = \frac{1}{A}u_\ell\,.$$

We have therefore exposed an explicit process of reconstruction for the target function f.

Remark 5.1.4. *Given (u_ℓ), there exists potentially several frames satisfying (5.1), yet the frame $(S^{-1}u_\ell)$ ensures a representation with minimal norm in $\ell^2(\mathbb{N})$. Namely, if $f \in \mathbb{H}$ has the representation $f = \sum_{\ell\geqslant 0} c_\ell u_\ell$, then*

$$\sum_{\ell\geqslant 0}|c_\ell|^2 = \sum_{\ell\geqslant 0}\langle f, S^{-1}u_\ell\rangle + \sum_{\ell\geqslant 0}\left|c_\ell - \langle f, S^{-1}u_\ell\rangle\right|^2.$$

Remark 5.1.5. *There exists other ways of characterizing frames. For example, the two conditions below are equivalent to $(u_\ell)_{\ell\geqslant 0}$ being a frame*

- *The synthesis operator T is a well defined mapping of $\ell^2(\mathbb{N})$ onto $\mathbb{H}$.*
- *There exists an orthonormal basis (e_ℓ) and a bounded operator $U : \mathbb{H} \to \mathbb{H}$ such that $u_\ell = U(e_\ell)$. This extends the fact that each Hilbert basis is the image of another Hilbert basis by a unitary operator U.*

We now turn to the setting up of a concrete frame in the context of spherical deconvolution, which relies on spherical harmonics, yet extends its performances.

5.2 Needlets

The goal of this section is to briefly introduce the theory of needlets, in order to expose the NEED-VD procedure in the direct case.
As mentioned earlier, the greater flexibility of the frame theory allows to model representative sets of functions with appropriate properties. A significant example is given by the Wavelet-Vaguelette decomposition: based on a bi-orthogonal system of functions (wavelets and vaguelettes) specifically designed for the operator $\boldsymbol{K}$ at stake so that a 'SVD-like' decomposition holds, and representing efficiently a wide variety of functions since it relies on a wavelet decomposition of the target signal. Let us mention the fact that vaguelettes actually enjoy an additional property which makes them 'more' than a frame, namely a Riesz-basis (we do not pursue the definition of these objects here, the reader is invited to consult [14]). The objective of needlets is somehow similar, yet the tools at stake in their construction, as well as the features they present, are globally different.
The requirements to be met by needlets are the following:

- Reproduce efficiently the local features of a signal.
- Provide a structure compatible with the inverse problem of spherical deconvolution.

The second requirement invites to take as a starting point the spherical harmonics basis, since, as it was mentioned before, they realize a blockwise-SVD of the operator. The first point will be reached through the coordination of two central tools : first, the Paley-Littlewood decomposition and second, the quadrature method on the sphere.

5.2.1 The needlet framework

Most of what follows now is directly inspired from [69], [68], and [48]. Although there exists a generic unifying framework (see Coulhon et al. [21]), we limit ourselves to a more pragmatic point of view here. The needlet theory relies on the orthogonal decomposition of the space $\mathbb{L}^2(\mathbb{S}^2)$:

$$\mathbb{L}^2(\mathbb{S}^2) = \bigoplus_{\ell \geqslant 0}^{\perp} \mathbb{H}_\ell \,,$$

where each $\mathbb{H}_\ell$ represents the space of spherical harmonics with degree ℓ. Along with this decomposition naturally come the orthogonal projectors $\boldsymbol{P}_\ell$ on $\mathbb{H}_\ell$ and their associated kernels

$$L_\ell(x,y) = L_\ell\big(\langle x,y\rangle_{\mathbb{R}^{2\ell+1}}\big) = \sum_{|m|\leqslant \ell} Y_{\ell,m}(x)\overline{Y_{\ell,m}(y)}\,.$$

Since L_ℓ is the kernel of an orthogonal projector, it satisfies the property

$$\int_{\mathbb{S}^2} L_\ell(x,y)L_k(y,z)dy = \delta_{\ell,k}L_\ell(x,z), \text{ for all } x,z \in \mathbb{S}^2\,. \tag{5.2}$$

Paley-Littlewood decomposition

The role of the Paley-Littlewood theory is to generalize some convenient properties of Hilbert bases to $\mathbb{L}^p$ spaces. This task is performed via a binary filtering of the projectors $\boldsymbol{P}_\ell$.

Let $a \in \mathcal{C}^\infty(\mathbb{R})$ be a symmetric function, compactly supported in $[-1,1]$ and decreasing on $\mathbb{R}^+$, such that for all $x \in \mathbb{R}$, $0 \leqslant a(x) \leqslant 1$ and for all $|x| \leqslant 1/2$, $|a(x)| = 1$. Define for all $x \in \mathbb{R}$, $b^2(x) = a(x/2) - a(x)$. b^2 is a positive function, supported in $[-2;-1/2]\bigcup[1/2;2]$, satisfying by construction $\sum_{j\geqslant 0} b^2(x2^{-j}) = 1$ for all $|x| \geqslant 1$. Define also the following projection kernels on $\mathbb{R}^2$

$$\Lambda_j(x,y) = \sum_{\ell\geqslant 0} b^2(\frac{\ell}{2^j})L_\ell(x,y)\,, \tag{5.3}$$

$$M_j(x,y) = \sum_{\ell\geqslant 0} b(\frac{\ell}{2^j})L_\ell(x,y)\,, \tag{5.4}$$

as well as the associated operators on $\mathbb{L}^2(\mathbb{S}^2)$,

$$B_j : \gamma \mapsto \int_{\mathbb{S}^2} \Lambda_j(x,y)\gamma(y)dy, \;\; A_J : \gamma \mapsto \sum_{j=-1}^{J} B_j\gamma\,,$$

with the convention $B_{-1}\gamma = \boldsymbol{P}_0\gamma$. Note that the sum in (5.3) and (5.4) is finite since $b(\frac{\ell}{2^j}) = 0$ if $\ell \notin L_j$, where we have noted L_j the set of integers ranging from 2^{j-1} to $2^{j+1}-1$. It is straightforward to show that, for all $f \in \mathbb{L}^2(\mathbb{S}^2)$,

$$\|A_J\gamma - \gamma\|_2 \to 0 \text{ as } J \to \infty\,. \tag{5.5}$$

One of the main results in Narcowich et al. [69] states that A_J also mimics the best polynomial approximation of γ with respect to $\|.\|_p$ for all $p \geqslant 1$, as expressed in the following theorem:

Theorem 5.2.1. *For all $p \in [1,\infty[$, if $f \in \mathbb{L}^p(\mathbb{S}^2)$, then*

$$\|A_J\gamma - \gamma\|_p \to 0 \text{ as } J \to \infty\,,$$

with uniform convergence if $f \in \mathcal{C}^0(\mathbb{S}^2)$.

Space discretization

The second ingredient in the construction of needlets is the polynomial structure of the spaces $\mathbb{H}_\ell$. Indeed, for all $\gamma \in \mathbb{H}_\ell$, $\gamma' \in \mathbb{H}_k$, we have $\gamma\gamma' \in \mathbb{H}_{\ell+k}$. Let us note $\mathcal{P}_\ell = \bigoplus_{k\leqslant\ell} \mathbb{H}_k$. A corresponding quadrature formula on every space $\mathcal{P}_\ell$ is available as well:

Proposition 5.2.2 (Quadrature formula)**.** *For all $\ell \geqslant 0$, there exists a finite set Z_ℓ of cubature points, associated to the cubature weights $(\lambda_\eta)_{\eta\in Z_\ell}$ such that, for all $\gamma \in \mathcal{P}_\ell$,*

$$\int_{\mathbb{S}^2} \gamma = \sum_{\eta\in Z_\ell} \lambda_\eta \gamma(\eta)\,.$$

Since $b(\frac{\ell}{2^j}) \neq 0$ only if $2^{j-1} \leqslant \ell < 2^{j+1}$ the function $z \mapsto M_j(x,z)$ belongs to $\mathcal{P}_{2^{j+1}-1}$, and $z \mapsto M_j(x,z)M_j(z,y)$ is an element of $\mathcal{P}_{2^{j+2}-2}$. For more convenience, we will note $\mathcal{Z}_j = Z_{2^{j+2}-2}$ the corresponding set of cubature points. It can be shown that the cubature points $\eta \in \mathcal{Z}_j$ and weights $(\lambda_\eta)_{\eta\in\mathcal{Z}_j}$ can be chosen so that the two following conditions are fulfilled:

$$c^{-1}2^{2j} \leqslant \text{card}(\mathcal{Z}_j) \leqslant c2^{2j} \text{ and } C^{-1}2^{-2j} \leqslant \lambda_\eta \leqslant C2^{-2j}\,, \tag{5.6}$$

for some constants $c, C > 0$. For all $j \geqslant 0$, B_j now satisfies:

$$\begin{aligned} B_j(\gamma) &= \int_{\mathbb{S}^2} \Big(\sum_{\eta\in\mathcal{Z}_j} \lambda_\eta M_j(x,\eta)M_j(\eta,y)dz\Big)\gamma(y)dy\,, \\ &= \sum_{\eta\in\mathcal{Z}_j} \sqrt{\lambda_\eta} M_j(x,\eta) \int_{\mathbb{S}^2} \sqrt{\lambda_\eta} M_j(\eta,y)\gamma(y)dy\,. \end{aligned} \tag{5.7}$$

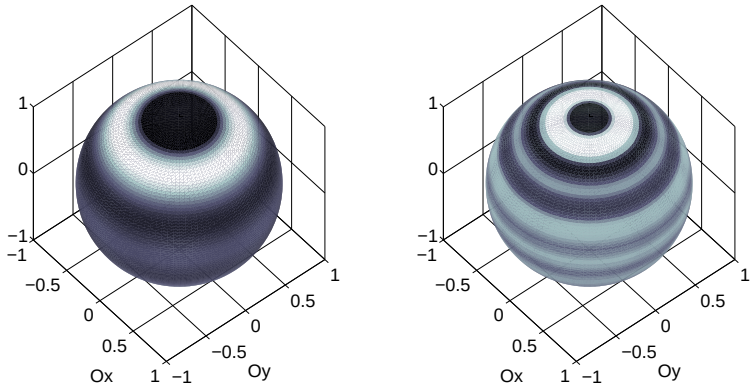

Figure 5.1: A Spherical representation of two needlets (level $j = 2, 3$ from left to right) centered around the point (0,0,1). The darkened zones correspond to the regions where the needlet is high. The concentration of the needlet around its center is more pronounced as the level j increases.

The functions $\boldsymbol{\psi}_{j,\eta} = \sqrt{\lambda_\eta} M_j(., \eta)$ appearing in (5.7) are called needlets. By extension we also define $\boldsymbol{\psi}_{-1,\eta} = \boldsymbol{\psi}_0 = (4\pi)^{-1}\mathbf{1}_{\{\mathbb{S}^2\}}$ the normalized constant on $\mathbb{S}^2$. An immediate consequence of (5.5) is the following: for all $\gamma \in \mathbb{L}^2(\mathbb{S}^2)$,

$$\|\gamma\|_2^2 = \langle \gamma, \boldsymbol{\psi}_0 \rangle^2 + \sum_{j \geqslant 0} \sum_{\eta \in \mathcal{Z}_j} \langle \gamma, \boldsymbol{\psi}_{j,\eta} \rangle^2 . \tag{5.8}$$

The next section shows that this property somehow generalizes to other $\mathbb{L}^p$ norms, $1 \leqslant p \leqslant \infty$.

5.2.2 Properties of needlets

By construction, needlets are compactly supported in the frequential domain. A crucial result proved by Narcowich et al. [69] shows that they are furthermore nearly exponentially localized in space:

Theorem 5.2.3. *Let $j \geqslant 0$, $\eta \in \mathcal{Z}_j$. For all $M > 0$, there exists $C_M > 0$ such that*

$$\forall x \in \mathbb{S}^2, \ |\boldsymbol{\psi}_{j,\eta}(x)| \leqslant \frac{C_M 2^j}{(1 + 2^j d(x, \eta))^M} . \tag{5.9}$$

where $d(x, y) = \arccos(\langle x, y \rangle)$ is the geodesic distance on the sphere. To illustrate this point, we represented two needlets of level $j = 2, 3$ on Figure 5.1. This property is central, since it allows to relate the $\mathbb{L}^p$ norm of the projection $\sum_{\eta \in \mathcal{Z}_j} \langle \gamma, \boldsymbol{\psi}_{j,\eta} \rangle \boldsymbol{\psi}_{j,\eta}$ to the discrete ℓ^p norm of the finite sequence $(|\langle \gamma, \boldsymbol{\psi}_{j,\eta} \rangle| \|\boldsymbol{\psi}_{j,\eta}\|_p)_{\eta \in \mathcal{Z}_j}$. Indeed, the two following propositions hold ([48]):

Proposition 5.2.4. *For all $1 \leqslant p \leqslant \infty$ (with the convention $1/\infty = 0$), there exist $c_p, C_p > 0$ such that*

$$c_p 2^{2j(\frac{1}{2} - \frac{1}{p})} \leqslant \|\boldsymbol{\psi}_{j,\eta}\|_p \leqslant C_p 2^{2j(\frac{1}{2} - \frac{1}{p})} . \tag{5.10}$$

Proposition 5.2.5. *For all $p \geqslant 1$, there exists a constant C_p such that for all $\gamma \in \mathbb{L}^p(\mathbb{S}^2)$,*

$$\|B_j(\gamma)\|_p \leqslant C_p\Big(\sum_{\eta\in\mathcal{Z}_j} |\langle\gamma, \boldsymbol{\psi}_{j,\eta}\rangle|^p \|\boldsymbol{\psi}_{j,\eta}\|_p^p\Big)^{1/p}. \tag{5.11}$$

Moreover, if $p = \infty$, there exists $C_\infty > 0$ such that

$$\|B_j(\gamma)\|_\infty \leqslant C_\infty 2^j \sup_{\eta\in\mathcal{Z}_j} |\langle\gamma, \boldsymbol{\psi}_{j,\eta}\rangle|. \tag{5.12}$$

5.2.3 Besov spaces

Besov spaces on the sphere naturally generalize the usual approximation properties of regular functions while being simply characterized with the help of needlets. A complete description, and the proofs of the results claimed in this part can be found in Narcowich et al. [68] or Kerkyacharian and Picard [48]. Let $\gamma : \mathbb{S}^2 \mapsto \mathbb{R}$ be a measurable function and let $E_{k,\pi}(\gamma)$ $(1 \leqslant \pi \leqslant \infty)$ be the distance of γ to $\mathcal{P}_k$ with respect to $\|.\|_\pi$, that is

$$E_{k,\pi}(\gamma) = \inf_{P\in\mathcal{P}_k} \|\gamma - P\|_\pi .$$

Theorem 5.2.6. *Let $0 < s < \infty$, $1 \leqslant p \leqslant \infty$ and $0 < r \leqslant \infty$. Let $\gamma \in L^\pi(\mathbb{S}^2)$. The following statements are equivalent and define the Besov space $B^s_{\pi,r}$ on $\mathbb{S}^2$:*

$$\Big(\sum_{k\geqslant 0} k^{rs} E_{k,\pi}(\gamma)^r \frac{1}{k}\Big)^{1/r} < \infty \tag{5.13}$$

$$\Big(\sum_{j\geqslant 0} 2^{jrs} E_{2^j,\pi}(\gamma)^r\Big)^{1/r} < \infty \tag{5.14}$$

$$\exists\, \xi_j \in \ell^r(\mathbb{N}),\ \|B_j\gamma\|_\pi = \xi_j 2^{-js} \tag{5.15}$$

$$\exists\, \xi_j \in \ell^r(\mathbb{N}),\ \Big(\sum_{\eta\in\mathcal{Z}_j} |\langle\gamma, \boldsymbol{\psi}_{j,\eta}\rangle|^\pi \|\boldsymbol{\psi}_{j,\eta}\|_\pi^\pi\Big)^{1/\pi} = \xi_j 2^{-js} \tag{5.16}$$

$B^s_{\pi,q}$ is a Banach space, endowed with the norm

$$\|\gamma\|_{B^s_{\pi,r}} = \Big\| \Big(2^{j(s+2(\frac{1}{2}-\frac{1}{\pi}))}\Big(\sum_{\eta\in\mathcal{Z}_j} |\langle\gamma, \boldsymbol{\psi}_{j,\eta}\rangle|^\pi\Big)^{1/\pi}\Big)_{j\geqslant 0}\Big\|_{\ell^r(\mathbb{N})}.$$

Besov embeddings

In order to conduct a procedure of estimation on Besov spaces, it is important to understand how they relate to each other as the values of the parameters s, π, r change. This is resumed in the following proposition:

Proposition 5.2.7 (Besov embeddings)**.** *Let $s > 0$, $1 \leqslant p, \pi, r \leqslant \infty$. We have*

- $B^s_{\pi,r} \subset B^s_{p,r}$ *if* $\pi \geqslant p$.
- $B^s_{\pi,r} \subset B^{s-2(\frac{1}{\pi}-\frac{1}{p})}_{p,r}$ *if* $\pi < p$ *and* $s - 2(1/\pi - 1/p) > 0$.
- $B^s_{\pi,r} \subset \mathcal{C}^0(\mathbb{S}^2)$ *if* $s > 2/\pi$, *where* $\mathcal{C}^0(\mathbb{S}^2)$ *is the set of continuous functions on* $\mathbb{S}^2$.

Note that Besov spaces on the sphere indeed generalize the Sobolev spaces $\mathcal{W}^s$ since it can be shown that $\mathcal{W}^s = B^s_{2,2}$.

5.3 The NEED-VD procedure

Let us now expose how needlets are used in the context of inverse problems such as spherical deconvolution. Since the projectors $\boldsymbol{P}_\ell$ constitute their building blocks, it is natural that the procedure of deconvolution exposed in Healy et al. [39] extends to a needlet counterpart. We shall see that the performances extend as well in term of squared loss, and improve in terms of $\mathbb{L}^p$ losses ($p \geqslant 1$).
The basic observation at the start of the NEED-VD procedure is that each needlet coefficient of $\boldsymbol{f}$ can be decomposed, thanks to Parseval's formula, in the following way

$$\begin{aligned}\langle \boldsymbol{f}, \boldsymbol{\psi}_{j,\eta}\rangle &= \sum_{\ell\geqslant 0}\langle \boldsymbol{P}_\ell \boldsymbol{f}, \boldsymbol{P}_\ell \boldsymbol{\psi}_{j,\eta}\rangle \\ &= \sum_{\ell\in L_j}\langle \boldsymbol{f}_\ell, \boldsymbol{\psi}_{j,\eta,\ell}\rangle\,.\end{aligned}$$

Applied to $\boldsymbol{f} = \boldsymbol{K}^{-1}\boldsymbol{K}\boldsymbol{f}$, this property entails

$$\begin{aligned}\langle \boldsymbol{f}, \boldsymbol{\psi}_{j,\eta}\rangle &= \sum_{\ell\in L_j}\langle \left(\boldsymbol{K}^{-1}\boldsymbol{K}\boldsymbol{f}\right)_\ell, \boldsymbol{\psi}_{j,\eta,\ell}\rangle \\ &= \sum_{\ell\in L_j}\langle \boldsymbol{K}_\ell^{-1}(\boldsymbol{K}\boldsymbol{f})_\ell, \boldsymbol{\psi}_{j,\eta,\ell}\rangle\,,\end{aligned}$$

thanks to the blockwise-SVD property 1.11. A natural unbiased estimator of $\langle \boldsymbol{f}, \boldsymbol{\psi}_{j,\eta}\rangle$ in the context of the white noise model with no error in the operator (3) is hence given by

$$\widehat{\boldsymbol{\beta}}_{j,\eta} \triangleq \sum_{\ell\in L_j}\langle \boldsymbol{K}_\ell^{-1}\boldsymbol{Y}_{\varepsilon,\ell}, \boldsymbol{\psi}_{j,\eta,\ell}\rangle\,.$$

Moreover, the elements $\boldsymbol{\psi}_{j,\eta,\ell}$ are easily computable, since, by construction,

$$\boldsymbol{\psi}_{j,\eta,\ell} = \langle \boldsymbol{\psi}_{j,\eta}, Y_{\ell,m}\rangle = b(\frac{\ell}{2^j})\overline{Y_{\ell,m}(\eta)} \text{ for all } \ell \in L_j, |m| \leqslant \ell\,.$$

It remains to control the variance of these estimators via an adapted thresholding procedure. If $\boldsymbol{K}$ satisfies the following assumption

Assumption 5.3.1. *There exists $\nu \geqslant 0$, $Q_1, Q_2 \geqslant 0$ such that, for all $\ell \in \mathbb{N}$,*

$$Q_1(\ell^\nu \vee 1) \leqslant \|\boldsymbol{K}_\ell^{-1}\|_{op} \leqslant Q_2(\ell^\nu \vee 1)\,. \tag{5.17}$$

We note $\mathcal{K}_\nu(Q_1, Q_2)$ the set of operators satisfying this assumption.

, then we readily obtain the tail control

$$\mathbb{P}\left(|\widehat{\boldsymbol{\beta}}_{j,\eta} - \langle \boldsymbol{f}, \boldsymbol{\psi}_{j,\eta}\rangle| > t\right) \leqslant C \exp\left(-\frac{t^2}{\varepsilon^2 2^{2j\nu}}\right),$$

which invites to set $\tau 2^{j\nu}\varepsilon\sqrt{|\log\varepsilon|}$ ($\tau > 0$) as a thresholding level for each computed coefficient. Remark that this property only requires the upper bound on $\|\boldsymbol{K}_\ell^{-1}\|_{\mathrm{op}}$ in Assumption 5.3.1. Note also that Assumption 5.3.1 is implied by Assumption 3.2.2. We can actually do more : since Assumption 5.3.1 also provides the lower bound $\|\boldsymbol{K}_\ell^{-1}\|_{\mathrm{op}} \geqslant Q_1\ell^\nu$, then provided that $Q_1 > 0$, we can safely replace $2^{j\nu}$ by $\|\boldsymbol{K}_{2^j}^{-1}\|_{\mathrm{op}}$ in the expression of the threshold level. The gain is notable, since we no longer require the knowledge of ν in the definition of the procedure.

Let us now enter into the core of the algorithm which was designed in the density framework by Kerkyacharian et al. [51]. We chose as a maximal level J such that

$$2^J \sim (\varepsilon\sqrt{|\log\varepsilon|})^{-1}\,. \tag{5.18}$$

As mentioned before, we set the signal thresholding level to

$$S_{j,\varepsilon} = \tau\|\boldsymbol{K}_{2^j}^{-1}\|_{\mathrm{op}}\varepsilon\sqrt{|\log\varepsilon|}\,, \tag{5.19}$$

for a positive constant τ and naturally define the estimator $\widetilde{f}$ as

$$\widetilde{f} = \sum_{j\leqslant J}\sum_{\eta\in\mathcal{Z}_j} \widehat{\boldsymbol{\beta}}_{j,\eta}\mathbf{1}_{\left\{|\widehat{\boldsymbol{\beta}}_{j,\eta}|\geqslant S_{j,\varepsilon}\right\}}\boldsymbol{\psi}_{j,\eta}\,. \tag{5.20}$$

Let us now expose the performances of this new estimator.

Theorem 5.3.2. *Let $\pi \geqslant 1$, $s > \frac{2}{\pi}$, $r \geqslant 1$ and $M > 0$. Let $\nu \geqslant 0$, let $Q_2 \geqslant Q_1 > 0$. Then for sufficiently large κ and τ, for all $p \in [1, +\infty[$,*

$$\sup_{f\in B^s_{\pi,r}(M), \boldsymbol{K}\in\mathcal{K}_\nu(Q_1,Q_2)} \mathbb{E}\,\|\tilde{f} - f\|_p^p \lesssim (|\log\varepsilon|)^{p-1}(\varepsilon\sqrt{|\log\varepsilon|})^{p\mu}\,,$$

where $\lesssim$ means inequality up to a multiplicative constant depending only on $p, s, \pi, r, M, \nu, Q_1, Q_2, \lambda, \kappa,$ and τ_{op}, and where the exponents μ are defined by

$$\mu = \begin{cases} \frac{s}{s+\nu+1} & \text{if } s > (\nu+1)(\frac{p}{\pi}-1) \\ & \text{or } s = (\nu+1)(\frac{p}{\pi}-1) \text{ and } r \leqslant \pi\,, \\ \frac{s-2/\pi+2/p}{s-2/\pi+\nu+1} & \text{if } \frac{2}{\pi} < s < (\nu+1)(\frac{p}{\pi}-1)\,. \end{cases}$$

Theorem 5.3.3. *Under the same hypotheses as Theorem 6.2.2,*

$$\sup_{f\in B^s_{\pi,r}(M),\boldsymbol{K}\in\mathcal{K}_\nu(Q_1,Q_2)} \mathbb{E}\,\|\tilde{f}-f\|_\infty \lesssim \sqrt{|\log\varepsilon|}(\varepsilon\sqrt{|\log\varepsilon|})^{\mu'}\,,$$

where the exponents μ' are defined by

$$\mu' = \frac{s-2/\pi}{s-2/\pi+\nu+1}\,.$$

Hence, the NEED-VD generalizes the $\mathbb{L}^2$ procedure (we remind to this end that the spaces $B^s_{2,2}$ and W^s coincide), in that they allow to consider broader classes of functions, and broader types of losses. The procedure is adaptive with respect to $\boldsymbol{f}$ and $\boldsymbol{K}$ in that it doesn't require any prior knowledge of M, s, π, r, Q_1, Q_2, nor ν. If $Q_1 = 0$, one can still reach those rates of convergence provided the preliminary knowledge of ν (see to this end [51]). Furthermore, those convergence rates can easily be proved to be minimax, up to a logarithmic term in ε, in the present setting (see the sketch of proof in [85]).

Chapter 6

Application of second generation wavelets to blind spherical deconvolution

This chapter is a slightly different version of an article submitted to a scientific review. It can be read separately from the rest of the manuscript, except for the section 5.2 of Chapter 5 which defines needlets.

Abstract:We address the problem of spherical deconvolution in a non parametric statistical framework, where both the signal and the operator kernel are subject to error measurements. After a preliminary treatment of the kernel, we apply a thresholding procedure to the signal in a second generation wavelet basis. Under standard assumptions on the kernel, we study the theoretical performance of the resulting algorithm in terms of $\mathbb{L}^p$ losses ($p \geqslant 1$) on Besov spaces on the sphere. We hereby extend the application of second generation spherical wavelets to the blind deconvolution framework [51]. The procedure is furthermore adaptive with regard both to the target function sparsity and smoothness, and the kernel blurring effect. We end with the study of a concrete example, putting into evidence the improvement of our procedure on the recent blockwise-SVD algorithm [23].

Contents

6.1 Introduction **130**

6.2 Estimation procedure **135**

6.3 Proofs **142**

6.1 Introduction

6.1.1 Statistical framework

Consider the following problem : we aim at recovering a signal $\boldsymbol{f}$ defined on the 2-dimensional sphere $\mathbb{S}^2$. $\boldsymbol{f}$ is not observed directly, but through the action of a blurring process modeled by a linear operator $\boldsymbol{K}$, and further contaminated by an additive Gaussian white noise. This is resumed in the classic white noise model

$$\boldsymbol{Y}_\varepsilon = \boldsymbol{K}\boldsymbol{f} + \varepsilon \dot{\boldsymbol{W}}\,, \tag{6.1}$$

where $\dot{\boldsymbol{W}}$ is a white noise on $\mathbb{L}^2(\mathbb{S}^2)$ and $\boldsymbol{K} : \mathbb{L}^2(\mathbb{S}^2) \to \mathbb{L}^2(\mathbb{S}^2)$ is a measurable operator. We shall further restrict the shape of $\boldsymbol{K}$ by assuming that it is a convolution operator on $\mathbb{L}^2(\mathbb{S}^2)$, a classic framework ([39], [52] and [51]) enjoying convenient mathematical properties (see section 6.1.2). Namely, we suppose that there exists $\boldsymbol{h} \in \mathbb{L}^2(\mathrm{SO}(3))$ such that

$$\boldsymbol{K}\boldsymbol{f}(\omega) = \int_{\mathrm{SO}(3)} \boldsymbol{f}(g^{-1}\omega)\boldsymbol{h}(g)dg\,, \tag{6.2}$$

where dg is the Haar measure on $\mathrm{SO}(3)$. So to speak, $\boldsymbol{f}$ is averaged on a neighborhood of ω and weighted according to $\boldsymbol{h}(g)$ for each rotation g^{-1} applied to ω. Alternatively, in a density estimation framework, one observes a random n-sample $(\boldsymbol{\theta}_1 X_1, ..., \boldsymbol{\theta}_n X_n)$ of $Z = \boldsymbol{\theta} X$ with density $\boldsymbol{K}\boldsymbol{f}$, where $\boldsymbol{\theta}$ is a random element in $\mathrm{SO}(3)$ (the group of rotations on $\mathbb{R}^3$) with density $\boldsymbol{h}$, and X has density $\boldsymbol{f} \in \mathbb{L}^2(\mathbb{S}^2)$. Formally we have $\varepsilon \sim n^{-1/2}$, and one can show that (6.2) holds as well ([39]). In practice, the blurring operator $\boldsymbol{K}$ is seldom directly observable and rather subject to measurement errors. For example $\boldsymbol{K}$ can be unknown but approximated via preliminary inference, or it can be the result of an unknown perturbation applied to a known operator. Following Efromovich and Koltchinskii [30] and Hoffmann and Reiß [40], we model the error in the operator as an additive Gaussian operator white noise. The observed result is a noisy version $\boldsymbol{K}_\delta$, satisfying

$$\boldsymbol{K}_\delta = \boldsymbol{K} + \delta \dot{\boldsymbol{B}}\,, \tag{6.3}$$

where $\dot{\boldsymbol{B}}$ is a Gaussian operator white noise on $\mathcal{L}\big(\mathbb{L}^2(\mathbb{S}^2)\big)$ the set of linear endomorphisms of $\mathbb{L}^2(\mathbb{S}^2)$, independent from $\dot{\boldsymbol{W}}$. The meaning of models (6.1) and (6.3) is as follows: for $u, v, w, \in \mathbb{L}^2(\mathbb{S}^2)$, observable quantities take the form

$$\big\langle \boldsymbol{K}\boldsymbol{f}, u\big\rangle + \varepsilon\alpha(u), \;\; \big\langle \boldsymbol{K}v, w\big\rangle + \delta\beta(v, w)\,,$$

where $\alpha(u)$ and $\beta(v, w)$ are both Gaussian centered variables with respective variances $\|u\|_2^2$ and $\|v\|_2^2\|w\|_2^2$. Moreover, if $u', v', w' \in \mathbb{L}^2(\mathbb{S}^2)$ are other candidate functions, we have

$$\begin{aligned}\mathbb{E}[\alpha(u)\alpha(u')] &= \langle u, u'\rangle_{\mathbb{L}^2(\mathbb{S}^2)} \\ \mathbb{E}[\beta(v, w)\beta(v', w')] &= \langle v, v'\rangle_{\mathbb{L}^2(\mathbb{S}^2)}\langle w, w'\rangle_{\mathbb{L}^2(\mathbb{S}^2)}\,.\end{aligned}$$

Many scientific fields call upon simple and efficient tools for the resolution of (6.1). Spherical deconvolution is for example well illustrated by the study of ultra high energy cosmic rays (UHECR), which are high energy radiations hitting the earth from apparently random directions. They could originate from long-lived relic particles from the Big Bang. Alternatively, they could be generated by the acceleration of standard particles, such as protons, in extremely violent astrophysical phenomena. They could also originate from Active Galactic Nuclei (AGN), or from neutron stars surrounded by extremely high magnetic fields. Discriminating among these different hypotheses involves the precise reconstruction of the probability density generating their observations. One could ask for example whether the latter is uniformly distributed among the sphere, or if it is constituted of superimposed localized spikes. In practice however, observations $(X_1, ..., X_n)$ of such radiations are often subject to various physical perturbations. We model these by a random rotation $\boldsymbol{\theta}$, which is to say we actually observe $(\boldsymbol{\theta}_1 X_1, ...\boldsymbol{\theta}_n X_n)$, n realizations of the random variable $Z = \boldsymbol{\theta} X$. The difficulty of the problem is characterized by the spreading of $\boldsymbol{h}$, the density of $\boldsymbol{\theta}$, around the neutral element of SO(3) : the less localized, the more difficult the estimation of $\boldsymbol{f}$. Moreover, the law of $\boldsymbol{\theta}$ is not known in general, even if some assumptions can restrict its shape. In this case, preliminary inference is necessary, and leads to an estimator $\boldsymbol{K}_\delta$ of $\boldsymbol{K}$ according to (6.3).

Case of a known operator

We shall consider here the case where $\delta = 0$, and expose the path which finally led to the introduction and use of needlets. Spherical harmonics constitute the most natural set of functions to expand $\boldsymbol{f} \in \mathbb{L}^2(\mathbb{S}^2)$. Their frequency localization furthermore makes them ideally suited to spherical deconvolution, as they realize a blockwise SVD of $\boldsymbol{K}$ (as shown in (6.1.1)), a property which guarantees the stability of its inversion. It prompted Healy et al. [39] to solve the spherical deconvolution problem with their use, hereby reaching optimal $\mathbb{L}^2$ rates of convergence on Sobolev spaces (Kim and Koo [52]). Unfortunately their performances can prove quite poor when the loss is measured by other $\mathbb{L}^p$ norms , $1 \leqslant p \leqslant \infty$, since they lack localization in the spatial domain (see [37]). The recent development of spherical wavelets ([77], [67]) reversed this compromise, the latter being well localized in the spatial domain but very poorly in the frequential one. This makes them useful when a direct estimation of $\boldsymbol{f}$ is involved (see for example Freeden and Schreiner [31] or Freeden and Michel [32] for applications to geophysics and atmospheric sciences), but irrelevant in the setting of spherical deconvolution. The solution to this problem was finally brought by Narcowich et al. [69], who introduced a new set of functions, called needlets, which preserve the frequential localization of spherical harmonics and remedy their lack of spatial localization. Thereby, needlets inherit the stability of spherical harmonics in spherical deconvolution. They were subsequently exploited by Kerkyacharian et al. [51], who designed a procedure involving needlets attaining near-minimax rates of convergence for $\mathbb{L}^p$ losses ($1 \leqslant p \leqslant \infty$) on Besov spaces (which definition is given in section 5.2.3). Needlets also found various

applications in the case of a direct estimation of $\boldsymbol{f}$, whether in astrophysics ([62],[37]) or brain shape modeling ([80]).

Case of an unknown operator and Galerkin projection

The main methods in the context of blind deconvolution involve SVD and Galerkin schemes (see [11],[12],[40] for example). Galerkin projections were for example successfully applied to blind deconvolution on Hilbert spaces ([30]) or on Besov spaces on $[0,1]^d$ ([40], [12]). They are based upon a discretization of (6.1) and (6.3) through the choice of appropriate test functions. Suppose we want to recover a function f from the observation of $g = Kf$. Let $(V_n)_{n\geqslant 0}$ and $(W_n)_{n\geqslant 0}$ be two increasing sequences of finite n-dimensional subspaces in $\mathbb{L}^2(\mathbb{S}^2)$, which admit the respective orthogonal bases $\boldsymbol{\varphi} = (\varphi_k)_{k\leqslant n}$ and $\boldsymbol{\psi} = (\psi_k)_{k\leqslant n}$. The Galerkin approximation $f_G \in V_n$ of f is the solution of the equation

$$\langle Kf_G, v\rangle \ = \langle g, v\rangle, \ \forall v \in W_n \tag{6.4}$$

This equation actually amounts to solving a finite dimensional linear system. Indeed, for $\gamma \in V_n$, note γ^n the vector whose components are $(\langle \gamma, \varphi_k\rangle)_{k\leqslant n}$ and K^n the matrix with entries $(\langle K\varphi_k, \psi_k\rangle)_{k,k'\leqslant n}$. Then $f_G \in V_n$ and we have

$$g^n = K^n f_G^n$$

The presence of noise in the signal and the operator raises additional issues. First, the algorithm must include and articulate two essential steps, namely the inversion of $\boldsymbol{K}$ and the regularization of the datas which we will perform through a projection/thresholding scheme. Note that both the signal and the operator $\boldsymbol{K}$ can (and will) be subject to regularization (see [40],[23]). The second practical problem concerns the choice of the test functions $\boldsymbol{\varphi}, \boldsymbol{\psi}$. This choice should answer the dilemma to find a set which is compatible both with the sparsity of $\boldsymbol{f}$ and with the structure of $\boldsymbol{K}$ (see [40], [23]). Spherical harmonics respond optimally to this problem in the case of spherical deconvolution on Sobolev spaces for a $\mathbb{L}^2$ error, since they realize a blockwise SVD of $\boldsymbol{K}$, as shown in (6.1.1). More importantly here, they allow a fine treatment of $\boldsymbol{K}_\delta$ thanks to the sparse structure of the original operator $\boldsymbol{K}$ in that basis. This structure was exploited by Delattre et al. [23] in the context of blind spherical deconvolution: by an adequate regularization of $\boldsymbol{K}_\delta$ and $\boldsymbol{Y}_\varepsilon$, the authors exhibited optimal rates of convergence under common assumptions on $\boldsymbol{f}$ and $\boldsymbol{K}$. This procedure is exposed in details in section 6.2.1.

6.1.2 Harmonic analysis on $\mathrm{SO}(3)$ and $\mathbb{S}^2$

The present part provides useful mathematical tools in the context of spherical deconvolution. It is a quick overview of harmonic analysis on the spaces $\mathbb{S}^2$ and $\mathrm{SO}(3)$ which

is mostly inspired by Healy et al. [39], and will end up with the blockwise SVD property. Let us define the Euler matrices

$$u(\varphi) = \begin{pmatrix} \cos\varphi & -\sin\varphi & 0 \\ \sin\varphi & \cos\varphi & 0 \\ 0 & 0 & 1 \end{pmatrix}, \; a(\theta) = \begin{pmatrix} \cos\theta & 0 & \sin\theta \\ 0 & 1 & 0 \\ -\sin\theta & 0 & \cos\theta \end{pmatrix}$$

where $\varphi \in [0, 2\pi)$, $\theta \in [0, \pi)$.
Every rotation g in SO(3) is the product of 3 elementary rotations :

$$\varepsilon = u(\varphi)a(\theta)u(\psi) \tag{6.5}$$

where $\varphi, \psi \in [0, 2\pi)$, $\theta \in [0, \pi)$ are the Euler angles of g. Let $\ell \in \mathbb{N}$ and $-\ell \leqslant m, n \leqslant \ell$. We also define the rotational harmonics

$$R_{\ell,m,n}(\varphi, \theta, \psi) = e^{-i(m\varphi + n\psi)} P_{\ell,m,n}(\cos(\theta)) \,, \tag{6.6}$$

where $P_{\ell,m,n}$ are the second type Legendre functions (see [84]).
The functions $R_{\ell,m,n}$, $\ell \in \mathbb{N}$, $|m|, |n| \leqslant \ell$ are the eigenfunctions of the Laplace-Beltrami operator on SO(3), associated with the eigenvalues $2\ell + 1$. Therefore, the system $(\sqrt{2\ell+1} R_{\ell,m,n})_{\ell \geqslant 0, |m|, |n| \leqslant \ell}$ forms a complete orthonormal basis of $\mathbb{L}^2(\mathrm{SO}(3))$. Let $h \in \mathbb{L}^2(\mathrm{SO}(3))$. For all $\ell \geqslant 0$, the projection of h on the space of rotational harmonics with degree ℓ is

$$\sum_{m,n=-\ell}^{\ell} \hat{h}_{\ell,m,n} R_{\ell,m,n}$$

where $\hat{h}_{\ell,m,n}$ is the (ℓ, m, n) Fourier coefficient of h, defined by

$$\hat{h}_{\ell,m,n} = \int_{\mathrm{SO}(3)} h(g) \overline{R_{\ell,m,n}(g)} dg \,, \tag{6.7}$$

and dg is the Haar measure on SO(3). An analogous study is available on $\mathbb{S}^2$. Any point $\omega \in \mathbb{S}^2$ is determined by its spherical coordinates (θ, φ):

$$\omega = (\sin(\theta)\cos(\varphi), \sin(\theta)\sin(\varphi), \cos(\theta)) \,, \tag{6.8}$$

where $\theta \in [0, \pi)$ and $\varphi \in [0, 2\pi)$. Let ℓ a positive integer and m, n two integers ranking from $-\ell$ to ℓ. Define the spherical harmonics on $\mathbb{S}^2$ by :

$$Y_{\ell,m}(\theta, \varphi) = (-1)^m \sqrt{\frac{2\ell+1}{4\pi} \frac{(\ell-m)!}{(\ell+m)!}} P_{\ell,m}(\cos(\theta)) e^{im\varphi} \,, \tag{6.9}$$

where $P_{\ell,m}$ are the Legendre functions (see [84]). The set $(Y_{\ell,m})_{\ell \geqslant 0, |m| \leqslant \ell}$ constitutes an orthonormal basis of $\mathbb{L}^2(\mathbb{S}^2)$. Note $\mathbb{H}_\ell$ the space of spherical harmonics with degree ℓ and $\boldsymbol{P}_\ell$ the orthogonal projector onto $\mathbb{H}_\ell$. Then for every function $\gamma \in \mathbb{L}^2(\mathbb{S}^2)$,

$$\boldsymbol{P}_\ell \gamma = \sum_{m=-\ell}^{\ell} \hat{\gamma}_{\ell,m} Y_{\ell,m} \,,$$

where $\hat{\gamma}_{\ell,m}$ is the (ℓ, m) Fourier coefficient of f, defined by

$$\hat{\gamma}_{\ell,m} = \int_{\mathbb{S}^2} \gamma(\omega)\overline{Y_{\ell,m}(\omega)}d\omega\,.$$

The term 'blockwise SVD' finds its roots in the following proposition, which links the Fourier coefficients of $h * \gamma$ to those of h and γ. A proof is present in [39].

Proposition 6.1.1 (Blockwise SVD property)**.** *Let $h \in \mathbb{L}^2(\mathrm{SO}(3))$ and $\gamma \in \mathbb{L}^2(\mathbb{S}^2)$ The Fourier coefficients of $h * \gamma$ are*

$$\widehat{(h * \gamma)}_{\ell,m} = \sum_{n=-\ell}^{\ell} \hat{h}_{\ell,m,n}\hat{\gamma}_{\ell,n} = \sum_{n=-\ell}^{\ell} \langle h * Y_{\ell,n}, Y_{\ell,m}\rangle\langle \gamma, Y_{\ell,n}\rangle\,.$$

Consequences on the Galerkin projection

Proposition 6.1.1 has interesting implications in terms of the Galerkin projection of (6.1) and (6.3) on spherical harmonics. Indeed, note $\boldsymbol{K}_\ell \in M_{2\ell+1}(\mathbb{C})$ the matrix

$$\boldsymbol{K}_\ell = \big(\langle \boldsymbol{K}Y_{\ell,n}, Y_{\ell,m}\rangle\big)_{|m|,|n|\leqslant\ell}$$

and, for $\gamma \in \mathbb{L}^2(\mathbb{S}^2)$, note $\gamma_\ell \in \mathbb{C}^{2\ell+1}$ the vector $\big(\langle \gamma, Y_{\ell,m}\rangle\big)_{|m|\leqslant\ell}$. Proposition 6.1.1 then translates into

$$\big(\boldsymbol{K}\boldsymbol{f}\big)_\ell = \boldsymbol{K}_\ell \boldsymbol{f}_\ell\,.$$

Let us hence turn back to the Galerkin scheme (6.4). Take $W_n = V_n$ to be the subspace of $\mathbb{L}^2(\mathbb{S}^2)$ spanned by all spherical harmonics with degree less than n. Proposition 6.1.1 implies the following:

1. $\boldsymbol{f}_G = \sum_{\ell\leqslant n} \boldsymbol{P}_\ell \boldsymbol{f}$
2. The Galerkin matrix $\boldsymbol{K}^n$ is a sparse block matrix, with blocks $\boldsymbol{K}_\ell$, $\ell \leqslant n$, along its diagonal. This justifies the denomination of blockwise SVD.

In the sequel, if $\gamma \in \mathbb{L}^2(\mathbb{S}^2)$, we will refer indifferently to $\boldsymbol{P}_\ell\gamma$ or γ_ℓ. Similarly, if $\boldsymbol{K}$ is a convolution operator on $\mathbb{L}^2(\mathbb{S}^2)$, we will refer indifferently to $\boldsymbol{P}_\ell\boldsymbol{K}\boldsymbol{P}_\ell$ or $\boldsymbol{K}_\ell$. Due to Parseval's formula, we also have

$$\begin{aligned}\|\boldsymbol{P}_\ell\,\gamma\|_{\mathbb{L}^2(\mathbb{S}^2)} &= \|\gamma_\ell\|_{\ell^2(\mathbb{C}^{2\ell+1})}\\ \|\boldsymbol{P}_\ell\boldsymbol{K}\boldsymbol{P}_\ell\|_{\mathbb{L}^2(\mathbb{S}^2)\to\mathbb{L}^2(\mathbb{S}^2)} &= \|\boldsymbol{K}_\ell\|_{op}\,,\end{aligned}$$

where we have noted $\|.\|_{op}$ the spectral norm of a matrix. Turning back to the original problem and reminding Proposition 6.1.1, we can reformulate the equivalent problem, obtained by projecting (6.1) and (6.3) onto every space $\mathbb{H}_\ell$:

$$\forall \ell \geqslant 0, \qquad \boldsymbol{Y}_{\varepsilon,\ell} = \boldsymbol{K}_\ell \boldsymbol{f}_\ell + \varepsilon\dot{\boldsymbol{W}}_\ell\,, \tag{6.10}$$

$$\forall \ell \geqslant 0, \qquad \boldsymbol{K}_{\delta,\ell} = \boldsymbol{K}_\ell + \delta\dot{\boldsymbol{B}}_\ell\,, \tag{6.11}$$

where $\dot{\boldsymbol{W}}_\ell$ is a centered Gaussian vector with covariance $\boldsymbol{I}_{2\ell+1}$, and $\dot{\boldsymbol{B}}_\ell$ is a $(2\ell+1)\times(2\ell+1)$ matrix whose entries are i.i.d. $\mathcal{N}(0,1)$ variables.

An alternative point of view

The blockwise SVD property allows to avoid considering the inner products $\langle \boldsymbol{K}_\delta Y_{\ell,m}, Y_{\ell' n}\rangle$ when $\ell \neq \ell'$ and provides hereby $\boldsymbol{K}_\delta$ with a sparse structure consisting in $(2\ell+1)\times(2\ell+1)$ matrices on its diagonal. This is a consequence of the convolutive structure of $\boldsymbol{K}$. Actually, an alternative way to get to (6.11) is to consider that the kernel $\boldsymbol{h}$ of $\boldsymbol{K}$ is directly polluted by an additive Gaussian white noise on $\mathbb{L}^2(\mathrm{SO}(3))$. Namely we would observe $\boldsymbol{h}_\delta = \boldsymbol{h} + \delta\dot{\boldsymbol{b}}$ where $\dot{\boldsymbol{b}}$ is a Gaussian white noise on $\mathbb{L}^2(\mathrm{SO}(3))$. Observations conducted on $\boldsymbol{K}_\delta$ would hence become

$$\langle \boldsymbol{K}_\delta Y_{\ell,m}, Y_{\ell',n}\rangle = \langle \boldsymbol{h}_\delta * Y_{\ell,m}, Y_{\ell',n}\rangle$$

and would be null if $\ell \neq \ell'$ as a consequence of Proposition 6.1.1.

6.2 Estimation procedure

We turn to the presentation of our procedure of Blind Deconvolution using Needlets, which we will denote by **BND**, and derive rates of convergence when the loss is measured in $\mathbb{L}^p$ norm, $1 \leqslant p \leqslant \infty$, on Besov spaces. It is natural to suggest needlets as the test functions to be used in the Galerkin projection (6.4), since they efficiently represent any function $\boldsymbol{f} \in B^s_{\pi,r}$. Unfortunately, the ensuing Galerkin matrix

$$\big(\langle \boldsymbol{K}\boldsymbol{\psi}_{j,\eta}, \boldsymbol{\psi}_{h,\alpha}\rangle\big)_{j\geqslant 0,\eta\in\mathcal{Z}_j,h\geqslant 0,\alpha\in\mathcal{Z}_h}$$

has many non-zero entries, due to the fact that the inner product $\langle \boldsymbol{K}\boldsymbol{\psi}_{j,\eta}, \boldsymbol{\psi}_{h,\alpha}\rangle$ is not necessarily null when $|j-h| \leqslant 1$. This is a direct consequence of (6.1.1) and the definition of needlets. The functions $Y_{\ell,m}$ constitute a more interesting choice since the inner product $\langle \boldsymbol{Y}_\varepsilon, \boldsymbol{\psi}_{j,\eta}\rangle$ can be expressed in terms of the matrices $\boldsymbol{K}_\ell$. Indeed, Parseval's formula entails

$$\langle \boldsymbol{Y}_\varepsilon, \boldsymbol{\psi}_{j,\eta}\rangle = \sum_{\ell\in L_j} \langle \boldsymbol{K}_\ell \boldsymbol{f}_\ell + \varepsilon \dot{\boldsymbol{W}}_\ell, \boldsymbol{\psi}_{j,\eta,\ell}\rangle\,.$$

Before entering into the core of our procedure, we need to precise the blurring effect of $\boldsymbol{K}$. This will be realized through the introduction of a constant ν which controls the increase of the norms $\|\boldsymbol{K}_\ell^{-1}\|_{op}$.

Assumption 6.2.1 (Degree of ill-posedness)**.** *There exists $\nu \geqslant 0$, $Q_1, Q_2 \geqslant 0$ such that, for all $\ell \in \mathbb{N}$,*

$$Q_1\big(\ell^\nu \vee 1\big) \leqslant \|\boldsymbol{K}_\ell^{-1}\|_{op} \leqslant Q_2\big(\ell^\nu \vee 1\big) \tag{6.12}$$

We note $\mathcal{K}_\nu(Q_1,Q_2)$ the set of operators satisfying this assumption, and call ν the degree of ill-posedness (DIP) of $\boldsymbol{K}$.

Assumption 6.2.1 actually states that even if $\boldsymbol{K}$ is continuous from $\mathbb{L}^2(\mathbb{S}^2)$ to $\mathbb{L}^2(\mathbb{S}^2)$, its inverse is not bounded and hence not computable in a satisfying way. However the weaker continuity of $\boldsymbol{K}^{-1} : \mathcal{W}^{\nu/2} \to \mathcal{W}^{-\nu/2}$ holds, where we have noted $\mathcal{W}^s = B^s_{2,2}$ the Sobolev space with parameter $s > 0$ on $\mathbb{S}^2$.
Let us now give an intuition of the main procedure in this paper. The decomposition of the inner product $\langle \boldsymbol{Kf}, \boldsymbol{\psi}_{j,\eta} \rangle$ onto every space $\mathbb{H}_\ell$, $\ell \geqslant 0$ via Parseval's formula, coupled with Proposition 6.1.1 gives

$$\langle \boldsymbol{f}, \boldsymbol{\psi}_{j,\eta} \rangle = \sum_{\ell \in L_j} \langle \boldsymbol{K}_\ell^{-1} (\boldsymbol{Kf})_\ell, \boldsymbol{\psi}_{j,\eta,\ell} \rangle .$$

Hence, a first natural estimator of $\langle \boldsymbol{f}, \boldsymbol{\psi}_{j,\eta} \rangle$ is

$$\tilde{\boldsymbol{\beta}}_{j,\eta} = \sum_{\ell \in L_j} \langle \boldsymbol{K}_{\delta,\ell}^{-1} \boldsymbol{Y}_{\varepsilon,\ell}, \boldsymbol{\psi}_{j,\eta,\ell} \rangle . \tag{6.13}$$

Remark that the elements $\boldsymbol{\psi}_{j,\eta,\ell}$, $\ell \in L_j$ are easily computable thanks to the identity

$$\langle \boldsymbol{\psi}_{j,\eta}, Y_{\ell,m} \rangle = b(\frac{\ell}{2^j}) \overline{Y_{\ell,m}(\eta)} \text{ for all } \ell \in L_j, |m| \leqslant \ell .$$

However, the presence of noises contaminating both the signal $\boldsymbol{Kf}$ and the operator $\boldsymbol{K}$ requires an additional treatment. Schematically, a regularized version of $\boldsymbol{K}_\delta$ is plugged into (6.13), and the resulting estimator is subsequently thresholded in order to control the variance induced by the two types of noises.

6.2.1 Main procedure

Suppose that Assumption 6.2.1 holds, and define J the maximal resolution level such that

$$2^J = \lambda \lfloor \left(\varepsilon \sqrt{|\log \varepsilon|} \right)^{-1} \wedge \left(\delta \sqrt{|\log \delta|} \right)^{-2} \rfloor \tag{6.14}$$

for a positive parameter λ. Set the operator thresholding level $O_\ell(\delta)$ to

$$O_\ell(\delta) = \kappa \sqrt{2\ell + 1} \delta \sqrt{|\log \delta|} , \tag{6.15}$$

where $\kappa > 0$. For $j \in \mathbb{N}$, let

$$\ell_j = \min \{ \ell \in L_j, \ \| \boldsymbol{K}_{\delta,\ell}^{-1} \|_{op} \leqslant O_\ell(\delta)^{-1} \}$$

(with the convention $\min \varnothing = +\infty$), and, for positive constants τ_{sig}, τ_{op}, define the signal thresholding level

$$S_j(\delta, \varepsilon) = \begin{cases} \| \boldsymbol{K}_{\delta,\ell_j}^{-1} \|_{op} \Big(\tau_{sig} \varepsilon \sqrt{|\log \varepsilon|} \vee \tau_{op} 2^{-j/2} \delta \sqrt{|\log \delta|} \Big) \text{ if } \ell_j < \infty , \\ +\infty \text{ if } \ell_j = +\infty . \end{cases} \tag{6.16}$$

Define now the estimator $\widehat{\boldsymbol{\beta}}_{j,\eta}$ similarly to $\widetilde{\boldsymbol{\beta}_{j,\eta}}$ but where $\boldsymbol{K}_{\delta}^{-1}$ is replaced by its thresholded version

$$\widehat{\boldsymbol{\beta}}_{j,\eta} = \sum_{\ell=2^{j-1}}^{2^{j+1}} \langle \boldsymbol{K}_{\delta,\ell}^{-1} \mathbf{1}_{\left\{\|\boldsymbol{K}_{\delta,\ell}^{-1}\| \leqslant O_\ell(\delta)^{-1}\right\}} \boldsymbol{Y}_{\varepsilon,\ell}, \boldsymbol{\psi}_{j,\eta,\ell} \rangle \,.$$

The final estimator $\tilde{\boldsymbol{f}}$ of $\boldsymbol{f}$ is

$$\tilde{\boldsymbol{f}} = \sum_{j \leqslant J} \sum_{\eta \in \mathcal{Z}_j} \widehat{\boldsymbol{\beta}}_{j,\eta} \mathbf{1}_{\left\{|\widehat{\boldsymbol{\beta}}_{j,\eta}| > S_j(\delta,\varepsilon)\right\}} \boldsymbol{\psi}_{j,\eta} \,.$$

For the sake of brevity, we shall denote this procedure as **BND** (for Blind Deconvolution using Needlets). Before establishing the convergence rates of this algorithm in a minimax framework, let us give some precisions about the shape of the thresholding levels. Usual thresholds ([40],[51]) involve an upper bound on the variance of the coefficients $\widehat{\boldsymbol{\beta}}_{j,\eta}$, and thereby the knowledge of the constant ν. The term $\|\boldsymbol{K}_{\delta,\ell_j}^{-1}\|_{op}$ in (6.16) is meant to replace the more often used upper bound $2^{j\nu}$. Indeed, Lemmas 6.3.1 and 6.3.2 show that with high probability these two quantities coincide up to a multiplicative constant. This trick endows the procedure with adaptivity with regard to the parameters s, π, r and Q_1, Q_2, ν, and subsequently means that no a priori knowledge on $\boldsymbol{f}$ nor $\boldsymbol{K}$ is required in order to set it up.
Lemma 6.3.2 however heavily relies on the non negativity of Q_1. As a matter of fact, the rates of convergence derived below fall apart when the latter is null. In that case, a preliminary knowledge of ν is essential, as well as the subsequent following adaptations: the signal level $S_j(\delta,\varepsilon)$ is changed to

$$\widetilde{S}_j(\delta,\varepsilon) = 2^{j\nu}\Big(\tau_{sig}\varepsilon\sqrt{|\log\varepsilon|} \vee \tau_{op}2^{-j/2}\delta\sqrt{|\log\delta|}\Big)$$

and the new maximal level of resolution $\tilde{J}$ satisfies

$$2^{\tilde{J}} = \lambda\big\lfloor \big(\varepsilon\sqrt{|\log\varepsilon|}\big)^{\frac{-1}{\nu+1}} \wedge \big(\delta\sqrt{|\log\delta|}\big)^{\frac{-1}{\nu+1/2}} \big\rfloor \,.$$

The tuning down of the maximal level is not essential, yet it permits to avoid unnecessary calculations. As a matter of fact, computations of the needlet coefficients are quite heavy, due to the absence of a simplifying algorithm (such as the pyramidal algorithm for wavelets, see [61]). Thus, the computation of a single needlet coefficient $\langle \gamma, \boldsymbol{\psi}_{j,\eta,\ell} \rangle$, which number grows exponentially as the resolution level increases, requires the determination of $2.2^j - 1$ inner products $\langle \gamma_\ell, \boldsymbol{\psi}_{j,\eta,\ell} \rangle$.
Let us now turn to the convergence rates of the procedure in a minimax framework, when the loss is measured in $\mathbb{L}^p$ norm ($1 \leqslant p \leqslant \infty$) and $\boldsymbol{f}$ belongs to a Besov body.

Theorem 6.2.2. *Let $\pi \geqslant 1$, $s > 2/\pi$, $r \geqslant 1$ and $M > 0$. Let $\nu \geqslant 0$, let $Q_1 \geqslant Q_2 > 0$. Then for sufficiently large $\kappa, \tau_{sig}, \tau_{op}$, for all $p \in [1, +\infty[$,*

$$\sup_{\boldsymbol{f} \in B^s_{\pi,r}(M),\, \boldsymbol{K} \in \mathcal{K}_\nu(Q_1,Q_2)} \mathbb{E}\,\|\tilde{\boldsymbol{f}} - \boldsymbol{f}\|_p^p \lesssim \mathcal{R}_p(\delta,2,1) \vee \mathcal{R}_p(\varepsilon,2,2)$$

where $\lesssim$ means inequality up to a multiplicative constant depending only on $p, s, \pi, r, M, \nu, Q_1, Q_2, \lambda, \kappa,$ and τ_{op}. The convergence rates $\mathcal{R}_p(x,d)$ are defined, for all $x > 0$, $1 \leqslant p < \infty$ and $d \in \mathbb{N}$ by

$$\mathcal{R}_{x,p}(d,d') = (|\log x|)^{p-1}(x\sqrt{|\log x|})^{p\mu(d,d')}\,,$$

where we noted

$$\mu(d,d') = \begin{cases} \frac{s}{s+\nu+\frac{d'}{2}} & \text{if } s > (\nu + d'/2)(p/\pi - 1) \\ & \text{or } s = (\nu + d'/2)(p/\pi - 1) \text{ and } r \leqslant \pi\,, \\ \frac{s-d/\pi+d/p}{s-d/\pi+\nu+d'/2} & \text{if } \frac{d}{\pi} < s < (\nu + d'/2)(p/\pi - 1)\,. \end{cases}$$

Theorem 6.2.3. *Under the same hypotheses as in Theorem 6.2.2,*

$$\sup_{\boldsymbol{f}\in B^s_{\pi,r}(M),\, \boldsymbol{K}\in\mathcal{K}_\nu(Q_1,Q_2)} \mathbb{E}\,\|\tilde{\boldsymbol{f}} - \boldsymbol{f}\|_\infty \lesssim \mathcal{R}_\infty(\delta,2,1) \vee \mathcal{R}_\infty(\varepsilon,2,2) \tag{6.17}$$

where

$$\mathcal{R}_\infty(x,d,d') = \sqrt{|\log x|}(x\sqrt{|\log x|})^{\mu'(d,d')}$$

and

$$\mu'(d,d') = \frac{s - d/\pi}{s - d/\pi + \nu + d'/2}$$

The speeds of convergence exhibit an explicit interplay between the noise levels δ and ε, including the possible case where $\delta \gg \varepsilon$. The convergence rates obtained when $\delta = 0$ and $\varepsilon = 0$ are very similar, except that the problem $\varepsilon = 0$ reveals rates corresponding to a problem in dimension 1. This indicates that the denoising of $\boldsymbol{K}_\delta$ results in the same rates as the denoising of $\boldsymbol{Y}_\varepsilon$, but with a dimension parameter given by the size of the blocks appearing in the blockwise SVD (that is to say the integer d' such that $\dim \mathbb{H}_\ell \sim \ell^{d'}$).

If $\delta = 0$, the rates coincide with the results of Kerkyacharian et al. [51] (actually, the algorithms themselves are nearly identical), which can be proved to be optimal in a minimax sense (up to a logarithmic factor, see Willer [85] for a sketch of proof). The optimality when $\delta \gg \varepsilon$ is not yet established, and we won't address it in the present paper. The two regions $s \geqslant (\nu + d/2)(\frac{p}{\pi} - 1)$ and $s < (\nu + d/2)(\frac{p}{\pi} - 1)$ are classic in non-parametric estimation in inverse problems, and respectively referred to as the regular case and the sparse case.

Although we chose to work in a white noise model for the convenience of calculations, the algorithm and ensuing results should be easily adapted to the density estimation framework mentioned in section 6.1.1, in which one observes direct realizations $(\boldsymbol{\theta}_1 X_1, ..., \boldsymbol{\theta}_n X_n)$ of $\boldsymbol{\theta} X$ and a noisy version $\boldsymbol{K}_\delta$ of $\boldsymbol{K}$.

Adaptation to other dimensions and comparison with existing works

A close inspection of the proofs of Theorems 6.2.2 and 6.2.3 shows that the presence of a blockwise SVD decomposition, combined with properties of the ensuing needlet frame similar to those in section 5.2, ensures the applicability of the scheme with adapted convergence rates.
This includes in particular the corresponding 1-dimensional problem, equivalent to deconvolution in a periodic setting ([28]). Here the Meyer's periodized wavelets can endorse the role of needlets in the present setting, since they are compactly supported in the frequential domain as well. In the Fourier basis on $[0,1]$, $\boldsymbol{K}$ is directly diagonalized, which corresponds to a blockwise SVD with dimensionality $d'=0$. The adapted algorithm henceforth reaches the rates $\mathcal{R}_p(\delta,1,0)\vee\mathcal{R}_p(\varepsilon,1,1)$, $1\leqslant p\leqslant\infty$. It outperforms the one developed in Hoffmann and Reiß [40] which corresponds formally to $\mathcal{R}_2(\delta,1,1)\vee\mathcal{R}_2(\varepsilon,1,1)$. The reason to it is that a Galerkin projection on wavelets is agnostic to the blockwise structure of $\boldsymbol{K}$. Moreover, our procedure widens the possible range of considered $\mathbb{L}^p$ losses.
In image processing, a signal $\boldsymbol{f}\in\mathbb{L}^2([0,1]^2)$ is observed through its convolution with a function $\boldsymbol{k}\in\mathbb{L}^2([0,1]^2)$ called the Point Spread Function of the measuring device, which requires to be estimated in first instance (see [72],[55]). A careful adaptation of the main results in this paper allows to treat this problem as well (for the definition of needlets on $[0,1]^2$, see [43]).
Another relevant example concerns the operators defined on $\mathbb{S}^d$, $d\geqslant 1$ via

$$\boldsymbol{K}f(\xi)=\int_{\mathbb{S}^d}\varphi(\langle\xi,\omega\rangle)f(\omega)d\omega\,,$$

where φ is a bounded integrable function on $[-1,1]$. In this case, as shown by the Funk-Hecke theorem (see [36]), spherical harmonics realize a SVD of $\boldsymbol{K}$. On the other hand, the construction of needlets generalizes naturally to $\mathbb{S}^d$ (see [69]), and the rates derived hence change to $\mathcal{R}_p(\delta,d,0)\vee\mathcal{R}_p(\varepsilon,d,d)$, $1\leqslant p\leqslant\infty$.

Comparison with the blockwise SVD algorithm of Delattre et al. [23]

In this section we present the blockwise SVD algorithm **BBD** (for Blind Blockwise Deconvolution) depicted in Delattre et al. [23], and compare it to **BND**. **BBD** also relies on the blockwise SVD property (6.1.1), but tackles the thresholding of the signal and the operator differently. Namely, define the maximal resolution level

$$L\sim\lfloor\big(\varepsilon\sqrt{|\log\varepsilon|}\big)^{-1}\wedge\big(\delta\sqrt{|\log\delta|}\big)^{-2}\rfloor$$

and the signal thresholding level $\mathcal{E}_\ell(\varepsilon)=\tau\sqrt{2\ell+1}\varepsilon\sqrt{|\log\varepsilon|}$, $\tau>0$. The estimator $\tilde{f}$ provided by the **BBD** algorithm is

$$\boldsymbol{f}=\sum_{\ell\leqslant L}\boldsymbol{K}_{\delta,\ell}^{-1}\mathbf{1}_{\left\{\|\boldsymbol{K}_{\delta,\ell}^{-1}\|_{op}<O_\ell(\delta)^{-1}\right\}}\boldsymbol{Y}_{\varepsilon,\ell}\mathbf{1}_{\left\{\|\boldsymbol{Y}_{\varepsilon,\ell}\|>\mathcal{E}_\ell(\varepsilon)\right\}}\,. \tag{6.18}$$

It is quickly seen that **BBD** is still adaptive with respect to $\boldsymbol{f}$ and $\boldsymbol{K}$. This estimator is however fundamentally different from ours: first, the signal regularization is directly performed on the observed signal $\boldsymbol{Y}_\varepsilon$ rather than on $\boldsymbol{K}_\delta^{-1}\boldsymbol{Y}_\varepsilon$. Secondly, this regularization step is anterior to the inversion of $\boldsymbol{K}_\delta$, whereas in **BND** the signal is first inverted and then thresholded. These differences imply differences as well in the setting in which **BBD** will perform well. Namely, Delattre et al. [23] require that the two following inequalities hold:

$$\|\boldsymbol{K}_\ell\|_{op} \leqslant R_1 \ell^{-\nu} \text{ and } \|\boldsymbol{K}_\ell^{-1}\|_{op} \leqslant R_2 \ell^{\nu} \tag{6.19}$$

for $R_1, R_2 > 0$. Let us note $\mathcal{G}(R_1, R_2)$ the set of operators satisfying (6.19). (6.19) unilaterally entails Assumption 6.2.1 which means that **BND** applies in the context of **BBD** but the reverse is false. As a matter of fact, (6.19) restricts the scope of application of **BBD** to quasi diagonal operators. The setting of **BND** is much more generic. Finally, due to the shape of the threshold performed on each $\boldsymbol{Y}_{\varepsilon,\ell}$, **BBD** performs well only when the loss in measured in quadratic risk, and when $\boldsymbol{f}$ belongs to a Sobolev space (which corresponds to $\boldsymbol{f} \in B^s_{2,2}$).
The counterpart to such restrictive assumptions is the remarkably fast rates of convergence it attains in the case $\varepsilon = 0$. Indeed, it can be proved that, for $s, M > 0$, $R_1, R_2 > 0$ and $\nu \geqslant 0$,

$$\sup_{\substack{\boldsymbol{f}\in\mathcal{W}^s(M)\\ \boldsymbol{K}\in\mathcal{G}(R_1,R_2)}} \mathbb{E}\,\|\tilde{\boldsymbol{f}} - \boldsymbol{f}\|_2 \lesssim \left(\delta\sqrt{|\log\delta|}\right)^{1\wedge\frac{2s}{2\nu+1}} \vee \left(\varepsilon\sqrt{|\log\varepsilon|}\right)^{\frac{2s}{2s+2\nu+1}}. \tag{6.20}$$

This clearly outperforms **BND** in the case $\pi = r = 2$, and $p = 2$.

6.2.2 Practical study

We present the practical numerical performances of **BND** and compare it to the Blind Blockwise Deconvolution algorithm (**BBD**) of Delattre et al. [23]. The sets of cubature points in the simulations that follow have been taken from the web site of R. Womersley `http://web.maths.unsw.edu.au/~rsw`. We proceed with the following choices of parameters :
Data: the target density $\boldsymbol{f}$ is given by

$$\boldsymbol{f}(\omega) = \exp(-2 * \|\omega - \omega_1\|_{\ell^1(\mathbb{R}^3)})/c$$

with $\omega_1 = (0, 1, 0)$ and $c = 0.6729$. Concerning the operator $\boldsymbol{K}$, we choose it among the class of Rosenthal laws on SO(3). These distributions find their origins in random walks on groups (see [75]). $\boldsymbol{K}$ is said to follow a Rosenthal distribution of parameters $\alpha \in]0;\pi]$ and $\nu > 0$ on SO(3) if, for $\ell \geqslant 0$, $|m| \leqslant \ell$, we have

$$\boldsymbol{K}_{\ell,m,n} = \left(\frac{\sin((\ell+1/2)\alpha)}{(2\ell+1)\sin(\alpha/2)}\right)^{\nu} \mathbf{1}_{\{m=n\}}.$$

κ	0.3	0.4	0.5	0.6	0.7	0.8
Nr_{op}	10	9	9	8	2	0

Table 6.1: Choosing of κ. Nr_{op} is the average number, computed on a base of $N = 10$ realizations, of levels $\ell \leqslant 10$ such that $\|\boldsymbol{K}_{\delta,\ell}^{-1}\|_{op} \leqslant O_\ell(\delta)^{-1}$. We have $\delta = 10^{-3}$.

A Rosenthal law hence provides a concrete example of operator with DIP $\nu \geqslant 0$. We will take $\alpha = \pi$ and $\nu = 1$.

Tuning parameters: we set $\lambda = 1$ in 6.14. The concrete choice of adequate thresholding constants κ and τ is a complex issue. Our practical choices will be based on the following remark, inspired from Donoho and Johnstone [27]: in the case of direct estimation on real line, the universal threshold which is both efficient and simple to implement, takes the form $2\sqrt{|\log \varepsilon|}$. A consistent interpretation is to consider that this threshold should kill any pure noise signal. We will adapt this reasoning to the case of interest.

Choice of κ : we use as a benchmark the case where $\boldsymbol{K}_\ell$ is the null matrix of $M_{2\ell+1}(\mathbb{R})$ for $\ell \geqslant 1$ (this corresponds to the case where the law of $\boldsymbol{\theta}$ is uniform over SO(3)). Given δ large enough, the smallest value κ such that

$$\|\boldsymbol{K}_{\delta,\ell}^{-1}\|_{op} > O_\ell(\delta)^{-1} \text{ for all } \ell \leqslant 10$$

is retained. The results are reported in Table 6.1 and give $\kappa = 0.8$.

Choice of τ_{sig} and τ_{op}: It is clear that the role of τ_{sig} (resp. τ_{op}) is to control the influence of the signal (resp. the operator) error. In order to compute τ_{sig} (resp. τ_{op}), we therefore work with noise levels $\varepsilon_{sig} > \delta_{sig} > 0$ (resp. $\delta_{op} > \varepsilon_{op} > 0$) large enough. We make use of the uniform density $\boldsymbol{u}$ on $\mathbb{S}^2$, satisfying $\boldsymbol{u}_\ell = 0$ for $\ell \geqslant 1$ as a benchmark. Henceforth $\langle \boldsymbol{u}, \boldsymbol{\psi}_{j,\eta} \rangle = 0$ for $j \geqslant 0$, $\eta \in \mathcal{Z}_j$, which means that the observations $\langle \boldsymbol{Y}_{\varepsilon_{sig}}, \boldsymbol{\psi}_{j,\eta} \rangle$, $j \geqslant 0$ are pure noise. Taking advantage of this remark, we simulate $\boldsymbol{K}_{\delta_{sig}}$ and, integrating the previously computed value of κ, apply the procedure for increasing values of τ_{sig} (resp. τ_{op}) until all the computed coefficients $\langle \tilde{\boldsymbol{u}}, \boldsymbol{\psi}_{j,\eta} \rangle$ are killed for $j \leqslant 3$. The results are reported in Table 6.2 and give $\tau_{sig} = 0.9$, $\tau_{op} = 0.2$.

We compare the performances of **BBD** (with parameters $\kappa = 0.8$ and $\tau = 1$ taken from [23]) and **BND** for $\delta \in \{3.10^{-3}, 10^{-3}, 10^{-4}\}$, $\varepsilon \in \{10^{-3}, 10^{-4}\}$. The (normalized) mean squared error and supremum norm error are computed with a Monte-Carlo method based on $N = 200$ simulations. Each loss is approximated by its discrete equivalent calculated on a uniform grid of 4096 points on $\mathbb{S}^2$ at each step. Results are reported in Table 6.3. They clearly illustrate the rates of convergence derived in Theorems 6.2.2 and 6.2.3 in that the loss in always higher when the signal noise level ε is predominant. Besides, it also confirms the relationship between the rates in Theorems 6.2.2 and 6.2.3 and (6.20). Indeed, since $\boldsymbol{K}$ also verifies (6.19), the rates (6.20) are available and Table 6.3 exposes the outperforming of **BND** over **BBD** in every situation except when the operator noise is highly predominant (corresponding to $(\delta, \varepsilon) = (3.10^{-3}, 10^{-4})$).

For particular realizations of $\boldsymbol{Y}_\varepsilon$ and $\boldsymbol{K}_\delta$, we plot in Figure 6.1 : the original shape of

τ_{sig}	0.5	0.6	0.7	0.8	0.9
$j=0$	3	0	3	0	0
$j=1$	10	6	0	0	0
$j=2$	20	9	2	1	0
$j=3$	94	22	8	4	0

τ_{op}	0.1	0.2
$j=0$	0	0
$j=1$	0	0
$j=2$	4	0
$j=3$	127	0

Table 6.2: Choosing of τ. For $(\delta_{sig}, \varepsilon_{sig}) = (\varepsilon_{op}, \delta_{op}) = (10^{-4}, 10^{-3})$ and each value of τ, we computed 10 times the described procedure and reported the average number of remaining needlet coefficients at level j.

δ	ε	$E\|\tilde{\boldsymbol{f}} - \boldsymbol{f}\|_2$		$E\|\tilde{\boldsymbol{f}} - \boldsymbol{f}\|_\infty$	
		BBD	**BND**	**BBD**	**BND**
3.10^{-3}	10^{-3}	0.2210	0.1695	0.3867	0.3464
	10^{-4}	0.1013	0.1603	0.2146	0.3374
10^{-3}	10^{-3}	0.2195	0.1242	0.3870	0.2204
	10^{-4}	0.0839	0.0594	0.1931	0.1569
10^{-4}	10^{-3}	0.2194	0.1267	0.3863	0.2257
	10^{-4}	0.0825	0.0584	0.1924	0.1571

Table 6.3: Average normalized $\mathbb{L}^2$ and $\mathbb{L}^\infty$ loss of **BBD** and **BND**.

the density, and the results of the different algorithms in the form of spherical views seen 'from above'. The figures emphasize the better adaptivity of **BND** to the 'spiky' shape of the target density.

6.3 Proofs

Preliminary lemmas

The establishment of the convergence rates in Theorems 6.2.2 and 6.2.3 requires the control of the tails of the variables $|\widehat{\boldsymbol{\beta}}_{j,\eta} - \boldsymbol{\beta}_{j,\eta}|$. This will be the subject of Lemma 6.3.3. Two results upstream of this Lemma involve the control of the tails of the variables $\|\dot{\boldsymbol{B}}_\ell\|_{op}$ (Lemma 6.3.1), as well as a control of $\|\boldsymbol{K}_{\delta,\ell}^{-1}\|_{op}$ on a particular set (Lemma 6.3.2). We won't perform the proofs of the two latter results, but will provide references where they are conducted.

Lemma 6.3.1 (Davidson and Szarek [22], Theorem 2.4)**.** *There exists two constants $\beta_0, c_0 \geqslant 0$ independent from $\ell \in \mathbb{N}$ such that*

$$\forall t \geqslant \beta_0,\ \mathbb{P}((2\ell+1)^{-1/2}\|\dot{\boldsymbol{B}}_\ell\|_{op} > t) \leqslant \exp(-c_0 t(2\ell+1)^2)\,.$$

A simple corollary is the following upper bound on the moments of $\|\dot{\boldsymbol{B}}_\ell\|_{op}$

$$\mathbb{E}[\|\dot{\boldsymbol{B}}_\ell\|_{op}^p] \lesssim \ell^{p/2}\,.$$

Lemma 6.3.2 (Delattre et al. [23], proof of Theorem 3.1)**.** *We introduce further the events $\mathcal{A}_\ell = \{\|(\boldsymbol{K}_{\delta,\ell})^{-1}\|_{op} \leqslant O_\ell(\delta)^{-1}\}$ and $\mathcal{B}_\ell = \{\|\delta\dot{\boldsymbol{B}}_\ell\|_{op} \leqslant a_\ell\}$ with $a_\ell = \rho O_\ell(\delta)$ for some $0 < \rho < \frac{1}{2}$. On $\mathcal{A}_\ell \cap \mathcal{B}_\ell$, we have*

$$\|\boldsymbol{K}_{\delta,\ell}^{-1}\|_{op} \leqslant \frac{\rho}{1-\rho}\|\boldsymbol{K}_\ell^{-1}\|_{op}$$
$$\text{and } \|\boldsymbol{K}_\ell^{-1}\|_{op} \leqslant (1-\rho)^{-1}\|\boldsymbol{K}_{\delta,\ell}^{-1}\|_{op}$$

Lemma 6.3.3. *Let $\overline{S_j}(\delta,\varepsilon) = \tau 2^{j\nu}\big(\varepsilon\sqrt{|\log\varepsilon|} \vee 2^{-j/2}\delta\sqrt{|\log\delta|}\big)$ with $\tau = \tau_{siq} \vee \tau_{op}$. In the setting of Theorem 6.2.2, for all $j \leqslant J$, $\eta \in \mathcal{Z}_j$, for all $p \geqslant 1$*

$$\mathbb{P}(|\widehat{\boldsymbol{\beta}}_{j,\eta} - \boldsymbol{\beta}_{j,\eta}| > \overline{S_j}(\delta,\varepsilon)) \lesssim \varepsilon^{\kappa^2} \vee \delta^{\kappa^2}\,, \tag{6.21}$$
$$\mathbb{E}[|\widehat{\boldsymbol{\beta}}_{j,\eta} - \boldsymbol{\beta}_{j,\eta}|^p] \lesssim (\varepsilon 2^{j\nu})^p \vee (\delta 2^{j(\nu-1/2)})^p \vee |\boldsymbol{\beta}_{j,\eta}|^p \mathbf{1}_{\{j \geqslant j_0\}}\,, \tag{6.22}$$
$$\mathbb{E}[\sup_{\eta\in\mathcal{Z}_j}|\widehat{\boldsymbol{\beta}}_{j,\eta} - \boldsymbol{\beta}_{j,\eta}|^p] \lesssim (j+1)^p\Big[(\varepsilon 2^{j\nu})^p \vee (\delta 2^{j(\nu-1/2)})^p\Big] \vee |\boldsymbol{\beta}_{j,\eta}|^p \mathbf{1}_{\{j \geqslant j_0\}}\,, \tag{6.23}$$

where $2^{j_0} \gtrsim \big(\delta\sqrt{|\log\delta|}\big)^{-\frac{2}{2\nu+1}}$.

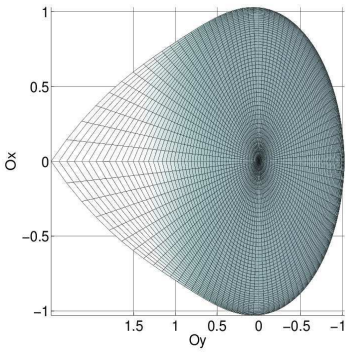

(a) Target Density

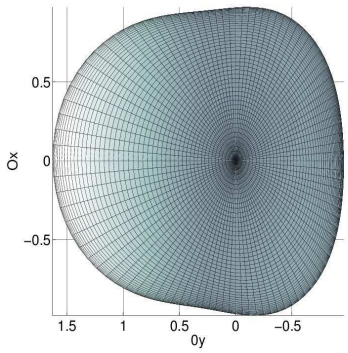

(b) **BBD**, $\varepsilon = 10^{-3}$

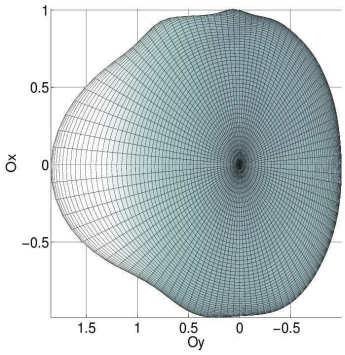

(c) **BND**, $\varepsilon = 10^{-3}$

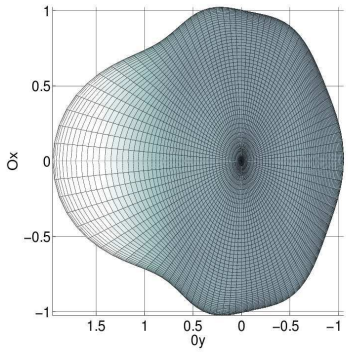

(d) **BBD**, $\varepsilon = 10^{-4}$

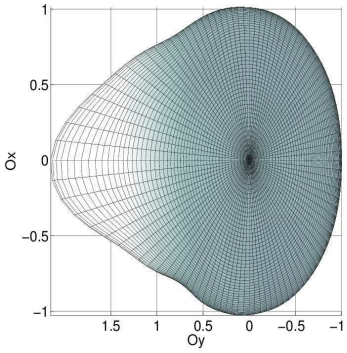

(e) **BND**, $\varepsilon = 10^{-4}$

Figure 6.1: Spherical view from above of the results of the two algorithms with noise level $\delta = 10^{-3}$

Proof of Lemma 6.3.3. All inequalities can be derived from the study of $\mathbb{P}(|\widehat{\boldsymbol{\beta}}_{j,\eta}-\boldsymbol{\beta}_{j,\eta}| > t)$ in each case. Resorting to the identity

$$\boldsymbol{K}_{\delta,\ell}^{-1}(\boldsymbol{K}_\ell \boldsymbol{f}_\ell + \varepsilon \dot{\boldsymbol{W}}_\ell) - \boldsymbol{f}_\ell = -\delta \boldsymbol{K}_{\delta,\ell}^{-1}\dot{\boldsymbol{B}}_\ell \boldsymbol{f}_\ell + \boldsymbol{K}_{\delta,\ell}^{-1}\varepsilon \dot{\boldsymbol{W}}_\ell \tag{6.24}$$

which holds for every $\ell \in \mathbb{N}$, and using Parseval's formula, we decompose $\widehat{\boldsymbol{\beta}}_{j,\eta} - \boldsymbol{\beta}_{j,\eta} = I + II + II$ where

$$\begin{aligned} I &= \sum_{\ell \in L_j} \langle -\delta \boldsymbol{K}_{\delta,\ell}^{-1} \mathbf{1}_{\mathcal{A}_\ell} \dot{\boldsymbol{B}}_\ell \boldsymbol{f}_\ell, \boldsymbol{\psi}_{j,\eta,\ell} \rangle, \\ II &= \sum_{\ell \in L_j} \langle \boldsymbol{K}_{\delta,\ell}^{-1} \mathbf{1}_{\mathcal{A}_\ell} \varepsilon \dot{\boldsymbol{W}}_\ell, \boldsymbol{\psi}_{j,\eta,\ell} \rangle, \\ III &= -\sum_{\ell \in L_j} \langle \boldsymbol{f}_\ell, \boldsymbol{\psi}_{j,\eta,\ell} \rangle \mathbf{1}_{\mathcal{A}_\ell^c}. \end{aligned}$$

We now have to study the deviation bounds of I, II, III. Term I can be decomposed as $I = IV + V$ where

$$\begin{aligned} IV &= -\sum_{\ell \in \boldsymbol{L}_j} \langle \delta \boldsymbol{K}_{\delta,\ell}^{-1} \dot{\boldsymbol{B}}_\ell \boldsymbol{f}_\ell, \boldsymbol{\psi}_{j,\eta,\ell} \rangle \mathbf{1}_{\mathcal{A}_\ell} \mathbf{1}_{\mathcal{B}_\ell} \\ V &= -\sum_{\ell \in \boldsymbol{L}_j} \langle \delta \boldsymbol{K}_{\delta,\ell}^{-1} \dot{\boldsymbol{B}}_\ell \boldsymbol{f}_\ell, \boldsymbol{\psi}_{j,\eta,\ell} \rangle \mathbf{1}_{\mathcal{A}_\ell} \mathbf{1}_{\mathcal{B}_\ell^c}. \end{aligned}$$

In order to treat the Term IV, we introduce the operator

$$\boldsymbol{Q}_j = \sum_{\ell \in L_j} \boldsymbol{K}_{\delta,\ell}^{-1} \mathbf{1}_{\mathcal{A}_\ell} \mathbf{1}_{\mathcal{B}_\ell} \dot{\boldsymbol{B}}_\ell$$

defined for $j \leqslant J$. Since $\boldsymbol{K}$ and $\dot{\boldsymbol{B}}$ are both stable with regard to every space $\mathbb{H}_\ell$, and since $\langle \boldsymbol{\psi}_{j,\eta}, \boldsymbol{\psi}_{h,\alpha} \rangle = 0$ if $|j-h| > 1$, we have

$$IV = -\langle \delta \boldsymbol{Q}_j f, \boldsymbol{\psi}_{j,\eta} \rangle = -\sum_{h=j-1}^{j+1} \sum_{\alpha \in \mathcal{Z}_h} \langle \delta \boldsymbol{Q}_j \boldsymbol{\psi}_{h,\alpha}, \boldsymbol{\psi}_{j,\eta} \rangle \langle f, \boldsymbol{\psi}_{h,\alpha} \rangle.$$

Henceforth

$$\begin{aligned} |IV| \leqslant & \Big(\sum_{h=j-1}^{j+1} \sum_{\alpha \in \mathcal{Z}_h} |\langle \delta \boldsymbol{Q}_j \boldsymbol{\psi}_{h,\alpha}, \boldsymbol{\psi}_{j,\eta} \rangle|^{\pi'} \Big)^{\frac{1}{\pi'}} \Big(\sum_{h=j-1}^{j+1} \sum_{\alpha \in \mathcal{Z}_h} |\langle f, \boldsymbol{\psi}_{h,\alpha} \rangle|^{\pi} \Big)^{\frac{1}{\pi}} \mathbf{1}_{\{\pi \leqslant 2\}} \\ & + \Big(\sum_{h=j-1}^{j+1} \sum_{\alpha \in \mathcal{Z}_h} |\langle \delta \boldsymbol{Q}_j \boldsymbol{\psi}_{h,\alpha}, \boldsymbol{\psi}_{j,\eta} \rangle|^{\pi} \Big)^{\frac{1}{\pi}} \Big(\sum_{h=j-1}^{j+1} \sum_{\alpha \in \mathcal{Z}_h} |\langle f, \boldsymbol{\psi}_{h,\alpha} \rangle|^{\pi'} \Big)^{\frac{1}{\pi'}} \mathbf{1}_{\{\pi > 2\}} \end{aligned}$$

where we used Hölder's inequality with $\pi^{-1} + (\pi')^{-1} = 1$. Now, if $\pi \leqslant 2$, then $\pi' \geqslant 2$ and (5.8) together with Proposition 5.2.4 entail

$$\begin{aligned}\Big(\sum_{h=j-1}^{j+1} \sum_{\alpha \in \mathcal{Z}_h} |\langle \delta \boldsymbol{Q}_j \boldsymbol{\psi}_{h,\alpha}, \boldsymbol{\psi}_{j,\eta} \rangle|^{\pi'} \Big)^{\frac{1}{\pi'}} &\leqslant \Big(\sum_{h=j-1}^{j+1} \sum_{\alpha \in \mathcal{Z}_h} |\langle \delta \boldsymbol{Q}_j \boldsymbol{\psi}_{h,\alpha}, \boldsymbol{\psi}_{j,\eta} \rangle|^{2} \Big)^{\frac{1}{2}} \\ &\leqslant \|\delta^T \boldsymbol{Q}_j \boldsymbol{\psi}_{j,\eta}\| \\ &\lesssim \delta 2^{j(\nu+1/2)} \,.\end{aligned}$$

Moreover, since $\boldsymbol{f} \in B^s_{\pi,r}$, we have

$$\Big(\sum_{h=j-1}^{j+1} \sum_{\alpha \in \mathcal{Z}_h} |\langle f, \boldsymbol{\psi}_{h,\alpha} \rangle|^{\pi} \Big)^{\frac{1}{\pi}} \lesssim 2^{-j(s-\frac{2}{\pi}+1)} \,.$$

If $\pi > 2$, a similar argument added with the Besov embedding $B^s_{\pi,r} \subset B^{s-2(1/\pi-1/\pi')}_{\pi',r}$ leads to the same bound. Finally,

$$\begin{aligned}\mathbb{P}(|IV| > t) &\leqslant \mathbb{P}\left(\|\delta^T \boldsymbol{Q}_j\|_{op} 2^{-j(s-\frac{2}{\pi}+1)} \gtrsim t \right) \\ &\leqslant \mathbb{P}(2^{-j/2} \|\widetilde{\boldsymbol{P}}_{\ell_j} \dot{\boldsymbol{B}} \widetilde{\boldsymbol{P}}_{\ell_j}\|_{op} \gtrsim t \delta^{-1} 2^{j(\nu-1/2-(s-2/\pi))}) \\ &\leqslant \exp\Big(- \frac{c_0 t^2 2^{2j}}{2^{2j(\nu-\frac{1}{2})}} \Big) \mathbf{1}_{\left\{ t \gtrsim \beta_0 2^{j(\nu-\frac{1}{2})} \right\}} \end{aligned} \tag{6.25}$$

where we noted $\widetilde{\boldsymbol{P}}_{\ell_j}$ the orthogonal projector onto $\bigoplus_{\ell \in L_j} \mathbb{H}_\ell$ and used Lemmas 6.3.1 and 6.3.2 together with the fact that $s > 2/\pi$. Turning to the Term V, a direct application of Lemma 6.3.1 entails

$$\mathbb{P}(\|\delta \dot{\boldsymbol{B}}_\ell\|_{op} > \boldsymbol{a}_\ell) \leqslant \delta^{c_0 \rho^2 (2\ell+1)^2 \kappa^2} \,. \tag{6.26}$$

So we have

$$\begin{aligned}\mathbb{P}(|V| > t) &\leqslant \mathbb{P}\Big(\sum_{\ell \in \boldsymbol{L}_j} \delta \|\boldsymbol{K}^{-1}_{\delta,\ell} \dot{\boldsymbol{B}}_\ell\|_{op} \|\boldsymbol{f}_\ell\| \|\boldsymbol{\psi}_{j,\eta,\ell}\| \mathbf{1}_{\mathcal{A}_\ell} \mathbf{1}_{\mathcal{B}^c_\ell} > t \Big) \\ &\leqslant \sum_{\ell \in \boldsymbol{L}_j} \mathbb{P}(\|\boldsymbol{K}^{-1}_{\delta,\ell} \dot{\boldsymbol{B}}_\ell\|_{op} \mathbf{1}_{\mathcal{A}_\ell} \mathbf{1}_{\mathcal{B}^c_\ell} > t) \\ &\lesssim \sum_{\ell \in \boldsymbol{L}_j} \mathbb{P}(\|\boldsymbol{K}^{-1}_{\delta,\ell} \dot{\boldsymbol{B}}_\ell\|_{op} \mathbf{1}_{\mathcal{A}_\ell} > t)^{1/2} \, \mathbb{P}(\|\delta \dot{\boldsymbol{B}}_\ell\|_{op} > \boldsymbol{a}_\ell)^{1/2} \\ &\lesssim \sum_{\ell \in \boldsymbol{L}_j} \mathbb{P}((2\ell+1)^{-1/2} \|\dot{\boldsymbol{B}}_\ell\|_{op} > t\kappa \log^{1/2} \delta)^{1/2} \delta^{c_0 \rho^2 (2\ell+1)^2 \kappa^2/2} \\ &\lesssim \delta^{c_0 \rho^2 2^{2j} \kappa^2/2} \sum_{\ell \in \boldsymbol{L}_j} \exp(-c_0 (2\ell+1)^2 t^2 \kappa^2 \log \delta/2) \\ &\lesssim \delta^{c_0 \rho^2 2^{2j} \kappa^2/2} \exp(-c_0 2^{2j} t^2 \kappa^2 \log \delta/2) \,.\end{aligned}$$

Turning to the term II, we decompose in a similar fashion $II = VI + VII$ where

$$VI = \sum_{\ell \in \boldsymbol{L}_j} \langle \varepsilon \boldsymbol{K}_{\delta,\ell}^{-1} \dot{\boldsymbol{W}}_\ell, \boldsymbol{\psi}_{j,\eta,\ell} \rangle \mathbf{1}_{\mathcal{A}_\ell} \mathbf{1}_{\mathcal{B}_\ell} \,,$$
$$VII = \sum_{\ell \in \boldsymbol{L}_j} \langle \varepsilon \boldsymbol{K}_{\delta,\ell}^{-1} \dot{\boldsymbol{W}}_\ell, \boldsymbol{\psi}_{j,\eta,\ell} \rangle \mathbf{1}_{\mathcal{A}_\ell} \mathbf{1}_{\mathcal{B}_\ell^c} \,.$$

Conditioning on $(\dot{\boldsymbol{B}}_\ell)_{\ell \in L_j}$ and applying Lemma 6.3.2, we derive for all $t > 0$,

$$\begin{aligned} \mathbb{P}(|VI| > t) &= \mathbb{P}\Big(\big| \sum_{\ell \in \boldsymbol{L}_j} \langle \varepsilon \boldsymbol{K}_{\delta,\ell}^{-1} \dot{\boldsymbol{W}}_\ell, \boldsymbol{\psi}_{j,\eta,\ell} \rangle \mathbf{1}_{\mathcal{A}_\ell} \mathbf{1}_{\mathcal{B}_\ell} \big| > t \Big) \\ &\leqslant \exp\big(- \frac{t^2}{2\varepsilon^2 2^{2j\nu}} \big) \,. \end{aligned} \tag{6.27}$$

As for the Term VII, employing Cauchy-Scwharz inequality, (6.26), and conditioning on $(\dot{\boldsymbol{B}}_\ell)_{\ell \in L_j}$, we write

$$\begin{aligned} \mathbb{P}(|VII| > t) &= \mathbb{P}(|\sum_{\ell \in \boldsymbol{L}_j} \langle \varepsilon \boldsymbol{K}_{\delta,\ell}^{-1} \dot{\boldsymbol{W}}_\ell, \boldsymbol{\psi}_{j,\eta,\ell} \rangle \mathbf{1}_{\mathcal{A}_\ell} \mathbf{1}_{\mathcal{B}_\ell^c}| > t) \\ &\leqslant \sum_{\ell \in \boldsymbol{L}_j} \mathbb{P}(|\langle \varepsilon \boldsymbol{K}_{\delta,\ell}^{-1} \dot{\boldsymbol{W}}_\ell, \boldsymbol{\psi}_{j,\eta,\ell} \rangle \mathbf{1}_{\mathcal{A}_\ell} \mathbf{1}_{\mathcal{B}_\ell^c}| > t) \\ &\leqslant \sum_{\ell \in \boldsymbol{L}_j} \mathbb{P}(|\langle \varepsilon \boldsymbol{K}_{\delta,\ell}^{-1} \mathbf{1}_{\mathcal{A}_\ell} \dot{\boldsymbol{W}}_\ell, \boldsymbol{\psi}_{j,\eta,\ell} \rangle| > t)^{1/2} \, \mathbb{P}(\delta \|\dot{\boldsymbol{B}}_\ell\|_{op} > \boldsymbol{a}_\ell)^{1/2} \\ &\lesssim \exp\big(- \frac{t^2 \delta^2 |\log \delta| 2^j}{4\varepsilon^2} \big) \delta^{c_0 \rho^2 2^{2j} \kappa^2 / 2} \,. \end{aligned}$$

It remains to treat the Term III. We claim that

$$\mathcal{A}_\ell^c \subset \big\{ \|\delta \dot{\boldsymbol{B}}_\ell\| \geqslant O_\ell(\delta) \big\} \bigcup \big\{ \|\boldsymbol{K}_\ell^{-1}\|_{op} \geqslant O_\ell(\delta)^{-1}/2 \big\} \tag{6.28}$$

(for a proof, we refer to Delattre et al. [23]). Hence, $III \leqslant VIII + IX$ where

$$VIII = |\sum_{\ell \in L_j} \langle \boldsymbol{f}_\ell, \boldsymbol{\psi}_{j,\eta,\ell} \rangle| \mathbf{1}_{\left\{ \|\delta \dot{\boldsymbol{B}}_\ell\| \geqslant O_\ell(\delta) \right\}} \,,$$
$$IX = |\sum_{\ell \in L_j} \langle \boldsymbol{f}_\ell, \boldsymbol{\psi}_{j,\eta,\ell} \rangle| \mathbf{1}_{\left\{ \|\boldsymbol{K}_\ell^{-1}\|_{op} \geqslant O_\ell(\delta)^{-1}/2 \right\}} \,.$$

As

$$\big\{ \|\boldsymbol{K}_\ell^{-1}\|_{op} > O_\ell(\delta)^{-1}/2 \big\} \subset \big\{ \ell > c(\delta \sqrt{|\log \delta|})^{-\frac{1}{\nu+1/2}} \big\} \tag{6.29}$$

for a constant c depending only on κ and Q_2, we derive that, noting $j_0 = \lfloor c(\delta \sqrt{|\log \delta|})^{-\frac{1}{\nu+1/2}} \rfloor + 1$, we have

$$\mathbb{P}(|IX| > t) \leqslant \mathbf{1}_{\left\{ t < |\boldsymbol{\beta}_{j,\eta}| \right\}} \mathbf{1}_{\{ j \geqslant j_0 \}} \,. \tag{6.30}$$

Indeed, for all $j < j_0$, for all $\ell \in L_j$, we have $\|\boldsymbol{K}_\ell^{-1}\|_{op} > O_\ell(\delta)^{-1}/2$. Now, a quick application of Lemma 6.3.1 entails

$$\mathbb{P}\left(\|\delta\dot{\boldsymbol{B}}_\ell\| \geqslant O_\ell(\delta)\right) \leqslant \delta^{c_0\kappa^2(2\ell+1)^2}.$$

Hence,

$$\begin{aligned}
P(|VIII| > t) &\leqslant \mathbb{P}\left(|\sum_{\ell\in L_j}\langle \boldsymbol{f}_\ell, \boldsymbol{\psi}_{j,\eta,\ell}\rangle \mathbf{1}_{\left\{\|\delta\dot{\boldsymbol{B}}_\ell\|\geqslant O_\ell(\delta)\right\}}| > t\right)\\
&\lesssim \sum_{\ell\in L_j} P\big(\mathbf{1}_{\left\{\|\delta\dot{\boldsymbol{B}}_\ell\|\geqslant O_\ell(\delta)\right\}} > t\big)\\
&\lesssim \sum_{\ell\in L_j} \mathbb{E}[\mathbf{1}_{\left\{\|\delta\dot{\boldsymbol{B}}_\ell\|\geqslant O_\ell(\delta)\right\}}\mathbf{1}_{\{t\leqslant 1\}}]\\
&\lesssim \sum_{\ell\in L_j} \mathbb{P}\left(\|\delta\dot{\boldsymbol{B}}_\ell\| \geqslant O_\ell(\delta)\right)^{1/2}\mathbf{1}_{\{t\leqslant 1\}}\\
&\lesssim \delta^{c_0\kappa^2 2^{2j}/2}\mathbf{1}_{\{t\leqslant 1\}}.
\end{aligned}$$

This ends the study of the tail of $|\widehat{\boldsymbol{\beta}}_{j,\eta} - \boldsymbol{\beta}_{j,\eta}|$. If κ and τ_{sig}, τ_{op} are large enough, the leading terms are given by (6.25), (6.27) and (6.30). (6.21) now results directly from the previous deviation inequalities. (6.22) is an application of the well known formula

$$E[|X|^p] = \int_{u>0} pu^{p-1}\,\mathbb{P}(|X| > u)du \leqslant p\int_{u>0} u^{p-1}\big(1\wedge\mathbb{P}(|X|>u)\big)du$$

if X is a real random variable. As for inequality (6.23), we have

$$\begin{aligned}
\mathbb{E}[\sup_{\eta\in\mathcal{Z}_j}|\widehat{\boldsymbol{\beta}}_{j,\eta} - \boldsymbol{\beta}_{j,\eta}|^p] &\leqslant \int_{u>0} pu^{p-1}\big(1\wedge\mathbb{P}(\sup_{\eta\in\mathcal{Z}_j}|\widehat{\boldsymbol{\beta}}_{j,\eta} - \boldsymbol{\beta}_{j,\eta}| > u)\big)du\\
&\leqslant p\int_{u>0} u^{p-1}\big(1\wedge 2^{2j}\,\mathbb{P}(|\widehat{\boldsymbol{\beta}}_{j,\eta} - \boldsymbol{\beta}_{j,\eta}| > u)\big)du.
\end{aligned}$$

Moreover, considering only the terms (6.25), (6.27) and (6.30) as mentioned above, we have

$$\begin{aligned}
2^{2j}\,\mathbb{P}(|\widehat{\boldsymbol{\beta}}_{j,\eta} - \boldsymbol{\beta}_{j,\eta}| > u) \lesssim & e^{-\frac{u^2}{2\varepsilon^2 2^{2j\nu}}+2j\log 2} + e^{-\frac{u^2}{2\delta^2 2^{j(2\nu-1)}}+2j\log 2}\\
&+ 2^{2j}\mathbf{1}_{\left\{u\lesssim\delta 2^{j(2\nu-1)}\right\}} + 2^{2j}\mathbf{1}_{\left\{u\leqslant|\boldsymbol{\beta}_{j,\eta}|\right\}}\mathbf{1}_{\{j\geqslant j_0\}},
\end{aligned}$$

which entails (6.23). □

6.3.1 Proof of Theorem 6.2.2

Proof. We shall only investigate the case where $p > \pi$, since for $p \leqslant \pi$, we have $B^s_{\pi,r} \subset B^s_{p,r}$. The $\mathbb{L}^p$ loss of the procedure can be decomposed as follows:

$$\mathbb{E}\,\|\tilde{\boldsymbol{f}} - \boldsymbol{f}\|_p^p \lesssim \mathbb{E}\,\|\sum_{j\leqslant J}\sum_{\eta\in\mathcal{Z}_j}\langle\tilde{\boldsymbol{f}} - \boldsymbol{f}, \boldsymbol{\psi}_{j,\eta}\rangle\boldsymbol{\psi}_{j,\eta}\|_p^p + \|\sum_{j>J}\sum_{\eta\in\mathcal{Z}_j}\boldsymbol{\beta}_{j,\eta}\boldsymbol{\psi}_{j,\eta}\|_p^p.$$

Since $f \in B^s_{\pi,r}$, we have

$$\| \sum_{j>J} \sum_{\eta \in \mathcal{Z}_j} \boldsymbol{\beta}_{j,\eta} \boldsymbol{\psi}_{j,\eta} \|_p^p \lesssim 2^{-Jp\left(s-2(1/\pi-1/p)\right)} .$$

Now it is proved in Kerkyacharian et al. [51] that for all $\nu, d' \geqslant 0$, we have

$$\frac{s-2(1/\pi-1/p)}{\nu+d'/2} \geqslant \mu(2,d') . \tag{6.31}$$

Since $2/d' \geqslant (\nu+d'/2)^{-1}$, the choice of the maximal level J ensures that this term is properly bounded by the desired rates of convergence. Bounding $\mathbb{E}\,\| \sum_{j \leqslant J} \sum_{\eta \in \mathcal{Z}_j} \langle \tilde{\boldsymbol{f}} - \boldsymbol{f}, \boldsymbol{\psi}_{j,\eta} \rangle \boldsymbol{\psi}_{j,\eta} \|_p^p$ is more involved. First we apply Hölder's inequality and (5.11) and decompose it as

$$\mathbb{E}\,\| \sum_{j \leqslant J} \sum_{\eta \in \mathcal{Z}_j} \langle \tilde{\boldsymbol{f}} - \boldsymbol{f}, \boldsymbol{\psi}_{j,\eta} \rangle \boldsymbol{\psi}_{j,\eta} \|_p^p \lesssim B + S ,$$

where

$$\begin{aligned} B =& J^{p-1} \sum_{j \leqslant J} \sum_{\eta \in \mathcal{Z}_j} \mathbb{E}\left[|\hat{\boldsymbol{\beta}}_{j,\eta} - \boldsymbol{\beta}_{j,\eta}|^p \mathbf{1}_{\left\{|\hat{\boldsymbol{\beta}}_{j,\eta}| > S_j(\delta,\varepsilon)\right\}} \right] \|\boldsymbol{\psi}_{j,\eta}\|_p^p , \\ S =& J^{p-1} \sum_{j \leqslant J} \sum_{\eta \in \mathcal{Z}_j} \mathbb{E}\left[|\boldsymbol{\beta}_{j,\eta}|^p \mathbf{1}_{\left\{|\hat{\boldsymbol{\beta}}_{j,\eta}| \leqslant S_j(\delta,\varepsilon)\right\}} \right] \|\boldsymbol{\psi}_{j,\eta}\|_p^p . \end{aligned}$$

The first step is to replace $S_j(\delta,\varepsilon)$ in B and S by a quantity explicitly depending on $2^{j\nu}$, namely $\overline{S_j}(\delta,\varepsilon)$. Remark to this end that on the event $\{\ell_j = +\infty\}$, we have $|\hat{\boldsymbol{\beta}}_{j,\eta}| \leqslant S_j(\delta,\varepsilon)$ almost surely. We subsequently write

$$\begin{aligned} B =& J^{p-1} \sum_{j \leqslant J} \sum_{\eta \in \mathcal{Z}_j} \mathbb{E}\left[|\hat{\boldsymbol{\beta}}_{j,\eta} - \boldsymbol{\beta}_{j,\eta}|^p \mathbf{1}_{\left\{|\hat{\boldsymbol{\beta}}_{j,\eta}| > S_j(\delta,\varepsilon)\right\}} \mathbf{1}_{\{\ell_j < +\infty\}} \mathbf{1}_{\mathcal{B}_{\ell_j}} \right] \|\boldsymbol{\psi}_{j,\eta}\|_p^p \\ &+ J^{p-1} \sum_{j \leqslant J} \sum_{\eta \in \mathcal{Z}_j} \mathbb{E}\left[|\hat{\boldsymbol{\beta}}_{j,\eta} - \boldsymbol{\beta}_{j,\eta}|^p \mathbf{1}_{\{\ell_j < +\infty\}} \mathbf{1}_{\mathcal{B}^c_{\ell_j}} \right] \|\boldsymbol{\psi}_{j,\eta}\|_p^p \\ \lesssim& J^{p-1} \sum_{j \leqslant J} \sum_{\eta \in \mathcal{Z}_j} \mathbb{E}\left[|\hat{\boldsymbol{\beta}}_{j,\eta} - \boldsymbol{\beta}_{j,\eta}|^p \mathbf{1}_{\left\{|\hat{\boldsymbol{\beta}}_{j,\eta}| > \overline{S_j}(\delta,\varepsilon)\right\}} \right] \|\boldsymbol{\psi}_{j,\eta}\|_p^p \\ &+ J^{p-1} \sum_{j \leqslant J} \sum_{\eta \in \mathcal{Z}_j} \mathbb{E}\left[|\hat{\boldsymbol{\beta}}_{j,\eta} - \boldsymbol{\beta}_{j,\eta}|^{2p} \right]^{p/2} \delta^{c_0 \rho^2 (22^j+1)^2 \kappa^2/2} \|\boldsymbol{\psi}_{j,\eta}\|_p^p \end{aligned} \tag{6.32}$$

where we successively applied Lemma 6.3.2, (6.26) and Cauchy-Schwarz inequality. It is clear that (6.32) is negligible for κ large enough. In a similar way,

$$\begin{aligned}
S =& J^{p-1}\sum_{j\leqslant J}\sum_{\eta\in\mathcal{Z}_j}\mathbb{E}\Big[|\boldsymbol{\beta}_{j,\eta}|^p\mathbf{1}_{\{|\widehat{\boldsymbol{\beta}}_{j,\eta}|\leqslant S_j(\delta,\varepsilon)\}}\mathbf{1}_{\{\ell_j<+\infty\}}\mathbf{1}_{\mathcal{B}_{\ell_j}}\Big]\|\boldsymbol{\psi}_{j,\eta}\|_p^p \\
&+ J^{p-1}\sum_{j\leqslant J}\sum_{\eta\in\mathcal{Z}_j}|\boldsymbol{\beta}_{j,\eta}|^p\,\mathbb{P}(\ell_j=+\infty)\|\boldsymbol{\psi}_{j,\eta}\|_p^p \\
&+ J^{p-1}\sum_{j\leqslant J}\sum_{\eta\in\mathcal{Z}_j}|\boldsymbol{\beta}_{j,\eta}|^p\,\mathbb{P}(\mathcal{B}_{\ell_j}^c)\|\boldsymbol{\psi}_{j,\eta}\|_p^p \\
\lesssim& J^{p-1}\sum_{j\leqslant J}\sum_{\eta\in\mathcal{Z}_j}\mathbb{E}\Big[|\boldsymbol{\beta}_{j,\eta}|^p\mathbf{1}_{\{|\widehat{\boldsymbol{\beta}}_{j,\eta}|\leqslant\overline{S_j}(\delta,\varepsilon)\}}\Big]\|\boldsymbol{\psi}_{j,\eta}\|_p^p \qquad (6.33)\\
&+ J^{p-1}\sum_{j\leqslant J}\sum_{\eta\in\mathcal{Z}_j}|\boldsymbol{\beta}_{j,\eta}|^p\,\mathbb{P}(\ell_j=+\infty)\|\boldsymbol{\psi}_{j,\eta}\|_p^p \qquad (6.34)\\
&+ J^{p-1}\sum_{j\leqslant J}\sum_{\eta\in\mathcal{Z}_j}|\boldsymbol{\beta}_{j,\eta}|^p\delta^{c_0\rho^2(22^j+1)^2\kappa^2/2}\|\boldsymbol{\psi}_{j,\eta}\|_p^p\,. \qquad (6.35)
\end{aligned}$$

(6.35) is small enough for κ large enough. Moreover, thanks to (6.28),

$$\big\{\ell_j=+\infty\big\}\subset\mathcal{A}_{2^j}^c\subset\big\{\|\delta\dot{\boldsymbol{B}}_{2^j}\|\geqslant O_{2^j}(\delta)\big\}\bigcup\big\{\|(\boldsymbol{K}_{2^j})^{-1}\|_{op}\geqslant O_{2^j}(\delta)^{-1}/2\big\}\,.$$

Thus, thanks to (6.29) and (6.26), the term (6.34) is negligible as well. We subsequently deduce that

$$\mathbb{E}\,\|\sum_{j\leqslant J}\sum_{\eta\in\mathcal{Z}_j}\langle\tilde{\boldsymbol{f}}-\boldsymbol{f},\boldsymbol{\psi}_{j,\eta}\rangle\boldsymbol{\psi}_{j,\eta}\|_p^p\lesssim J^{p-1}\big(Bb+Bs+Sb+Ss\big)$$

with

$$\begin{aligned}
Bb&=\sum_{j\leqslant J,\eta\in\mathcal{Z}_j}\mathbb{E}\big[|\widehat{\boldsymbol{\beta}}_{j,\eta}-\boldsymbol{\beta}_{j,\eta}|^p\mathbf{1}_{\{|\widehat{\boldsymbol{\beta}}_{j,\eta}|>\overline{S_j}(\delta,\varepsilon)\}}\mathbf{1}_{\{|\boldsymbol{\beta}_{j,\eta}|>\overline{S_j}(\delta,\varepsilon)/2\}}\big]\|\boldsymbol{\psi}_{j,\eta}\|_p^p\,,\\
Bs&=\sum_{j\leqslant J,\eta\in\mathcal{Z}_j}\mathbb{E}\big[|\widehat{\boldsymbol{\beta}}_{j,\eta}-\boldsymbol{\beta}_{j,\eta}|^p\mathbf{1}_{\{|\widehat{\boldsymbol{\beta}}_{j,\eta}|>\overline{S_j}(\delta,\varepsilon)\}}\mathbf{1}_{\{|\boldsymbol{\beta}_{j,\eta}|\leqslant\overline{S_j}(\delta,\varepsilon)/2\}}\big]\|\boldsymbol{\psi}_{j,\eta}\|_p^p\,,\\
Sb&=\sum_{j\leqslant J,\eta\in\mathcal{Z}_j}|\boldsymbol{\beta}_{j,\eta}|^p\,\mathbb{E}\big[\mathbf{1}_{\{|\widehat{\boldsymbol{\beta}}_{j,\eta}|\leqslant\overline{S_j}(\delta,\varepsilon)\}}\mathbf{1}_{\{|\boldsymbol{\beta}_{j,\eta}|>2\overline{S_j}(\delta,\varepsilon)\}}\big]\|\boldsymbol{\psi}_{j,\eta}\|_p^p\,,\\
Ss&=\sum_{j\leqslant J,\eta\in\mathcal{Z}_j}|\boldsymbol{\beta}_{j,\eta}|^p\,\mathbb{E}\big[\mathbf{1}_{\{|\widehat{\boldsymbol{\beta}}_{j,\eta}|\leqslant\overline{S_j}(\delta,\varepsilon)\}}\mathbf{1}_{\{|\boldsymbol{\beta}_{j,\eta}|\leqslant2\overline{S_j}(\delta,\varepsilon)\}}\big]\|\boldsymbol{\psi}_{j,\eta}\|_p^p\,.
\end{aligned}$$

We can now treat the terms Bs, Bb, Sb and Ss. Applying (5.11), (6.21) and Cauchy-Schwarz inequality:

$$\begin{aligned}
Bs&\leqslant J^{p-1}\sum_{j\leqslant J}\sum_{\eta\in\mathcal{Z}_j}\mathbb{E}\big[|\widehat{\boldsymbol{\beta}}_{j,\eta}-\boldsymbol{\beta}_{j,\eta}|^p\mathbf{1}_{\{|\widehat{\boldsymbol{\beta}}_{j,\eta}-\boldsymbol{\beta}_{j,\eta}|>\overline{S_j}(\delta,\varepsilon)/2\}}\big]\|\boldsymbol{\psi}_{j,\eta}\|_p^p\\
&\leqslant J^{p-1}\sum_{j\leqslant J}\sum_{\eta\in\mathcal{Z}_j}\mathbb{E}[|\widehat{\boldsymbol{\beta}}_{j,\eta}-\boldsymbol{\beta}_{j,\eta}|^{2p}]^{1/2}\,\mathbb{P}(|\widehat{\boldsymbol{\beta}}_{j,\eta}-\boldsymbol{\beta}_{j,\eta}|>\overline{S_j}(\delta,\varepsilon)/2)^{1/2}\|\boldsymbol{\psi}_{j,\eta}\|_p^p\\
&\lesssim J^{p-1}\sum_{j\leqslant J}\sum_{\eta\in\mathcal{Z}_j}\big((\varepsilon 2^{j\nu})^p\vee(\delta 2^{j(\nu-1/2)})^p\vee|\boldsymbol{\beta}_{j,\eta}|^p\mathbf{1}_{\{j\geqslant j_0\}}\big)2^{jp}\big(\varepsilon^{\tau^2}\vee\delta^{\tau^2}\big)\,.
\end{aligned}$$

Moreover,

$$\begin{aligned} Sb &\leqslant J^{p-1} \sum_{j \leqslant J} \sum_{\eta \in \mathcal{Z}_j} |\boldsymbol{\beta}_{j,\eta}|^p \, \mathbb{P}(|\widehat{\boldsymbol{\beta}}_{j,\eta} - \boldsymbol{\beta}_{j,\eta}| > \overline{S_j}(\delta, \varepsilon)) \|\boldsymbol{\psi}_{j,\eta}\|_p^p \\ &\lesssim J^{p-1} \left(\varepsilon^{\tau^2} \vee \delta^{\tau^2} \right), \end{aligned}$$

since $f \in B_{p,r}^{s-2(1/\pi - 1/p)}$. Hence in both cases the rate of convergence is smaller than what is claimed for sufficiently large τ. Turning to Bb and Ss, we write, for all $z, z' \geqslant 0$,

$$\begin{aligned} Bb \lesssim & J^{p-1} \sum_{j \leqslant J} \sum_{\eta \in \mathcal{Z}_j} \mathbb{E}[|\widehat{\boldsymbol{\beta}}_{j,\eta} - \boldsymbol{\beta}_{j,\eta}|^p] \mathbf{1}_{\left\{|\boldsymbol{\beta}_{j,\eta}| > \overline{S_j}(\delta,\varepsilon)/2\right\}} \|\boldsymbol{\psi}_{j,\eta}\|^p \\ \lesssim & \sum_{j \leqslant J} \sum_{\eta \in \mathcal{Z}_j} \left((\varepsilon 2^{j\nu})^p \vee (\delta 2^{j(\nu-1/2)})^p \vee |\boldsymbol{\beta}_{j,\eta}|^p \mathbf{1}_{\{j \geqslant j_0\}} \right) \mathbf{1}_{\left\{|\boldsymbol{\beta}_{j,\eta}| > \overline{S_j}(\delta,\varepsilon)/2\right\}} \|\boldsymbol{\psi}_{j,\eta}\|^p \\ \lesssim & J^{p-1} \left(\varepsilon \sqrt{|\log \varepsilon|} \right)^{p-z} \sum_{j \leqslant J} 2^{j[\nu(p-z)+p-2]} \sum_{\eta \in \mathcal{Z}_j} |\boldsymbol{\beta}_{j,\eta}|^z \\ & + J^{p-1} \left(\delta \sqrt{|\log \delta|} \right)^{p-z'} \sum_{j \leqslant J} 2^{j[(\nu-1/2)(p-z')+p-2]} \sum_{\eta \in \mathcal{Z}_j} |\boldsymbol{\beta}_{j,\eta}|^{z'} \\ & + J^{p-1} 2^{-j_0 p \left(s - 2(\frac{1}{\pi} - \frac{1}{p}) \right)} \end{aligned}$$

and

$$\begin{aligned} Ss \lesssim & J^{p-1} \sum_{j \leqslant J} \sum_{\eta \in \mathcal{Z}_j} |\boldsymbol{\beta}_{j,\eta}|^z \mathbf{1}_{\left\{|\boldsymbol{\beta}_{j,\eta}| \leqslant 2\tau 2^{j\nu} \varepsilon \sqrt{|\log \varepsilon|}\right\}} \|\boldsymbol{\psi}_{j,\eta}\|_p^p \\ & + J^{p-1} \sum_{j \leqslant J} \sum_{\eta \in \mathcal{Z}_j} |\boldsymbol{\beta}_{j,\eta}|^z \mathbf{1}_{\left\{|\boldsymbol{\beta}_{j,\eta}| \leqslant 2\tau 2^{j(\nu-1/2)} \delta \sqrt{|\log \delta|}\right\}} \|\boldsymbol{\psi}_{j,\eta}\|_p^p \\ \lesssim & J^{p-1} \left(\varepsilon \sqrt{|\log \varepsilon|} \right)^{p-z} \sum_{j \leqslant J} 2^{j[\nu(p-z)+p-2]} \sum_{\eta \in \mathcal{Z}_j} |\boldsymbol{\beta}_{j,\eta}|^z \|\boldsymbol{\psi}_{j,\eta}\|_p^p \\ & + J^{p-1} \left(\delta \sqrt{|\log \delta|} \right)^{p-z'} \sum_{j \leqslant J} 2^{j[(\nu-1/2)(p-z')+p-2]} \sum_{\eta \in \mathcal{Z}_j} |\boldsymbol{\beta}_{j,\eta}|^{z'} \|\boldsymbol{\psi}_{j,\eta}\|_p^p . \end{aligned}$$

The term

$$2^{-j_0 p \left(s - 2(1/\pi - 1/p) \right)} \sim (\delta \sqrt{|\log \delta|})^{p \frac{s-2(1/\pi-1/p)}{\nu+1/2}}$$

is readily bounded thanks to (6.31), which leaves us in both cases with the term $R(\varepsilon, \nu, z) + R(\delta, \nu - 1/2, z')$ to control, where

$$R(x, y, z) = J^{p-1} \left(x \sqrt{|\log x|} \right)^{p-z} \sum_{j \leqslant J} 2^{j[y(p-z)+p-2]} \sum_{\eta \in \mathcal{Z}_j} |\boldsymbol{\beta}_{j,\eta}|^z \|\boldsymbol{\psi}_{j,\eta}\|_p^p .$$

We only give a brief overview of the treatment of $R(x, y, z)$, a detailed one is present in Kerkyacharian et al. [51]. First, we split it as follows

$$\begin{aligned} R(x, y, z) = J^{p-1} \Big[& \left(x \sqrt{|\log x|} \right)^{p-z_1} \sum_{j \leqslant J_0} 2^{j[y(p-z_1)+p-2]} \sum_{\eta \in \mathcal{Z}_j} |\boldsymbol{\beta}_{j,\eta}|^{z_1} \|\boldsymbol{\psi}_{j,\eta}\|_p^p \\ & + \left(x \sqrt{|\log x|} \right)^{p-z_2} \sum_{j > J_0} 2^{j[y(p-z_2)+p-2]} \sum_{\eta \in \mathcal{Z}_j} |\boldsymbol{\beta}_{j,\eta}|^{z_2} \|\boldsymbol{\psi}_{j,\eta}\|_p^p \Big] \end{aligned}$$

where z_1, z_2, J_0 are to determine. Consider first the case where $s \geqslant (y+1)(p/\pi - 1)$. Note $q = p(y+1)(s+y+1)^{-1}$. Taking $z_2 = \pi$, $z_1 = \tilde{q} < q$ and $2^{J_0 \frac{p}{q}(y+1)} \sim (x\sqrt{|\log x|})^{-1}$ entails

$$R(x, y, J_0) \lesssim (\log x)^{p-1}(x\sqrt{|\log x|})^{p-q}$$

which is the desired bound. Now consider the case where $s < (y+1)(p/\pi - 1)$ and note $q = p(y+1-2/p)(y+1+s-2/\pi)^{-1}$. Take $z_1 = \pi$, $z_2 = \tilde{q} > q$ and $2^{J_0 \frac{p}{q}(y+1-2/p)} \sim (x\sqrt{|\log x|})^{-1}$. We obtain

$$R(x, y, J_0) \lesssim (\log \varepsilon)^{p-1}(x\sqrt{|\log x|})^{p-q}$$

which ends the proof. □

6.3.2 Proof of Theorem 6.2.3

Proof. Write similarly

$$\|\tilde{\boldsymbol{f}} - \boldsymbol{f}\|_\infty \leqslant \mathbb{E}\,\|\sum_{j \leqslant J}\sum_{\eta \in \mathcal{Z}_j} (\widehat{\boldsymbol{\beta}}_{j,\eta} - \boldsymbol{\beta}_{j,\eta})\boldsymbol{\psi}_{j,\eta}\|_\infty + \|\sum_{j > J}\sum_{\eta \in \mathcal{Z}_j} \boldsymbol{\beta}_{j,\eta}\boldsymbol{\psi}_{j,\eta}\|_\infty\,.$$

The term $\|\sum_{j>J}\sum_{\eta\in\mathcal{Z}_j}\boldsymbol{\beta}_{j,\eta}\boldsymbol{\psi}_{j,\eta}\|_\infty$ can be handled as in Theorem 6.2.2. Moreover, (5.12) for $p = \infty$ entails, similarly to the proof of Theorem 6.2.2,

$$\mathbb{E}\,\|\sum_{j \leqslant J}\sum_{\eta \in \mathcal{Z}_j} (\widehat{\boldsymbol{\beta}}_{j,\eta} - \boldsymbol{\beta}_{j,\eta})\boldsymbol{\psi}_{j,\eta}\|_\infty \lesssim Bb + Bs + Sb + Ss$$

with

$$\begin{aligned}
Bb &= \sum_{j\leqslant J} 2^j\,\mathbb{E}\big[\sup_{\eta\in\mathcal{Z}_j}|\widehat{\boldsymbol{\beta}}_{j,\eta} - \boldsymbol{\beta}_{j,\eta}|\mathbf{1}_{\{|\widehat{\boldsymbol{\beta}}_{j,\eta}|>\overline{S_j}(\delta,\varepsilon)\}}\mathbf{1}_{\{|\boldsymbol{\beta}_{j,\eta}|>\overline{S_j}(\delta,\varepsilon)/2\}}\big]\,,\\
Bs &= \sum_{j\leqslant J} 2^j\,\mathbb{E}\big[\sup_{\eta\in\mathcal{Z}_j}|\widehat{\boldsymbol{\beta}}_{j,\eta} - \boldsymbol{\beta}_{j,\eta}|\mathbf{1}_{\{|\widehat{\boldsymbol{\beta}}_{j,\eta}|>\overline{S_j}(\delta,\varepsilon)\}}\mathbf{1}_{\{|\boldsymbol{\beta}_{j,\eta}|\leqslant\overline{S_j}(\delta,\varepsilon)/2\}}\big]\,,\\
Sb &= \sum_{j\leqslant J} 2^j \sup_{\eta\in\mathcal{Z}_j}|\boldsymbol{\beta}_{j,\eta}|\,\mathbb{E}\big[\mathbf{1}_{\{|\widehat{\boldsymbol{\beta}}_{j,\eta}|\leqslant\overline{S_j}(\delta,\varepsilon)\}}\mathbf{1}_{\{|\boldsymbol{\beta}_{j,\eta}|>2\overline{S_j}(\delta,\varepsilon)\}}\big]\,,\\
Ss &= \sum_{j\leqslant J} 2^j \sup_{\eta\in\mathcal{Z}_j}|\boldsymbol{\beta}_{j,\eta}|\,\mathbb{E}\big[\mathbf{1}_{\{|\widehat{\boldsymbol{\beta}}_{j,\eta}|\leqslant\overline{S_j}(\delta,\varepsilon)\}}\mathbf{1}_{\{|\boldsymbol{\beta}_{j,\eta}|\leqslant2\overline{S_j}(\delta,\varepsilon)\}}\big]\,.
\end{aligned}$$

Now we have, using inequality (6.23),

$$\begin{aligned}
Bb &\leqslant \sum_{j\leqslant J} 2^j\,\mathbb{E}\sup_{\eta\in\mathcal{Z}_j}|\widehat{\boldsymbol{\beta}}_{j,\eta} - \boldsymbol{\beta}_{j,\eta}|\mathbf{1}_{\{|\boldsymbol{\beta}_{j,\eta}|>\overline{S_j}(\delta,\varepsilon)/2\}}\\
&\leqslant \sum_{j\leqslant J} 2^j \mathbf{1}_{\{\exists\eta\in\mathcal{Z}_j,\,|\boldsymbol{\beta}_{j,\eta}|\geqslant\overline{S_j}(\delta,\varepsilon)/2\}} 2^j\,\mathbb{E}\sup_{\eta\in\mathcal{Z}_j}|\widehat{\boldsymbol{\beta}}_{j,\eta} - \boldsymbol{\beta}_{j,\eta}|\\
&\lesssim \sum_{j\leqslant J} 2^j \mathbf{1}_{\{\exists\eta\in\mathcal{Z}_j,\,|\boldsymbol{\beta}_{j,\eta}|\geqslant\overline{S_j}(\delta,\varepsilon)/2\}}(j+1)\big(\varepsilon 2^{j\nu} \vee \delta 2^{j(\nu-1/2)}\big) \vee |\boldsymbol{\beta}_{j,\eta}|\mathbf{1}_{\{j\geqslant j_0\}}\\
&\lesssim 2^{J_1(\nu+1)}(J_1+1)\varepsilon + 2^{I_1(\nu+3/2)}(I_1+1)\delta + \sum_{j\geqslant j_0} 2^j|\boldsymbol{\beta}_{j,\eta}|
\end{aligned}$$

where J_1 is chosen so that, for $j \geqslant J_1$, $|\boldsymbol{\beta}_{j,\eta}| \leqslant \tau\varepsilon\sqrt{|\log\varepsilon|}2^{j\nu}/2$. We can take for example (see [51]) J_1 verifying, for a certain constant B,

$$2^{J_1} = B\big(\varepsilon\sqrt{|\log\varepsilon|}\big)^{-(s+\nu+1-2/\pi)^{-1}}.$$

Similarly, taking

$$2^{I_1} = C\big(\delta\sqrt{|\log\delta|}\big)^{-(s+\nu+1/2-2/\pi)^{-1}}$$

for a certain constant C implies $|\boldsymbol{\beta}_{j,\eta}| \leqslant \tau\delta\sqrt{|\log\delta|}2^{j(\nu-1/2)}/2$ for all $j \leqslant I_1$. The term $\sum_{j\geqslant j_0} 2^j|\boldsymbol{\beta}_{j,\eta}|$ is easily treated. This finally leads to the rates

$$Bb \lesssim |\log\varepsilon|\varepsilon^{\mu'(2)} \vee |\log\delta|\delta^{\mu'(1)}$$

and

$$\begin{aligned} Ss &\leqslant \sum_{j\leqslant J} 2^j \sup_{\eta\in\mathcal{Z}_j} |\boldsymbol{\beta}_{j,\eta}| \mathbf{1}_{\{|\boldsymbol{\beta}_{j,\eta}|\leqslant 2\overline{S_j}(\delta,\varepsilon)\}} \\ &\lesssim \Big[\sum_{j\leqslant J_1} 2^j\varepsilon\sqrt{|\log\varepsilon|}2^{j\nu} + \sum_{j>J_1} 2^j|\boldsymbol{\beta}_{j,\eta}|\Big] \\ &\qquad\qquad \vee \Big[\sum_{j\leqslant I_1} 2^j\delta\sqrt{|\log\delta|}2^{j(\nu-1/2)} + \sum_{j>I_1} 2^j|\boldsymbol{\beta}_{j,\eta}|\Big], \end{aligned}$$

which are of the proper order. Turning to Bs and Sb, we write, using inequalities (6.21) and (6.23)

$$\begin{aligned} Bs &\leqslant \sum_{j\leqslant J} 2^j\,\mathbb{E}\big[\sup_{\eta\in\mathcal{Z}_j} |\widehat{\boldsymbol{\beta}}_{j,\eta} - \boldsymbol{\beta}_{j,\eta}| \mathbf{1}_{\{|\widehat{\boldsymbol{\beta}}_{j,\eta}-\boldsymbol{\beta}_{j,\eta}|>\overline{S_j}(\delta,\varepsilon)/2\}}\big] \\ &\leqslant \sum_{j\leqslant J} 2^j\,\mathbb{E}[\sup_{\eta\in\mathcal{Z}_j} |\widehat{\boldsymbol{\beta}}_{j,\eta} - \boldsymbol{\beta}_{j,\eta}|^2]^{1/2}\,\mathbb{P}(\exists\eta\in\mathcal{Z}_j,\ |\widehat{\boldsymbol{\beta}}_{j,\eta} - \boldsymbol{\beta}_{j,\eta}| > \overline{S_j}(\delta,\varepsilon)/2)^{1/2} \\ &\lesssim \sum_{j\leqslant J} 2^j\Big[(j+1)\big(\varepsilon 2^{j\nu} \vee \delta 2^{j(\nu-1/2)}\big) \vee |\boldsymbol{\beta}_{j,\eta}|\mathbf{1}_{\{j\geqslant j_0\}}\Big]\Big[2^{2j}(\varepsilon^{\tau^2} \vee \delta^{\tau^2})\Big]^{1/2}. \end{aligned}$$

Now apply inequality (6.21) and the fact that $|\boldsymbol{\beta}_{j,\eta}| \lesssim 2^{-j}$ to derive

$$\begin{aligned} Sb &\leqslant \sum_{j\leqslant J} 2^j\,\mathbb{E}\big[\sup_{\eta\in\mathcal{Z}_j} |\boldsymbol{\beta}_{j,\eta}| \mathbf{1}_{\{|\widehat{\boldsymbol{\beta}}_{j,\eta}-\boldsymbol{\beta}_{j,\eta}|>\overline{S_j}(\delta,\varepsilon)\}}\big] \\ &\lesssim \sum_{j\leqslant J} 2^{2j}\,\mathbb{P}\big(|\widehat{\boldsymbol{\beta}}_{j,\eta} - \boldsymbol{\beta}_{j,\eta}| > \overline{S_j}(\delta,\varepsilon)\big) \\ &\lesssim \sum_{j\leqslant J} 2^{2j}(\varepsilon^{\tau^2} \vee \delta^{\tau^2}). \end{aligned}$$

It is clear that for a well chosen τ these terms are smaller than the announced rates. □

Acknowledgements

The author would like to thank his advisor Dominique Picard for numerous and fruitful discussions and suggestions.

Appendix A

Wavelets and Besov spaces in statistical estimation.

Contents

A.1 Multi Resolution Analysis 155

A.2 Wavelets and approximation theory 157

A.3 Statistical estimation using wavelets 159

Even if we don't make an explicit use of it, wavelets and Besov spaces on $\mathbb{R}^d$ inspire (conceptually as well as historically) a wide part of the results and techniques at stake in this thesis. For these reasons, we proceed to a brief introduction to their theory (in the case $d = 1$), reviewing the main steps of their construction in a summary way (section A.1) as well as their main connections with functional analysis and approximation theory (section A.2). We show then how they conveniently apply to the field of statistical estimation (section A.3), either in the case of direct estimation or inverse problems. This chapter relies for the most part on [41], [60] and [16].

A.1 Multi Resolution Analysis

We tackle the introduction of wavelets via the definition of a MRA. A MRA is a nested sequence of spaces meant to capture finer details of signals as the level (the resolution) increases.

Definition A.1.1 (Multi Resolution Analysis)**.** *A MRA of* $\mathbb{L}^2(\mathbb{R})$ *is an increasing sequence of closed subsets* $(V_j)_{j\in\mathbb{Z}}$ *such that*

1. $\bigcap_{j\in\mathbb{Z}} V_j = \{0\}$.
2. $\overline{\bigcup_{j\in\mathbb{Z}} V_j} = \mathbb{L}^2(\mathbb{R})$.
3. $\forall f \in \mathbb{L}^2(\mathbb{R})$, $\forall j \in \mathbb{Z}$, $f(x) \in V_j \Leftrightarrow f(2x) \in V_{j+1}$.

4. $\forall f \in \mathbb{L}^2(\mathbb{R})$, $\forall k \in \mathbb{Z}$, $f(x) \in V_0 \Leftrightarrow f(x-k) \in V_0$.

5. *There exists a function* $\boldsymbol{\varphi} \in V_0$*, called a scaling function or father wavelet, such that the set* $\{\boldsymbol{\varphi}(x-k), k \in \mathbb{Z}\}$ *constitutes an orthonormal basis of* V_0.

The basis $\{\boldsymbol{\varphi}(x-k), k \in \mathbb{Z}\}$ gives way for a refinement in V_j, since by construction the set $\{\boldsymbol{\varphi}_{j,k}(x) = 2^{j/2}(2^j x - k), k \in \mathbb{Z}\}$ constitutes an orthonormal basis of V_j. However the projection $\boldsymbol{P}_{V_j} f$ and $\boldsymbol{P}_{V_{j+1}} f$ are partly redundant, since V_j and V_{j+1} are not orthogonal. This means that, for any function $f \in \mathbb{L}^2(\mathbb{R})$, we can't make use of

$$\boldsymbol{P}_{V_j} f = \sum_{k \in \mathbb{Z}} \langle f, \boldsymbol{\varphi}_{j,k} \rangle \boldsymbol{\varphi}_{j,k}$$

to compute rapidly $\boldsymbol{P}_{V_{j+1}} f$, and we have to calculate all the coefficients $\big(\langle f, \boldsymbol{\varphi}_{j+1,k} \rangle\big)_{k \in \mathbb{Z}}$. A more convenient framework is to work with the part of V_{j+1} which remains orthogonal to V_j

$$W_j = V_{j+1} \ominus V_j \,,$$

so that we can write

$$\boldsymbol{P}_{V_{j+1}} f = \boldsymbol{P}_{V_j} f + \boldsymbol{P}_{W_j} f \,,$$

where the sum is orthogonal. A handy result from wavelet theory asserts that the space W_j is itself spanned by the translations and rescaling of a single function $\boldsymbol{\psi}$ called a mother wavelet. Namely,

$$W_j = \operatorname{span}\{\boldsymbol{\psi}_{j,k}, k \in \mathbb{Z}\} \,,$$

with obvious notations. We hence have decomposed $\mathbb{L}^2(\mathbb{R})$ into the orthogonal sum

$$\mathbb{L}^2(\mathbb{R}) = V_0 \overset{\perp}{\bigoplus} \overset{\perp}{\bigoplus_{j \geqslant 1}} W_j$$

Note that the index 0 is in fact arbitrary and can be set to any integer $j_0 \in \mathbb{N}$. We can now safely write, for any function $f \in \mathbb{L}^2(\mathbb{R})$, the decomposition

$$f = \sum_{k \in \mathbb{Z}} \alpha_{j_0} \boldsymbol{\varphi}_{j_0,k} + \sum_{j > j_0} \sum_{k \in \mathbb{Z}} \beta_{j,k} \boldsymbol{\psi}_{j_0,k} \,,$$

where the wavelet coefficients are defined as $\alpha_{j_0,k} = \langle f, \boldsymbol{\varphi}_{j_0,k} \rangle$ and $\beta_{j,k} = \langle f, \boldsymbol{\psi}_{j,k} \rangle$. Of course, the constraints imposed by the MRA property imply constraints on the mother and the father wavelets as well (see [41, Chapter 5]). Also, the quality of the MRA is dictated by the features of those functions, such as null moments and support. The Daubechies wavelets (see [60, Chap. 7]) for example provide compactly supported wavelets with arbitrary null-moments.

A.2 Wavelets and approximation theory

In this section we show how the wavelet coefficients of a function $f \in \mathbb{L}^2(\mathbb{R})$ relate to its regularity in a certain sense. To this end, we first introduce the Besov spaces $B^s_{\pi,r}$ on $\mathbb{R}$. These include for example the Sobolev space $\mathcal{W}^s = B^s_{2,2}$ as well as the Hölder spaces H^s for certain values of s. There exists several ways to define such spaces, via the moduli of continuity, via interpolation theory or Littlewood-Paley decomposition for example. We first follow the definition from Cohen [16, Chap. 3] based on the moduli of continuity.

A.2.1 Besov spaces

Definition A.2.1. *Let $f \in \mathbb{L}^\pi(\mathbb{R})$, $1 \leqslant \pi \leqslant \infty$. Let $\tau_h f(x) = f(x-h)$ and $\Delta_h f = \tau_h f - f$. For $t \geqslant 0$, the n-th order $\mathbb{L}^p$ modulus of smoothness of f is defined by*

$$\omega_n(f,t)_p = \sup_{|h| \leqslant t} \|\Delta_h^n f\|_p \,.$$

The modulus of smoothness is decreasing as a function of t, and translates the degree of accuracy to which $\tau_h f$ approximates f in $\mathbb{L}^p$.

Definition A.2.2. *Let $\pi, r \geqslant 1$, $s > 0$. The Besov space $B^s_{\pi,r}(\mathbb{R})$ is defined as the set of functions $f \in \mathbb{L}^\pi(\mathbb{R})$ such that*

$$\left(2^{js} w_n(f, 2^{-j})_\pi\right)_{j \geqslant 0} \in \ell^r$$

where n is an integer such that $s < n$. A natural norm on $B^s_{\pi,r}$ is hence

$$\|f\|_{B^s_{\pi,r}} = \|f\|_\pi + \left\|\left(2^{js} w_n(f, 2^{-j})_\pi\right)_{j \geqslant 0}\right\|_{\ell^r} .$$

As stated before, Besov spaces include several classical functional spaces. For example, we have $H^s = B^s_{\infty,\infty}$ when $s \notin \mathbb{N}$ as well as $W^{s,p} = B^s_{p,p}$ when s is not an integer, or when $p = 2$.

A.2.2 Besov spaces and Littlewood-Paley decomposition

It is noteworthy that Besov spaces also have a characterization in terms of Littlewood-Paley decomposition. This reveals the link between the construction of wavelets and the construction of needlets performed in section 5.2. The material of this section echoes [41, Chapter 9]. We consider here the usual Schwartz space $S'(\mathbb{R})$.
We remind that b is a function satisfying the following : let a be a $\mathcal{C}^\infty(\mathbb{R})$ symmetric function, compactly supported in $[-1,1]$, decreasing on $\mathbb{R}^+$, such that for all $x \in \mathbb{R}$, $0 \leqslant a(x) \leqslant 1$ and for all $|x| \leqslant 1/2$, $|a(x)| = 1$. Define , for all $x \in \mathbb{R}$,

$$b^2(x) = a(\frac{x}{2}) - a(x) \,.$$

b^2 is a positive function, supported in $[-2;-1/2]\bigcup[1/2;2]$, satisfying by construction

$$\forall |x| \geqslant 1, \sum_{j\geqslant 0} b^2(\frac{x}{2^j}) = 1\,. \tag{A.1}$$

For every function $f \in S'(\mathbb{R})$, one can write

$$f(\xi) = a(\xi)\hat{f}(\xi) + \sum_{j=0}^{\infty} b(\frac{\xi}{2^j})\hat{f}(\xi)\,, \tag{A.2}$$

where $\hat{\cdot}$ denotes the Fourier transform. A different way of formulating (A.2) is

$$f = \sum_{j=-1}^{\infty} \mathcal{D}_j f \,(weakly)\,,$$

where $\mathcal{D}_j f = \beta * f$ for $j = 0, 1, ...$ and $\mathcal{D}_{-1} f = \alpha * f$, and where α and β are the two functions whose Fourier transform are a and b respectively. The behavior of the atoms $\mathcal{D}_j f$ actually characterize its belonging to the Besov space $B^s_{\pi,r}$, as stated in the theorem below:

Theorem A.2.3. *Let $1 \leqslant \pi, r \leqslant \infty$, $s > 0$ and $f \in \mathbb{L}^\pi(\mathbb{R})$. Then f belongs to $B^s_{\pi,r}$ if and only if*

$$\|\mathcal{D}_{-1} f\|_\pi < \infty \text{ and } \left(2^{js}\|\mathcal{D}_j f\|_\pi\right)_{j\geqslant 0} \in \ell^r\,.$$

A.2.3 Characterization of Besov spaces via wavelet expansion

The power of the wavelet theory is to provide a way to represent Besov spaces sequentially, via the behavior of the wavelet coefficients of a function. Hereby, wavelets capture a wide variety of phenomenons embodied by the different values of π, r and s. We have the following theorem:

Theorem A.2.4. *Let $N \in \mathbb{N}$, $0 < s < N+1$, $1 \leqslant \pi, r \leqslant \infty$ and $\boldsymbol{\varphi}, \boldsymbol{\psi}$ a scaling function/wavelet system. Suppose there exists a positive decreasing function H such that*

1. $\forall x, y,\ |\sum_k \boldsymbol{\varphi}(x-k)\boldsymbol{\varphi}(y-k)| \leqslant H(|x-y|)$.
2. $\int H(u)du|u|^{N+1}du < \infty$.
3. $\boldsymbol{\varphi}^{N+1}$ *exists and* $\sup_{x\in\mathbb{R}} |\sum_k \boldsymbol{\varphi}^{N+1}(x-k)| < \infty$.

Then f belongs to the Besov body $B^s_{\pi,r}$ if and only if f belongs to $\mathbb{L}^\pi(\mathbb{R})$ and there exists a positive sequence $(\varepsilon_j)_{j\geqslant 0} \in \ell^r$ such that for all $j \geqslant 0$, $\|f - \boldsymbol{P}_{V_j} f\|_p \leqslant 2^{-js}\varepsilon_j$.

Thus, the Besov body $B^s_{\pi,r}$ is equipped with the (equivalent) norm

$$\|f\|_{B^s_{\pi,r}} = \|\alpha_0\|_{\ell^\pi} + \left\|\left(2^{j(s-1/\pi+1/2)}\|(\beta_{j,k})_{k\leqslant 2^j}\|_{\ell^\pi}\right)_{j\geqslant 0}\right\|_{\ell^r}\,.$$

A.3 Statistical estimation using wavelets

A.3.1 Direct estimation ($\boldsymbol{K} = \boldsymbol{I}$) using wavelets; linear and thresholding estimators

In this section we will detail the motivations underlying thresholding procedures. To this end, we will consider the minimax risk induced by the $\mathbb{L}^p$ norm on Besov spaces $B^s_{\pi,r}$

$$\inf_{\tilde{\boldsymbol{f}}} \sup_{\boldsymbol{f} \in B^s_{\pi,r}(M)} \|\tilde{\boldsymbol{f}} - \boldsymbol{f}\|_p \,.$$

A notable fact is that the exponents π and p need not be the same a priori (the case $p = \pi$ is referred to as the 'matched' case in the literature). As a matter of fact, in order to assess the quality of an algorithm, one is usually brought to consider more specific losses than the usual quadratic risk. An underlying motivation is for example that a good approximation of $\boldsymbol{f}$ in $\mathbb{L}^2$ norm can perform very poorly locally. In a more generic manner, different types of $\mathbb{L}^p$ losses for $1 \leqslant p \leqslant \infty$ will translate different type of information on the convergence of $\tilde{\boldsymbol{f}}$ to $\boldsymbol{f}$. Indeed, one localized but important error will affect the $\mathbb{L}^\infty$ norm much more than its $\mathbb{L}^2$ counterpart, while a small error all along the space of definition will be exacerbated by the $\mathbb{L}^1$ norm more than by the $\mathbb{L}^2$ norm. For these reasons, there is no loss which is considered as superior to the others in terms of quality of approximation, and an efficient procedure should provide rates of convergence available for a wide range of such losses.
Wavelet based procedures on Besov spaces allow to do so. Of course, the rates will depend on the relation between the chosen index p and the regularity parameters s, π, q. A remarkable feature is that the type of procedure achieving the minimax rates also depends on these regions. Rates of convergence for generic lossed $\mathbb{L}^p(\mathbb{R})$, $p > 1$ on Besov spaces were first exhibited in the paper of Donoho et al. [28], in the context of density estimation. Suppose hence we observe a sample $(X_1, ..., X_n)$ with common density $\boldsymbol{f}$. Let us first define a refinement of the above Besov spaces. We consider, for a fixed $L > 0$, the set

$$\widetilde{B}^s_{\pi,r}(M) = \left\{ \boldsymbol{f} \text{ s.t } \int \boldsymbol{f} = 1, \text{supp}\boldsymbol{f} \subset [-L, L] \text{ and } \boldsymbol{f} \in B^s_{\pi,r}(M) \right\},$$

and also study the corresponding linear minimax risk where the set of estimators is restricted to the linear ones. Let us start with a "negative" result. We have the

Theorem A.3.1 (Härdle et al. [41], Theorem 10.3 and Theorem 10.4)**.**

$$\inf_{\tilde{\boldsymbol{f}}\ linear} \sup_{\boldsymbol{f} \in B^s_{\pi,r}(M)} \|\tilde{\boldsymbol{f}} - \boldsymbol{f}\|_p^p \sim C n^{-\frac{s'p}{2s'+1}} \,,$$

where $s' = s - (1/\pi - 1/p)_+$.

The reason why it is negative, as we shall see, is that if $p > \pi$, this rate is actually not minimax. This means that only non linear estimators (such as thresholding ones) can attain the minimax optimum on certain zones. Indeed, by an adequate thresolding procedure, Donoho et al. [28] exhibited the following rates of convergence:

$$\inf_{\tilde{\boldsymbol{f}}} \sup_{\boldsymbol{f}\in\widetilde{B}^s_{\pi,r}} \|\tilde{\boldsymbol{f}} - \boldsymbol{f}\|_p^p \leqslant \begin{cases} C(\log n)^{\delta} n^{-\alpha_1 p} & \text{if } \pi > \frac{p}{2s+1},\ \alpha_1 = \frac{s}{2s+1}\,, \\ C(\log n)^{\delta'} \left(\frac{\log n}{n}\right)^{\alpha_2 p} & \text{if } \pi = \frac{p}{2s+1},\ \alpha_2 = \frac{s-1/\pi+1/p}{2(s-1/\pi)+1}\,, \\ C\left(\frac{\log n}{n}\right)^{\alpha_2 p} & \text{if } \pi < \frac{p}{2s+1}\,. \end{cases}$$

These results call for several comments:
First, they confirm the tendency that linear estimators are sub-optimal in the case where $p > \pi$ since in this case, $s - 1/\pi + 1/p < s$.
Second, the techniques used to derived these upper bounds on the minimax risk are classical thresholding procedures performed on each empirical wavelet coefficient $\widehat{\boldsymbol{\beta}}_{j,k} = n^{-1}\sum_{i=1}^n \boldsymbol{\psi}_{j,k}(X_i)$, the thresholding level being proportional to $\sqrt{\log n/n}$.
Third, the convergence rates present an 'elbow phenomenon' depending on the relative value of p, π and s. The zones $\pi > p(2s+1)^{-1}$ and $\pi \leqslant p(2s+1)^{-1}$ are referred to as the regular and sparse zone respectively, according to the wavelet coefficients' behavior of the functions living in each of these zones.
Finally, all these rates of convergence are essentially minimax, up to logarithmic factors in n. We do not detail this here, and invite the reader to refer to Härdle et al. [41] for a full discussion on the subject.

A.3.2 Application of wavelets to inverse problems

This section echoes section 1.4.1, and we refer to the latter for precision on the framework. Remark that $\boldsymbol{f}$ is now defined on $[0,1]$ (and not $\mathbb{R}$). Here, we present the estimator more in details, and its corresponding rates of convergence on $\mathbb{L}^p$ spaces. Define the estimator $\widetilde{\boldsymbol{\beta}}_{j,k}$ of $\boldsymbol{\beta}_{j,k}$ as

$$\widetilde{\boldsymbol{\beta}}_{j,k} = \widehat{\boldsymbol{\beta}}_{j,k} \mathbf{1}_{\left\{|\widehat{\boldsymbol{\beta}}_{j,k}| > \tau 2^{j\nu}\sqrt{\frac{\log n}{n}}\right\}}\,.$$

Pick $2^J \sim \left(\frac{\log n}{n}\right)^{-\frac{1}{2\nu+1}}$ and define

$$\tilde{\boldsymbol{f}} = \sum_{j\leqslant J}\sum_{k\leqslant 2^j} \widetilde{\boldsymbol{\beta}}_{j,k}\boldsymbol{\psi}_{j,k}\,.$$

We have the

Theorem A.3.2 (Donoho et al. [28], Proposition 1). *Let $p, \pi \geqslant 1$, $s > 1/\pi$ and*

$$r \leqslant \min\left\{\frac{p(2\nu+1)}{2(\nu+s)+1}, \frac{(2\nu+1)p-2}{2(s+\nu)-2/\pi+1}\right\}.$$

The above estimator achieves the following rates of convergence:

$$\sup_{\boldsymbol{f}\in B^s_{\pi,r}(M)} \|\widetilde{\boldsymbol{f}} - \boldsymbol{f}\|_p^p \leqslant \begin{cases} C\big(\frac{\log n}{n}\big)^{\alpha_1 p} & \text{if} \quad s \geqslant (2\nu+1)\big(\frac{p}{2\pi} - \frac{1}{2}\big), \\ & \alpha_1 = \frac{s}{2(s+\nu)+1} \\ C\big(\frac{\log n}{n}\big)^{\alpha_2 p} & \text{if} \quad \frac{1}{\pi} - \frac{1}{2} - \nu \leqslant s < (2\nu+1)\big(\frac{p}{2\pi} - \frac{1}{2}\big), \\ & \alpha_2 = \frac{(s-1/\pi+1/p)}{1+2(s+\nu-1/\pi)} \end{cases}$$

As above, we notice an 'elbow effect' in the expression of the rates, depending this time on the DIP ν as well. These rates can also be proved to be minimax in the present setting (see for example [85]).
This 'wavelet scenario' type of convergence also appears in some algorithms derived from needlets, as in Kerkyacharian et al. [51], and is hereby to be related with the results of Chapter 6 (in the case $\delta = 0$). This is not surprising since the tools at stake here meet those used for the construction of needlets (in particular, the fact that the wavelets used present a compact frequential support).

Appendix B

Proof of the lower bound in (2.5)

Theorem B.0.3. *Let $Q > 0$, $s, M > 0$ and suppose that $\boldsymbol{K}$ belongs to the set $\mathcal{K}(Q) \triangleq \{\boldsymbol{K}, \|(\boldsymbol{K}^\ell)^{-1}\| \leqslant Q\ell^\nu\}$. Then*

$$\inf_{\tilde{\boldsymbol{f}}} \sup_{\substack{\boldsymbol{f}\in\mathcal{W}^s(M)\\ \boldsymbol{K}\in\mathcal{K}(Q)}} \|\tilde{\boldsymbol{f}} - \boldsymbol{f}\| \gtrsim \delta^{\frac{2s}{2(s+\nu)+1}} \vee \varepsilon^{\frac{2s}{2(s+\nu)+1}}\,.$$

Proof. This proof is performed in Efromovich and Koltchinskii [30] in a parallel way, where both the operator and target function are blurred with random noise. We follow a different path here, based on an 'Assouad' strategy. The case $\delta = 0$ is classic and will not be treated. We concentrate instead on the case where $\varepsilon = 0$. We will follow the directive ideas in Hoffmann and Reiß [40] and define the set of test functions $\boldsymbol{f}_0, ..., \boldsymbol{f}_m$ via $\boldsymbol{f}_i = \boldsymbol{K}_i^{-1}\boldsymbol{K}\boldsymbol{f}_0$ where $\boldsymbol{K}_i$ is an adequate perturbation of a reference operator $\boldsymbol{K}$ (and $\boldsymbol{K}_0 = \boldsymbol{I}$). The proper functioning of the proof requires the tuning of several constants which we will denote by c_i where i is an integer. We will not perform this task thoroughly, but rather indicate that the correct choice of such constants leads to the desired property.
Let hence $L \sim \delta^{-\frac{2}{2(s+\nu)+1}}$ and $\boldsymbol{f}_0 = c_0\mathbf{1}$. Obviously, $\boldsymbol{f}_0 \in \mathcal{W}^s(M)$ for a small enough c_0. We define the diagonal operator $\boldsymbol{K}$ via $(\boldsymbol{K})_{m,n} = c_1 L^{-\nu}\mathbf{1}_{\{m=n\}}$, $m, n \leqslant L$, and the perturbing matrices with size $L \times L$

$$(\boldsymbol{H}_i)_{m,n} = \mathbf{1}_{\{m=i,n=1\}},\ i = 1, ..., L\,.$$

Let $\omega \in \{0,1\}^L$ and define

$$\boldsymbol{K}_\omega = \boldsymbol{K} + c_2\delta\boldsymbol{H}_\omega,\ \text{where } \boldsymbol{H}_\omega = \sum_{i\leqslant L}\omega_i\boldsymbol{H}_i\,.$$

Since, for all $\omega \in \{0,1\}^L$, we have $\|\boldsymbol{H}_\omega\|_{op} \leqslant CL^{\frac{1}{2}}$, we also have

$$\delta\|\boldsymbol{K}^{-1}\|_{op}\|\boldsymbol{H}_\omega\|_{op} \leqslant C\delta^{\frac{2s}{2(s+\nu)+1}} \lesssim 1\,.$$

Thus by the usual Neumann series argument (see the proof of Theorem 3.3.1), $\boldsymbol{K}_\omega \in \mathcal{K}(Q)$ for well adjusted constants.
In the sequel, we will make use of the following decompositions: first, note that

$$\begin{aligned}\boldsymbol{f}_\omega - \boldsymbol{f}_{\overline{\omega}} = \delta \boldsymbol{K}^{-1}\big(\boldsymbol{H}_\omega - \boldsymbol{H}_{\overline{\omega}}\big)\boldsymbol{f}_0 + \big(\delta \boldsymbol{K}^{-1}\boldsymbol{H}_\omega\big)^2\big(\boldsymbol{I} + \delta \boldsymbol{K}^{-1}\boldsymbol{H}_\omega\big)^{-1}\boldsymbol{f}_0 \\ - \big(\delta \boldsymbol{K}^{-1}\boldsymbol{H}_{\overline{\omega}}\big)^2\big(\boldsymbol{I} + \delta \boldsymbol{K}^{-1}\boldsymbol{H}_{\overline{\omega}}\big)^{-1}\boldsymbol{f}_0\,. \qquad \text{(B.1)}\end{aligned}$$

This is equivalent to

$$\begin{aligned}\boldsymbol{f}_\omega - \boldsymbol{f}_{\overline{\omega}} &= \delta \boldsymbol{K}^{-1}\big(\boldsymbol{H}_\omega - \boldsymbol{H}_{\overline{\omega}}\big)\boldsymbol{f}_0 + \sum_{k\geqslant 2}\big(\delta \boldsymbol{K}^{-1}\boldsymbol{H}_\omega\big)^k\boldsymbol{f}_0 - \sum_{k\geqslant 2}\big(\delta \boldsymbol{K}^{-1}\boldsymbol{H}_{\overline{\omega}}\big)^k\boldsymbol{f}_0 \\ &= \delta \boldsymbol{K}^{-1}\big(\boldsymbol{H}_\omega - \boldsymbol{H}_{\overline{\omega}}\big)\boldsymbol{f}_0 + \sum_{k\geqslant 2}\delta^k L^{k\nu}\big(\boldsymbol{H}_\omega^k - \boldsymbol{H}_{\overline{\omega}}^k\big)\boldsymbol{f}_0 \\ &= \delta \boldsymbol{K}^{-1}\big(\boldsymbol{H}_\omega - \boldsymbol{H}_{\overline{\omega}}\big)\boldsymbol{f}_0 + \delta^2 L^{2\nu}\sum_{k\geqslant 0}\delta^k L^{k\nu}\big(\boldsymbol{H}_\omega^{k+2} - \boldsymbol{H}_{\overline{\omega}}^{k+2}\big)\boldsymbol{f}_0\,. \qquad \text{(B.2)}\end{aligned}$$

Let us define, for all ω, $\boldsymbol{f}_\omega = \boldsymbol{K}_\omega^{-1}\boldsymbol{K}\boldsymbol{f}_0$. Then, in virtue of (B.1), $\boldsymbol{f}_\omega \in \mathcal{W}^s(M)$. Indeed, in this decomposition, the first term satisfies

$$\begin{aligned}\|\delta \boldsymbol{K}^{-1}\big(\boldsymbol{H}_\omega - \boldsymbol{H}_{\overline{\omega}}\big)\boldsymbol{f}_0\|_{\mathcal{W}^s}^2 &= \delta^2\sum_{\ell\leqslant L}\ell^{2s}\langle \boldsymbol{K}^{-1}\big(\boldsymbol{H}_\omega - \boldsymbol{H}_{\overline{\omega}}\big)\boldsymbol{f}_0, e_\ell\rangle^2 \\ &\leqslant C\delta^2 L^{2\nu+2s+1} \\ &\lesssim 1\,,\end{aligned}$$

whereas the second (and third) term can be bounded by

$$\begin{aligned}\|\big(\delta \boldsymbol{K}^{-1}\boldsymbol{H}_\omega\big)^2\big(\boldsymbol{I} + \delta \boldsymbol{K}^{-1}\boldsymbol{H}_\omega\big)^{-1}\boldsymbol{f}_0\|_{\mathcal{W}^s}^2 &= \delta^4\sum_{\ell\leqslant L}\ell^{2s}\langle \boldsymbol{K}^{-1}\boldsymbol{H}_\omega\big(\boldsymbol{I} + \delta \boldsymbol{K}^{-1}\boldsymbol{H}_\omega\big)^{-1}\boldsymbol{f}_0 \\ &\qquad\qquad , {}^{\boldsymbol{t}}\boldsymbol{H}_\omega\,{}^{\boldsymbol{t}}\boldsymbol{K}^{-1}e_\ell\rangle^2 \\ &\leqslant C\delta^4\sum_{\ell\leqslant L}\ell^{2s}L^{2\nu+1}L^{2\nu} \\ &\leqslant C\delta^2 L^{2\nu+2s+1}L^{2\nu+1} \\ &\lesssim \delta^{\frac{4s}{2(s+\nu)+1}}\,.\end{aligned}$$

The next step in the establishment of the lower bound is to lower-bound the $\mathbb{L}^2$ differences between two candidate functions. More precisely, we have to show (see Korostelev and Tsybakov [54]) that, if ω and $\overline{\omega}$ only differ by one coordinate, then $\|\boldsymbol{f}_\omega - \boldsymbol{f}_{\overline{\omega}}\| \geqslant C\delta L^\nu$. We will hence make this assumption. In order to lower bound $\|\boldsymbol{f}_\omega - \boldsymbol{f}_{\overline{\omega}}\|$, we use (B.2). In that decomposition, the first term satisfies

$$\|\delta \boldsymbol{K}^{-1}\big(\boldsymbol{H}_\omega - \boldsymbol{H}_{\overline{\omega}}\big)\boldsymbol{f}_0\| = \delta L^\nu\sum_{i\leqslant L}|\omega_i - \overline{\omega}_i| = \delta L^\nu$$

whereas the second term is upper-bounded by

$$\begin{aligned}\|\delta^2 L^{2\nu}\sum_{k\geqslant 0}\delta^k L^{k\nu}\big(\boldsymbol{H}_\omega^{k+2}-\boldsymbol{H}_{\overline{\omega}}^{k+2}\big)\boldsymbol{f}_0\| &\leqslant \delta^2 L^{2\nu}\sum_{k\geqslant 1}\delta^k L^{k\nu}(k+2)L^{\frac{k+1}{2}}\|\boldsymbol{H}_\omega-\boldsymbol{H}_{\overline{\omega}}\|_{op}\|\boldsymbol{f}_0\|\\ &\leqslant C\delta^2 L^{2\nu+1/2}\\ &\leqslant C\delta L^\nu \delta^{\frac{2s}{2(s+\nu+1)}}\,.\end{aligned}$$

Thus, for well chosen constants, $\|\boldsymbol{f}_\omega-\boldsymbol{f}_{\overline{\omega}}\|\geqslant C\delta L^\nu$.
Also, the likelihood of $\mathbb{P}^{\boldsymbol{K}_\omega}$ under he law $\mathbb{P}^{\boldsymbol{K}_{\overline{\omega}}}$ corresponding to the parameters $\boldsymbol{K}_\omega$ and $\boldsymbol{K}_{\overline{\omega}}$ is

$$\Lambda(\boldsymbol{K}_\omega,\boldsymbol{K}_{\overline{\omega}})=\exp\big(\delta^{-1}\langle\boldsymbol{K}_\omega-\boldsymbol{K}_{\overline{\omega}},\boldsymbol{B}\rangle_{\mathrm{HS}}-\frac{1}{2}\delta^{-2}\|\boldsymbol{K}_\omega-\boldsymbol{K}_{\overline{\omega}}\|_{\mathrm{HS}}^2\big)$$

and the two models remain contiguous as soon as the Hilbert-Schmidt norm $\|\boldsymbol{K}_\omega-\boldsymbol{K}_{\overline{\omega}}\|_{\mathrm{HS}}$ remains of order δ, which is the case here.
The rest of the proof can be deduced following the lines of Korostelev and Tsybakov [54], Theorem 2.6.4. □

Bibliography

[1] J. Abate, G.L. Choudhury, and W. Whitt. On the Laguerre method for numerically inverting Laplace transforms. *INFORMS Journal on Computing*, 8:413–427, 1996.

[2] F. Abramovich and B. W. Silverman. Wavelet decomposition approaches to statistical inverse problems. *Biometrika*, 85:115–129, 1998.

[3] F. Abramovich, M. Pensky, and Y. Rozenholc. Laplace deconvolution with noisy observations. *EJS*, 7:1094–1128, 2013.

[4] M. Ameloot, J.M. Beechem, and L. Brand. Simultaneous analysis of multiple fluorescence decay curves by Laplace transforms. deconvolution with reference or excitation profiles. *Biophys Chem.*, 23(3-4):155–71, 1986.

[5] L. Birgé. An alternative point of view on Lepski's method. *Lecture Notes-Monograph Series*, 36:113–133, 2001.

[6] B. Bongioanni and J. L. Torrea. What is a Sobolev space for the laguerre function systems? *Studia Mathematica*, 192:147–172, 2009. doi: 10.4064/sm192-2-4.

[7] A. Böttcher and S.M. Grudsky. *Spectral Properties of Banded Toeplitz Matrices.* Siam edition, 2005.

[8] O. Bousquet. A Bennett concentration inequality and its application to suprema of empirical processes. *C.R. Math. Acad. Sci. Paris*, 334:495–500, 2002.

[9] T. Cai. Adaptive wavelet estimation: A block thresholding and oracle inequality approach. *Ann. Statist.*, 27:898–924, 1999.

[10] T. Cai and H. Zou. A data-driven block thresholding approach to wavelet estimation. *Ann. Statist.*, 37:569–595, 2009.

[11] L. Cavalier and N. W. Hengartner. Adaptive estimation for inverse problems with noisy operators. *Inverse Problems*, 21:1345–1361, 2005.

[12] L. Cavalier and M. Raimondo. Wavelet deconvolution with noisy eigenvalues. *IEEE Trans. Signal Processing*, 55:2414–2424, 2007.

[13] L. Cavalier and A. Tsybakov. Sharp adaptation for inverse problems with random noise. *Probab. Theory Relat. Fields*, 123:323–354, 2002.

[14] O. Christensen. *An Introduction to Frames and Riesz Bases*. Birkhäuser, 2007.

[15] A.C. Cinzori and P.K. Lamm. Future polynomial regularization of ill-posed volterra equations. *SIAM J. Num. Anal.*, 37:949–979, 2000.

[16] A. Cohen. *Numerical analysis of wavelet methods, Vol32 of Studies in mathematics and its application*. Elsevier, 2003.

[17] A. Cohen, M. Hoffmann, and M. Reiß. Adaptive wavelet Galerkin methods for linear inverse problems. *SIAM J. Numer. Anal.*, 42:1479–1501, 2004.

[18] F. Comte and C. Lacour. Data-driven density estimation in the presence of additive noise with unknown distribution. *J. R.l Stat. Soc. Ser. B Statist. Methodol.*, 73 (4):601–627, 2011.

[19] F. Comte, C. Guenod, M. Pensky, and Y. Rozenholc. Laplace deconvolution and its application to dynamic contrast enhanced imaging. *hal-00715943*, 2012.

[20] J.G. McNally C. Preza J.A. Conchello and L.J. Thomas. Artifacts in computational optical-sectioning microscopy. *J. Opt. Soc. Am. A*, 11:1056–1067, 1994.

[21] T. Coulhon, G. Kerkyacharian, and P. Petrushev. Heat kernel generated frames in the setting of Dirichlet spaces. *Journal of Fourier Analysis and Applications*, 18: 995–1066, 2012.

[22] K. R. Davidson and S. J. Szarek. *Local operator theory, random matrices and Banach spaces. In Handbook on the Geometry of Banach Spaces 1*. North-Holland, Amsterdam, (w. b. johnson and j. lindenstrauss, eds.) edition, 2001.

[23] S. Delattre, M. Hoffmann, D. Picard, and T. Vareschi. Blockwise SVD with error in the operator and application to blind deconvolution. *EJS*, 6:2274–2308, 2012.

[24] D. Delyon and A. Juditsky. On minimax wavelet estimators. *Applied and Computational Harmonic Analysis*, 3(3):215 – 228, 1996.

[25] A.K. Dey, C.F. Martin, and F.H. Ruymgaart. Input recovery from noisy output data, using regularized inversion of Laplace transform. *IEEE Trans. Inform. Theory*, 44:1125–1130, 1998.

[26] D. Donoho. Nonlinear solution of linear inverse problems by wavelet-vaguelette decomposition. *Appl. Comput. Harmon. Anal.*, 2:101–126, 1995.

[27] D. Donoho and I Johnstone. Ideal spatial adaptation by wavelet shrinkage. *Biometrika*, 81(3):425–455, 1994.

[28] D. Donoho, I. Johnstone, G. Kerkyacharian, and D. Picard. Density estimation by wavelet thresholding. *Ann. Statist.*, 24(2):508–539, 1996.

[29] D. L. Donoho and I. M. Johnstone. Adapting to unknown smoothness via wavelet shrinkage. *J. Amer. Statist. Assoc.*, 90:1200–1224, 1995.

[30] S. Efromovich and V. Koltchinskii. On inverse problems with unknown operators. *IEEE Trans. Inf. Theory*, 47:2876–2894, 2001.

[31] Gervens T. Freeden, W. and M. Schreiner. *Constructive Approximation on the Sphere (With Applications to Geomathematics).* Oxford Sciences Publication. Clarendon Press, Oxford., 1998.

[32] Michel D. Freeden, W. and V. Michel. Local multiscale approximations of geostrophic oceanic flow: theoretical background and aspects of scientific computing. *Mar. Geod.*, 28:313–329, 2005.

[33] S.F. Gibson and F. Lanni. Diffraction by a circular aperture as a model for three-dimensional optical microscopy. *J. Opt. Soc. Am. A*, 6, 1357–1367.

[34] Y. Golubev. On universal oracle inequalities related to high-dimensional linear models. *Ann. Statist.*, 38-(5):2751–2780, 2010.

[35] I.S. Gradshteyn and I.M. Ryzhik. *Table of Integrals, Series, and Products.* Academic press, new york edition, 1980.

[36] H. Groemer. *Geometric Applicatons of Fourier Series and Spherical Harmonics.* Cambridge Univ. Press. 1996.

[37] F. Guilloux, G. Faÿ, and F. Cardoso. Practical wavelet design on the sphere. *Appl. Comput. Harmon. Anal.*, 26(2):143–160, 2009.

[38] P. Hall, G. Kerkyacharian, and D. Picard. On the minimax optimality of block thresh- olded wavelet estimators. *Statist. Sinica*, 9:33–50, 1999.

[39] D.M. Healy, H. Hendriks, and P.T. Kim. Spherical deconvolution. *J. Multivariate Anal.*, 67, 1–22.

[40] M. Hoffmann and M. Reiß. Nonlinear estimation for linear inverse problems with error in the operator. *Ann. Statist.*, 36:310–336, 2008.

[41] W. Härdle, G. Kerkyacharian, D. Picard, and A. Tsybakov. *Wavelets, Approximation, and Statistical Applications.* Lecture Notes in Statistics, Vol.129. Springer edition, 2007. ISBN 978-0-387-98453-7.

[42] I.A. Ibragimov and R.Z Hasminskii. *Statistical Estimation. Asymptotic Theory.* Springer-Verlag, 1981.

[43] K. Ivanov, P. Petrushev, and Y. Xu. Decomposition of spaces of distributions induced by tensor product bases. *Journal of Functional Analysis*, 263(5):1147 – 1197, 2012.

[44] G. Johnstone, I. Kerkyacharian, D. Picard, and M. Raimondo. Wavelet deconvolution in a periodic setting. *J. R. Stat. Soc. Ser. B Statist. Methodol.*, 66:547–573, 2004.

[45] I.M. Johnstone and B.W. Silverman. Discretization effects in statistical inverse problems. *J. Complexity*, 7(1):1–34, 1991.

[46] J. Keilson and W.R. Nunn. Laguerre transformation as a tool for the numerical solution of integral equations of convolution type. *Appl. Math. and Comput.*, 5(4): 313–359, 1979.

[47] H. E. Keller. *Handbook of Biological Confocal Microscopy.* Plenum Press, New York, 2nd edition edition, 1995. chapter Objective lenses for confocal microscopy.

[48] G. Kerkyacharian and D. Picard. New generation wavelets assiociated with statistical problems. *8th Workshop on Stochastic Numerics, Research Institute for Mathematical Sciences, Kyoto University,*, page 119–146, 2009.

[49] G. Kerkyacharian, P. Petrushev, D. Picard, and T. Willer. Needlet algorithms for estimation in inverse problems. *EJS*, 1, 2007.

[50] G. Kerkyacharian, G. Kyriazis, E. Le Pennec, P. Petrushev, and D. Picard. Inversion of noisy Radon transform by SVD based needlets. *Appl. Comput. Harmonic Anal.*, 28:24–45, 2010.

[51] G. Kerkyacharian, T.M. Pham Ngoc, and D. Picard. Localized spherical deconvolution. *Ann. Statist.*, 39:1042–1068, 2011.

[52] P.T. Kim and Y.J. Koo. Optimal spherical deconvolution. *J. Multivariate Anal.*, 80:21–42, 2002.

[53] A. Kirsch. *An Introduction to the mathematical theory of inverse problems.* Springer. 2011.

[54] A.P. Korostelev and A.B. Tsybakov. *Minimax theory of image reconstruction.* Springer, 1993.

[55] D. Kundur and D. Hatzinakos. Blind image deconvolution. *IEEE Sig. Proc. Mag.*, 13:43–64, 1996.

[56] P.K. Lamm. Variable-smoothing local regularization methods for first-kind integral equations. *Inverse problems*, 19:195–216, 2003.

[57] O.V. Lepski. Asymptotically minimax adaptive estimation. I: Upper bounds. optimally adaptive estimates. *Theory. Probab. Appl.*, 36:682–697, 1991.

[58] T.N. Lien, D.D Trong, and A.P.N. Dinh. Laguerre polynomials and the inverse Laplace transform using discrete data. *J. Math. Anal. Appl.*, 337:1302–1314, 2008.

[59] P. Linz. *Analytical and Numerical Methods for Volterra Equations*. Siam edition, 1985.

[60] S. Mallat. *A wavelet tour of signal processing*. Academic Press. 2008.

[61] S.G. Mallat. A theory for multiresolution signal decomposition: the wavelet representation. *Pattern Analysis and Machine Intelligence, IEEE Transactions on*, 11 (7):674–693, 1989.

[62] D. Marinucci, D. Pietrobon, A. Balbi, P. Baldi, P. Cabella, G. Kerkyacharian, P. Natoli, D. Picard, and N. Vittorio. Spherical needlets for CMB data analysis. *Monthly Notices of the Royal Astronomical Society*, 383(2):143–160, 2008.

[63] C. Marteau. Regularization of inverse problems with unknown operator. *Math. Methods Statist.*, 15(4):415–443, 2006.

[64] P. Massart. *Concentration inequalities and model selection*. Ecole d'Eté de Probabilités de Saint-Flour XXXIII (Jean Picard ed.), Lecture Notes in Mathematics 1986. Springer, 2007.

[65] P. Mathe and S.V. Pereverzev. Geometry of linear ill-posed problems in variable Hilbert scales. *Inverse problems*, 19:789–803, 2003.

[66] M.W. Meckes. On the spectral norm of a random Toeplitz matrix. *Elect. Comm. in Probab.*, 12:315–325, 2007.

[67] F. Narcowich and J. Ward. Nonstationary wavelets on the m-sphere for scattered data. *Appl. Comput. Harm. Anal.*, 3:324–336, 1996.

[68] F. Narcowich, P. Petrushev, and J. Ward. Decomposition of Besov and Triebel-Lizorkin spaces on the sphere. *J. Funct. Anal.*, 238(2):530–564, 2006.

[69] F. Narcowich, P. Petrushev, and J. Ward. Localized tight frames on spheres. *J. Funct. Anal.*, 238(2):530–564, 2006.

[70] Michael H. Neumann and O. Hössjer. On the effect of estimating the error density in nonparametric deconvolution. *J. Nonparametric Statist.*, 7(4):307–330, 1997. URL `http://www.tandfonline.com/doi/abs/10.1080/10485259708832708`.

[71] M. Nussbaum and S.V. Pereverzev. The degree of ill-posedness in stochastic and deterministic models. *Preprint No. 509, Weierstrass Institute (WIAS), Berlin*, 1999.

[72] P. Pankajakshan L. Blanc-Féraud B. Zhang Z. Kam J-C. Olivo-Marin and J. Zerubia. Parametric blind deconvolution for confocal laser scanning microscopy (clsm)-proof of concept. *Projet INRIA Ariana, research report 6493*, 2008.

[73] G. Ramm. *Mathematical and Analytical Techniques with Applications to Engineering*. Springer. 2004.

[74] P.K. Rathnakumar. A localization theorem for Laguerre expansions. *Proceedings of the Indian Academy of Sciences - Mathematical Sciences*, 105(3):303–314, 1995.

[75] J.S. Rosenthal. Random rotations: characters and random walks on SO(N). *Ann. Probab.*, 22(1):398–423, 1994.

[76] G. Reiner C. Cremer S. Hell and E.H.K. Stelzer. Aberrations in confocal fluorescence microscopy induced by mismatches in refractive index. *J. Microscopy*, 169: 391–405, 1993.

[77] P. Shröder and W. Sweldens. Spherical wavelets: Efficiently representing functions on the sphere. *Computer Graphics Proceedings*, 95, 161-172.

[78] P.A. Stokseth. Properties of a defocused optical system. *J. Opt. Soc. Am. A*, 59: 1314–1321, 1969.

[79] M. Talagrand. Majorizing measures: the generic chaining. *Ann. Probab.*, 24(3): 1049–1103, 1996.

[80] J.D. Tournier, F. Calamante, D.G. Gadian, and A. Connelly. Direct estimation of the fiber orientation density function from diffusion-weighted MRI data using spherical deconvolution. *Neuroimage*, 23:1176–1185, 2004.

[81] A.B. Tsybakov. On the best rate of adaptive estimation in some inverse problems. *C.R. Acad. Sci. Paris Sér. I Math.*, 330:835–840, 2000.

[82] A.B. Tsybakov. *Introduction to nonparametric estimation*. Springer. 2008.

[83] A.C.M. Van Rooij and F.H. Ruymgaart. Regularized deconvolution on the circle and the sphere. *Nonparametric Functional Estimation and Related Topics*, 335: 679–690, 1991.

[84] N.J. Vilenkin. *Fonctions spéciales et théorie de la représentation des groupes*. Monographies Universitaires de Mathématiques, 33. Dunod, Paris, 1969.

[85] T. Willer. Optimal bounds for inverse problems with Jacobi-type eigenfunctions. *Statist. Sinica*, 19(2):785–800, 2009.

Résumé: Cette thèse étudie l'effet de l'imprécision sur un opérateur intervenant dans la résolution d'un problème inverse. La problématique habituelle des problèmes inverses est l'approximation d'un signal d'entrée à partir de son image par un opérateur régularisant. A l'incertitude habituelle contaminant l'observation du signal de sortie, on ajoute cette erreur commise sur l'opérateur que l'on modélise par un processus Gaussien d'une certaine amplitude, potentiellement différente de la précédente. Nous nous intéressons plus particulièrement au cas où l'opérateur en question est un opérateur à noyau, lorsque ce dernier est lui même bruité. Ce modèle recouvre par exemple les cas de la convolution de Fourier périodique, de Laplace/Volterra, ou bien la convolution sphérique.
Nous développons des procédures statistiques d'estimation dans chacun de ces cas, en traitant de manière adéquate la nouvelle erreur commise sur le noyau selon la forme de la matrice associée à un schéma de Galerkin. Plus précisément, nous étudions le risque quadratique dans le cas où cette dernière est diagonale, diagonale par blocs ou bien triangulaire inférieure et de Toeplitz. Dans chacun de ces cas, nous mettons en évidence de nouvelles vitesses de convergence faisant intervenir de manière explicite les deux paramètres d'incertitude (sur le signal de sortie et sur le noyau) et dont nous prouvons l'optimalité au sens minimax. Enfin, nous étudions spécifiquement le cas de la déconvolution sphérique en mettant à profit les needlets sphériques, sorte d'équivalent d'ondelettes sur la sphère, dans la construction d'une procédure qui traite ce même problème pour un risque en norme Lp.

Mots-clés: Estimation non-paramétrique, Problèmes inverses, Bruit dans l'opérateur, Déconvolution aveugle, Adaptativité, Déconvolution de Laplace, Déconvolution sphérique.

Discipline : Mathématiques

Abstract: This thesis focuses on the impact of the imprecision on a linear operator when the latter is at stake in an inverse problem. The usual framework of an inverse problem involves the recovery of an input signal, when one observes its response through a linear operator (the output signal) . The output signal is usually observed with an additive random Gaussian noise, and we suppose that the operator is observed with an additive Gaussian noise as well, independent of the former, the error amplitudes being potentially different. We will study more precisely the case of kernel operators, when the kernel is subject to observation noise. This covers the case of periodic Fourier convolution, Laplace/Volterra convolution or spherical convolution. In each of those preceding cases, we develop statistical procedures of estimation, which rely on the adequate treatment of the Galerkin matrix involved when discretizing the inverse problem. More precisely, we study the quadratic risk in the case where the latter matrix is diagonal, block-diagonal or lower triangular Toeplitz. In each case we put into evidence new rates of convergence with an explicit dependency on the two noise amplitudes (noise contaminating the output signal or the kernel) and we prove them to be minimax. Finally, we focus on the specific case of spherical deconvolution and show how the spherical needlets (a kind of wavelet defined on the sphere) allow us to design a procedure which controls the risk measured in Lp norm.

Key words: Nonparametric estimation, Inverse problems, Noise in the operator, Blind deconvolution, Adaptivity, Laplace deconvolution, Spherical deconvolution.

Laboratoire de Probabilités et Modèles Aléatoires,
CNRS-UMR 7599, UFR de Mathématiques, case 7012
Université Paris 7, Denis Diderot
Avenue de France, 75205 Paris Cedex 13.